

**Imperial College  
London**



**NOVEL APPLICATIONS FOR PAPER SLUDGE ASH**

by

**CHARIKLEIA SPATHI**

*A thesis submitted in fulfilment of the requirements for the degree of  
Doctor of Philosophy*

**Faculty of Engineering**

*Department of Civil and Environmental Engineering*

**November 2015**

I, Charikleia Spathi, declare that this thesis, submitted for the degree of Doctor of Philosophy of Imperial College London, is the result of my own work and all information derived from other researchers has been specifically acknowledged. No part of the work has previously been presented for another qualification elsewhere.

*Charikleia Spathi*



Date: 24/11/2015

Supervisors:

**Professor Chris R. Cheeseman**

Department of Civil and Environmental Engineering  
Imperial College London  
South Kensington Campus  
SW7 2AZ

**Dr Luc J. Vandeperre**

Department of Materials  
Imperial College London  
South Kensington Campus  
SW7 2AZ

**Imperial College London**  
**Department of Civil and Environmental Engineering**  
**South Kensington Campus**  
**London SW7 2AZ**

First published in Great Britain by Imperial College London 2015

Copyright © Charikleia Spathi 2015

Charikleia Spathi asserts the moral right to be identified as the author of this work.

The copyright of this thesis rests with the author and is made available under a Creative Commons Attribution Non-Commercial No Derivatives licence. Researchers are free to copy, distribute or transmit the thesis on the condition that they attribute it, that they do not use it for commercial purposes and that they do not alter, transform or build upon it. For any reuse or redistribution, researchers must make clear to others the licence terms of this work.

*‘Αν μή πηλόν τύψης, κέραμος ου γίγνεται.’*

Archytas of Tarentum, Pythagorean philosopher  
(428-347 BC)

## ABSTRACT

The disposal of paper sludge ash (PSA) generated by the UK paper industry has caused environmental concerns and there is a need to provide more sustainable management options as an alternative to landfill. This study investigated and developed viable technologies for the production of waste-derived lightweight filler (LWF) particles with high strength-to-density ratios and hydrophobic materials.

Two types of PSA, supplied by Aylesford Newsprint and UPM-Shotton recycled paper mills, were processed into LWFs and hydrophobic powders. They were both composed of gehlenite ( $\text{Ca}_2\text{Al}_2\text{SiO}_7$ ), calcite ( $\text{CaCO}_3$ ), calcium silicate ( $\alpha\text{-Ca}_2\text{SiO}_4$ ), lime ( $\text{CaO}$ ) and quartz ( $\text{SiO}_2$ ). Given that PSA exhibited low sintering reactivity at temperatures up to 1200 °C, recycled soda-lime glass was used to promote sintering while minimising the energy intensity of the proposed thermal treatment. Wet-milling of glass with PSA addition up to 20 wt. % produced foamed lightweight materials ( $\sim 1 \text{ g}\cdot\text{cm}^{-3}$ ) after rapid sintering at 800 °C. This was shown to be because of extensive growth of pores caused by gas evolution from the decomposition of, primarily, calcium carbonate present in PSA. Thermodynamic considerations for the 80/20 glass/PSA system also showed that the amount of gas evolved and entrapped within the sintered body determined the extent of closed-cell porosity for mixes of given viscosity and particle size characteristics. This was found to be a time-sensitive mechanism on a minutes scale. Incorporation of such low water permeability LWFs in cement mortars corroborated their use as structural, thermal-insulating materials.

Dry milling of PSA particles with stearic acid led to unexpected surface functionalization inducing super-hydrophobicity. Both PSA samples exhibited water contact angles in the region of 150° when treated with 4 wt. % of stearic acid under optimised process conditions. This was due to the formation of calcium stearate self-assembling layers physically and chemically adsorbed on fracture PSA surfaces. PSA particles exhibited higher hydrophobicity when treated with stearic acid compared to other inorganic substrates and organic acids investigated.

Research findings indicate that manufacturing of glass/PSA LWFs and PSA-based hydrophobic materials was technically feasible at laboratory scale. Economic and environmental benefits could drive commercial exploitation of research outputs.

## ACKNOWLEDGEMENTS

I would like to express my sincere gratitude to my supervisor, Professor Chris Cheeseman, for providing me the opportunity to work on this challenging research topic. I highly admire his creative thinking and can-do attitude. I feel truly fortunate to have been academically trained under and alongside him. I would like to particularly thank him for introducing me into the world of student entrepreneurship. His constant support and encouragement, especially during hard times, have been the reasons this project was completed.

I could not thank more Dr Luc Vandeperre for his scientific contribution in the course of this project. In particular, his guidance in helping me understand the thermodynamics of the sintering process presented herein, is greatly acknowledged. I feel honoured to have worked with such an inspiring academic and person.

This project would not have been possible without the financial support of EPSRC and the industrial partners, Smithers PIRA, Aylesford Newsprint Ltd and UPM-Shotton Ltd. In particular, my interactions with Rachel Bain, Paul Richards, Andrew Bronnert, Taru Päiväläinen and Pasi Virtanen have been mostly valuable.

My special thanks go to Dr Martin Kay who, apart from providing his expertise in paper industry-related issues, initiated the discussions with the industrial sponsors and he believed from day one in my capability to deliver the project.

I also acknowledge the academic and personal support of Dr Costas Velis in the course of my MSc thesis and during my PhD project. I would like to thank Dr Geoff Fowler and Mrs. Carol Edwards in the Roger Perry laboratory for their technical help and support. I would also like to thank Dr Jerry Heng from the Chemical Engineering Department for his guidance in hydrophobicity-related topics.

Many thanks to all the MSc and undergraduate students I had the opportunity to collaborate with. Peter, Neale, Robert, Paphawee, Ioannis and Joy, your research findings greatly influenced the direction of my own research.

I would like to thank Thanos (Dr Άχρηστος!) for his incredible support and all the fun we had in the lab. I also thank fellow researchers, Nicolas, Ding, Veronica, Maria, Carsten, Tingting, Eliana, Steve, Rosie, Carlos, Jelena, Xavier, Giuseppe, Haris, Simon and Wen for all the good times we had outside office hours. PIG, go raibh maith agat gan déanamh an tionscadal seo! Thodoris, Maria and Michalis, thank you for all the crazy London moments.

I have no words to express my appreciation for Edo, Manuel, Rob, Acile and Karl. In particular, I would like to express my gratitude to Dr Karl Smith for being such an amazing friend. I will never forget the care and love he showed when I was at my worst. Karl, I promise I will compensate soon for all the negative energy I might have passed on you!

I could not thank more Dr Fei Zhang and Dr Quentin Cheok for their unfailing motivation. All the talks, holiday escapes, dinner nights as well as the Snowdonia adventure and the bike ride to Richmond will stay with me for life. A big thanks to Quentin, Rita and Alkis for being the best flatmates I could ever ask for. You made our London house a home for me.

A huge thanks to Katerina (my Barbie girl!) for her friendship. She has always been next to me through good and bad moments. Special thanks also go to my beautiful, lifelong friends in Greece, Amani, Voula, Georgia, Fay, Costas, Sofia, Irene, Katerina, Lefteris and Myrto for their continuous support and encouragement. Finally, I am particularly thankful to my beloved cousin, Eleni, for always believing in me.

Finally, my deepest appreciation goes out to my family, my parents, Thanasis and Eleni, and my brother, Panayiotis, for their devotion and support throughout my life. I would also like to thank Evi, the new member of our family, for her support. Their patience, particularly during the writing-up period of my PhD thesis, has been catalytic for the completion of this project.

## PUBLICATIONS AND ACHIEVEMENTS

### Journal publications

Spathi, C., Young, N., Heng, J.Y-Y., Vandeperre, L.J.M. & Cheeseman, C.R. (2015)  
A simple method for preparing super-hydrophobic powder from paper sludge ash.  
*Materials Letters*, 142 (1), pp. 80-83.

Spathi, C., Vandeperre, L.J.M. & Cheeseman, C.R. (2015) Production of Lightweight  
Fillers from Waste Glass and Paper Sludge Ash. *Waste and Biomass Valorization*,  
6 (5), pp. 875-881.

### Achievements associated with this PhD project

**International Patent P60507WO**  
(filed in June 2015)

**Imperial Innovations, UK**

*The invention relates to a waste-derived super-hydrophobic powder for use as coating material or as concrete additive*

**Althea-Imperial 2015 Prize, Winner**

**The Althea Foundation, US  
Imperial College London, UK**

*The Althea-Imperial Programme is a personal and professional development programme aimed at women studying at Imperial. It consists of a series of workshops designed to help develop enterprising ideas.*

**Business idea:** PSA-based hydrophobic materials

**Team members:** Spathi, C., Minson, K., Clancy, R., Heng, J.Y-Y., Vandeperre, L. & Cheeseman, C.R.

**Venture Catalyst Challenge, Finalist**

**Create Lab, UK**

*An annual competition with over 200 applications from startups, judged for innovation and commercial viability.*

**Business idea:** PSA-based hydrophobic materials

**Team members:** Spathi, C., Minson, K. & Clancy, R.

# TABLE OF CONTENTS

<b>ABSTRACT .....</b>	<b>5</b>
<b>ACKNOWLEDGEMENTS .....</b>	<b>6</b>
<b>PUBLICATIONS AND ACHIEVEMENTS.....</b>	<b>8</b>
<b>TABLE OF CONTENTS .....</b>	<b>9</b>
<b>LIST OF FIGURES.....</b>	<b>13</b>
<b>LIST OF TABLES.....</b>	<b>21</b>
<b>ABBREVIATIONS AND TERMS .....</b>	<b>23</b>
<b>CHAPTER 1        INTRODUCTION.....</b>	<b>24</b>
1.1     BACKGROUND TO RESEARCH .....	24
1.2     SUSTAINABILITY IN THE PAPER INDUSTRY.....	24
1.3     SUSTAINABILITY IN THE CONSTRUCTION MATERIALS SECTOR .....	26
1.3.1    Relevant legislation for the construction sector.....	28
<b>CHAPTER 2        AIM AND OBJECTIVES.....</b>	<b>31</b>
2.1     RESEARCH AIM.....	31
2.2     RESEARCH OBJECTIVES.....	31
2.3     EXPERIMENTAL STRUCTURE.....	31
<b>CHAPTER 3        LITERATURE REVIEW.....</b>	<b>33</b>
3.1     WASTE MANAGEMENT IN THE PAPER INDUSTRY.....	33
3.1.1    The production process for deinked pulp from recycled paper.....	33
3.1.2    Waste streams resulting from paper making.....	34
3.1.3    Paper sludge generation and characteristics .....	36
3.1.4    Paper sludge disposal methods in Europe and the UK .....	37
3.2     PAPER SLUDGE ASH (PSA) .....	41
3.2.1    Typical chemical composition and leachability of PSA .....	42
3.2.2    Current reuse applications .....	44
3.2.3    Novel reuse applications.....	46
3.3     LIGHTWEIGHT MINERAL CONSTRUCTION MATERIALS.....	47
3.3.1    Lightweight Aggregates (LWAs) .....	47
3.3.2    Lightweight fillers (LWFs).....	48
3.3.3    Properties of lightweight materials .....	49
3.3.4    Key factors affecting lightweight materials properties .....	50
3.4     WASTE MATERIALS IN LIGHTWEIGHT MATERIALS PRODUCTION .....	53
3.4.1    Waste glass and its use in lightweight materials.....	54

3.5	PRINCIPLES OF HYDROPHOBICITY.....	56
3.5.1	Young’s wetting model.....	56
3.5.2	Wenzel’s wetting model .....	57
3.5.3	Cassie-Baxter wetting model.....	58
3.5.4	Formation of self-assembling monolayers (SAMs) on mineral particles .....	60
<b>CHAPTER 4</b>	<b>MATERIALS AND EXPERIMENTAL METHODOLOGY.....</b>	<b>62</b>
4.1	MATERIALS.....	62
4.1.1	Materials used for the production of LWFs.....	62
4.1.2	Materials used for the production of cement mortars .....	63
4.1.3	Materials used for the production of hydrophobic particles .....	63
4.2	PREPARATION OF SAMPLES.....	64
4.2.1	Preparation of lightweight fillers (LWFs).....	64
4.2.2	Preparation of cement mortars.....	65
4.2.3	Preparation of hydrophobic particles .....	66
4.3	CHARACTERISATION TECHNIQUES.....	66
4.3.1	Particle size analysis by laser diffraction.....	67
4.3.2	Density analysis.....	68
4.3.3	Water absorption.....	70
4.3.4	Apparent open porosity.....	70
4.3.5	Microstructural analysis.....	71
4.3.6	Chemical analysis .....	72
4.3.7	Leachability .....	74
4.3.8	Heat stability.....	76
4.3.9	Workability of cement mortars .....	77
4.3.10	Thermal conductivity.....	78
4.3.11	Mechanical strength tests.....	79
4.3.12	Water Contact Angle (WCA) test.....	80
4.3.13	Surface roughness.....	81
4.4	RESULTS AND ERROR CALCULATION .....	81
4.4.1	Statistical significance: t-Test.....	82
<b>CHAPTER 5</b>	<b>PRODUCTION OF LIGHTWEIGHT FILLERS (LWFS).....</b>	<b>83</b>
5.1	INTRODUCTION.....	83
5.1.1	Characterisation of raw materials .....	84
5.1.2	Lab-based manufacturing process .....	91
5.2	FEASIBILITY STUDY: SCREENING EXPERIMENTS .....	91
5.3	EFFECT OF GLASS ADDITION ON LWF PHYSICAL PROPERTIES .....	93
5.4	EFFECT OF SINTERING TIME ON PROPERTIES OF END-PRODUCTS.....	96
5.4.1	Effect of sintering time on the 80/20 glass/PSA_ ANP mix.....	96
5.4.2	Effect of sintering time on the 90/10 glass/PSA_ UPM mix .....	97

5.4.3	Microstructural evolution during sintering .....	98
5.5	EFFECT OF PARTICLE SIZE OF RAW MATERIALS AND SINTERING TIME ON THE PROPERTIES OF 80/20 GLASS/PSA MIXES.....	99
5.5.1	Physical and microstructural properties of sintered products .....	99
5.5.2	Performance of optimum LWFs of different grain sizes .....	104
5.5.3	Crushing strength of optimum LWFs .....	105
5.5.4	Mineralogy of optimum 80/20 glass/PSA LWFs.....	106
5.6	LEACHABILITY OF AS-RECEIVED PSA AND OPTIMUM 80/20 GLASS/PSA LWFs.....	107
5.6.1	Acid Neutralisation Capacity (ANC).....	108
5.6.2	Leachate analysis .....	110
5.6.3	Inclusive leaching behaviour .....	114
5.7	CONCLUDING REMARKS .....	115
<b>CHAPTER 6</b>	<b>MICROSTRUCTURAL EVOLUTION DURING SINTERING.....</b>	<b>118</b>
6.1	INTRODUCTION.....	118
6.2	THERMODYNAMIC ASPECTS OF CALCIUM HYDROXIDE AND CALCITE DECOMPOSITION.....	118
6.3	VISCOUS GROWTH OF PORES DURING SINTERING.....	121
6.3.1	Volumetric expansion of glass/PSA mixes: Geometrical aspects.....	121
6.4	CONCLUDING REMARKS .....	125
<b>CHAPTER 7</b>	<b>CEMENT MORTARS: A VIABLE APPLICATION FOR GLASS/PSA LWFs.</b>	<b>126</b>
7.1	INTRODUCTION.....	126
7.2	MATERIALS AND PREPARATION OF MORTARS.....	126
7.3	RESULTS AND DISCUSSION .....	127
7.3.1	Workability and water absorption.....	127
7.3.2	Dry bulk density and thermal conductivity.....	129
7.3.3	Compressive strength and microstructure.....	131
7.4	CONCLUDING REMARKS .....	134
<b>CHAPTER 8</b>	<b>PSA-BASED HYDROPHOBIC MATERIALS .....</b>	<b>136</b>
8.1	INTRODUCTION.....	136
8.1.1	Surface functionalization of waste materials .....	137
8.2	EXPERIMENTAL METHODOLOGY .....	138
8.3	RESULTS AND DISCUSSION .....	139
8.3.1	Effect of dry milling time and stearic acid addition on PSA hydrophobicity .....	139
8.3.2	Effect of SFAs on PSA hydrophobicity under optimum conditions.....	142
8.3.3	Hydrophobicity of different inorganic substrates .....	143
8.3.4	PSA: Formation of a hydrophobic monolayer .....	147
8.3.5	Heat and humidity resistance .....	148
8.4	CONCLUDING REMARKS .....	151
<b>CHAPTER 9</b>	<b>DISCUSSION .....</b>	<b>152</b>

9.1	PRODUCTION OF LIGHTWEIGHT FILLERS FROM WASTE GLASS AND PAPER SLUDGE ASH.....	152
9.2	PSA-BASED HYDROPHOBIC POWDERS .....	158
<b>CHAPTER 10</b>	<b>CONCLUSIONS AND RECOMMENDATIONS .....</b>	<b>162</b>
10.1	THESIS CONCLUSIONS .....	162
10.2	RECOMMENDATIONS FOR FURTHER WORK .....	163
<b>REFERENCES.....</b>		<b>165</b>
<b>APPENDIX A.....</b>		<b>181</b>
<b>APPENDIX B.....</b>		<b>183</b>
<b>APPENDIX C.....</b>		<b>185</b>

## LIST OF FIGURES

<b>Figure 1.1</b> Waste management hierarchy (Adapted from: European Commission, 1999). .....	26
<b>Figure 1.2</b> Suggested paper sludge reduction technologies (Adapted from: Mahmood & Elliott, 2006). .....	26
<b>Figure 1.3</b> Construction sector: a) typical life cycle of a construction; b) estimated contribution of each construction stage to total CO <sub>2</sub> emissions arising from construction (Adapted from Dept. for BIS, 2010). .....	28
<b>Figure 1.4</b> Major carbon-reduction targets and relevant legislation for aspects of the construction life cycle .....	29
<b>Figure 2.1</b> Schematic diagram of the experimental approach for the development of reuse applications for PSA. ....	32
<b>Figure 3.1</b> A single-loop deinking process for pulp production from recovered paper. Rejects yields at each stage have been taken from Mäkinen et al. (2013). ....	34
<b>Figure 3.2</b> Overview of waste streams generated during papermaking. ....	35
<b>Figure 3.3</b> Principal stages of wastewater treatment at a mill. ....	36
<b>Figure 3.4</b> Disposal methods for pulp and paper industry residues in 2008 (Adapted from: CEPI, 2011). ....	39
<b>Figure 3.5</b> Schematic of a typical PSA production process (Adapted from: WRAP, 2008). .....	42
<b>Figure 3.6</b> Comparison between typical and high-performance lightweight granules (Adapted from Hammer, 1998). ....	49
<b>Figure 3.7</b> Schematic diagram of the process stages involved in manufacturing of lightweight materials. Key mechanisms affecting the pelletisation and sintering stage are explained in detail. ....	53
<b>Figure 3.8</b> Liquid droplet on a solid surface exhibiting different levels of hydrophobicity: a) non-hydrophobic/wetting surface, b) hydrophobic surface and c) super-hydrophobic surface. The contact angle ( $\theta_c$ ) is formed when equilibrium is reached between the various interfacial tension forces, i.e. solid-liquid ( $\gamma_{SL}$ ), solid-vapour ( $\gamma_{sv}$ ) and liquid-vapour ( $\gamma_{LV}$ ). .....	57
<b>Figure 3.10</b> Liquid droplet on a rough surface after: a) the Wenzel's wetting model and b) after the Cassie-Baxter wetting model. ....	59

<b>Figure 3.11</b> Schematic of self-assembling monolayer (SAM): a) indicating bonding between the headgroup-substrate while leaving endgroups to the exterior and b) different energies associated with adsorption of a surfactant to substrate: $\Delta E_{ads}$ stands for adsorption energy, $\Delta E_{corr}$ corrugation of substrate potential experienced by molecule, $\Delta E_{hyd}$ van der Waals interaction of hydrocarbon tails, and $\Delta E_g$ energy of gauche defect expressing the deviation from fully stretched backbone (Adapted from Schreiber, 2000).	61
<b>Figure 4.1</b> Laboratory manufacturing process for the production of lightweight fillers.	65
<b>Figure 4.2</b> Parallel batch test for the pH dependence test. 15 PSA samples and LWF particles were analysed in order to assess the leaching behaviour at various pH conditions.	75
<b>Figure 4.3</b> Schematic of a Netzsch 402 E dilatometer (Adapted from Netzsch, 2006).	77
<b>Figure 4.4</b> Schematic diagram of the TT-TC probe arrangement used for measuring thermal conductivity based on the transient hot wire method.	78
<b>Figure 4.5</b> Crushing strength test apparatus and results: a) dimensions of the set-up, b) test container filled with LWF sample and load application, c) typical deformation curve with the CS(10) value identified at 10 % deformation.	80
<b>Figure 4.6</b> Typical sessile drop formed on the surface of disc samples made from different hydrophobic powders.	81
<b>Figure 5.1</b> A schematic of interlinkages of key process parameters determining the end-microstructure of sintered products. The ‘golden section’, i.e. the desired microstructure, is attained when optimum powder mixes are processed under optimised conditions prior to and during sintering.	83
<b>Figure 5.2</b> Particle size distribution of as-received PSA samples and milled glass (via TEMA milling for 60 s) (n=3).	87
<b>Figure 5.3</b> Scanning electron micrographs of PSA agglomerated particles: a-b) PSA_ANP and c-d) PSA_UPM.	87
<b>Figure 5.4</b> X-Ray patterns of the as-received PSA samples: a) PSA_ANP and b) PSA_UPM. The major crystalline phases present are: calcium silicate ( $\text{Ca}_2\text{SiO}_4$ ), calcite ( $\text{CaCO}_3$ ), gehlenite ( $\text{Ca}_2\text{Al}_2\text{SiO}_7$ ), lime ( $\text{CaO}$ ), mayenite ( $\text{Ca}_{12}\text{Al}_{14}\text{O}_{33}$ ) and quartz ( $\text{SiO}_2$ ) (n=3).	88

**Figure 5.5** TGA and DSC results for the as-received PSA samples: a) PSA\_ANP and b) PSA\_UPM. Major weight loss between 600 and 780 °C is due to the decomposition of calcite (CaCO<sub>3</sub>) to lime (CaO) with simultaneous generation of CO<sub>2</sub> through:  $CaCO_3 \rightarrow CaO + CO_2$ . The maximum gas evolved during sintering is a key parameter for attaining maximum porosity in the final sintered body. Between 600 °C and 780 °C, being the temperature region of primary importance for further sintering processing, PSA\_ANP exhibits a weight loss of 8.5 wt. % whereas PSA\_UPM a loss of 6.7 wt.% (n=3). .....89

**Figure 5.6** Dilatometer results for glass and PSA\_ANP. The softening point of glass is observed at 594 °C, when shrinkage due to dissolution and smelting of the sample occurred. In contrast, PSA\_ANP particles (pressed into discs) exhibit low sintering reactivity with samples failing to densify when slowly sintered at high temperatures. This was confirmed for PSA\_UPM samples (top right image). .....90

**Figure 5.7** The effect of sintering temperature on density and water absorption of the 80/20 glass/PSA\_ANP mix (n=10). Lightweight materials are formed with enhanced properties compared to Poraver at the optimum sintering temperature of 800 °C. The sintering time was kept fixed at 20 minutes. ....93

**Figure 5.8** Effect of PSA addition on the density and water absorption of glass-PSA pellets fired at 800 °C for 20 minutes: a) PSA\_ANP and b) PSA\_UPM. All mixes were wet milled for 1h prior to pelletisation and sintering. The two types of ashes behave differently during sintering, with PSA\_ANP exhibiting better sintering reactivity. The 50 PSA\_UPM – 50 glass mixes failed to provide strong testable sintered products. Lightweight materials, with the maximum possible PSA content, are produced for the 80/20 glass/ PSA\_ANP (in wt. %) mix and the 90/10 glass/PSA\_UPM (in wt. %) mix. (n=10). ....95

**Figure 5.9** Effect of sintering time on particle density and water absorption of the 20 PSA\_ANP – 80 glass mix when fired at 800 °C. Raw materials were wet milled for 1h prior to pelletising and sintering. Beyond 15 minutes, an abrupt change in permeability of the sintered body was observed indicating piercing of the outer layer of the pellets (n=10). ....96

**Figure 5.10** Effect of sintering time on particle density and water absorption of the 90/10 glass/PSA\_UPM mix when fired at 800 °C. Raw materials were wet milled for 1h prior to pelletising and sintering. At 15 minutes, an abrupt change in permeability

of the sintered body was observed indicating piercing of the outer layer of the pellets (n=10). .....97

**Figure 5.11** Morphology of LWFs prepared with glass-PSA mixes wet milled for 1h prior to sintering at 800 °C : a-d) Cross-sections of 80/20 glass/PSA\_ANP pellets sintered for 5, 10, 15 and 20 minutes respectively, and e-f) Cross-sections of 90/10 glass/PSA\_UPM pellets sintered for 2 and 10 minutes respectively. ....98

**Figure 5.12** Scanning electron micrographs of: a-b) Commercial LWF Poraver particles of 600-850 µm in diameter and c) 100 % glass pellets sintered at 800 °C for 15 minutes having a particle density of 1.12 g·cm<sup>-3</sup> and water absorption of 3.8 wt. %. .....99

**Figure 5.13** Particle size distributions for the 80/20 glass/PSA mixes achieved after wet milling for 1, 2 and 4 hours. Mixes containing PSA\_UPM showed better size reduction properties compared to the PSA\_ANP ones. At 4 hours of wet milling, PSA\_ANP mixes formed agglomerates, This can be attributed to the reaction of free lime (CaO) present in the PSA\_ANP and water in the mill for the formation of calcium hydroxide according to:  $CaO s + H_2O (l) \leftrightarrow Ca(OH)_2 (aq)$ . ..... 100

**Figure 5.14** Effect of wet milling and sintering time on (a-b) the particle density and water absorption of 80/20 glass/PSA\_ANP and (c-d) particle density and water absorption of 80/20 glass/PSA\_UPM of sintered pellets at 800 °C (n=10). ..... 101

**Figure 5.15** Morphology of 80/20 glass/PSA pellets sintered at 800 °C: Cross-section of 80/20 glass/PSA\_ANP pellets after 20 minutes of sintering for the 1h (a), 2h (b) and 4h (c) wet milling times; Cross-section of 80/20 glass/PSA\_UPM pellets for the 1h (d), 2h (e) and 4h (f) wet milling times. .... 102

**Figure 5.16** Microstructure of 80/20 glass/PSA\_UPM LWFs sintered at 800 °C: Cross-section of pellets prepared with glass-PSA mixes wet milled for 4h after sintering for 2 minutes (a), 10 minutes (b) and 20 minutes (c). ..... 103

**Figure 5.17** Microstructure of optimum LWFs prepared with glass-PSA\_UPM mixes which were wet milled for 4h prior to being sintered at 800 °C for 10 minutes: a) whole LWF particle and b) cross-section of (a). ..... 103

**Figure 5.18** Optimum LWFs produced at 800 °C for 10 minutes with mixes of: a) 80/20 glass/PSA\_ANP wet milled for 1 hour and b) 80/20 glass/PSA\_UPM wet milled for 4 hours. .... 104

**Figure 5.19** Effect of pellet diameter on particle density (a) and water absorption (b) of optimum 80/20 glass/PSA LWFs and Poraver (n=10). ..... 105

**Figure 5.20** XRD patterns of optimum 80/20 glass/PSA LWFs prepared with 20 wt. % of PSA\_ANP (a) and 20 wt. % of PSA\_UPM (b) sintered at 800 °C for 10 minutes. Representative LWF samples were manually ground to form powders with a mean particle size of 35 µm..... 106

**Figure 5.21** Acid Neutralisation Capacity of the as-received PSA\_ANP and PSA\_UPM samples; 80/20 glass/PSA LWFs sintered at 800 °C for 10 minutes. Sintered LWFs exhibited decreased ANC (n=15). ..... 109

**Figure 5.22** Leaching data for (a) Ca, (b) Na, (c) Mg and (d) K as a function of leachate pH for the as received PSA\_ANP and PSA\_UPM samples (left column) as well as optimum LWFs produced after sintering optimised 80/20 glass/PSA mixes (right column) (n=15)..... 112

**Figure 5.23** Leaching data for Al as a function of leachate pH for the as received PSA\_ANP and PSA\_UPM samples (left) as well as optimum LWFs produced after sintering optimised 80/20 glass/PSA mixes (right) (n=15)..... 113

**Figure 5.24** Leaching data for Fe (left) and Zn (right) as a function of leachate pH for the as received PSA\_ANP and PSA\_UPM samples as well as optimum LWFs produced after sintering optimised 80/20 glass/PSA mixes (n=15)..... 114

**Figure 5.25** Leaching data for Mn (left) and As (right) as a function of leachate pH for the as received PSA\_ANP and PSA\_UPM samples as well as optimum LWFs produced after sintering optimised 80/20 glass/PSA mixes (n=15)..... 114

**Figure 6.1** Equilibrium partial pressure of CO, CO<sub>2</sub> or H<sub>2</sub>O as a function of temperature for the decomposition reactions of CaCO<sub>3</sub> (in the absence or presence of free carbon) and Ca(OH)<sub>2</sub>, which could contribute to bloating during rapid sintering provided the sum of the equilibrium partial pressures exceeds 1 atm. .... 120

**Figure 6.2** Schematic of single pores growth into a grid of regular cubes. Single-bubble hollow spherical will give rise to the same scaling during growth and hence the pore size depends on the distribution of the pore former..... 123

**Figure 6.3** Predicting final pore size: Maximum pore diameter at piercing as a function of the calcite diameter (black line). The dashed red line indicates a typical pore size at piercing for samples with 20 wt. % ANP ash suggesting the calcite particles are at least 5 µm in size. .... 124

**Figure 7.1** Effect of sand replacement by optimum glass/PSA and Poraver LWFs on workability of cement mortars. CM is the control mortar prepared with a cement:sand:water = 1:3:0.5. The w/c ratio was kept fixed for all samples (n=5). . 128

**Figure 7.2** Effect of sand replacement by LWFs (% w/w) on density (n=5). CM is the control mortar prepared with a cement:sand:water = 1:3:0.5. Lines represent predicted density values based on the mass fraction and skeletal density of each of the mix components. .... 130

**Figure 7.3** Effect of sand replacement by LWFs (% w/w) on thermal conductivity of mortar samples (n=5). Dry samples were used to assess the thermal conductivity using a TT-TC probe. Five faces of samples were tested and average values are reported. .... 131

**Figure 7.4** Effect of sand replacement by LWFs (% w/w) on the 28-day compressive strength of saturated mortar samples (n=5)..... 132

**Figure 7.5** Correlation between dry bulk density of mortars and 28-day compressive strength. Within each subgroup of samples prepared with different % w/w of LWFs, a decrease in strength was observed with decreasing density..... 133

**Figure 7.6** Morphology of lightweight cement mortars: a) Image of cross-section of mortar samples containing 40 % w/w of glass/PSA\_UPM LWFs, b) Optical microscopy micrograph of control mortar showing the distribution of sand grains in the cement matrix and c) LWF particle bonded with the cement paste in mortar sample shown in (a). No pores were developed in the interfacial transition zone of the filler-cement matrix..... 134

**Figure 8.1** Effect of dry milling time (a) and stearic acid addition (b) on WCA of PSA\_UPM and ANP samples treated with 1 wt. % stearic acid in (a) and dry milled for 4 and 8 hours respectively in (b) (n=10). .... 140

**Figure 8.2** Effect of dry milling time on the PSA\_ANP particle size distribution. Grinding of PSA for 16 hours resulted in agglomeration of particles (n=3). .... 141

**Figure 8.3** Images of water droplets on hydrophobic surfaces used to determine the water contact angle ( $\theta_c$ ) by the sessile drop method. The droplets shown are for PSA\_ANP dry milled for different times with 1 wt.% addition of stearic acid (A, 2 hours; B, 4 hours; C, 8 hours and D, 16 hours)..... 142

**Figure 8.4** The effect of different surface functionalization agents on the WCA of PSA samples (n=10). SFAs used are saturated fatty acids with different carbon chain lengths. .... 143

<b>Figure 8.5</b> WCA of various inorganic substrates dry milled for 8 hours with 4 wt. % addition of stearic acid (n=10). .....	144
<b>Figure 8.6</b> The effect of stearic acid addition (by weight) on calcium carbonate and lime samples dry milled for 8 hours (n=10). .....	145
<b>Figure 8.7</b> Surface roughness profiles of calcium carbonate and lime powders dry milled for 8 hours with 8 wt. % of stearic acid after pressing them into pellets with an applied force of a 25 N (a) and 100 N (b). .....	146
<b>Figure 8.8</b> FTIR spectra of PSA powders treated with different stearic acid additions and milled for 8 hours: a) PSA as received; b) 1 wt. % addition; c) 4 wt. % addition and d) 8 wt. % addition. The adsorption band at 1588 cm <sup>-1</sup> indicates binding of stearic acid to the substrate surface through the formation of calcium stearate (n=3). .....	148
<b>Figure 8.9</b> Thermal stability of PSA-based and calcium carbonate hydrophobic powders: a) effect of temperature on WCA of functionalised substrates (n=10), b) TGA/DSC analysis of stearic acid (n=3) and c) TGA/DSC analysis of PSA_ANP dry milled for 8 hours with 4 wt. % stearic acid (n=3). .....	149
<b>Figure 8.10</b> Effect of humidity on hydrophobicity of PSA-based hydrophobic samples (n=3). The relative humidity was kept constant at 95 % at 23±2 °C. ....	150
<b>Figure 9.1</b> Melt viscosity variations as a function of temperature for the 80/20 glass/PSA mixes prepared with two different types of PSA (PSA_ANP and PSA_UPM). Data was calculated according to a literature model (Fluegel, 2007). .....	155
<b>Figure 9.2</b> The microstructural evolution of LWF particles from waste glass and paper sludge ash (PSA) is described by the following steps: a) particle packing of initial raw materials, b) bloating of particles during sintering due to gas evolved from PSA constituents being entrapped in the vitrified body and c) final closed-cell porous structures achieved after optimisation of key process parameters. ....	156
<b>Figure 9.3</b> Schematic of porous structures of highly water-absorbent LWF glass/PSA pellets. Sintering of pellets beyond the critical sintering time, as identified for each mix design, resulted in interconnectivity of pores and high water absorption values. ....	157
<b>Figure 9.4</b> Schematic diagram of the surface functionalization of PSA particles by stearic acid molecules via prolonged dry milling. The possible structure of organic layers formed on fractured surfaces of PSA involves formation of bonds between stearate ions and Ca <sup>+2</sup> from calcite particles present in PSA. Chemisorption reactions led to the formation of a monolayer with the hydrocarbon tails perpendicular to the	

Ca<sup>2+</sup> surface. Physisorption is also identified due to the local bilayers formed by the tail-to-tail arrangement of hydrocarbon chains. Free stearic acid molecules can also be found. .... 160

**Figure B.1** Leaching controlling factors and mechanisms of release of elements into the environment when a porous solid material comes in contact with a liquid, called the '*leachant*'. In this study, pH was selected as an important factor to investigate. .... 183

## LIST OF TABLES

<b>Table 3.1</b> Composition and energy content of dry matter content of sludges and rejects (CEPI, 2011) .....	35
<b>Table 3.2</b> Total solid waste generated by different types of pulp and paper mills in Europe (IPPC, 2013) .....	36
<b>Table 3.3</b> Composition of the final sludge (combined primary and secondary sludge) from fibre recovery and wastewater treatment (European Commission, 2014) .....	37
<b>Table 3.4</b> Leading waste treatment options applied by the pulp and papermaking industry in Europe (Adapted from: CEPI, 2011) .....	38
<b>Table 3.5</b> Selected research publications on reuse applications for paper sludge.....	40
<b>Table 3.6</b> Combustion of paper sludge in England and Wales, 2006 (Adapted from: WRAP, 2007).....	42
<b>Table 3.7</b> Chemical composition (in mg/kg) of paper sludge ash (WRAP, 2008)....	43
<b>Table 3.8</b> Typical leachability of PSA at L/S <sup>1</sup> 10 (mg/kg) (WRAP, 2008) .....	44
<b>Table 3.9</b> LWA classification (British Standards Institution, 2002).....	48
<b>Table 3.10</b> LWAs available in the UK .....	48
<b>Table 3.11</b> Lightweight fillers available in the UK.....	49
<b>Table 4.1</b> Main components of cement mortar mixes .....	63
<b>Table 4.2</b> Surface functionalization agents (SFAs) and mineral substrates used to investigate the potential of inducing hydrophobicity via a dry milling process .....	63
<b>Table 4.3</b> Characterisation methods for raw materials and end-products .....	67
<b>Table 5.1</b> Chemical composition of waste glass from Day Aggregates Ltd and as-received PSA samples supplied by Aylesford Newsprint Ltd. and UPM-Shotton Ltd., denoted ‘ <i>PSA_ANP</i> ’ and ‘ <i>PSA_UPM</i> ’ respectively. The powders were pressed into discs and analysed by XRF. Results are expressed as oxides on a dry basis by weight % (n=3). .....	87
<b>Table 5.2</b> Key properties of raw materials (n=3). .....	87
<b>Table 5.3</b> Experimental design matrix for the production of LWFs. Process parameters and desired performance properties were benchmarked against the leading lightweight filler product, Poraver <sup>®</sup> and project-oriented objectives.....	91
<b>Table 5.4</b> Qualitative observation results for PSA-glass mixes fired for 20 minutes at different sintering temperatures .....	92

<b>Table 5.5</b> Crushing strength of optimum 80/20 glass/PSA LWFs and Poraver LWFs (n=10).....	106
<b>Table 5.6</b> Composition of metals on acid digested as-received PSA samples and corresponding maximum leaching concentrations of optimum 80/20 glass/PSA LWFs. Analysis was performed by ICP-AES (n=15).....	115
<b>Table 5.7</b> Key process parameters to obtain optimum LWF properties.....	117
<b>Table 7.1</b> Composition of mortars containing optimum glass/PSA and Poraver LWFs. Water was added at a fixed water: cement ratio of 0.5. No additives were used.....	127
<b>Table 7.2</b> Water absorption (wt. %) of cement mortars prepared with optimum glass/PSA and Poraver LWFs (n=5). .....	129
<b>Table A.1</b> Properties of wastes which render them hazardous.....	181
<b>Table B.1</b> Leaching limit values for inert, non-hazardous and hazardous granular wastes calculated at L/S=10 l/kg for total release (Adapted from Council Decision 2003/33/EC).....	184

## **ABBREVIATIONS AND TERMS**

<b>ANP</b>	Aylesford Newsprint Ltd.
<b>BOD</b>	Biochemical Oxygen Demand
<b>CA</b>	Contact Angle
<b>CEN</b>	European Committee of Standardisation
<b>CEPI</b>	Confederation of European Paper Industries
<b>CM</b>	Control Mortar
<b>DEFRA</b>	Department for Environmental, Food and Rural Affairs
<b>EA</b>	Environment Agency
<b>EPSRC</b>	Engineering and Physical Sciences Research Council
<b>ESCSI</b>	Expanded Shale, Clay and Slate Institute
<b>FA</b>	Fly Ash
<b>LECA</b>	Lightweight Expanded Clay Aggregate
<b>LPS</b>	Liquid phase sintering
<b>LWA</b>	Lightweight aggregate
<b>LWAC</b>	Lightweight aggregate concrete
<b>LWF</b>	Lightweight filler
<b>PC</b>	Portland cement
<b>PIRA</b>	Paper Industry Research Association
<b>PSA</b>	Paper sludge ash
<b>CoGAP</b>	Codes of Good Agricultural Practice
<b>RDF</b>	Refuse-Derived Fuel
<b>RCF</b>	Recycled Fibre
<b>RHA</b>	Rice Husk Ash
<b>SAMs</b>	Self-Assembling monolayers
<b>SEM</b>	Scanning electron microscope
<b>SFA</b>	Surface Functionalization Agent
<b>TGA</b>	Thermogravimetric Analysis
<b>WA</b>	Water Absorption
<b>WCA</b>	Water Contact Angle
<b>WRAP</b>	Waste & Resources Action Programme

## **CHAPTER 1 Introduction**

### **1.1 Background to research**

This was an Industrial Case Award PhD project funded by EPSRC and supported by Smithers PIRA, which provides technology-based consulting services to the paper industry. The key industry collaborators were Aylesford Newsprint Ltd. and UPM-Shotton, both producing newsprint paper from recycled paper. Both UK paper mills employ combustion of wastes as a means of, primarily, disposing of waste streams generated during the paper making process. Although this method significantly reduces the volume of waste, it is not waste-free. Paper sludge ash (PSA), being the residue from this combustion, was the starting material in the present research, which aimed to develop novel, long-term, higher-value PSA-based applications. This could significantly reduce, if not eliminate, the increased expenditures of landfill and help the paper industry meet current and emerging sustainability targets.

Recycled lightweight fillers (LWFs) were identified as a promising end-application for the increasing volumes of PSA, given the need for high-performance, sustainable construction materials. Addition of waste glass in PSA mixes was found to be essential in processing PSA into LWF particles. However, as the project evolved, the prospect of engineering hydrophobic materials from PSA arose and was also investigated as a potential way of upcycling PSA. Both types of proposed end-products can serve as substitutes for traditionally mined or chemically synthesised construction materials or as additives in a range of material applications.

At European level, resource efficiency has been the flagship initiative of the Europe 2020 Strategy as communicated in the ‘Roadmap to a Resource Efficient Europe’ document (European Commission, 2011). In this context, the current research project suggested resource efficient technologies to reduce natural resources consumption while promoting industrial symbiosis between the paper and construction industries.

### **1.2 Sustainability in the paper industry**

Paper production is fully automated and a great range of paper grades are available to consumers for various applications. In the 21<sup>st</sup> century, the use of recycled paper became an increasingly important raw material for the production of paper-based

materials. This maximises the efficient use of wood material and limits its impact on biomass availability (CEPI, 2010).

The UK paper industry is the most successful recycler with a remarkable 73 % of the fibre used throughout the sector coming from recovered paper. However, with an annual production of approximately 4.5 million tonnes of various types of paper (graphics, boards, tissue etc.), the sector is also a significant waste generator, primarily due to the large volumes of paper sludge produced from de-inking and water treatment stages throughout the papermaking process. Focus is, hence, placed on waste disposal and reuse, an aspect of the papermaking cycle that had been long neglected.

Increased emphasis on the environment both at European and worldwide level, accompanied by the implementation of tighter legislation, has had an impact on the pulp and paper industry. Focusing on sustainable waste management, the Waste Framework Directive, last amended in November 2008, lays down a number of suggested measures that should be taken in order to prevent waste generation and/or make reuse of waste materials in secondary products. The suggested waste management hierarchy, to be followed by both individual consumers and producers, is depicted in **Figure 1.1** (European Council, 1999). In addition, the EU Landfill Directive and the constantly increasing Landfill Tax in the UK add more responsibilities to the UK paper industry for diverting waste from landfill and encourage converting waste materials into valuable by-products (European Council, 1999).

In this context, the pulp and paper industry has adopted more sustainable waste management approaches. A number of waste reduction methods have been adopted in order to convert waste streams into added-value, marketable products. As detailed in Chapter 3, paper sludge is the main waste stream generated from the overall paper making process. Mahmood and Elliott (2006) have evaluated the predominant paper sludge treatment methods, as outlined in **Figure 1.2**. The sludge reduction technologies can be broadly grouped into two categories: 1) process changes to minimise sludge yield and 2) post-treatment to reduce the amount to be disposed of. The former approach is more advantageous over the latter in the sense that decreased sludge production is achieved in the first place having subsequent decreased sludge management costs. Although combined employment of process changes and post-

treatment methods will lead to optimum waste minimisation results, complete elimination of waste is not feasible. It is, hence, essential to divert focus on circular economy approaches.

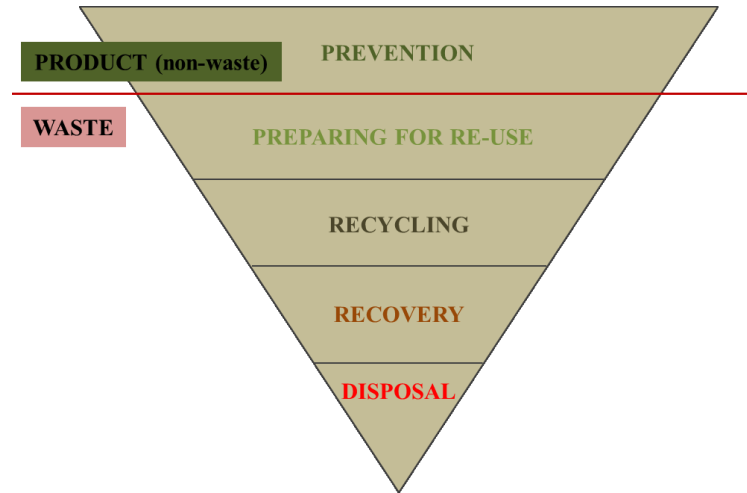


**Figure 1.1** Waste management hierarchy (Adapted from: European Commission, 1999).

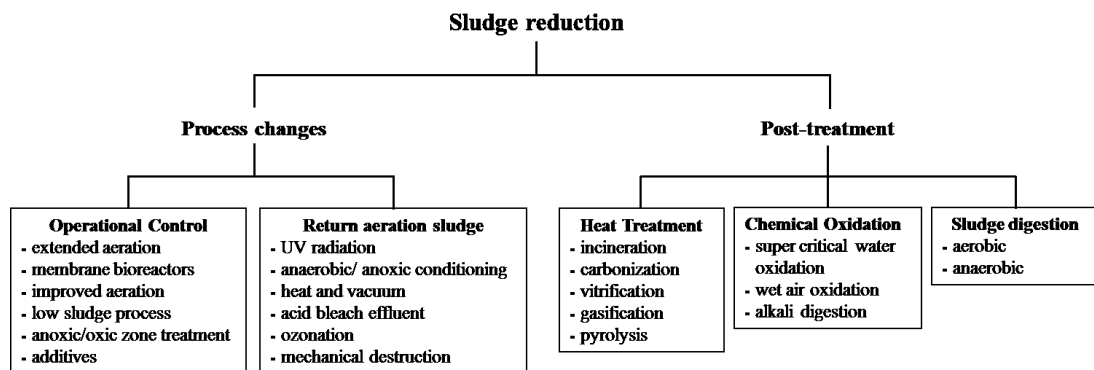


**Figure 1.2** Suggested paper sludge reduction technologies (Adapted from: Mahmood & Elliott, 2006).

### 1.3 Sustainability in the construction materials sector

The construction and maintenance of buildings and other structures account for approximately half of UK CO<sub>2</sub> emissions. In order to achieve the UK Government target of 80 % reduction in total carbon emissions vs. 1990 levels by 2050, sustainable practices should be adopted by the construction industry. The amount of construction materials consumed in the UK should be considered reason enough to promote and disseminate such practices. The long lives of buildings and infrastructure make them promising high-volume stores of waste-derived construction materials. Therefore, an environment-conscious choice of materials could help the sector meet current

sustainability challenges while ensuring engineering creativity through the introduction of novel construction materials.

A holistic approach for a sustainable built environment should consider embodied carbon arising from all aspects of the design, extraction and/or manufacture of materials and components, transport of people and materials, construction process, occupancy and demolition of buildings and infrastructure. As shown in **Figure 1.3**, 83 % of total CO<sub>2</sub> emissions are generated ‘downstream’ during the use phase of a building due to the use of lighting, heating, ventilation and air-conditioning, water use and thermal insulation options available. Another tangible 17 % of total CO<sub>2</sub> emissions are associated with the construction process and the manufacture and distribution of construction materials.

It is estimated that the industry consumes 6 tonnes of materials per annum for every person living in the UK. It is the largest consumer of natural, non-renewable resources (90 % of extracted minerals are used in the construction industry) having a significant impact on the sustainability of the UK (Constructing Excellence, 2008). Depleting natural sources of raw materials and increasing energy costs are key drivers towards increased sustainability in the construction sector.

In addition to pure environmental concerns, a survey conducted by PricewaterhouseCoopers (PwC) in 2012 on behalf of the Construction Products Association (CPA), also indicates that the majority of the industry identifies the potential for innovation and economic growth presented by sustainability. The survey involved companies of various sizes covering a broad range of building materials produced such as concrete, aggregates, ceramics, metals etc. (PwC and CPA, 2012). Deploying a green agenda, therefore, makes both sustainable and economic sense.

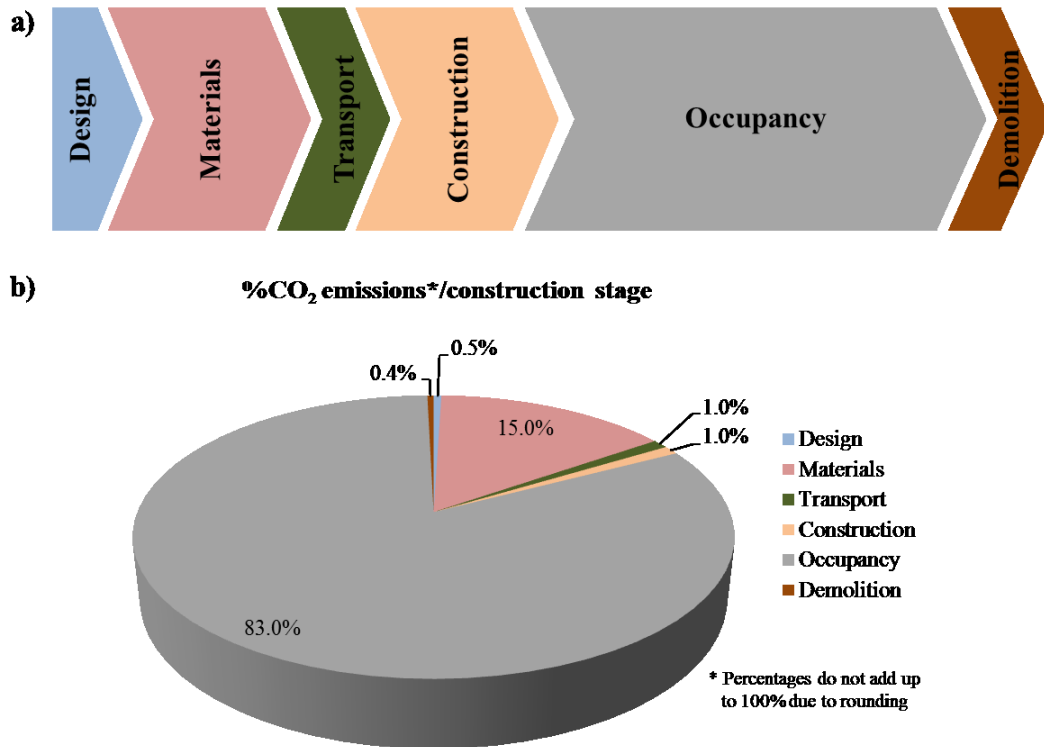


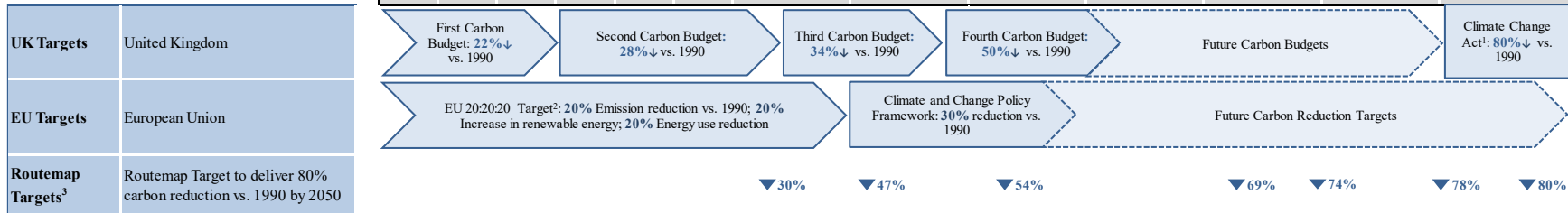
**Figure 1.3** Construction sector: a) typical life cycle of a construction; b) estimated contribution of each construction stage to total CO<sub>2</sub> emissions arising from construction (Adapted from Dept. for BIS, 2010).

### 1.3.1 Relevant legislation for the construction sector

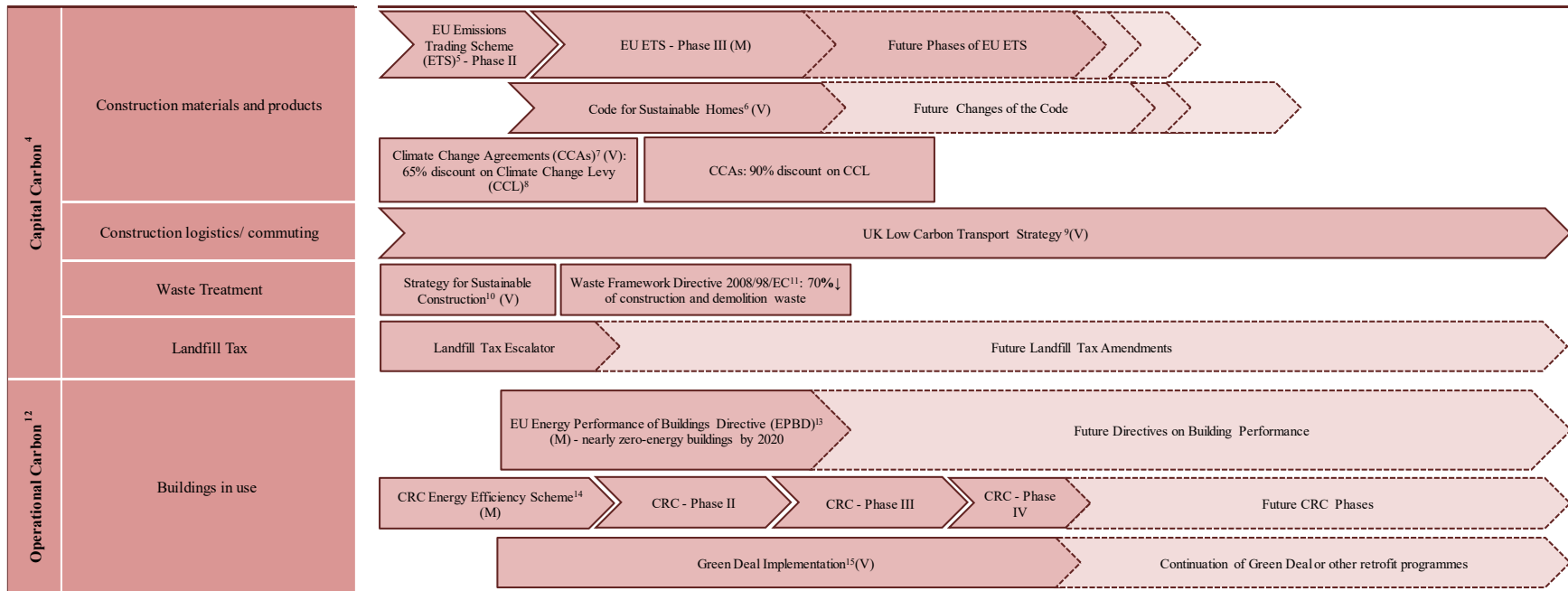
In order to meet the Climate Change Act (2008) target for 80 % reduction in total CO<sub>2</sub> emissions compared to 1990 levels by 2050 in the built environment, all involved stakeholders should take action towards sustainability. A number of mandatory and voluntary policies and strategies have been put into force to incentivise such actions. An overview of the carbon-reduction related legislation for various aspects of construction life cycle is provided in Figure 1.4.

Systematic efforts are also being made by organisations to voluntarily report to stakeholders on the sustainability practices they embed into their corporate activities. Increasing demand for business operations transparency and customer awareness of the environmental footprint of products and services are additional drivers for transition to a ‘green’ building industry. In future, the sector will need to be more resourceful in order to improve stakeholders’ credibility.

**Carbon Reduction Targets**



**Policy and Strategy**



**Key**  
 (M): mandatory  
 (V): voluntary

**Figure 1.4** Major carbon-reduction targets and relevant legislation for aspects of the construction life cycle.

- 
- <sup>1</sup> Great Britain. *Climate Change Act 2008: Elizabeth II. Chapter 27*. (2008) London, The Stationer Office.
- <sup>2</sup> European Commission (2010) *Analysis of options to move beyond 20% greenhouse gas emission reductions and assessing the risk of carbon leakage*. European Commission.
- <sup>3</sup> The Green Construction Board (2013) *The Low Carbon Routemap for the Built Environment*. [Online] Available from: <http://www.greenconstructionboard.org/index.php/resources/routemap> [Accessed 10th December 2014].
- <sup>4</sup> Capital Carbon: covers emissions associated with the extraction/manufacture of materials, transport of materials and people, on-site activities, demolition of buildings and infrastructure.
- <sup>5</sup> European Commission (2003) Directive 2003/87/EC: *Emissions Trading Scheme (ETS)*. European Commission.
- <sup>6</sup> Code for sustainable homes: rating system for new homes in England and Wales. Assessment is completed against 9 criteria (related to energy, water and waste).
- <sup>7</sup> Climate Change Agreements (CCAs): voluntary agreements between the industry and the Environment Agency to reduce energy use and CO<sub>2</sub> emissions.
- <sup>8</sup> Climate Change Levy (CCL): tax added to electricity and fuel bills.
- <sup>9</sup> Department for Transport (2009) *Low Carbon Transport: A Greener Future* [Online] Available from: <http://webarchive.nationalarchives.gov.uk/+http://www.dft.gov.uk/pgr/sustainable/carbonreduction/low-carbon.pdf> [Accessed 10th December 2014].
- <sup>10</sup> HM Government (2008) *Strategy for Sustainable Construction* [Online] Available from: <http://www.strategicforum.org.uk/pdf/1381-Report.pdf> [Accessed 21st January 2015].
- <sup>11</sup> European Commission (2008) Directive 2008/98/EC: *Waste Framework Directive*. European Commission.
- <sup>12</sup> Operational Carbon: covers emissions from lighting, heating, waste from construction and demolition waste.
- <sup>13</sup> European Commission (2010) Directive 2010/31/EC: *Energy Performance of Building*. European Commission.
- <sup>14</sup> CRC Energy Efficiency Scheme is designed to incentivise energy efficiency (large organisations only).
- <sup>15</sup> Green Deal promotes energy-saving improvements. It targets property owners.

## CHAPTER 2 Aim and Objectives

### 2.1 Research aim

In alignment with the current legislative landscape that shapes future trends in the paper industry, this research project aims to develop closed-loop, high-value applications for paper sludge ash (PSA), a so-far classified waste material. In particular, this research explores the potential of using PSA for the production of lightweight fillers (LWFs) and hydrophobic particles. The use of PSA in similar applications has not been previously publicly reported.

### 2.2 Research Objectives

The research aim was achieved by meeting the following objectives:

- Characterising the physical and chemical properties of as-received PSA;
- Designing raw material mixes and optimising the laboratory manufacturing processes for the production of lightweight fillers (LWFs);
- Evaluating the leaching properties of as-received PSA and optimised LWFs by conducting pH-dependence tests;
- Evaluating the thermal insulation properties of cement mortars prepared with optimum LWFs;
- Investigating the feasibility of engineering PSA-based hydrophobic powders via dry milling using various organic surface functionalization agents (SFAs);
- Assessing the properties of LWFs produced against commercially available LWFs, Poraver, and of PSA-based hydrophobic particles against those produced using alternative inorganic substrates.

### 2.3 Experimental structure

The experimental approach adopted for the completion of this PhD project is depicted schematically in Figure 2.1.

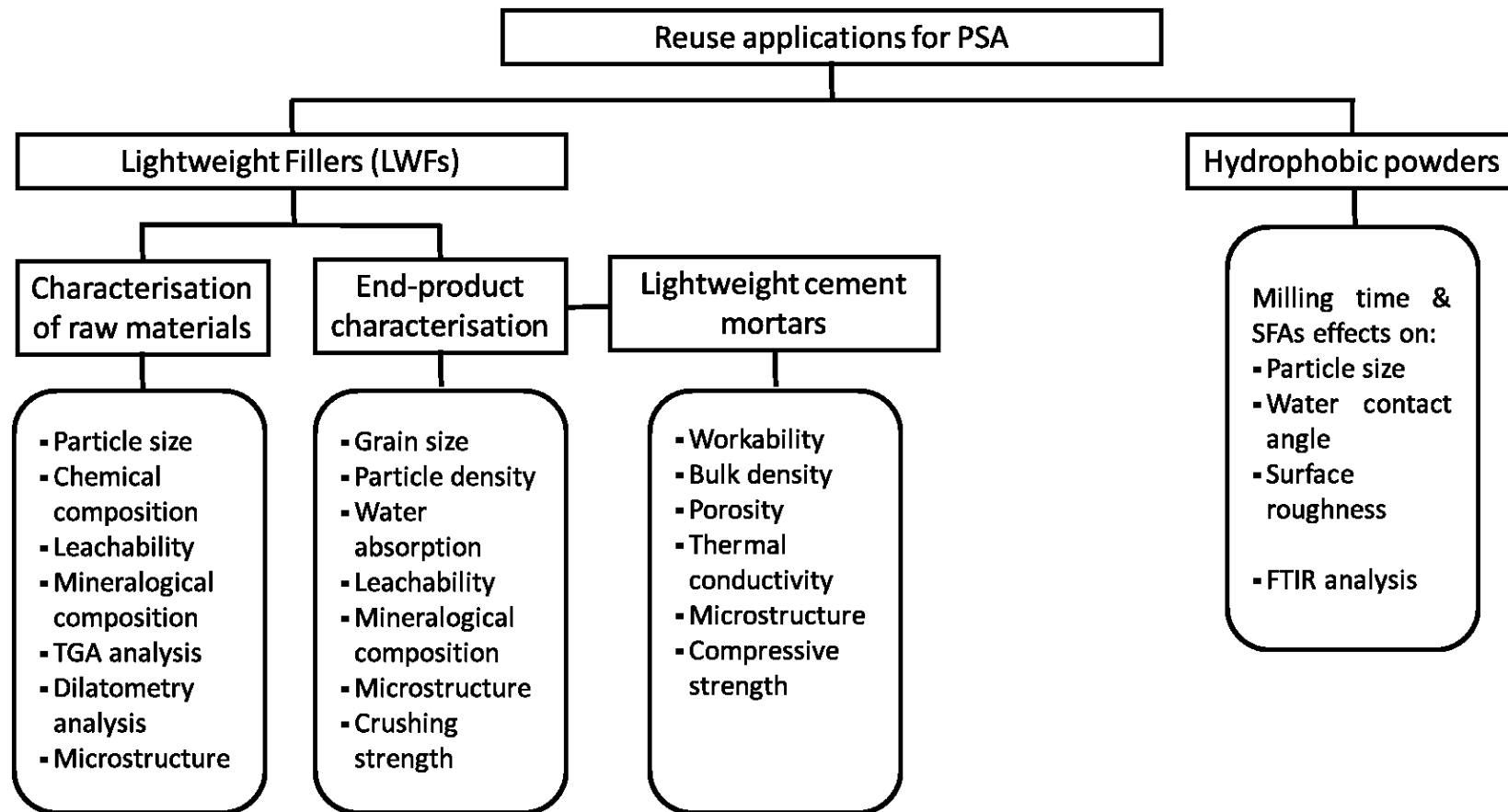


**Figure 2.1** Schematic diagram of the experimental approach for the development of reuse applications for PSA.

## CHAPTER 3 Literature Review

### 3.1 Waste management in the paper industry

Paper recycling and deinked paper production might be both economically and environmentally advantageous over virgin fibre pulp manufacturing but they have also led to increased volumes of waste paper sludge, mainly due to the extensive cleaning processes required to remove the contaminants in recovered paper feedstock. This has associated disposal problems and entails high risks of hazardous substances leaching into the environment unless the waste is appropriately treated (CEPI, 2004).

#### 3.1.1 The production process for deinked pulp from recycled paper

Recycled fibre (RCF) has become an indispensable raw material for the paper industry, accounting for more than 50 % of the total raw materials. In theory, paper can be recycled up to seven times. In practice, though, indefinite recycling is not possible as fibres get shorter and weaker to form a continuous sheet of paper. The current average fibre recycling rate in Europe is 3.5 times (CEPI, 2013). According to the preliminary statistics for 2014 reported by CEPI, an estimated total utilization of paper for recycling is 47.5 million tonnes, increased by 5 % compared to the 2009 pre-financial crisis levels.

In general, the processing of recycled fibres can be divided in two main categories (IPPC, 2013):

- processes with mechanical cleaning, i.e. without a deinking stage, used for products such as testliner, corrugating medium, uncoated board and cartonboard;
- processes with both mechanical cleaning and deinking, comprising products such as newsprint, tissue, printing and copy paper, magazine papers (super-calendered and lightweight coated), coated board and cartonboard.

In order to improve the quality of the RCF, which primarily consists of old newspapers and magazines, and convert them into chemical pulp suitable for papermaking, a series of screening and cleaning operations are combined. The methods used may vary from mill to mill but the aim is always set to separate fibrous material from impurities and contaminants with the aid of warm water and chemical additives.

A simplified single-loop deinking process line for producing pulp for newsprint is depicted in **Figure 3.1**. Once large non-paper items have been removed and pulp has been produced, a series of cleaning stages follow. The main deinking process is a selective floatation process during which air bubbles are fed into the pulp suspension. In this way, hydrophobic particles, i.e. ink, stickies, fillers, coating pigments and binders, become attached to them and form a foam which is then skimmed off. This froth reject is the main waste stream during pulp production from recovered paper. Hydrophilic particles will remain in the pulp suspension, such as some fibres. In most cases, several floatation stages may be required in order to increase the deinking efficiency. Finally, depending on optical specifications for the end-product, deinked pulp may be further dispersed and bleached.

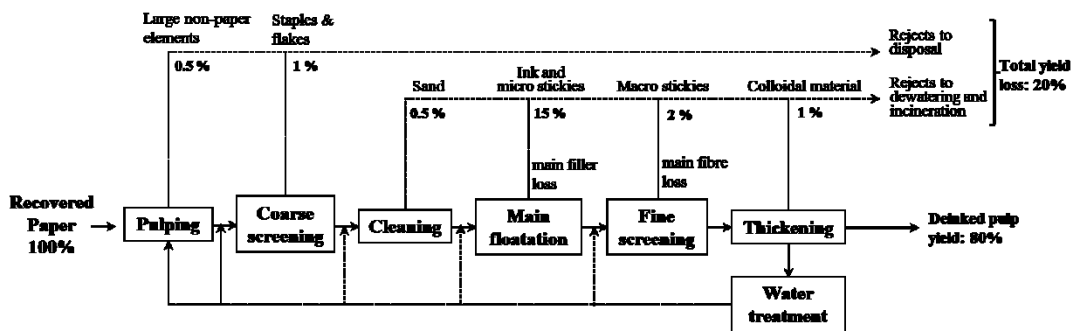


**Figure 3.1** A single-loop deinking process for pulp production from recovered paper. Rejects yields at each stage have been taken from Mäkinen et al. (2013).

For the purposes of this study, however, special emphasis will be placed on the waste streams formed from the production line. In an attempt to appreciate the value one could add on those materials, a detailed description of the various solid wastes generated at a recycled paper mill and their subsequent treatment will be given in the following sections.

### 3.1.2 Waste streams resulting from paper making

During paper production using either virgin wood or recycled paper various solid waste streams are formed, as presented in **Figure 3.2** (Monte et al., 2009). Amongst those, current waste management challenges for the pulp and paper industry are primarily associated with the great paper sludge volumes produced from the wastewater treatment operations at a mill. Herein, the term sludge is used to denote the semi-solid slurry collected in the effluent treatment units, as defined in section 3.1.3. The composition and energy content of the dry matter content of both sludges

and solid rejects are presented in **Table 3.1**. Typically, screen and coarse rejects are removed and treated separately in contrast to the various types of sludges which are combined prior to the selected treatment method employed. A note, yet, should be made about the variability these figures could present depending on the specific operational conditions at each mill. Further, the amount and composition of the solid wastes depend on the paper grade produced, the raw materials used and the process methods applied. As depicted in **Table 3.2**, the total amount of waste generated/ton of product is highly dependent on the type of mill and increases significantly in the case of recovered paper processing, where deinking is applied.

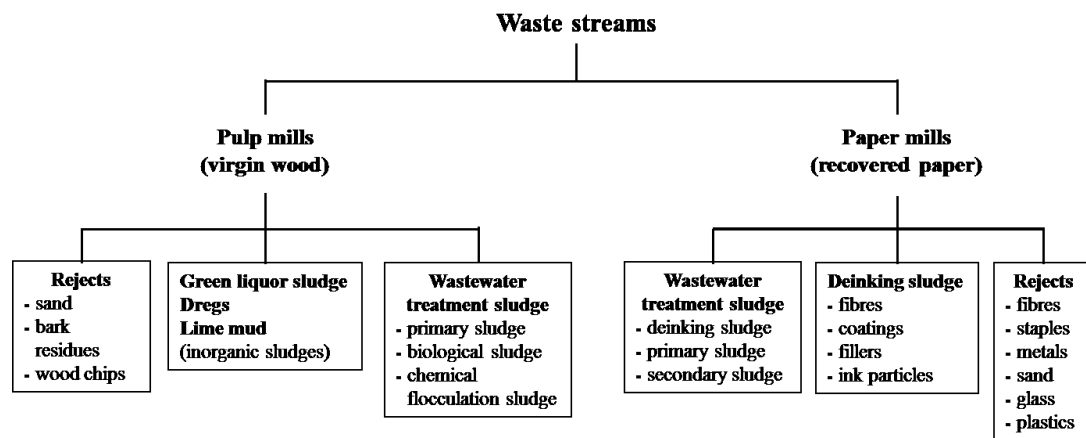


**Figure 3.2** Overview of waste streams generated during papermaking.

**Table 3.1** Composition and energy content of dry matter content of sludges and rejects (CEPI, 2011)

Type of waste stream	Composition	Energy content (MJ/ton <sub>wet</sub> )
Screen rejects	Cellulose, plastics, hair, stickies	8,000
Coarse rejects	Recyclable fibres, wet strength fibres, plastics, wood, metal, others	12,000
Deinking sludge	Cellulose fibres, calcium carbonate, kaolin, ink	3,000
Primary sludge	Fibres, fillers, coating clay, calcium carbonate	2,690
Secondary (biological sludge)	Calcium carbonate, copper, microorganisms, fibres, proteins	4,000-5,000

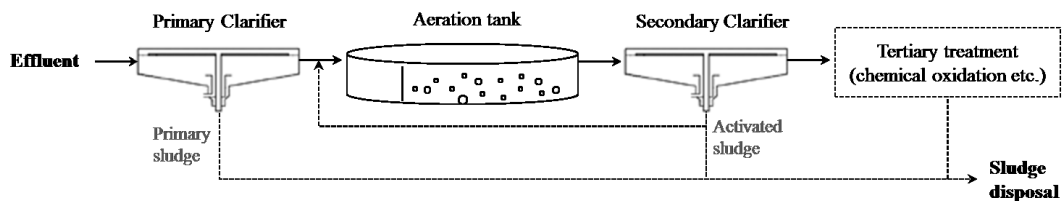
**Table 3.2** Total solid waste generated by different types of pulp and paper mills in Europe (IPPC, 2013)

Process	Kraft pulp	Sulphite pulp	Mechanical and semi-chemical pulp	Wood-free	Recovered paper
Total solid waste (kg/t <sub>paper</sub> )	60-80	60-80	60	33	50-600

With recovered paper being the primary raw material in the UK, increased waste disposal issues arise. It is, therefore, critical for the paper industry to consider and deploy more sustainable solutions to minimize and treat sludge wastes.

### 3.1.3 Paper sludge generation and characteristics

Effluents from the various stages of paper production are treated in a wastewater treatment plant, generally comprising of three stages: a) primary, b) secondary and c) tertiary treatments. This results in great amounts of sludge to be disposed of. A schematic of a typical wastewater treatment arrangement is shown in **Figure 3.3**.

**Figure 3.3** Principal stages of wastewater treatment at a mill.

Although the composition of solid wastes in the pulp and paper industry is well known and constant and has been minimised through efficient process recycling, sludge compositions vary widely throughout the industry and depend on the type of operations at each mill, as shown in **Table 3.3**. Paper sludge compositions also vary depending on the water treatment process they result from. Primary treatment sludge is mainly composed of fibres, fines and fillers lost throughout paper production due to inefficient solid/liquid separations. The lost materials collected through gravity settling in the primary clarifier may account from up to 4 % for pulp mills to a maximum of 30 % for the waste paper mills (Trutschler, 1999). Although, intensive efforts to improve fibre recovery have led to a decrease in primary sludge production, the production of secondary sludge, which is the residue from biological treatment, is likely to increase for two reasons: a) increased BOD loading as a result of increased

production and 2) improved BOD and suspended solids (SS) removal compelled by more stringent regulations (Mahmood and Elliott, 2006).

Secondary sludge is mainly biological in nature and therefore, difficult to dewater mechanically. In order to facilitate further treatment, primary and secondary sludges are mixed together. The combined sludge is, then, dewatered using gravity tables or drums and disc thickeners to achieve high dry matter content, varying from 5 to 75 % by weight (Engel and Moore, 1998; Kudra et al., 2002). Dewatering is useful in reducing sludge storage capacities, facilitating transport and increasing its calorific value.

**Table 3.3** Composition of the final sludge (combined primary and secondary sludge) from fibre recovery and wastewater treatment (European Commission, 2014)

Parameter	Unit	Values range
Dry solid (DS) content	%	29.4 – 52.7
Organic solids	% DS	25.5 – 76.1
Lead	mg/kg DS	10.0 – 210
Cadmium	mg/kg DS	0.01 – 0.98
Chromium	mg/kg DS	8.8 – 903
Copper	mg/kg DS	19.9 – 195
Nickel	mg/kg DS	<10 – 31.3
Mercury	mg/kg DS	0.1 – 0.89
Zinc	mg/kg DS	34.2 – 1,320

#### 3.1.4 Paper sludge disposal methods in Europe and the UK

Amid several waste management options adopted by European paper mills, the ones widely practised are presented in more detail in **Table 3.4**. Incineration with energy recovery as well as re-use of paper residues in industrial processes are becoming the predominant waste treatment methods. **Figure 3.4** clearly indicates that the proportion of residues disposed of in landfills has been constantly decreasing in Europe over recent years in favour of waste valorization. Landfilling has become the least favorable disposal method, with certain European countries banning the landfilling of waste coming from the pulp and paper industry.

**Table 3.4** Leading waste treatment options applied by the pulp and papermaking industry in Europe (Adapted from: CEPI, 2011)

Waste treatment process/ utilization options	Description
Incineration or combustion	Incineration of residues (both rejects and sludge) is based on their complete combustion in an incinerator. It is regulated in Europe by Directive 2000/76/EC, which requires all plants to keep incineration at a temperature of at least 850 °C for at least 2 s.
Pyrolysis	The organic waste is heated (400 – 800 °C) in the absence of oxygen to produce a mixture of gaseous and liquid fuels, with a solid inert residue (mainly carbon).
Steam reforming	It is based on an innovative technology of combustion-induced oscillations which promote high heat release and achieve more complete combustion.
Wet oxidation	Organic contaminants, in liquid or solid form, are extracted into water where they come into contact with an oxidant under conditions that promote their rapid destruction.
Super critical water oxidation	It exploits the capacity of supercritical water to dissolve both oxygen and non-polar organic compounds, thereby allowing organic waste to be oxidised into carbon dioxide and water.
Gasification	It is a based on the conversion of a combustible material into an inflammable gas and an inert residue employing air or oxygen.
Utilization in the cement/ brick industry	The energy content of the paper residues can be used as feedstock for the cement rotary kiln.

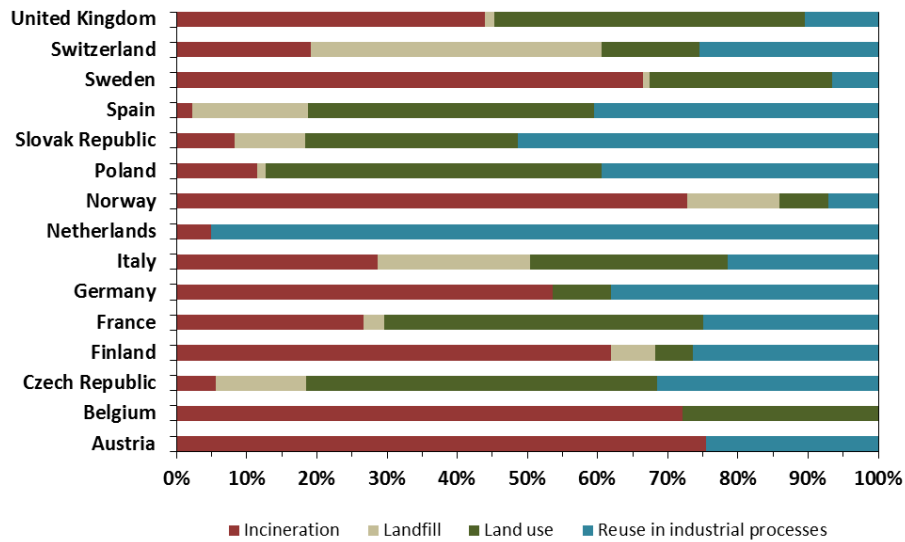


**Figure 3.4** Disposal methods for pulp and paper industry residues in 2008 (Adapted from: CEPI, 2011).

In the UK, besides incineration and landfilling, alternative reuses of paper sludge in industrial processes and land spreading have attracted interest from both researchers and industry. At present, paper sludge is either being disposed of in landfills or used for the production of refuse-derived fuel (RDF), cement-based construction materials, for land recovery, or as animal bedding. Some interesting reuse applications for paper sludge have been selected, based on their relevance to the UK reality, and are included in **Table 3.5**. Landspreading of paper sludges is regulated through the Environmental Permitting Regime (EPR) and it is also covered by Duty of Care with respect to the transport and transfer of the sludges (CPI, 2014). Sludge utilisation as a cementitious material in concrete products is also gaining significant attention, and promising results have been reported in some of the hereunder mentioned studies.

The scope of landspreading, though, is limited as it requires great space capacity and it is restricted to certain periods throughout the year in order to achieve optimum biological action. Also, reliability issues over suitability of the material for land application constrain its wide use by farmers. Utilisation of sludges in construction materials, although promising, is only feasible at low proportions due to durability deterioration of end-products. Long-term contracts with the construction industry are also difficult to achieve. This means that sludge disposal via land application and utilisation in building products does not standalone represent an inclusive solution for the large volumes of sludge the industry generates at national and worldwide level.

**Table 3.5** Selected research publications on reuse applications for paper sludge

Reference	Type of application	Key findings
Phillips et al., 1997	Soil amendment	Increased carbon content for various soil types (clay, sandy loam) and crop types (grass, wheat).
Barriga et al., 2010	Soil amendment	Improved soil fertility and biological functioning.
Demeyer and Verloo, 1999	Alternative crop fertilizer	Immobilisation of N in soils with high N content.
Ribeiro et al., 2010	Alternative crop fertilizer	Correction of organic content and acidity of soils.
Moo-Young et al., 1996	Landfill cover	Paper sludge used as hydraulic barrier provided an effective impermeable cover, meeting regulatory requirements.
Beauchamp et al., 2002	Animal bedding	No effect on animal growth when de-inking sludge was used as bedding.
WRAP, 2004	Construction materials	Prototypes developed for the following types of materials containing sludge: a) low-density cement blocks; b) hardboard; c) tiles; c) hybrid MDF; d) softboard and e) cement bonded sludge board.
Frias et al., 2008	Blended cements	Calcining of paper sludge at 650 °C for 2 h resulted in a cementitious material.
Ochoa de Alda, 2008	Paper and board	Primary sludge used for the production of low-grade paper and board met specifications.
Dunster, 2007	Portland cement production	Paper sludge can be used as an alternative fuel or as a cement clinker input material
Yan et al., 2011	Cement mortars	Addition of sludge at < 2.5 % by weight of cement produced acceptable mortars.

Therefore, despite the fact that mechanically dewatered paper sludge has relatively low calorific value (2.5-6.0 MJ/kg), co-combustion with biomass and plastics is increasingly applied as a method for energy recovery and sludge disposal in the UK (WRAP, 2007). Incineration of paper sludge achieves a reduction of the amount of material to be landfilled by about 80-90 %, generating paper sludge ash (PSA) as residual product. The combustion of this type of waste is regulated by the European Waste Incineration Directive and therefore, a minimum temperature of 850 °C for at least 2 seconds is required to ensure dioxins and furans are kept to trace levels (European Commission, 2000). An environmental permit under the Environmental Permitting (England and Wales) Regulations 2007 is also required for the operation of paper sludge combustors.

Based on unpublished data from the UK Environment Agency (EA), gathered through personal encounters with EA officers, there are currently 40 paper mills with a daily production capacity higher than 20 tonnes. Four of them employ sludge combustion on-site with energy recovery, generating 140 ktonnes of PSA annually. A significant 92 % of the ash generated is in the form of hazardous fly ash and the remainder is non-hazardous bottom ash. High fly ash volumes are due to the high ash and calcium carbonate content of dewatered paper sludge, which also explains the high pH values of PSA (pH ~ 12). Although, the above figures are very static, a new producer of paper sludge ash will be operating in the Manchester area and a couple more paper sludge combustors have been permitted and planned to operate in the next years, meaning that PSA production is expected to increase over time.

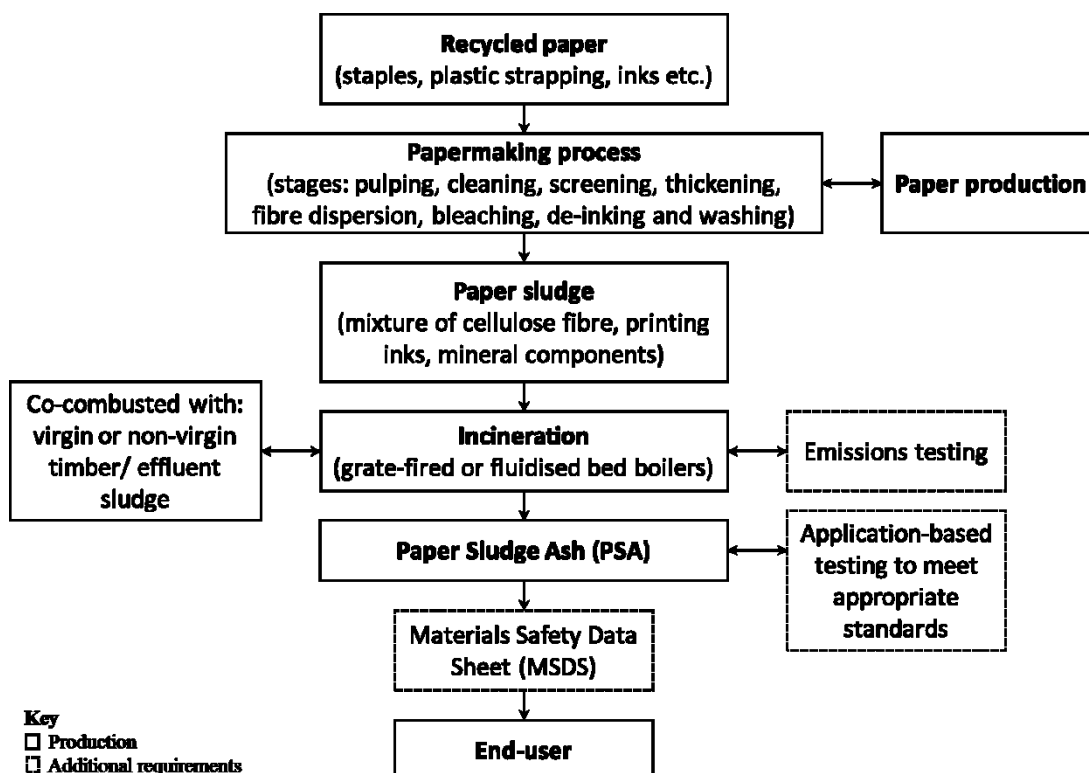
### **3.2 Paper Sludge Ash (PSA)**

Paper sludge ash (PSA) is the residue from the incineration of paper sludge and other input materials, such as virgin timber, effluent sludge and plastics, which arise from the process of papermaking. A breakdown of the materials fed to incinerators in England and Wales is given in **Table 3.6** and a typical PSA production process is depicted in **Figure 3.5**. Increasing volumes of PSA generated by the UK paper industry has caused environmental concerns and amplified the need for sustainable solutions for PSA disposal as an alternative to landfill. An overview of the characteristics of PSA and its current applications in the UK will be given in the following sections.

**Table 3.6** Combustion of paper sludge in England and Wales, 2006 (Adapted from: WRAP, 2007)

Material fed to incinerator	Amount (tonnes/year)*
Paper sludge	275,000
Biomass (virgin and non-virgin timber)	120,000
Plastics	17,000

\*All figures are on a dry basis.

**Figure 3.5** Schematic of a typical PSA production process (Adapted from: WRAP, 2008).

### 3.2.1 Typical chemical composition and leachability of PSA

Paper sludge ash is a fine powder with very low moisture content (~0.2 wt. %), very high pH levels (pH~ 12-13) and organic content ranging from 0.05-2.39 wt. %. The actual thermal treatment processes employed may vary between mills due to the nature of the paper sludge to be combusted. For instance, mills combusting only paper sludge produce ash with a high calcium oxide content (>10 %), while those co-combusting plastics with paper sludge produce PSA with a relatively high chlorine content. Variability in input feedstock, i.e. paper sludge, is effectively reflected on the chemical properties of produced PSA, as shown in **Table 3.7**.

**Table 3.7** Chemical composition (in mg/kg) of paper sludge ash (WRAP, 2008)

	<b>Determinand</b>	<b>Range of values</b>
<b>Major elements</b>	Calcium (Ca)	102,375 – 376,00
	Silicon (Si)	103,423 – 139,799
	Aluminium (Al)	57,368 – 86,952
	Magnesium (Mg)	121 – 31,119
	Potassium (K)	1,826 – 15,800
	Sulphur trioxide (SO <sub>3</sub> )	2,800 – 15,100
	Strontium (Sr)	280 – 7,001
	Iron (Fe)	1,748 – 5,106
	Phosphorus (P)	652 – 3,650
	Sodium (Na)	1,187 – 2,893
	Titanium (Ti)	0.210 – 1,918
	Manganese (Mn)	0.01 - 1781
	Barium (Ba)	71 - 1549
	<b>Trace elements</b>	Fluorine (F)
Copper (Cu)		98 - 562
Zinc (Zn)		68 - 449
Lead (Pb)		21 - 125
Chromium (Cr)		21 - 59
Thalium (Th)		48.7 – 50

Despite the fact that operators of paper sludge combustion are, in most cases, reluctant to share PSA quality and leachability data, Aylesford Newsprint, E-ON and UPM-Kymmene have released such data, as summarised in WRAP's (Waste & Resources Action Programme) technical report on PSA (2008). Leachability data of key elements of environmental concern found in PSA are presented in **Table 3.8**.

The composition of PSA may also vary in waste classification. In the UK, PSA is currently classified as waste and if it possesses any of the hazardous properties H1-H14 (see Appendix A), it may be classified as hazardous. Hazard arises from high free lime contents, rendering PSA a corrosive material. If considered hazardous, both PSA producers and end-users (if any) need to hold an environmental permit and use a

consignment note to transport or dispose it of (Environment Agency, 2007). In 2008, a Quality Protocol for PSA was publicly assessed through the Waste Protocols Project, initiated by the Environment Agency and WRAP, so that the utilisation of PSA in production processes is facilitated. The Quality Protocol was not issued despite identification of major markets for PSA. In most cases, however, the fact that no recognised standards exist to cover the use of PSA in potential applications creates ambiguity over its classification as waste or not. An exemption is, therefore, still required before PSA can be used in current or potential new applications, as outlined in sections 3.2.2 and 3.2.3 respectively.

**Table 3.8** Typical leachability of PSA at L/S<sup>1</sup> 10 (mg/kg) (WRAP, 2008)

<b>Determinand</b>	<b>Mean values</b>
Sulphate (SO <sub>4</sub> )	131
Barium (Ba)	35.3
Aluminium (Al)	30.6
Chlorine (Cl)	2.6
Fluorine (F)	2.3
Lead (Pb)	0.2
Thalium (Th)	0.2
Phosphorus (P)	0.2
Molybdenum (Mo)	0.1
Manganese (Mn)	0.1
Zinc (Zn)	0.1
Arsenic (As)	0.1

<sup>1</sup>L/S is an abbreviation for 'liquid to solid ratio'.

### 3.2.2 Current reuse applications

The minimum PSA market is estimated at 300,000 tonnes/year. The current amount supplied to end-markets is estimated to be 88,000 tonnes/year (WRAP, 2008). The major designated applications are listed below:

- as a liming agent for application to agricultural land;
- as a desiccant for animal bedding;
- as a sewage sludge stabiliser;
- in block manufacture;

- in cement manufacture and
- as a binder in steel slag manufacture.

The main current and potential markets for PSA, as identified by WRAP (2008), are discussed in more detail below:

**1. Agricultural liming agent:** PSA contains a range of calcium compounds, such as calcium oxide, which give liming properties. This means that it can be used as a direct replacement of non-waste lime products currently used by farmers. Depending on soil pH levels and types of cropping, appropriate application methods and dosages can be applied. Any land application of PSA should meet requirements laid down in the *Codes of Good Agricultural Practice (CoGAP)* for air, water and soils (DEFRA, 2009).

**2. Desiccant for animal bedding:** PSA can be used as a high pH biocide to dust down cubicle beds and straw yards with the aim to reduce the levels of pathogens. When combined with straw, increased absorbency, improved bedding conditions and reduced levels of mastitis can be achieved.

**3. Sewage sludge stabiliser:** Hydrated lime and quicklime are traditionally used as sewage sludge stabilisers. This results in a valuable product that can be applied to land. PSA could potentially substitute such purchased lime materials.

**4. Block manufacture (and other concrete products):** Conformation to existing standards and attainment of specifications are both required prior to PSA utilisation in block manufacture. Although PSA is already being used in block manufacture, higher lime content could enhance the performance of end-products and further increase PSA share of the concrete products market. This is an area that has attracted great attention from researchers. Many alternative reuse applications have exploited the inherent cementitious properties of PSA (Mozaffari et al., 2006; 2009; Segui et al., 2012; Fava et al., 2011, Bai et al., 2003). In all studies, the cementitious properties of PSA - standalone or blended with ground granulated blast furnace slag (GGBS) - were verified. There is hence, potential for increased PSA use as a binder for the production of low-grade concrete products.

**5. Cement manufacture:** Ongoing discussions with the cement industry on the potential of using PSA in the production of clinker to manufacture Portland cement (PC) have not yet led to tangible outcomes. As reported by Dunster (2007), one of the

major PSA producers in the UK, UPM-Shotton, have been previously involved in such discussions with Lafarge Ltd. Further details have not been publicly disclosed.

**6. Binder in steel slag manufacture:** This is a potential market for PSA. Given that the steel industry uses lime additions to attain desired alkalinity levels for steel slag, PSA could instead be used as a fluxing agent. However, PSA may affect the absorption of oxidised impurities from the molten iron and therefore, further investigation is needed.

### 3.2.3 Novel reuse applications

Given that PSA volumes are expected to increase over time, further research to identify and quantify appropriate end uses for PSA is required. The volume of PSA being beneficially reused should increase by the amount currently being landfilled. The potential for PSA to increase its current market share and stimulate new markets will depend on the specification, price and consumer confidence in PSA and PSA-based products.

Lightweight fillers (LWFs) have been identified as having potential for high volume use in construction products as demand for such materials increases in industrialised countries. This research project focused on the development of artificial lightweight materials from PSA. Manufacturing lightweight fillers using PSA would not only constitute a novel, value-added application for PSA, but it would also meet UK industry demand for low density fillers supplied at appropriate prices. Discussions with the pre-cast concrete products industry confirm that there are potential benefits of using lightweight materials but current sources are prohibitively expensive.

In addition, converting PSA into hydrophobic particles is a niche alternative reuse application which has not been previously investigated. It is a field that is worth exploring further given the great perspective that hydrophobic additives and coatings have in a number of applications and industries. The need for robust hydrophobic materials has been established through engagement with potential end-customers, such as manufacturers of waterproof concrete additives and engineering firms.

### 3.3 Lightweight mineral construction materials

Lightweight materials can be either natural or artificial materials obtained via thermal processing of raw materials. Heating is compulsory in order to form porosity within the ‘green’ body structure as it will be discussed in section 3.3.3. For the purposes of this work, lightweight materials are further divided in two categories: aggregates and fillers. The term ‘*aggregate*’ will be used to refer to a typical building aggregate and the term ‘*filler*’ will be used to denote a high-performance lightweight material, which has lower particle density and is smaller in size.

Cheeseman et al. (2004) suggested the following qualitative specifications for lightweight pellets in concrete applications:

- rigid but low-density and porous, sintered ceramic core;
- dense continuous surface layer to inhibit water permeability that should be pozzolanic to form a strong bond with concrete;
- approximately spherical shape to enhance fresh concrete properties.

#### 3.3.1 Lightweight Aggregates (LWAs)

Historically, LWAs production has been recorded in Roman times and continues today with the exploitation of naturally occurring low-density materials. As defined in BS EN 13055-1 (British Standards Institution, 2002), LWA is a particulate material from mineral origin with a particle density below  $2,000 \text{ kg m}^{-3}$  or a loose bulk density below  $1,200 \text{ kg m}^{-3}$ .

LWAs are classified in four categories: a) naturally occurring aggregates, b) aggregates produced from natural components or secondary materials of industrial processes, c) by-products of industrial processes and d) recycled aggregates (British Standards Institution, 2002). The materials used for the aggregates in these categories are listed in Table 3.9.

A tendency towards the manufacture of artificial LWAs became apparent around the end of the 19<sup>th</sup> century, along with the development of reinforced concrete. In Europe, however, it was not until 1931 that the manufacture of LECA (Lightweight Expanded Clay Aggregate) commenced in Denmark. Thereafter, many manufactured LWAs have been introduced in the international market.

**Table 3.9** LWA classification (British Standards Institution, 2002)

Type of aggregate	Materials
Natural	Pumice, volcanic cinders
Manufactured from natural components	Expanding clay, shale, siliceous rock or slate
Secondary products of industrial processes	Pulverized fuel ash (PFA), paper mills sludge, sewage sludge, expanded blast furnace slag
Recycled	Expanded glass

Artificial aggregates fall broadly in two categories: a) sintered ceramic aggregates formed by heat-treating clay, shale or slate, and b) products formed by intensely heat-treating industrial by-products. The ceramic LWAs are more established in construction and other applications compared to those based on recycled materials. ESCSI (Expanded Shale, Clay and Slate Institute) has reported a number of case studies on the suitability of LWAs in asphalt, geotechnical and other applications (ESCSI report, 2004). The widely commercially available LWAs in the UK are presented in Table 3.10. They are mainly used in high-rise structures.

**Table 3.10** LWAs available in the UK

Proprietary name	Type	Manufacturing process	Dry loose bulk density ( $\text{kg} \cdot \text{m}^{-3}$ ) <sup>1</sup>
Foamed slag	Foamed glass	Foaming bed	750
Leca/Fibo	Expanded clay	Rotary kiln	425
Lyttag	Sintered PFA	Sinter strand	825
Pellite	Blastfurnace slag	Pelletisation	900
Granulex	Expanded slate	Rotary kiln	700
Liapor	Expanded shale	Rotary kiln	650
Dupré Minerals	Expanded vermiculite	Vertical furnace	100
Alfa	Expanded clay	Belt conveyor furnace	800

<sup>1</sup>Average values obtained from manufacturers' technical data sheets.

### 3.3.2 Lightweight fillers (LWFs)

There is not a generally accepted definition for lightweight fillers and the distinction between LWAs and LWFs is not clear. As opposed to LWAs, LWFs are significantly finer with a size range between 0.5 to 4 mm, which makes them more versatile. The particle density is below  $1,000 \text{ kg m}^{-3}$ . A list of the most important available LWFs in the UK and key properties are presented in **Table 3.11**.

**Table 3.11** Lightweight fillers available in the UK

Proprietary name	Type	Manufacturing process	Particle size (mm) <sup>1</sup>	Loose bulk density (kg·m <sup>-3</sup> ) <sup>1</sup>
Poraver	Expanded glass	Rotary kiln	0.10 – 16.0	400-140
Liaver	Expanded glass	Rotary kiln	0.25 – 4.0	450-190
Rotec	Expanded silicate	Extraction	0.04 – 4.0	450-300
Ecoglass	Foamed glass	Belt sintering furnace	0.2 – 11.0	200-160

<sup>1</sup> All values obtained from manufacturers' technical data sheets.

Such materials have been used for more than 20 years to improve the properties of a variety of finished consumer products. They are used as dispersed fillers for plastic composites, as they are compatible with plastisols, thermoplastics, latex, polyesters, epoxies, phenolic resins, and urethanes. They have excellent flow properties and can either have a closed or open structure depending on the application to be used in.

This research project focuses on the development of fine, closed-structure LWFs with relatively low water ingress rates. A schematic comparison between a typical commercially available aggregate on the market and high-performance lightweight filler is given in **Figure 3.6**.

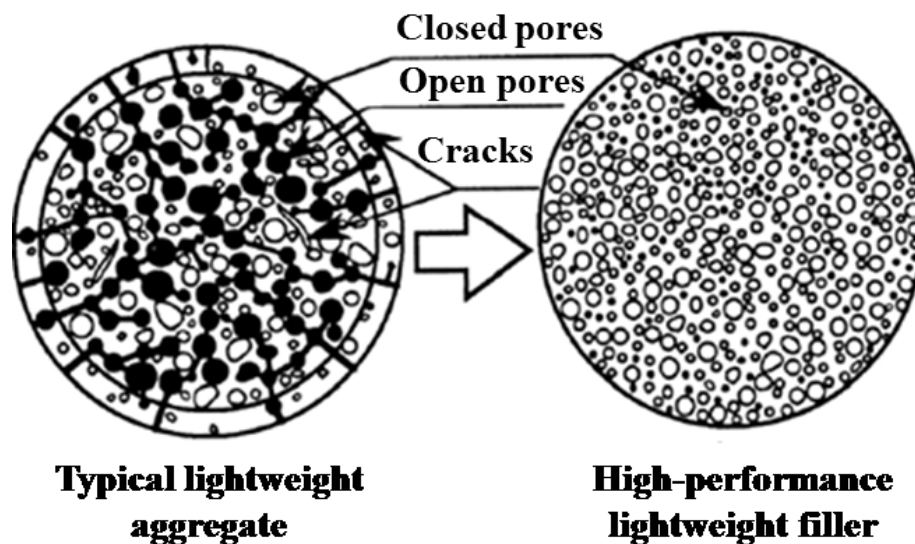


**Figure 3.6** Comparison between typical and high-performance lightweight granules (Adapted from Hammer, 1998).

### 3.3.3 Properties of lightweight materials

Key lightweight material properties are: (i) particle density ( $\rho_{rd}$ ); (ii) water absorption ( $WA$ ); and (iii) microstructure.  $WA$  is associated with the open porous structure and

interconnections between pores. When a combination of the aforementioned properties is available an extended range of potential applications opens up.

Properties of lightweight materials have to be determined prior to their use because they affect the end-product performance, i.e. strength, deformation, durability, water absorption, shrinkage and creep, thermal conductivity and abrasion resistance (Chandra and Berntsson, 2003). However, the necessity for testing and reporting all properties depends on the final use of the material.

For instance, high WA is not desirable if the aggregate is designed for the production of lightweight aggregate concrete (LWAC), as the aggregate will often compete with the cement for available water, hindering a well-controlled pozzolanic reaction to form calcium silicate and calcium alumina-silicate hydrates during cement hydration (Wei et al., 2011). Materials exhibiting low WA may be used as loose bulk fill to improve heat and sound insulating properties of ceilings, floors and walls.

### 3.3.4 Key factors affecting lightweight materials properties

Lightweight materials manufacturing process is complex as many factors affect the properties of the end-product. Key factors and mechanisms controlling the various stages of the manufacturing process and hence, the properties of the end-product are listed below:

a) **Raw materials** (type, particle size): Naturally occurring materials or industrial by-products can be used for the production of lightweight materials (see Table 3.10). The inherent characteristics of the raw materials used dictate, to a great extent, the performance of the end-product. The particle size of the raw materials is a highly influential factor given that formulations will undergo a sintering process. In ceramic science, the so called ‘grain growth dilemma’ questions the use of mono-size powders or unequal-size powders in terms of optimal microstructure attainment. Sintering models have been developed by Sivakumar et al. (1997) suggesting that processing the initial size of powders allows the controlling of the evolving microstructure during sintering. He and Ma (2005) also observed that particle size influences the controlling mechanism of sintering as it is linked with sintering reaction paths (grain-boundary diffusion path).

So far, little work has been done on the influence of fineness of raw materials used for the production of lightweight materials. Chindaprasirt et al. (2007) investigated the production of LWAs from rice husk ash (RHA) of three different degrees of fineness and reported that the properties of LWAs enhanced with the increase in fineness of RHA. Moreover, Manikandan and Ramamurthy (2007) investigated the influence of the fineness of fly ash (FA) on the aggregate pelletisation process. Increasing fineness of FA had an impact on the main factors, viz. speed of disk, angle of disk, duration, of the overall pelletisation process.

**b) Pelletisation** (particle packing, green density, binders): It is the term used for the formation of approximately spherical particles. The pellets are formed by agglomeration of particles. Agglomerates can be formed by granulation (pan, drum, cone or mixer granulation) or compaction (roll pressing, extrusion and pellet mills). In the former technique, tumbling forces are responsible for particle agglomeration. Cohesion forces between the particles increase with increasing amounts of bonding agent (most commonly water). In the latter, the green density of pellets depends on the process applied (Bijen, 1986). Correlations between initial compaction of particles in the green body and sintered density have attracted the interest of many researchers (Sweeny and Mayo, 2002; Occhionero & Halloran, 1984).

Binders aid the pelletisation of the material; amend the chemical and mineralogical consistency of sintered pellets and affect the strength of fresh and sintered pellets resulting in lower water absorption rates (Ramamurthy and Harikrishnan, 2006). The most commonly used binders are cement, lime, bentonite and some organic substances like dextrin, sulphate waste liquor, tars and alkali compounds.

**c) Rapid liquid phase sintering mechanism** (densification, microstructure evolution, expansion, sintering time and temperature): One of the most critical stages of lightweight materials manufacturing process is sintering. Sintering is a process in which particles bond together when heated approximately to three quarters of their melting temperature. The ultimate aim of sintering is to develop bonding within the 'green' pellets. The driving force is the net reduction in surface energy. Liquid-phase sintering (LPS) involves the formation of a liquid phase to promote higher densification rates and lower the sintering temperatures. Diffusion distances become shorter at the presence of a liquid phase able to wet the solid grains, providing a

capillary force that pulls them together. Depending on the solid-liquid solubility rates, different microstructure evolution pathways are possible. Because of cost and productivity advantages, it is estimated that over 70% of sintering products are processed using liquid-phase sintering (German et al., 2009).

In the lightweight materials engineering process, however, in order to achieve porous microstructures, rapid liquid phase sintering of raw materials takes place. In this case, further densification of the green body is undesirable and sintering is ended at the initial stage of viscous phase formation allowing enough time for simultaneous gas evolution and entrapment in the sintered body. Gas evolution can be due to: (i) volatilisation of sulphides from 400 °C, (ii) release of crystallised water from minerals at 600 °C, (iii) ignition of carbonates from 700 °C and (iv) liberation of oxygen from 1100 °C due to reaction of iron (III) oxide ( $\text{Fe}_2\text{O}_3$ ) traces present in the mixture. Expansion of sintered pellets is a dynamic balance of the gas liberated and the inhibiting effect of liquid viscosity of the semi-molten matrix. After sintering and bloating, the particle has to be instantly cooled down so as to prevent further expansion which could cause weakening of the pore structure and consequently decrease disintegration resistance when used in construction (Owens, 1993).

Expanding agents are usually used in order to promote the bloating phenomenon. A suitable expanding agent should decompose at a temperature higher than that of the liquid phase-providing component but still within the range where enough viscous phases have developed to encapsulate gas inside the pellet (Ducman et al., 2002).

A broad range of expanding agents has been tested to obtain foamed materials to be used in construction-related applications including: incinerator bottom ash (Cheeseman, 2004), masonry rubble (Mueller et al., 2008), anthracite (Anagnostopoulos and Stivanakis, 2009), harbour sediment (Wei et al., 2011) and sewage sludge (Cusido and Soriano, 2011).

Temperature is also crucial in the firing process because it determines the extent of bloating, which in turn affects the particle density of the end-product. An increase in temperature leads to a decrease in particle density due to: (i) the formation of more viscous phases able to encapsulate the gas liberated, (ii) a lowering of the viscosity of the viscous phases which enhances their ability to flow and (iii) the escape of more

gases (Wei et al., 2011). Microstructure control is also a time-dependent phenomenon given that the LPS microstructure is constantly evolving. Therefore, what it will be, in following chapters, denoted as ‘final’ microstructure is only a glimpse of the evolving structure, which determines the end-properties of the lightweight materials produced.

A schematic diagram of a typical manufacturing process of lightweight materials and the various factors affecting each stage is given in **Figure 3.7**.

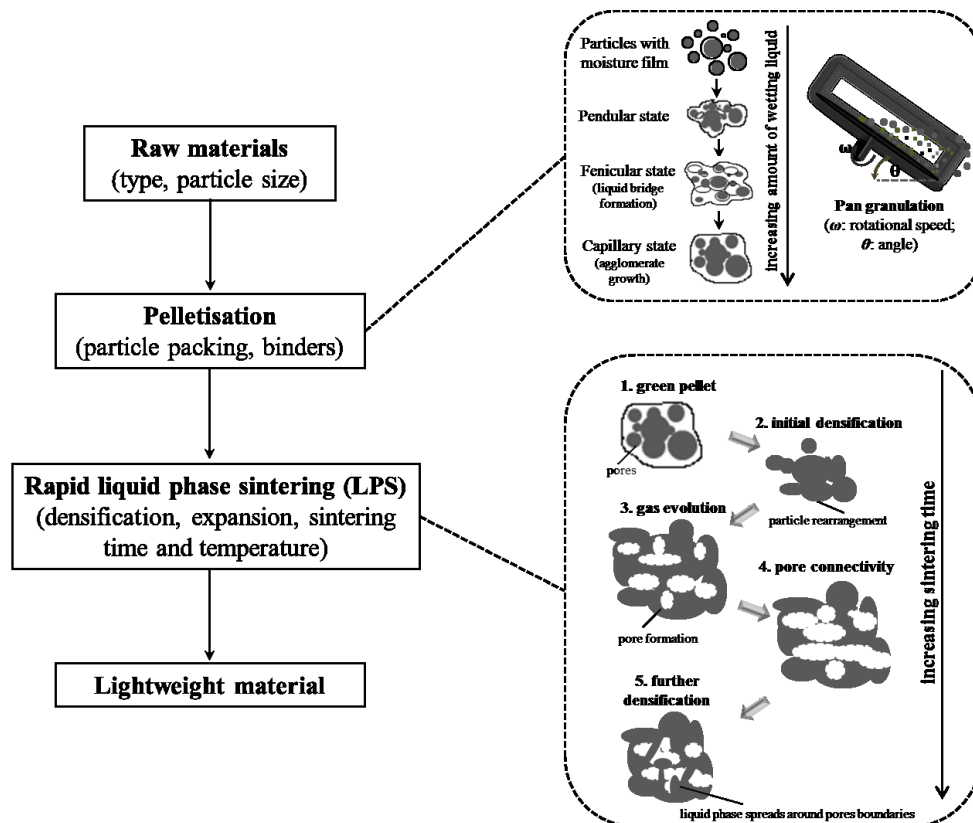


**Figure 3.7** Schematic diagram of the process stages involved in manufacturing of lightweight materials. Key mechanisms affecting the pelletisation and sintering stage are explained in detail.

### 3.4 Waste materials in lightweight materials production

Properties of lightweight materials vary depending on the raw materials and the process used for their production. Naturally occurring lightweight materials such as pumice, scoria, volcanic cinders or diatomite have been traditionally used for the production of LWAC. Expanding clays, shale or silica-rich rocks can be engineered by thermal treatment to produce lightweight materials, such as the commercially available LWFs Liapor, Optiroc and Perlite. Increasing tendency of reusing wastes in

construction has led to the valorisation of several industrial waste streams in the production of lightweight materials.

The potential of recycled lightweight materials as fillers in a wide range of construction materials/composites has recently been the main object of research. Recent studies have investigated the use of lignite coal fly ash (Kourti and Cheeseman, 2010; Anagnostopoulos and Stivanakis, 2009), incinerator bottom ash (Bethanis and Cheeseman, 2004; Huang et al., 2007; Cioffi et al., 2011), heavy metal sludge cake and mining residues (Huang et al., 2007), sewage sludge ash (Cheeseman and Viridi, 2005), rice husk ash (Chindapasirt, 2009) and harbour sludge (Wei et al., 2011) for the preparation of artificial LWAs.

It is primarily the optimisation of the mechanical properties of end-products that has attracted attention. Lightweight concretes containing expanded polystyrene (EPS) were developed by Babu et al. (2006) and exhibited acceptable compressive strength values of 20 MPa. Similar mechanical properties were achieved by Maldonado-Bandala et al. (2015) when using expanded polystyrene foam (EPSF) in concrete. According to de' Gennaro et al. (2009), structural concrete formed with granite sludge-based lightweight grains also had a compressive strength of 30 MPa. In contrast, Kralj (2009) reported low compressive strength values (~ 4 MPa) for concrete samples prepared with lightweight Poraver pellets. This justifies construction practitioners' choice to use Poraver in non-structural applications.

A limited number of studies has also addressed thermal insulating performance of concrete and cement mortars containing materials, including lightweight aggregates, cellulose and glass fibre, mineral wool, polystyrene, urethane foam, vermiculite and expanded polystyrene (Khedari et al., 2001; Zhou et al., 2010; Demharte, 1998; Vrana & Bjork, 2009; Ferrandiz-Mas et al., 2014). However, the fact that research findings range from promising to less favourable makes the need to find a viable solution more urgent.

### **3.4.1 Waste glass and its use in lightweight materials**

An estimated volume of 2.5 million tonnes of glass was consumed in the UK in 2012 (WRAP, 2013). This is classified in the following categories: a) container, b) flat, c)

fibre and d) domestic glass. For the manufacturing of glass products, a great quantity of virgin raw materials, mainly sand and limestone, is being consumed annually (British Glass Manufacturers' Confederation, 2009). Pressure for increasing glass recycling rates has been induced by the EU Directive on Packaging and Packaging Waste, setting a 60 % glass recycling target for all European members (European Commission, 2004). The UK glass recycling targets have been set to 80 %. This translates into greater recycling obligations for UK companies.

The recycling rate in the UK, as outlined in the WRAP 2013 report, was 65 % of total national consumption. Glass recycling is primarily divided into two categories: a) re-melting to produce new glass products and b) re-using glass cullet as aggregate in construction applications. In the former case, sorting of glass by type and colour is essential whereas in the latter, mixed-colour glass can be used. In recent years, increasing proportion of glass being collected co-mingled by local authorities has raised concerns over its quality. Mixed-colour glass not only requires sorting from the other dry recycle materials, but it also needs further size reduction, sorting by colour and removal of contaminants in order to meet the standards of the remelt sector (Resource Association, 2014).

Consequently, a notable 34 % of waste glass remains classified as non-remelt glass, mainly because of its poor quality for re-processing. Adding value to these misplaced glass residues by converting them into high-value lightweight construction products is part of the circular economy that both the glass and construction materials industries need to achieve.

Expanded glass-based lightweight materials appear to be more promising compared to other types of materials. Recycled glass is suitable for the formation of a viscous phase. It has high silica content, has an amorphous structure and large surface area when milled, and has been successfully used for the production of lightweight materials. Due to the high sodium oxide (Na<sub>2</sub>O) and calcium oxide (CaO) content, glass can be sintered at low temperature, and this reduces the firing time and energy consumption of the sintering process (Bernardo et al., 2007, Matteucci et al., 2002). The flux content (defined as the weight sum of Fe<sub>2</sub>O<sub>3</sub>, Na<sub>2</sub>O, K<sub>2</sub>O, CaO and MgO) aids the rapid sintering reaction (Wei et al., 2011).

For the preparation of lightweight materials from glass powder, expanding agents are typically used in order to promote the bloating effect. Sodium in the glass is responsible for the formation of a low-viscosity melt that is able to encapsulate the evolving gases. Expanded glass particles can therefore be produced by mixing finely ground glass with a suitable expanding agent and firing this mixture at a temperature above the softening point of glass where the viscosity is less than  $10^{6.6}$  Pa·s (Kingery et al., 1976).

### 3.5 Principles of hydrophobicity

Given recognized practical importance, wetting phenomena have been receiving increasing attention in a great range of industries. In this study, the opportunity of developing super-hydrophobic materials from paper sludge ash (PSA) originated from the unexpected hydrophobisation of PSA particles when dry milled with stearic acid, as part of the LWF production process. This was further explored as it represents an original reuse application for PSA, which has not been investigated before. The first part of this section on the fundamentals of hydrophobicity is followed by a review section on current research methods to produce super-hydrophobic solid particles.

A fundamental characteristic of a super-hydrophobic surface is a high contact angle (CA) formed by a water droplet deposited on such surfaces, as opposed to non-hydrophobic, or else hydrophilic, surfaces for which wetting by the deposited water is observed. Surfaces exhibiting a CA higher than  $90^\circ$  are simply called hydrophobic to distinguish them from the super-hydrophobic ones exhibiting a CA in excess of the critical value of  $150^\circ$ .

#### 3.5.1 Young's wetting model

A basic wetting model, describing the equilibrium achieved between the various interfacial tension forces, is that of a sessile drop on a flat, inert and uniform substrate, as defined by Young's equation (Young, 1805):

$$\cos \theta_c = \frac{\gamma_{SV} - \gamma_{SL}}{\gamma_{LV}} \quad (-1 < \cos \theta_c < 1; 0 < \theta_c < 180^\circ) \quad [\text{Eq. 3.1}],$$

where  $\gamma_{LV}$ ,  $\gamma_{SL}$  and  $\gamma_{SV}$  refer to liquid-vapour surface tension, solid-liquid and solid-vapour interfacial energies, respectively. The equation originates from the minimum free-energy condition applied at the droplet contact boundary where the

aforementioned interfaces meet, also called contact line  $L$  (which in the case of droplets is a circle). It is, hence, assumed that the energy remains fixed regardless of shifts ( $dx$ ) of the line position (De Gennes, 1985). The schematic diagram in **Figure 3.8** represents the different levels of hydrophobicity of a surface, classified into: a) non-hydrophobic, b) hydrophobic and c) super-hydrophobic surfaces, according to the CA formed when equilibrium of the various interfacial tensions is reached.

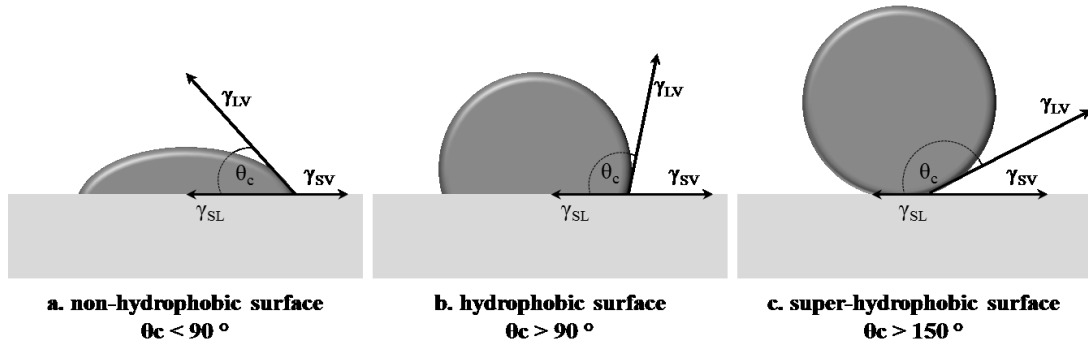


**Figure 3.8** Liquid droplet on a solid surface exhibiting different levels of hydrophobicity: a) non-hydrophobic/wetting surface, b) hydrophobic surface and c) super-hydrophobic surface. The contact angle ( $\theta_c$ ) is formed when equilibrium is reached between the various interfacial tension forces, i.e. solid-liquid ( $\gamma_{SL}$ ), solid-vapour ( $\gamma_{SV}$ ) and liquid-vapour ( $\gamma_{LV}$ ).

Although Young's equation can only be applied to ideal, smooth surfaces, the same minimum free-energy principle can also be applicable to non-uniform surfaces, leading to more generalised equations. These describe more complex phenomena, such as topographically rough surfaces. The most common equations of that type are the Wenzel equation and the Cassie-Baxter equation.

### 3.5.2 Wenzel's wetting model

The model describes the state where the liquid fully wets the surface asperities with air entrapment under the droplet. The model assumes homogenous wetting regime, as seen in Figure 3.10a. This is expressed by the following equation (Wenzel, 1936):

$$\cos \theta = r \cos \theta_c \quad [\text{Eq. 3.2}],$$

where  $\theta$  is the macroscopically observed CA,  $\theta_c$  is the Young's CA for an ideal surface and  $r$  is the roughness ratio, i.e. the ratio of the true area of the rough surface and that of the apparent/ projected area, In layman's terms,  $r$  is the factor that normalises the difference between a smooth surface, as defined in the Young's model scenario, and a rough surface.

This equation clearly illustrates that roughness enhances the wetting behaviour of a flat surface. For the non-hydrophobic surfaces ( $\theta_c < 90^\circ$ ), Equation 5.2 predicts that the observed CA  $\theta$  on the rough surface will be lower than  $\theta_c$ . Alike, for the hydrophobic surfaces ( $\theta_c > 90^\circ$ ), the observed CA  $\theta$  on the rough substrate will be higher than  $\theta_c$ . If the value of the  $r$  factor is high and the surface is a non-hydrophobic one, it is inferred from Equation 5.2 that  $\cos\theta$  can exceed 1, meaning that the wetting is complete. Applying the same logic, CA  $\theta$  can approach  $180^\circ$  for the super-hydrophobic surfaces. Although, in this scenario, the determining parameter for hydrophobicity is the surface roughness, it would be quite simplistic to induce hydrophobicity by just engineering rougher surfaces. This is because, in reality, the CAs generally spread in a large interval and that contradicts the yield of a unique angle derived from Equation 5.2 (Manakasettharn et al., 2011). This interval is called *hysteresis* and is responsible for the adhesion of droplets on the surface. The extent of adhesion depends on whether the liquid is advancing or receding on the surface and therefore, the energy equilibrium varies across the surface area (De Gennes, 1985). Super-hydrophobicity is, therefore, better explained using the Cassie-Baxter wetting model for rough surfaces, as detailed below.

### 3.5.3 Cassie-Baxter wetting model

In this state, the droplet only contacts the tips of the surface asperities, leaving layers of the substrate non-wetted, as shown in Figure 3.9b. The wetted fraction is denoted as  $f_s$ . The lower the value of  $f_s$  gets, i.e. greater air residing under the droplet, the higher the hydrophobicity. More precisely, the CA  $\theta$  of such a droplet is an average of the angle on the solid (of cosine  $\cos\theta$ ) and on the air (of cosine -1), weighted by the fractions  $f_s$  and  $1 - f_s$ , respectively. This is mathematically expressed by the following equation (Cassie and Baxter, 1944):

$$\cos \theta = -1 + f_s (\cos \theta_c + 1) \quad [\text{Eq. 3.3}]$$

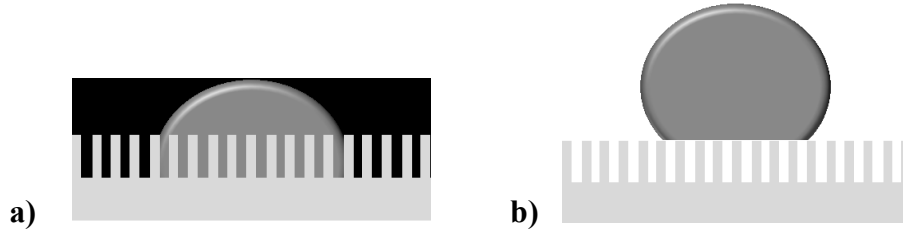


**Figure 3.9** Liquid droplet on a rough surface after: a) the Wenzel's wetting model and b) after the Cassie-Baxter wetting model.

The Cassie-Baxter model sufficiently explains the potential of a surface to become super-hydrophobic, provided low-enough values of  $f_s$  are in place. In order for a robust 'fakir' state to be maintained, the intrinsic CA  $\theta_c$  must exceed some critical value  $\theta_c^*$ . That value varies depending on layer topography (Patankar, 2003). For the most common superhydrophobic surfaces, the value of  $\theta_c^*$  is approximately  $90^\circ$ . A transition from the Cassie-Baxter to the Wenzel state is observed when the minimum requirement for  $\theta_c^*$  is not fulfilled.

The two most prominent factors affecting the stability of the Cassie-Baxter state and inducing the transition to a Wenzel state are associated with: 1) the introduction of some external force field and 2) nature of the liquids. A typical example of the latter would be the effect of the liquid hydrostatic pressure. Once this pressure exceeds the maximum possible capillary force, responsible for maintaining the position of the liquid-vapour interface at the tips of a structure (as shown in **Figure 3.9**), it results into wetting of the substrate (Callies and Quéré, 2005). With regard to the characteristics of the liquid involved, for a given substrate, a widely accepted method to assess the influence of the nature of the liquid on hydrophobicity is the Foz-Zisman's equation, which relates the surface tension of the liquid ( $\gamma_{LV}$ ) to Young's CA  $\theta_c$ :

$$\cos\theta_c = 1 - \varphi(\gamma_{LV} - \gamma_c) \quad [\text{Eq. 3.4}],$$

where  $\varphi$  is a parameter of the order of one depending on the chemistry of the liquid and  $\gamma_c$  is the critical liquid tension of a liquid below which complete spreading occurs (Fox and Zisman, 1950). This equation predicts eventual wetting (decrease in  $\theta_c$ ) of the substrate in a monotonic way with the decrease in surface tension of the liquid.

In order to circumvent this problem, the topography of the substrate needs to be designed in a way that a high energy barrier is established between the metastable

Cassie-Baxter state and the stable Wenzel state. Fabrication techniques to produce such stable superhydrophobic surfaces include photolithography and etching, template and master replication (e.g. by using poly-dimethylsiloxane (PDMS)), wet and electrochemical etching, chemical vapour deposition, sol-gel and colloidal processing and crystal growth (e.g. from reactions) (Manakasettharn et al., 2011).

However, a detailed review on fabrication methods to acquire superhydrophobic surfaces will not be included in the present study given that the primary research scope has been the production of superhydrophobic PSA-based powders rather than surfaces. Focus is, therefore, placed on creating self-assembling monolayers (SAMs) on the surface of micro-particulates, such being the case of PSA particles, in order to confer hydrophobicity on the surface of the particles.

#### **3.5.4 Formation of self-assembling monolayers (SAMs) on mineral particles**

Self-assembling monolayers are defined as ordered molecular assemblies that are formed spontaneously by the adsorption of a surfactant with a specific affinity of its functional group (or ‘headgroup’) to a substrate. A very attractive feature of such molecules is the possibility of using them to tailor, by virtue of different functional groups, the surface energies and hence, change the wetting properties of the substrate. The self-assembly process exploits this preferential, strong binding of one functional group of the surfactant on the substrate in order to engineer the surface properties. This is known as surface functionalization (Schreiber, 2000).

The adsorption of headgroups on the surface of a substrate is the strongest interaction and presumably the predominant driving force for the self-assembling process, as shown in **Figure 3.10**. However, the chain-chain interactions are not to be neglected, especially as the chain length increases and chain corrugations (zig-zag-like internal configurations) influence the final packing structure of the SAMs (Fenter et al., 1993). The final SAM structure depends on whether the chain-chain or the headgroup-substrate interactions dominate.

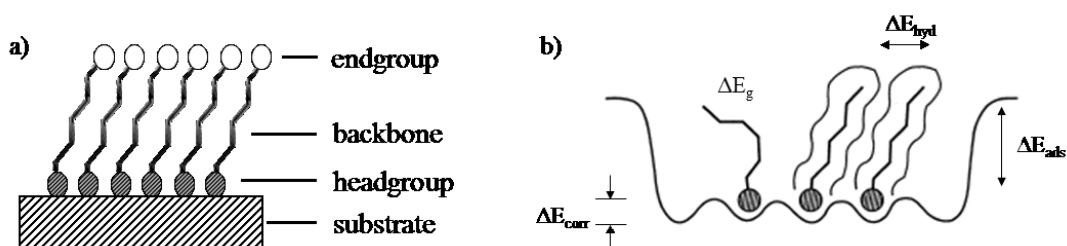


**Figure 3.10** Schematic of self-assembling monolayer (SAM): a) indicating bonding between the headgroup-substrate while leaving endgroups to the exterior and b) different energies associated with adsorption of a surfactant to substrate:  $\Delta E_{ads}$  stands for adsorption energy,  $\Delta E_{corr}$  corrugation of substrate potential experienced by molecule,  $\Delta E_{hyd}$  van der Waals interaction of hydrocarbon tails, and  $\Delta E_g$  energy of gauche defect expressing the deviation from fully stretched backbone (Adapted from Schreiber, 2000).

The current study focuses on tailoring the surface of inorganic PSA particles using various carboxylic acids as surface functionalization agents (SFAs). Similar treatments of waste materials have been reported by many research groups appreciating the availability and low-cost perspectives of such materials. Sakthivel et al. (2013) investigated the processing of coal fly ash particles into a hydrophobic material, which has high oil-sorption capacity and could therefore be used in oil spill cleanup applications. Similarly, Yao et al. (2013) also used stearic acid to functionalise the surface of coal fly ash particles to be used as filler material in polymer composites. The reported high levels of hydrophobicity of coated filler particles helped achieve enhanced mechanical properties of the end-polymer composite materials.

In general, surface functionalization of inorganic particles, primarily calcium carbonate, has delivered promising results for use as filler material in polymeric composites as postulated in the studies of Kim et al. (2006), Lin et al. (2011) and Rungruanga et al. (2006). It is to be highlighted, though, that the mechanisms of surface coating and filler-polymer matrix interactions are not fully understood in all cases.

## **CHAPTER 4 Materials and experimental methodology**

This chapter describes the experimental methodology deployed in order to prepare and evaluate the performance of lightweight fillers (LWFs), hydrophobic mineral particles as well as lightweight cement mortars. The materials used throughout this study and the sample preparation methods are detailed below. The methods used can, primarily, fall into the following broad categories: a) thermal processing for the production of LWFs, b) dry milling of raw material mixes for hydrophobic powder formation and c) standard preparation method for the production of cement mortars with partial substitution of sand by LWFs. The characterisation techniques used to assess key properties of both raw materials and end-products are also described. A combination of these techniques has been fundamental in assessing the performance of materials under different process conditions, varied based on the principles of parametric analysis for designing multi-factorial experiments.

### **4.1 Materials**

#### **4.1.1 Materials used for the production of LWFs**

Upcycling waste glass and paper sludge ash waste streams has been the foremost object of the present study. LWFs were identified as a viable application worth investigating after liaising with our project partners. PSA was supplied by the two UK paper mills partly sponsoring this PhD research, producing newsprint from recycled paper, Aylesford Newsprint in Kent and UPM-Shotton in Wales, denoted, for brevity, '*PSA\_ANP*' and '*PSA\_UPM*' respectively. They both use combustion in a fluidized bed boiler at 850 °C to manage waste paper sludge. The PSA produced is a fine grey powder. Waste glass was supplied by Day Aggregates Ltd., a collecting and sorting waste glass facility in Battersea, London. The material was received in the form of mixed-colour glass cullet of non-significant fibre contamination. It was further ground by attrition milling for 60 seconds in 50 g batches to produce a fine glass powder (see section 4.2.1). A detailed material characterisation study of all three main types of wastes used throughout this research project is given in Chapter 5.

### 4.1.2 Materials used for the production of cement mortars

Cement mortars were considered a potential application for LWFs manufactured from PSA and waste glass. Other than the LWFs, which were produced in this work and will be detailed in the results chapters, Portland cement (PC), sand and water were the main constituents of mortars, as detailed in Table 4.1.

**Table 4.1** Main components of cement mortar mixes

Name	Grade	Supplier
Portland cement	CEM II	Hope Construction Materials, UK
sand	< 2 mm	Sibelco, UK
water	distilled water	-

### 4.1.3 Materials used for the production of hydrophobic particles

In order to investigate the potential of engineering hydrophobic PSA-based powders, various carboxylic acids were used as surface functionalization agents (SFAs). The selection of SFAs was based on initial observations of hydrophobisation induced via dry milling PSA with stearic acid. In order to investigate the effects of alkyl chain length on hydrophobicity, suggested to be critical by Smith & Tanford (1973), were also used. Also, alternative inorganic minerals, based on the chemical affiliation to PSA composition, were tested for their hydrophobic properties when processed under the same conditions and were compared against both types of PSA samples. The chemicals involved in this investigation are summarised in **Table 4.2**.

**Table 4.2** Surface functionalization agents (SFAs) and mineral substrates used to investigate the potential of inducing hydrophobicity via a dry milling process

	Name	Formula	Density (g/cm <sup>3</sup> ) <sup>1</sup>	Supplier
SFAs	capric acid	C <sub>10</sub> H <sub>20</sub> O <sub>2</sub>	0.89	Sigma Aldrich (NH, USA)
	myristic acid	C <sub>14</sub> H <sub>28</sub> O <sub>2</sub>	0.99	Sigma Aldrich (NH, USA)
	stearic acid	C <sub>18</sub> H <sub>36</sub> O <sub>2</sub>	0.94	Sigma Aldrich (NH, USA)
	behenic acid	C <sub>22</sub> H <sub>44</sub> O <sub>2</sub>	0.82	Sigma Aldrich (NH, USA)
Substrates	calcium carbonate	CaCO <sub>3</sub>	2.71	VWR (PA, USA)
	calcium hydroxide	Ca(OH) <sub>2</sub>	2.24	Sigma Aldrich (NH, USA)
	silica fume	SiO <sub>2</sub> <sup>2</sup>	2.20	Elkem (Oslo, Norway)
	paper sludge ash	PSA	<b>Detailed characterisation in Chapter 5</b>	

<sup>1</sup> All density values were taken from the Material Safety Data Sheets of suppliers and refer to density values measured at 20 °C.

<sup>2</sup> Silicon oxide accounts for 97.6 wt. % according to chemical composition data reported in: Zhang, F. (2012) *Magnesium oxide based binders as low-carbon cements*. PhD thesis. Imperial College London.

## 4.2 Preparation of samples

### 4.2.1 Preparation of lightweight fillers (LWFs)

Lightweight fillers (LWFs) were prepared with various mixes of milled waste glass and paper sludge ash (PSA). Two types of PSA were used for comparison. The PSA addition to glass ranged from 0-100 wt. %. However, preliminary experimental work suggested that only up to a maximum of 50 wt. % addition of PSA would result into strong pellets after sintering to be used as construction materials. Hence, focus was placed on optimising those mixes, as explained in following chapters.

The waste glass cullet was initially ground to achieve particle size reduction via attrition/ TEMA milling for 60 seconds in 50 g batches to produce a fine glass powder which was used in all experiments. Milled waste glass was then mixed with PSA by wet ball milling (Pascal Engineering Ltd.) at a constant rate of 45 rpm for a duration ranging from 1-4 hours using 19 mm diameter alumina balls as the milling media. 500 g batches of raw materials were used with 1000 mL of water with a solid: milling media ratio of 1:5 and a milling media load: mill capacity ratio of 1:3. Wet-milling resulted in thick slurry which was dried at 105 °C for 24 hours (Gallenkamp Hotbox oven). The dried glass-PSA powder was manually ground using a pestle and mortar and sieved to < 475 µm. The powder was mixed with ~50 % (w/v) water and formed into approximately spherical pellets using a pan-pelletiser. The water content was adjusted to achieve optimum workability of the paste. The disc angle was fixed at 30°, the rotation speed was 6 rpm and the pelletising time varied from 10-40 minutes depending on the composition mix. It was observed that high PSA content mixes needed longer times for pelletisation. ‘Green’ pellets formed, ranging in diameter from 0.5–5 mm, were dried at 105 °C for 24 hours prior to sintering. Finally, they were fired in a Carbolite rotary tube electrical furnace. This had a 150 cm long tube with a 90 cm central heated zone. The speed of rotation was 10 rpm and it was kept horizontal to control sintering time. A schematic of the laboratory LWF manufacturing process is shown in Figure 4.1.

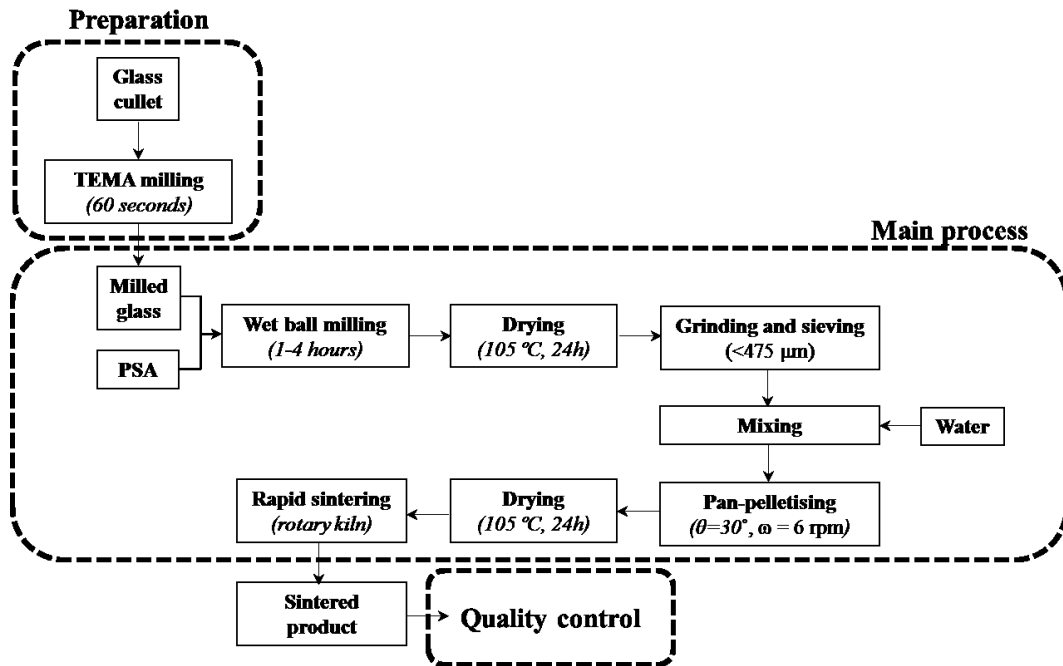


**Figure 4.1** Laboratory manufacturing process for the production of lightweight fillers.

#### 4.2.2 Preparation of cement mortars

Cement-based building materials are a potential application for LWFs. Hence, cement mortars were prepared using the optimum LWFs derived from the aforementioned manufacturing process in order to investigate the density, compressive strength and thermal conductivity and compare these properties against those of cement mortars prepared with normal aggregates (i.e. sand). The preparation method of mortars was adapted from BS EN 196-1:2005 (British Standards, 2005). The mass proportions of the cement, sand and water were kept fixed at 1:3:0.5 for the control mortars. The water: cement ratio was kept fixed at 0.5 for all experiments. Control batches consisted of (450±2) g of cement Type II (Hope Construction Materials), (1,350±5) g of sand (< 2 mm) and (225±1) g of distilled water. Substitution of sand by LWFs was done on a weight basis expressed as weight percentage of sand in the mix (% w/w).

Initially, the cement and water were mixed mechanically at low speed of (140±5) rpm for 30 seconds. Sand and LWFs were added steadily during the next 30 s and mixing continued for an additional 30 s at high speed of (285±10) rpm. Then, the mixing was stopped for 90 s to move the mortar adhering to the wall and bottom part of the bowl to the middle of the bowl by means of a rubber scrapper. Mixing continued at high speed for 60 s. These mixing operations and timings were carried out automatically.

Specimens were then moulded into 50x50x50 mm cubic moulds and placed on a vibration table for approximately 5 minutes. The excess mortar was levelled off with a metal straightedge and samples were covered with a glass plate to preserve moisture and left to set for 24 hours in a temperature controlled room at  $(22\pm 1)$  °C after which they were demoulded. In order to evaluate the compressive strength, demoulded mortars were soaked in tap water at  $(20\pm 1)$  °C for an aging time of 28 days, with vertical faces kept as cast vertical in the container. A detailed description of the compressive strength method is given in section 4.3.11.

### **4.2.3 Preparation of hydrophobic particles**

Hydrophobic particles were formed via dry milling with the addition of surface functionalization agents (SFAs) at addition ranges ranging from 0-8 wt. %. Dry milling was carried out using a ball mill (Pascal Engineering Ltd., UK) under the same ball milling conditions detailed in section 4.2.1. On this occasion, no water was added in the mix. The material was milled for a pre-determined duration ranging from 1-16 hours. The samples were kept in air tight bags to minimise moisture adsorption before testing.

## **4.3 Characterisation techniques**

The experimental methods and analytical techniques used to assess the characteristics of both raw materials and end-products produced are summarised in Table 4.3.

**Table 4.3** Characterisation methods for raw materials and end-products

Property assessed	Test method	Applied on
particle size	laser diffraction particle size analysis	<sup>1</sup> ◇ <sup>2</sup> □ <sup>3</sup> x
loose bulk density	in-house method	◇ □
skeletal density	He pycnometry	◇ □
apparent particle density	Archimedes principle	◇ <sup>4</sup>
water absorption	BS EN 1097-6:2013	◇
apparent porosity	BS EN 10545-3:1997	◇
microstructure/porosity	Scanning Electron Microscope (SEM)	◇ □ ◇ ● <sup>5</sup> x
mineralogical composition	X-Ray Diffraction (XRD)	◇ □ ◇
pH	in-house method	◇ □ ◇ ●
bulk elements	X-Ray Fluorescence (XRF)	◇ □
trace metals	Inductively Coupled Plasma – Atomic Emission Spectroscopy (ICP-AES), aqua-regia and pH dependence leaching tests	◇ □ ◇
chemical bonding	Fourier Transform Infrared Spectroscopy (FTIR)	x
heat stability	Thermogravimetric Analysis (TGA), dilatometry	□ x
workability of mortars	BS EN 1015-3:1999	●
thermal conductivity	TT-TC probe method	●
mechanical strength	compressive, crushing strength	◇ ●
hydrophobicity	Water Contact Angle (WCA)	x
surface roughness	LaserSurf non-destructive method	x

<sup>1</sup>◇: waste glass; <sup>2</sup>□: paper sludge ash (PSA); <sup>3</sup>x: hydrophobic powder; <sup>4</sup>◇: lightweight fillers (LWFs); <sup>5</sup>●: cement mortars.

#### 4.3.1 Particle size analysis by laser diffraction

The measurement of particle size by laser diffraction is a more versatile and robust method compared to more traditional methods, such as sieve analysis. The light scattered at various angles from dispersed particulates, as a laser beam passes through them, is captured and directed to the detector. The angle over which the light is diffracted is directly correlated to the particle size of a sample. The obtained scattering pattern is compared against an appropriate optical model allowing for the calculation of the particle size distribution. Between the two most widely used models, the Fraunhofer Approximation and Mie Theory, the former was selected given its simplicity and the relatively big size of the powder materials.

The particle size distribution of powder materials used throughout this study was, therefore, determined by laser diffraction (Beckman Coulter LS-100) in the range from 0.4 to 900  $\mu\text{m}$ , using tap water as the dispersant media. Approximately 0.2 g of powder (dependent upon density characteristics) was mixed with a few drops of surfactant (Teepol™ 610 S) and distilled water to ensure deglomeration of individual particles. The mix was placed into the laser diffractometer and sonicated for 60 seconds prior to measurement. Each mix was analysed in triplicate and the average is reported for each sample.

### 4.3.2 Density analysis

In this study, different density measurement methods were used to determine the density of powder samples, comprised of solid particles with a particle size of less than 1 mm, coarser filler materials with a particle size of less than 10 mm and dry cement mortars. Bulk density of loose powders and mortar samples is the simplest way to measure density considering both the solids and the pore space between particles. For the measurement of powder density, density analysis was conducted by helium pycnometry to obtain the ‘*skeletal*’ or ‘*apparent*’ density of solids. In order to measure the particle density of porous fillers, the Archimedes Principle was employed. A description of each method can be found below.

#### a) Loose bulk density

‘*Loose*’ bulk density is the freely settled bulk density based on volume and mass measurements taken without prior compaction of the powder sample, as opposed to the ‘*tapped*’ bulk density. Similarly, the calculation of dry bulk density of cement mortars is based on weighing of dry moulded specimens and dimensional measurements of specimens to define the apparent volume. The loose bulk density was calculated according to Equation 4.1:

$$\text{Bulk density (kg/m}^3\text{)} = \frac{m_{\text{dry}}}{V_{\text{dry}}} \quad [\text{Eq. 4.1}],$$

where  $m_{\text{dry}}$  is the mass of material/moulded specimen after drying at  $100 \pm 5$  °C until constant mass is obtained and  $V_{\text{dry}}$  is the volume occupied by the sample/moulded specimen. In the case of powders, a glass beaker of 50  $\text{cm}^3$  was filled with the powder which was levelled off to obtain a flat plane level. No tapping or application of

pressure took place whilst the sample was poured into the beaker to avoid any compaction. The sample was then weighed to measure the total mass  $m_{dry}$ . The loose bulk density results reported herein represent the average value of three measurements.

### b) Skeletal density

‘*Skeletal*’ or ‘apparent’ density considers solely the solids within the sample excluding the pores and void spaced between particles within the bulk sample. In order to measure the ‘apparent’ volume a helium pycnometer was used (Micromeritics, AccuPyc II 1340, Georgia, USA). This consists of two chambers, one with a removable lid for sample entry and a second one with a fixed volume  $V_c$ . Before the measurement, the second chamber was filled with helium gas (*He*) to a known pressure  $P_1$  while the chamber ( $V_r$ ) containing the sample ( $m_{dry}$ ) was evacuated. A pathway connects both chambers allowing for *He* to flow into the sample and enter even the smallest voids or pores. The new pressure  $P_2$  was measured and the volume  $V_s$  occupied by the sample was calculated according to Equation 4.2:

$$V_s \text{ (m}^3\text{)} = V_c + \frac{V_r}{\frac{P_1}{P_2} - 1} \quad [\text{Eq. 4.2}]$$

The skeletal density  $p_s$  was then derived using Equation 4.3:

$$p_s \text{ (kg/m}^3\text{)} = \frac{m_{dry}}{V_s} \quad [\text{Eq. 4.3}].$$

Results represent the average value of three measurements for each sample.

### c) Apparent particle density

The apparent particle density of LWFs (or specific gravity) was determined using the Archimedes principle after fully saturating particles with water ( $m_{sat}$ ), as described in BS EN1097-11:2013 (British Standards Institution, 2013). The method is based on the fact that the weight of the displaced water is proportional to its volume (assuming uniform density  $\rho_w$ ), while at the same time the immersed weight of the sample ( $m_{imm}$ ) equals the weight of the sample in air lessened by the weight of the displaced water. Hence, Archimedes principle can be reformulated to give the apparent particle density ( $p_{rd}$ ) of the sample on an oven-dried basis ( $m_{dry}$ ) according to Equation 4.4:

$$\rho_{rd} \text{ (kg/m}^3\text{)} = \rho_w \cdot \frac{m_{dry}}{m_{sat} - m_{imm}} \quad [\text{Eq.4.4}],$$

where the immersed mass is  $m_{imm}$  and the 24-h saturated surface-dry mass is  $m_{sat}$ . In order to ensure full saturation, samples were kept under water and under vacuum for 24 hours.

The distinct difference between the two methods lies on the fact that with pycnometry the volume measured excludes the pores and void spaces between particles within the bulk sample. In contrast, Archimedes principle accounts for the total porosity (open and closed) in the volume measurement. Apparent particle density results reported represent average values of ten individual samples tested.

### 4.3.3 Water absorption

With regard to lightweight fillers, water absorption ( $WA_{24}$ ) is defined in BS EN1097-6:2013 (British Standards Institution, 2013) as the increase in the mass of the particle (oven dried) due to the water impregnated in the open pores of the particle. All samples were placed in a vacuum chamber evacuated to a pressure of 10 kPa for 24h. While maintaining the vacuum, sufficient water was admitted to cover the samples by 5 cm.

The water absorption of LWFs produced was, then, calculated (as a percentage of the dry mass) for a set of ten particles from each batch, in accordance with the following formula:

$$WA_{24} \text{ (wt. \%)} = \frac{m_{sat} - m_{dry}}{m_{dry}} \times 100 \quad [\text{Eq. 4.5}],$$

where the meaning of the parameters involved is identical to that described above. Water absorption results reported represent average values of ten individual samples tested, representing 25 % of total batch production.

### 4.3.4 Apparent open porosity

Based on Archimedes principle, the apparent porosity,  $P$ , expressed as a percentage, is the relationship of the volume of the open pores of the samples to its exterior volume. The external volume ( $V$ ) is calculated using Equation 4.6, according to BS EN10545-3:1997 (British Standards Institution, 1997):

$$V \text{ (m}^3\text{)} = m_{sat} - m_{imm} \quad [\text{Eq. 4.6}]$$

The volume of open pores ( $V_o$ ) can be derived using Equation 4.7:

$$V_o \text{ (m}^3\text{)} = m_{sat} - m_{dry} \quad [\text{Eq. 4.7}],$$

where the terms used in both formulas are identical to those mentioned in section 4.3.2.

In the above calculations, the assumption is made that density of water is  $1 \text{ kg/m}^3$ , which is true for water at room temperature. Therefore, the apparent porosity  $P$  can be calculated using the following formula (Equation 4.8):

$$P (\%) = \frac{V_o}{V} \times 100 \quad [\text{Eq. 4.8}].$$

#### 4.3.5 Microstructural analysis

The microstructural characteristics of materials play a key role in both understanding their inherent properties and determining the properties of the final products in which they participate. It is, therefore, crucial to obtain information about the atom arrangement (crystallinity) and pore structure of materials. The techniques used to appreciate the microstructural characteristics of raw materials and finished products are given below.

##### a) Scanning Electron Microscope (SEM)

In order to evaluate the microstructural structure of raw materials and end-products, a Scanning Electron Microscope (SEM) was used. SEM involves directing an electron beam to the surface of the test object and detecting signals from the interactions between the resulting electrons (back scattering and secondary electrons) and the sample to generate images of the sample in its native state (Kazmiruk, 2012). Given that all materials used in this study had low electrical conductivities, they were coated with gold (Au) to avoid charging when observing the microstructure in the SEM. In this study, a JEOL JSM-5610LV (Massachusetts, USA) microscope was used. Main focus was placed on examining the shape and size of pores within the body of fractured LWFs and surface morphology of powdered raw materials.

##### b) Mineralogical composition using X-Ray Diffraction (XRD)

X-Ray Diffraction (XRD) is a versatile analytical technique for identification and quantitative determination of the various crystalline phases of compounds. In contrast to amorphous materials, crystalline materials are made of atoms arranged in regular three-dimensional arrays. They are arranged so that they form a series of parallel planes separated from one another by a distance  $d$ , which depends on the nature of the material. Typically, when a concentrated monochromatic beam of X-rays (of

wavelength  $\lambda$ ) is incident on the sample at an angle  $\theta$ , the atoms will cause the beam to diffract into many directions. According to Bragg's Law (Equation 4.9), constructive interference occurs only when the distance travelled by the rays reflected from successive planes differs by a complete number of wavelengths  $n$  (Waseda, 2011):

$$n\lambda = 2d \cdot \sin\theta \quad [\text{Eq. 4.9}].$$

By determining the d-spacings, which are unique for each crystalline compound, and comparing them to a database of known reference compounds, sample identification can be achieved. In this study, the powder samples were introduced into an X-Pert PRO MPD by PANalytical, with Cu K radiation and spectra were collected in the range of 5 to 70°. The acceleration voltage was fixed at 40 KV and a current of 40 mA were applied. Analysis of spectra was carried out using the X'Pert HighScore Plus software.

#### 4.3.6 Chemical analysis

##### a) pH analysis

The early age pH of as-received raw materials was measured by preparing mixes of dry powders (s:solids) with distilled water at a w/s ratio of 5. The mix was homogenised using a magnetic stirrer to form a slurry. The pH was measured at various times, with continuous stirring in between measurements. The pH meter used for testing was a Fischerbrand Hydrus 500 with a Mettler Toledo Inlab Routine Pro electrode. The pH meter was calibrated using buffer solutions of pH 4, 7 and 10. The pH measurements were repeated in triplicate and the results reported represent final pH values attained after equilibrium was achieved (i.e. pH difference between consecutive measurements was less than 0.1). The in-house pH analysis method is considered adequately consistent to allow comparisons between the various samples despite the lack of a standardised pH test method.

##### b) Bulk chemical composition: X-Ray Fluorescence (XRF)

X-Ray Fluorescence (XRF) is a proven, non-destructive method for quantitative and qualitative elemental analysis. It is a type of spectrometry based on the emission of characteristic radiation in the form of photons from an atom that has been excited by

X-rays. Given that the energy used to excite the sample is greater than the ionization potential of its atoms, electrons of the inner orbitals of the atom are ejected making the structure of the atom unstable. The ‘hole’ is covered by electrons in higher orbitals releasing energy. Such transitions yield fluorescent photons with energy equal to the difference of the two orbitals involved. The wavelength  $\lambda$  of this fluorescent radiation can be calculated using Planck’s Law:

$$\lambda = \frac{h \cdot c}{E} \quad [\text{Eq. 4.10}],$$

where  $h$  is Planck’s constant,  $c$  is the speed of light and  $E$  is the energy emitted. The fluorescent radiation is directly related to the amount of each element in the material (Jenkins, 1999). In this study, bulk samples of as-received PSA and waste glass were analysed using a Spectro 2000 X-Ray Fluorescence Analyser and results are expressed in the form of oxides as wt. % of total sample weight. For chemical analysis of samples with key elements present at low concentrations, ICP-AES was used as detailed below.

### **c) Trace metal analysis: Inductively Coupled Plasma – Atomic Emission Spectroscopy (ICP-AES) – Sulphates and Chlorides**

Inductively Coupled Plasma – Atomic Emission Spectroscopy (ICP-AES) is an analytical technique used to detect trace metals and semimetals. The highly ionized gas, plasma, is used to excite atoms or ions that emit electromagnetic radiation at wavelengths characteristic of a particular atom. Given that the intensity of the radiation is proportional to the concentration of the element in the sample, quantitative elemental analysis is also possible. The spectrometer used in this work was an ICP-AES Optima 7300 DV by Perkin Elmer with Argon gas used as an atmosphere for the plasma. In order to ensure that concentration of the species of interest falls within the detection limits of the spectrometer powder samples were diluted in distilled water and filtered through 0.45  $\mu\text{m}$  filter paper. The preparation process of the various test and blank solutions is described in detail in section 4.3.7. In the present study, the leachate of as-received PSA samples and optimum sintered LWFs were analysed using ICP-AES to evaluate environmental risk. The sulphates and chlorides analysis was carried out at MEDAC Ltd, Surrey, UK.

**d) Chemical bonding: Fourier Transform Infrared Spectroscopy (FTIR)**

The spectrum of IR absorption represents the ‘fingerprint’ of each molecule and helps determine the chemical bonds present and the overall structure of a compound. Only electrically charged molecules (with constant dipole moment) can interact with the IR radiation and stretch or bend. Those vibrations are detected and compared with a database of known molecules. In this study, a ThermoScientific Nicolet iS10 spectrometer (Massachusetts, USA) was used to assess the structure of PSA-based hydrophobic powders. Approximately 0.01 g of sample was mixed with 1 g KBr, pressed to a pellet and analysed.

FTIR was used to investigate the interaction between PSA particles and acid surface functionalization agents (Thermo Scientific Nicolet 6700 spectrometer with Omnic Spectra software). Sample powders were mixed (1-2 wt. %) with KBr and pressed to form 10 mm discs using a 10,000 kg load.

**4.3.7 Leachability**

Leaching tests play a key role in evaluating environmental impact associated with the use of waste materials in the production of LWFs. In order to determine the degree of immobilization of elements of environmental concern within the ceramic matrix of LWFs, formed after sintering at high temperatures, a comparison between as-received waste materials and optimum waste-derived LWFs was made. This is possible by bringing the solid matrix in contact with the liquid phase, called the *leachant*, allowing for inorganic and organic substances to dissolve out. The *Aqua-Regia* and *pH dependence* methods were employed to quantify the total content of trace elements and the leachability properties respectively. A full description of each method is given below.

**a) Aqua-Regia test**

The total content (TC) of trace heavy metals of environmental concern present in PSA samples was determined by ICP-AES after full acid digestion. The method followed was adopted from BS EN 13657:2002 (British Standards, 2002). 2.5 g of oven dried sample were transferred to boiling tubes with 5 mL of deionised water, 12 mL of Aristar grade HCl and 4 mL of concentrated HNO<sub>3</sub>. The tubes were heated at 100 °C

for 2 hours and left to cool for 15-30 minutes. The content of the tubes were then transferred to 100 mL volumetric flasks with washings of deionised water. The solutions were centrifuged at 3000 rpm for 5 minutes. The eluate collected was passed through 0.45  $\mu\text{m}$  filter paper into a beaker. 9 mL of liquid was mixed with 1 mL of concentrated hydrochloric acid to reduce the risk of metal salt precipitation and stored in sample tubes for analysis. Three samples of each type of PSA were tested and the average values obtained are reported.

### b) pH-dependence test

In this study, the leaching characteristics of samples were evaluated with the pH dependence test using a liquid to solid ratio of 10 covering the full pH range, according to BS-EN 12457-2:2002 (British Standards, 2002). For brevity, the test may also be referred to as '*pH static leach test*' (van der Sloot et al., 2007). The test involves parallel batch extractions of the material at  $L/S = 10$  ( $\text{L}\cdot\text{kg}^{-1}$ ) in sealed glass test tubes, where sub-samples (2 g) of as-received PSA and optimum LWFs of particle size less than 4 mm were dried and mixed with 20 ml of aqueous acid solutions that varied in concentrations between 0% and 100% 4.0 M nitric acid over 15 equal increments. Given that all samples were of high alkalinity ( $\text{pH} > 12$ ), there was no need to use base solutions to cover the pH range. All samples were agitated for 48 hours in a rotary extractor to equilibrate before measuring the pH of the leachates (Figure 4.2). These leachates were extracted and filtered through a 0.45  $\mu\text{m}$  membrane filter paper and analysed by ICP-AES (see section 4.3.6) for a wide range of elements including Ca, Na, Mg, K, Cr, Zn, Pb, Cu, and Al at pH ranging from 2 to 12.

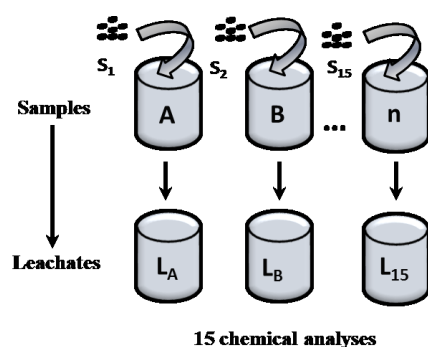


**Figure 4.2** Parallel batch test for the pH dependence test. 15 PSA samples and LWF particles were analysed in order to assess the leaching behaviour at various pH conditions.

In addition, the test represents an indirect way of measuring the acid neutralisation capacity (ANC), which corresponds to the buffering ability of the material. This parameter is a measure of appreciating the behaviour of the material at a potential pH stress, shifting the conditions into a more critical pH region. The pH dependence test is a reference test for all extended material evaluation allowing for easy comparisons among a wide range of materials, such as wastes, soil, construction materials and composites.

#### **4.3.8 Heat stability**

Manufacturing of LWFs is based on the mechanisms governing rapid sintering in an electrical rotational furnace. Hence, the behavior of raw materials during heating at high temperatures is of uttermost importance. Heat stability refers to the resistance of the material to chemical and physical changes during sintering, which ultimately determine the mechanical properties.

##### **a) Thermogravimetric analysis (TGA) and Differential Scanning Calorimetry (DSC)**

Thermogravimetric analysis (TGA) is an analytical technique that measures the mass change of a material under a controlled temperature programme,  $T(t)$ . Differential Scanning Calorimetry (DSC) measures the heat flow between a reference and filled crucible which relate to the nature of the phase transformations occurring (exothermic or endothermic). In this study, TGA/DSC was carried out to determine the weight loss of as-received PSA samples due to decomposition of thermally instable species in order to assess the potential for use as expanding agent in glass mixes during sintering. Measurements were carried out in air and sample weight is recorded as a function of temperature. Samples were heated from room temperature to 900 °C at a constant heating rate of 10 °C/ minute with measurements taken every 6 seconds. The equipment used was an STA (Simultaneous Thermogravimetric Analysis) 449 F1 from Netzsch (Germany) which has a sample (placed in an alumina crucible) and a reference alumina crucible, connected to a balance.

## b) Dilatometry

Dilatometry is a thermo-analytical technique used to determine the expansion or shrinkage of materials and glass transition temperature ( $T_g$ ) over controlled heating regime. The as-received PSA and waste glass samples were pressed into cylindrical pellets and placed in the sample holder against which a pushrod is pushed at 1.5 N. The length change is detected and is then converted into volumetric change which is plotted against temperature. The sample holder and pushrod are made of alumina ( $\text{Al}_2\text{O}_3$ ) to sustain temperatures as high as 1700 °C. The dilatometer used in this study was the Netzsch 402 E (Germany), as described schematically in Figure 4.3.

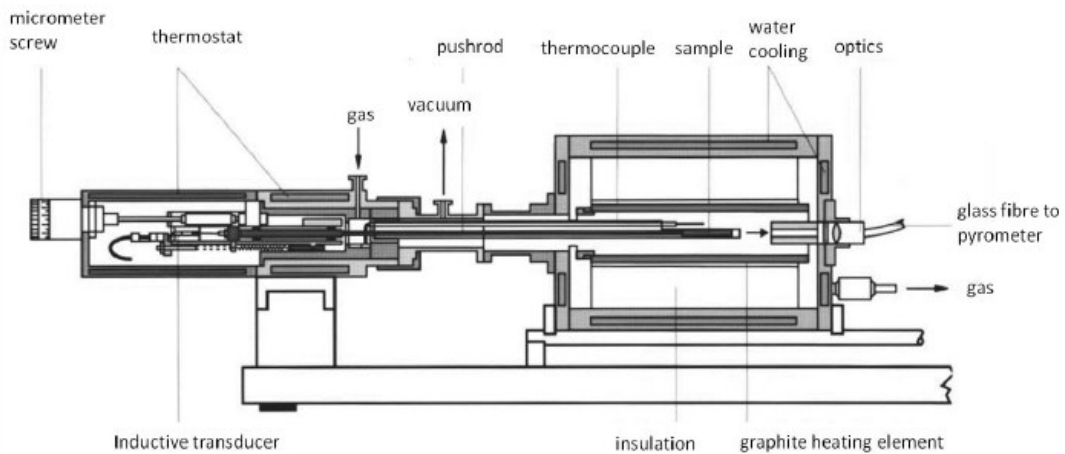


**Figure 4.3** Schematic of a Netzsch 402 E dilatometer (Adapted from Netzsch, 2006).

### 4.3.9 Workability of cement mortars

Workability of mortars, prepared as described in section 4.2.2, is a measure of evaluating the ease of use of the mortars by measuring the ease by which they flow. The standard flow test involved using a standard conical frustum shape of mortar with diameter of four inches, as defined in BS EN 1015-3:1999 (British Standards, 1999). This mortar was placed on a flow table and dropped 10 times within 15 seconds. As the mortar was dropped, it spreaded out on the flow table. The initial ( $D_i$ ) and final ( $D_f$ ) diameters of the mortar sample were used to calculate flow, expressed as percentage of the initial diameter, according to the following equation:

$$\text{Flow} = \frac{D_f - D_i}{D_i} \times 100 \quad [\text{Eq. 4.11}].$$

Mortar samples should have a flow of approximately 110. For the purposes of this study, the quantity of water in the mix was kept fixed given that all mortar samples were found to be ‘workable’.

#### 4.3.10 Thermal conductivity

Thermal conductivity (TC) is a measure of the rate of heat transfer through unit thickness and area of material. In technical terms, the thermal conductivity ( $k$ ) of a material is defined as the amount of heat that passes through  $1 \text{ m}^2$  of a material of  $1 \text{ m}$  thickness for a temperature difference of  $1 \text{ }^\circ\text{C}$  between the inner and outer faces. In this study, a non-destructive test method based on the Mathis modified hot-wire technique was employed (Schmidt et al., 2006). It is based on the principle that the temperature increase of the Ni wire, caused by a known electrical current, is inversely related to the thermal conductivity of the material. A correlation between the voltage rise over time and the thermal conductivity is established by assessing reference materials with known thermal properties. Dried mortar samples were used to determine thermal conductivity using a TT-TC probe (Therm Test Inc.) which measures the temperature rise at a defined distance from a linear heat source in contact with the test sample, as shown in Figure 4.4. The heating wire and the thermocouple are encapsulated in a probe that electrically insulates them from the test material.

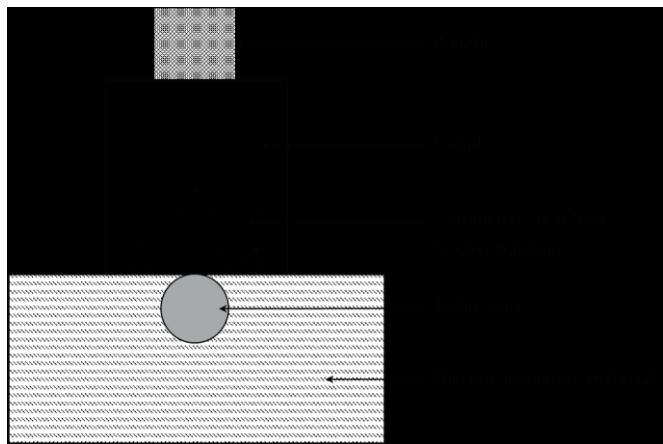


**Figure 4.4** Schematic diagram of the TT-TC probe arrangement used for measuring thermal conductivity based on the transient hot wire method.

The ideal mathematical model assumes that the hot wire is of infinite fineness and length and is surrounded by a homogeneous, isotropic material with constant initial temperature. Hence, for a constant heat output  $Q$  per unit time and length of the wire

( $\text{W} \cdot \text{m}^{-1}$ ), the temperature rise  $\Delta T(r,t)$  at radial position  $r$  is given by the following formula:

$$\Delta T(r,t) = \frac{Q}{4\pi k} \ln \frac{4at}{r^2 C} \quad [\text{Eq. 4.12}],$$

where  $a$  is the thermal diffusivity ( $\text{m}^2 \cdot \text{s}^{-1}$ ) (defined as  $a = k / \rho c_p$ , with  $\rho$  being the density ( $\text{kg} \cdot \text{m}^{-3}$ ) and  $c_p$  the heat capacity ( $\text{J} \cdot \text{kg}^{-1} \cdot \text{K}^{-1}$ ) of the test material) and  $C = \exp(\gamma)$ , where  $\gamma = 0,5772157$  is the Euler's constant (dimensionless). The above equation is valid only for  $r^2/4at \ll 1$ , i.e. for long time  $t$  and for short distance  $r$ . Therefore, the measurement of temperature rise  $\Delta T(r,t)$  as a function of the natural logarithm of time ( $\ln t$ ) is used to determine the thermal conductivity  $k$  by calculating the slope  $K$  of this linear relationship according to the following formula (Vozár, 1996):

$$k (\text{W} \cdot \text{m}^{-1} \cdot \text{K}^{-1}) = \frac{Q}{4\pi K} \quad [\text{Eq. 4.13}].$$

This technique has previously been used to evaluate the thermal conductivity of cement mortars and pastes (Olmeda et al., 2013; Ferrandiz-Mas et al., 2014).

#### 4.3.11 Mechanical strength tests

Mechanical strength describes the ability of a material to resist an external force without failure. The applied stress can be either compressive, tensile, or shear. In this study, only compressive strength properties of LWFs and cement mortars were evaluated as these are considered to be key to the performance of final building materials and other applications in which they could potentially be used. Two different test methods were employed to assess the compressive strength of mortars and LWFs as described below.

##### a) Compressive strength

The unconfined compressive strength of mortar samples, cured in water for 28 days, was measured using an ADR – Auto strength machine (ELE International) according to BS EN 196-1:2005 (British Standards, 2005). The loading rate was kept constant at 1 kN/s and the force at which the sample was fractured ( $F_{max}$ , in N) was recorded. The compressive strength of each sample was calculated according to the following equation:

$$R_c \text{ (MPa)} = \frac{F_{\max}}{A} \quad [\text{Eq. 4.14}],$$

where  $A$  is the area (in  $\text{mm}^2$ ) of the sample on which the force is applied. Five samples were tested under the same conditions to derive the average value and standard deviation, which are calculated as described in section 4.4.

### b) Crushing strength

The crushing strength of LWFs produced was determined by loading a bulk amount of 3-4 g of LWFs between two parallel plates until 10 % deformation is achieved. The equipment used was a Zwick/Roell Z010 (Germany) machine with a 10 kN load cell. The equipment configuration and a typical stress vs deformation curve are depicted in Figure 4.5. The confined compressive strength CS (10) was calculated according to:

$$\text{CS}(10) = \frac{F_{10}}{A} \quad [\text{Eq. 4.15}],$$

where  $F_{10}$  is the load (in N) recorded at 10 % deformation, and  $A$  is the area (in  $\text{mm}^2$ ) of the load distribution plate. All results reported herein represent average values of five samples tested.

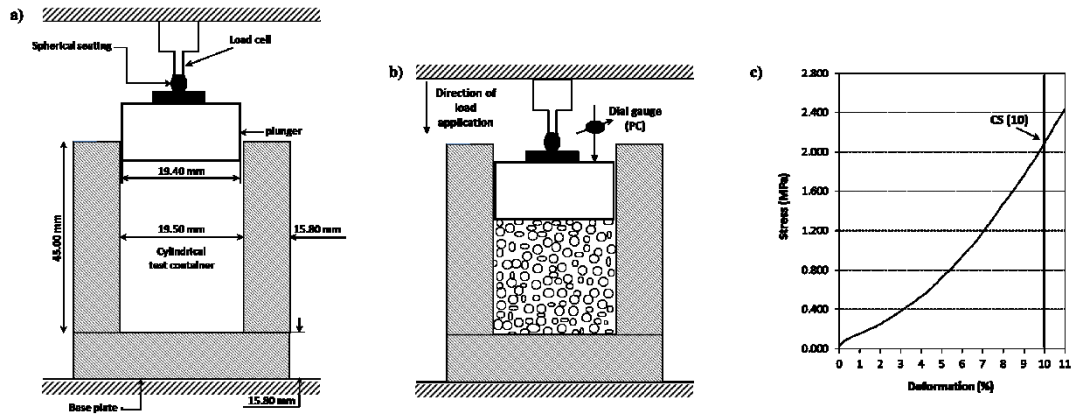


**Figure 4.5** Crushing strength test apparatus and results: a) dimensions of the set-up, b) test container filled with LWF sample and load application, c) typical deformation curve with the CS(10) value identified at 10 % deformation.

### 4.3.12 Water Contact Angle (WCA) test

The degree of hydrophobicity was assessed using the sessile drop method (Krüss Easy Drop tensiometer) measuring the static water contact angle (WCA) of a  $5 \mu\text{l}$  volume water drop formed on the surface of pressed disc samples. These were prepared by

pressing approximately 1 g of powder in a 19.7 mm diameter die at 4 kN to ensure a flat surface was obtained prior to testing. A typical sessile drop image can be seen in **Figure 4.6**. Assuming circular drop shape, the circle modelling method was applied to determine the contact angle of the deposited water droplet on the hydrophobic surface. Values for WCA reported represent the average of ten individual measurements on three pressed discs prepared.

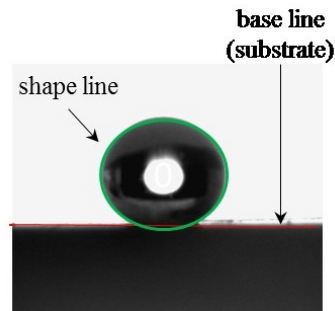


**Figure 4.6** Typical sessile drop formed on the surface of disc samples made from different hydrophobic powders.

#### 4.3.13 Surface roughness

Surface roughness of pressed discs was assessed using a non-contacting optical instrument (LaserSurf, WYKO NT9100 surface profiler). Samples prepared with various SFAs and substrates were assessed after pressing the powders into discs at 25, 50, 75 and 100 kN. Values for surface roughness reported represent the average of ten individual measurements on three pressed discs prepared with the various hydrophobic powders taken at different tracings along the disc surface to investigate surface roughness homogeneity.

### 4.4 Results and error calculation

All results reported represent average values using the arithmetic mean ( $\bar{x}$ ) of several measurements taken ( $n$ ). This can be calculated according to:

$$\bar{x} = \frac{1}{n} \sum_{i=1}^n x_i = \frac{1}{n} (x_1 + x_2 + \dots + x_n) \quad [\text{Eq. 4.16}]$$

In order to calculate the error, the standard deviation ( $\sigma$ ) was used. The standard deviation quantifies the variation of a set of data from the mean. Hence, low standard

deviation indicates that individual measurements are close to the mean value in contrast to high standard deviation values. It can be calculated according to:

$$\sigma = \sqrt{\frac{1}{n} \sum_{i=1}^n (x_i - \bar{x})^2} \quad [\text{Eq. 4.17}].$$

In the case of normally distributed data, it is expected that 68.2 % of the measured data falls within  $\pm$  one standard deviation of the mean, whilst 95.4 % of the measured data falls within  $\pm$  two standard deviations. All data presented in this research were normally distributed.

#### 4.4.1 Statistical significance: t-Test

In order to assess the statistical significance of experimental results, t-tests were performed. This allowed for the comparison of the mean values of different samples with known variance. The t-test was only employed in the cases in which a decision to be made about the direction of the research depended on the significance of the findings. In contrast, statistical significance was not considered critical in the case of experiments aimed to depict trends in findings rather than focus on absolute individual values of material properties tested.

Given that all data were normally distributed, the differences in means of two samples of independent variables (i.e.,  $\bar{x}_1, \bar{x}_2$ ) can be assessed with a hypothesis test at which:  $H_0$  (null hypothesis):  $\bar{x}_1 - \bar{x}_2 = 0$  (the means are equal) versus  $H_1: \bar{x}_1 \neq \bar{x}_2$ . Under the null hypothesis, the following equation may be used to test the hypothesis:

$$\frac{[(\bar{x}_1 - \bar{x}_2) - 0]}{\sqrt{\left[\left(\frac{\sigma_1^2}{n_1} + \frac{\sigma_2^2}{n_2}\right)\right]}} \sim N(0,1) \quad [\text{Eq. 4.18}]$$

Where  $n_1$  and  $n_2$  are the sizes of sample population 1 and 2 respectively. The t-distribution and tables were used to work out rejection regions and define significance at a 5 % significance level.

## CHAPTER 5 Production of lightweight fillers (LWFs)

### 5.1 Introduction

This chapter contains the results of the experimental work aimed at making lightweight fillers from paper sludge ash (PSA). First, material characterisation data for PSA samples, supplied by Aylesford Newsprint Ltd. and UPM-Shotton Ltd, are given followed by the actual LWF production results. Due to the fact that PSA standalone was found to be difficult to process into LWFs on its own, milled glass cullet was added and therefore, the characterisation of the raw materials also includes characterisation of the waste glass used.

Key process parameters, including waste glass and PSA content, particle size of the raw materials and sintering conditions were optimised. The optimisation procedure involved balancing the interdependencies between the inherent properties of raw materials used and the formation and sintering processes to produce end-products with microstructural characteristics defining the mechanical properties and hence, the potential end-applications of processed materials. This is depicted schematically in Figure 5.1. The effects of the various parameters on particle density, water absorption, mineralogy and microstructure of the sintered products are discussed.

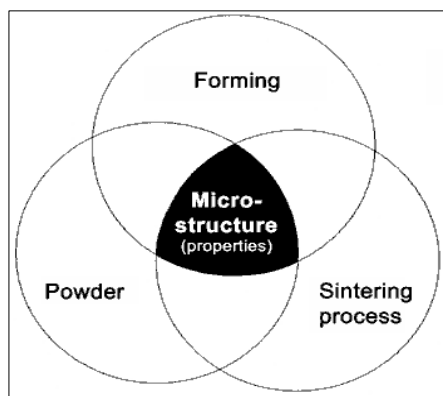


**Figure 5.1** A schematic of interlinkages of key process parameters determining the end-microstructure of sintered products. The ‘golden section’, i.e. the desired microstructure, is attained when optimum powder mixes are processed under optimised conditions prior to and during sintering.

LWF materials have higher economic value than normal weight or lightweight aggregates (LWAs) currently in use. In comparison with lightweight aggregates, LWFs have lower density and water absorption rates and are supplied in particle sizes typically ranging from 0.5 mm to 4 mm diameter. LWFs provide low-thermal conductivity, sound proofing properties and potentially improved fire-resistance in

addition to being light-weight. The sustainability credentials of recycled foam glass products have also been previously demonstrated through LCA (Blengini et al., 2012).

Throughout this chapter, as well as in subsequent chapters, LWFs produced are compared with commercially available LWFs supplied by the German company Poraver<sup>®</sup>, being the leading lightweight product imported in the UK. With that in mind and given lack of EU standardisation in the field of recycled lightweight fillers, the technical specifications of LWFs produced were benchmarked against the Poraver properties.

### 5.1.1 Characterisation of raw materials

#### a) Waste glass

Mixed-colour recycled glass cullet was used. This was ground using attrition milling for 60 seconds in 50 g batches to produce a fine glass powder, as described in section 4.2.1, which was used in all experiments, unless specified otherwise. The chemical composition of the recycled glass was determined by X-ray fluorescence (XRF Spectro 2000 Analyser) and is shown in Table 5.1. The chemical composition data confirmed that the samples were soda-lime glass. Particle size and pH analysis was performed as described in sections 4.3.1 and 4.3.6 respectively. The pH of the glass powder was 10.5. It had a  $d_{10}$  (10 % by volume of particles having a diameter smaller than this size) of 2  $\mu\text{m}$ , a  $d_{50}$  (mean diameter) of 11  $\mu\text{m}$  and  $d_{90}$  of 28  $\mu\text{m}$ . The particle size distribution is shown in Figure 5.2. The absolute density, measured using a helium gas pycnometer, as detailed in section 4.3.2, was 2.48  $\text{g}\cdot\text{cm}^{-3}$ . The glass transition temperature  $T_g$  was determined using a Netzsch 402 E dilatometer as described in section 6.3.8. As shown in Figure 5.6, glass powder exhibited shrinkage of 23.2 % between 594 °C and 664 °C, which indicates the temperature range within which glass softening occurs. This was comparable data to that reported by Karamanov et al. (2013). Key glass properties are summarised in Table 5.2.

#### b) Paper sludge ash (PSA)

Paper sludge ash (PSA) was supplied by two major paper mills, Aylesford Newsprint Ltd. and UPM-Shotton Ltd., both producing newsprint from recycled paper. For brevity, they are denoted ‘PSA\_ANP’ and ‘PSA\_UPM’ throughout this study. They

are both generated from the combustion of waste paper sludge onsite in a fluidized bed boiler at 850 °C for 2 s. The ash produced was a highly alkaline fine powder with pH values as high as 12.3 and 12.4 for PSA\_ANP and PSA\_UPM respectively. The chemical composition of both PSAs is presented in Table 5.1. The particle size distribution of the as-received PSAs was determined by laser diffraction as described in section 4.3.1. The particle size distributions of PSA\_ANP and PSA\_UPM are depicted in Figure 5.2. PSA\_ANP had a  $d_{10}$  of 23  $\mu\text{m}$ , a  $d_{50}$  of 156  $\mu\text{m}$  and  $d_{90}$  of 395  $\mu\text{m}$ . PSA\_UPM had a  $d_{10}$  of 13  $\mu\text{m}$ , a  $d_{50}$  of 140  $\mu\text{m}$  and  $d_{90}$  of 474  $\mu\text{m}$ . The absolute density was 2.85  $\text{g}\cdot\text{cm}^{-3}$  and 2.90  $\text{g}\cdot\text{cm}^{-3}$  for PSA\_ANP and PSA\_UPM, respectively. Key properties of PSA samples are summarised in Table 5.2.

The crystalline phases present in the PSA samples were determined by X-ray diffraction. As shown in Figure 5.4, the major crystalline phases present were gehlenite ( $\text{Ca}_2\text{Al}_2\text{SiO}_7$ ), calcite ( $\text{CaCO}_3$ ), calcium silicate ( $\text{a}'\text{-Ca}_2\text{SiO}_4$ ), lime ( $\text{CaO}$ ) and quartz ( $\text{SiO}_2$ ). In contrast to PSA\_UPM, in PSA\_ANP, mayenite ( $\text{Ca}_{12}\text{Al}_{14}\text{O}_{33}$ ) was also detected. PSA particles were porous and heterogeneous as shown by the SEM micrographs in Figure 5.3. Separate particles formed larger agglomerates as a consequence of the combustion process. Agglomerated particles were loosely bonded which was a favorable characteristic for PSA size reduction processing.

The characteristics of PSA samples at high temperatures were investigated via Thermogravimetric (TG) and dilatometry analysis, as shown in Figure 5.5. The initial step of weight loss from ambient temperature to 120 °C was associated with the evaporation of residual physically absorbed water. Weight loss at temperatures up to 400 °C is caused by thermal degradation of calcium hydroxide in PSA, as it was also reported by Bai et al. (2003). Weight loss between 600 °C and 780 °C is attributed to the decomposition of calcite ( $\text{CaCO}_3$ ) to lime ( $\text{CaO}$ ) with simultaneous generation of  $\text{CO}_2$ , while heat absorption is detected. This corresponds to a trough in the DSC curve, given that calcite decomposition is an endothermic phenomenon. These findings corroborate those reported by Fava et al. (2011). Evolution of  $\text{CO}_2$  gas within this temperature range makes PSA a promising expanding agent for preparing porous glass particles. Between the two types of PSA, there is a significant difference in terms of promoting-expansion potential, expressed as weight loss % by mass. It is clear that PSA\_ANP has higher calcite content compared to PSA\_UPM and therefore, gas

release will be more prominent during sintering for glass/PSA\_ANP samples. Dilatometry data revealed that PSA has low sintering reactivity as particles did not sinter together to form a rigid body and samples fell apart after heating to 1180 °C. As shown in Figure 5.6, in contrast to glass, solid-state reactions failed to lead to coalescence of PSA particles and densification.

**Table 5.1** Chemical composition of waste glass from Day Aggregates Ltd and as-received PSA samples supplied by Aylesford Newsprint Ltd. and UPM-Shotton Ltd., denoted ‘PSA\_ANP’ and ‘PSA\_UPM’ respectively. The powders were pressed into discs and analysed by XRF. Results are expressed as oxides on a dry basis by weight % (n=3).

	SiO <sub>2</sub>	CaO	Na <sub>2</sub> O	MgO	Al <sub>2</sub> O <sub>3</sub>	K <sub>2</sub> O	Fe <sub>2</sub> O <sub>3</sub>	SO <sub>3</sub>	TiO <sub>2</sub>	P <sub>2</sub> O <sub>5</sub>	Others
Glass	75.8	12.0	7.3	2.3	1.4	0.6	0.3	0.2	nd	nd	-
PSA_ANP	21.2	61.2	nd	2.8	12.6	0.4	0.9	0.2	0.3	0.1	0.1
PSA_UPM	17.7	62.6	0.5	3.5	8.8	1.2	1.5	1.7	0.7	0.4	1.3

nd: not detected

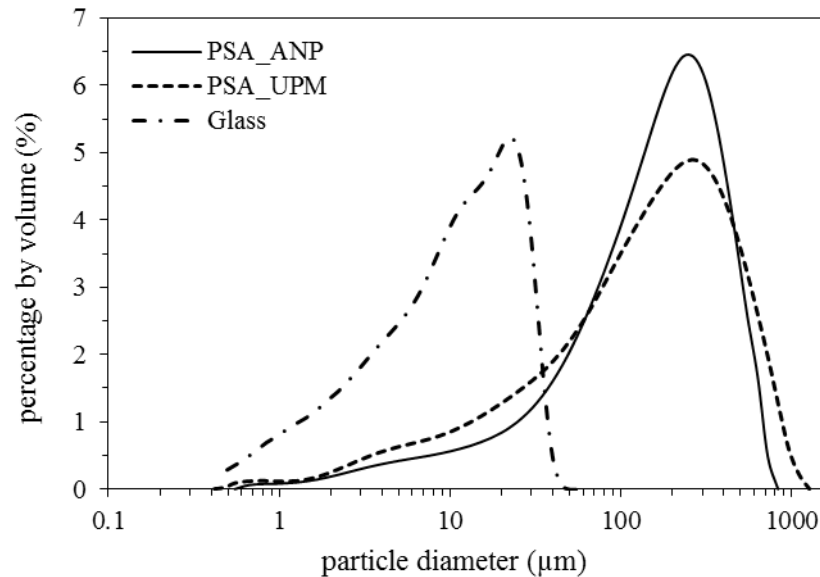


**Figure 5.2** Particle size distribution of as-received PSA samples and milled glass (via TEMA milling for 60 s) (n=3).

**Table 5.2** Key properties of raw materials (n=3).

	Glass	PSA_ANP	PSA_UPM
pH	10.5	12.3	12.4
$\rho_s$ (g/cm <sup>3</sup> )	2.48	2.85	2.90
T <sub>g</sub> (°C)	594	-	-

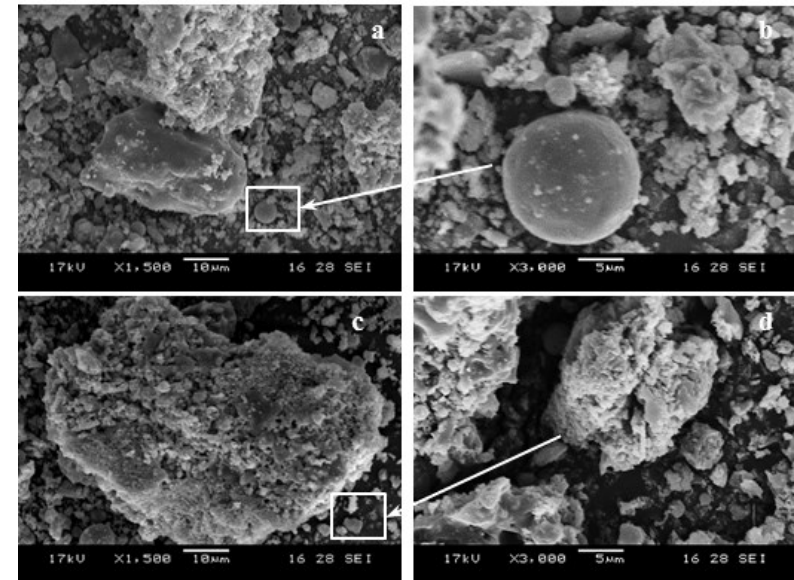


**Figure 5.3** Scanning electron micrographs of PSA agglomerated particles: a-b) PSA\_ANP and c-d) PSA\_UPM.

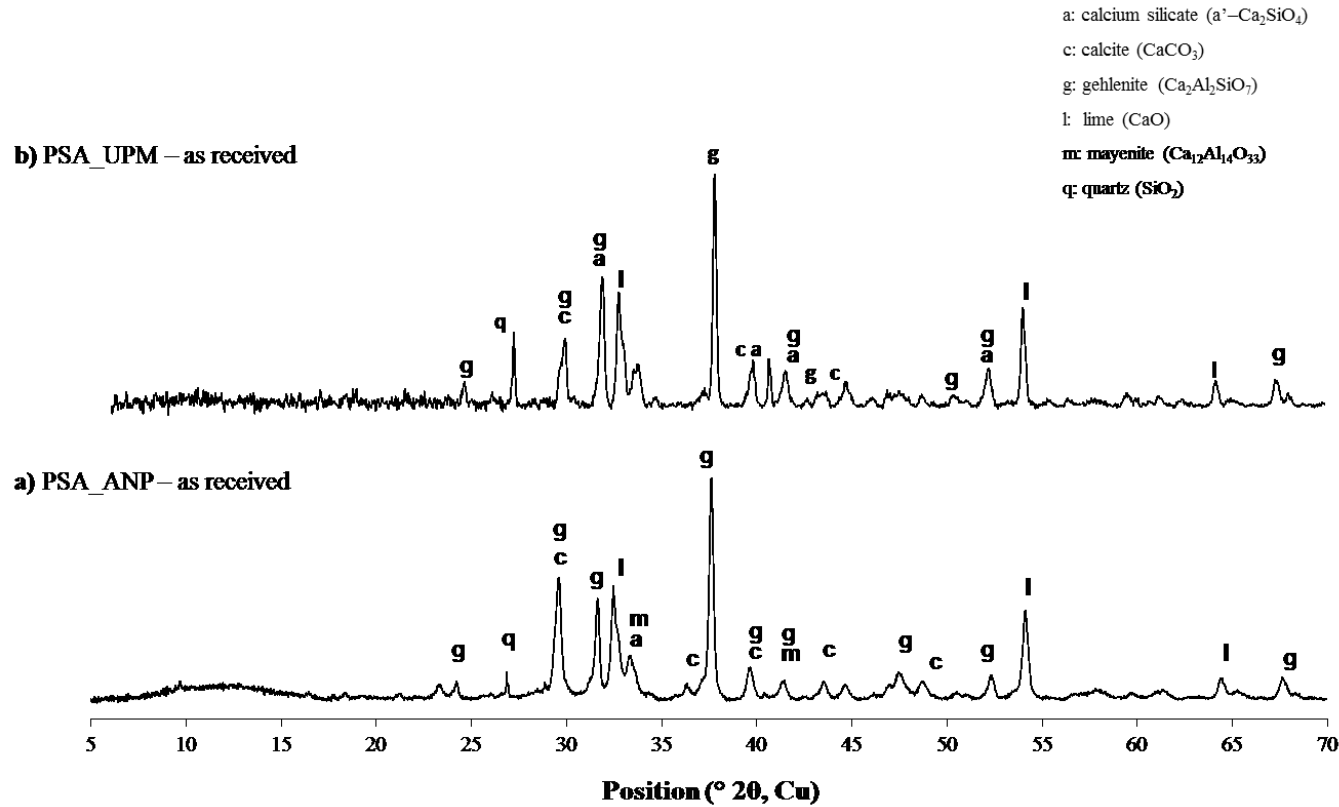


**Figure 5.4** X-Ray patterns of the as-received PSA samples: a) PSA\_ANP and b) PSA\_UPM. The major crystalline phases present are: calcium silicate ( $\text{Ca}_2\text{SiO}_4$ ), calcite ( $\text{CaCO}_3$ ), gehlenite ( $\text{Ca}_2\text{Al}_2\text{SiO}_7$ ), lime ( $\text{CaO}$ ), mayenite ( $\text{Ca}_{12}\text{Al}_{14}\text{O}_{33}$ ) and quartz ( $\text{SiO}_2$ ) ( $n=3$ ).

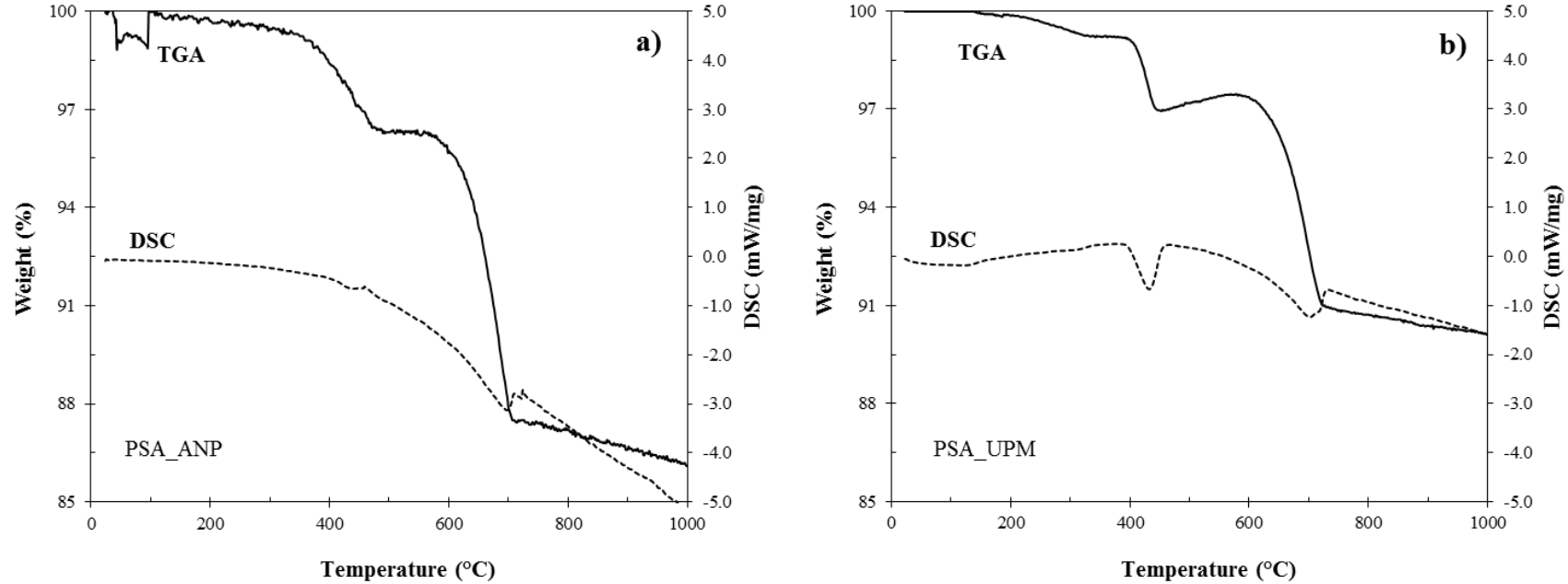


**Figure 5.5** TGA and DSC results for the as-received PSA samples: a) PSA\_ANP and b) PSA\_UPM. Major weigh loss between 600 and 780 °C is due to the decomposition of calcite ( $\text{CaCO}_3$ ) to lime ( $\text{CaO}$ ) with simultaneous generation of  $\text{CO}_2$  through:  $\text{CaCO}_3 \rightarrow \text{CaO} + \text{CO}_2 \uparrow$ . The maximum gas evolved during sintering is a key parameter for attaining maximum porosity in the final sintered body. Between 600 °C and 780 °C, being the temperature region of primary importance for further sintering processing, PSA\_ANP exhibits a weight loss of 8.5 wt. % whereas PSA\_UPM a loss of 6.7 wt.% (n=3).

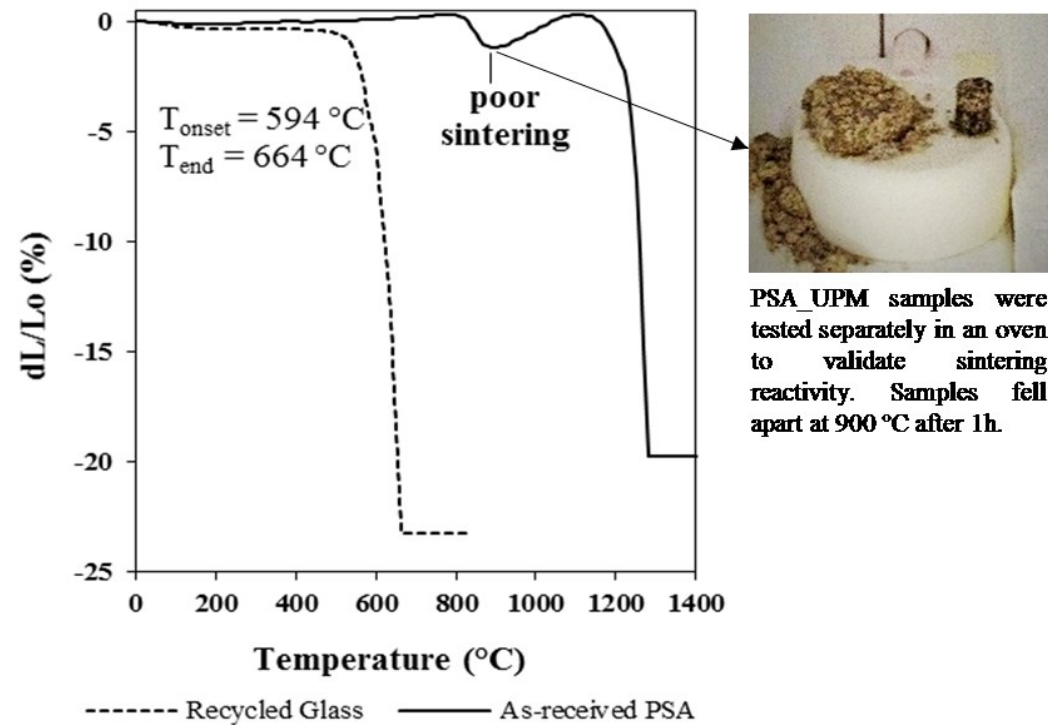


**Figure 5.6** Dilatometer results for glass and PSA\_ANP. The softening point of glass is observed at 594 °C, when shrinkage due to dissolution and smelting of the sample occurred. In contrast, PSA\_ANP particles (pressed into discs) exhibit low sintering reactivity with samples failing to densify when slowly sintered at high temperatures. This was confirmed for PSA\_UPM samples (top right image).

### 5.1.2 Lab-based manufacturing process

Early tests, confirmed by characterisation results presented above, indicated that low temperature thermal treatments could not sinter PSA samples into a coherent material. It was therefore decided to add waste glass as a binding agent. Obviously, it was attempted to maximise the PSA content in the mix. To evaluate whether the properties of LWFs produced from the glass/PSA binary system could meet current market requirements, it was decided to compare them with a commercial LWF product made from waste glass (Poraver<sup>®</sup> lightweight fillers). Table 5.3 summarises the properties of the commercial product, as reported in the Poraver<sup>®</sup> technical data sheets. In the present study, process parameters were varied to achieve desired properties for glass-PSA LWFs that are comparable or improved to the Poraver<sup>®</sup> values.

**Table 5.3** Experimental design matrix for the production of LWFs. Process parameters and desired performance properties were benchmarked against the leading lightweight filler product, Poraver<sup>®</sup> and project-oriented objectives.

	Criterion #	Poraver <sup>®</sup> *	Glass-PSA LWF
powders	Particle size of raw materials ( $\mu\text{m}$ )	< 30	minimum grinding
	Composition mix	100% waste glass	minimise waste glass / maximise PSA content
forming	Pelletisation	pan-pelletiser	pan-pelletiser counter current Eirich mixer
sintering	Sintering temperature ( $^{\circ}\text{C}$ )	900	< 900
	Sintering time (min)	na	minimum
properties	Particle size (mm)	0.1 – 8.0	0.5 – 4.0
	Apparent particle density ( $\text{g}\cdot\text{cm}^{-3}$ )	0.32 – 0.95	< 1
	Water absorption (w/w %)	30 - 120	< 50
	Thermal conductivity ( $\text{W}\cdot\text{m}^{-1}\text{K}^{-1}$ )	0.07	minimum
	Crushing strength ( $\text{N}\cdot\text{mm}^{-2}$ )	1.4 – 2.8	> 3.0
	Microstructure	unevenly distributed pores	evenly distributed pores

\* All values have been taken from the Poraver technical data sheets, as reported on their corporate website.

### 5.2 Feasibility study: screening experiments

Hand-rolled spherical ‘green’ pellets, using various as-received PSA-glass mixes, were rapidly fired at different pre-set temperatures for 20 minutes in order to determine the composition and temperature ranges within which a lightweight sintered material can be produced. Firing temperatures ranged between 700 and 900  $^{\circ}\text{C}$ , as imposed by

the TGA results for PSA (see Figure 5.5) and dilatometry data for glass (see Figure 5.6). Glass powder was added to as-received PSA on the basis of weight % varying from 0 wt. % to 100 wt. %, with an increment of 10 wt. % between trials. All mixes were fired at 700 and 900 °C and selective composition mixes of high and low PSA content were fired at intermediate temperatures. Based on past experience, a sintering time of 20 minutes was selected for conducting preliminary screening experiments (Spathi, 2011). Qualitative observation results are summarized in Table 5.4.

Promising lightweight pellets were produced at temperatures above 800 °C for the 80/20 glass/PSA (wt. %) and 90/10 glass/PSA (wt. %) composition mixes. Strong sintered pellets were also obtained for up to 50 wt. % addition of glass to as-received PSA when fired at 900 °C. Poor sintering was observed for the mixes having high PSA content, owing to the absence of solid-solid reactions between PSA particles or PSA-glass particles, which was expected based on dilatometry data for PSA.

**Table 5.4** Qualitative observation results for PSA-glass mixes fired for 20 minutes at different sintering temperatures

PSA (wt. %) <sup>1</sup>	Temperature (°C)				
	700	750	800	850	900
100	x <sup>2</sup>	x	x	x	x
90	x	x	x	x	x
80	x	<b>NO trials.</b> Focus on high and low PSA content mixes and low and high sintering temperatures.			x
70	x				x
60	x				x
50	⊙ <sup>3</sup>				⊙ <sup>3</sup>
40	⊙				⊙
30	⊙	⊙	⊙	⊙	⊙
20	⊙	⊙	✓ <sup>4</sup>	✓	✓
10	⊙	⊙	✓	✓	✓
0	⊙	⊙	⊙	⊙	⊙

<sup>1</sup> Both types of PSA gave similar results. Hence, observation results refer to both PSA\_ANP and PSA\_UPM. The remainder of the mix consists of TEMA milled glass powder.

<sup>2</sup> x: weak pellet

<sup>3</sup> ⊙: strong pellet, no expansion

<sup>4</sup> ✓: strong, lightweight pellet

Selected screening experiments to determine the optimum sintering temperature were performed with as-received PSA\_ANP samples. The 80/20 glass/ PSA\_ANP (in wt. %) mix was selected as a promising composition mix resulting in lightweight

materials. Sintering at 700, 750 800 and 850 °C for 20 minutes helped conclude that the sintering temperature of 800 °C is the optimum one for obtaining a foamed glass microstructure. Sintering at higher temperatures had no significant effect on decreasing the final particle density, as shown in Figure 5.7. Replicating the experiments with PSA\_UPM samples was not considered vital at this stage given the already established similar qualitative performance of this type of PSA-glass mixes. Hence, the assumption that PSA\_UPM samples would perform similarly was made.



**Figure 5.7** The effect of sintering temperature on density and water absorption of the 80/20 glass/PSA\_ANP mix (n=10). Lightweight materials are formed with enhanced properties compared to Poraver at the optimum sintering temperature of 800 °C. The sintering time was kept fixed at 20 minutes.

### 5.3 Effect of glass addition on LWF physical properties

The above observations set the decision framework for the following series of experiments in which focus was placed on optimising the mixes containing PSA from 0 to 50 wt. %. These were rapidly fired at the minimum sintering temperature of 800°C able to produce strong lightweight pellets. The sintering time was kept fixed at 20 minutes. In order to achieve optimised homogeneity of glass-PSA mixes, and potentially promote sintering reactivity of PSA particles by reducing the original particle size of raw materials, glass-PSA mixes were wet milled for 1h. Finally, pan-pelletising was opted as a more viable spherical ‘green’ pellet formulation process. Determining the optimum composition mix for LWF production, when sintering

occurs under pre-determined sintering conditions, is, hence, the object of this piece of work.

The effect of glass addition on density and water absorption of various glass-PSA mixes is shown in Figure 5.8, which also contains data for Poraver, a commercial LWF. Samples prepared with PSA\_ANP additions up to 20 wt. % have similar or lower densities than 5 mm commercial LWFs (Figure 5.8a). Given low sintering reactivity of PSA, further increases in the PSA content inhibits the formation of sufficient glassy phases to entrap the gases being evolved. Gas escape results in lack of pore formation and increased density. Peak density values observed at 30 wt. % addition of PSA\_ANP indicate sufficient viscous phase formation with simultaneous excessive gas evolution. This leads to collapse of the pore network, justifying peak density values. Further increases in the PSA content results in both decreased glassy phases formation and excessive gas escape with samples exhibiting a chalky surface. At 10 wt. % addition of PSA\_ANP, lightweight fillers with a particle density as low as  $0.45 \text{ g cm}^{-3}$  are obtained. However, excessive interconnection of pores and piercing of the vitrified layer formed, due to the presence of glass, results in high water absorption of 145 wt. %. In the case of PSA\_ANP, the optimum samples, combining low density and relatively low water absorption, contained 80 wt. % glass and 20 wt. % PSA. These had a density of  $0.75 \text{ g cm}^{-3}$  and water absorption of 75 %. In contrast, glass sintered pellets have a particle density of  $1.12 \text{ g cm}^{-3}$  and water absorption of 3.8 wt. %.

In contrast, samples prepared with PSA\_UPM have a different behaviour (Figure 5.8b). Lightweight sintered material having a low density of  $0.65 \text{ g cm}^{-3}$  is achieved when PSA\_UPM is added at 10 wt. % in the glass mix. This has a corresponding water absorption of 88 wt. %. Further addition of PSA\_UPM results in a more densified structure with peak densification observed at the 20 wt. % PSA\_UPM addition. This can be attributed to the limiting expanding potential of this type of ash, as inferred by the TGA results shown in Figure 5.5. Porosity is, hence, expected to be restrained by a less prominent gas evolution during sintering resulting in a more densified structure. Further PSA\_UPM addition in the glass mix, similarly to PSA\_ANP, hinders the formation of a vitreous 'sealing capsule' able to capture the evolving decomposition gas within the sintered body. Firing a 50 PSA\_UPM - 50 glass (wt. %) mix at  $800 \text{ }^\circ\text{C}$

for 20 minutes resulted in failing of the sintered samples, which were not appropriate for testing. This highlights the significance of the difference in sintering capacity of the two PSA samples in question. The difference in silica content in the two PSA samples (see Table 5.1) justifies the fact that PSA\_ANP has a more robust ‘sintering potential’ over PSA\_UPM.

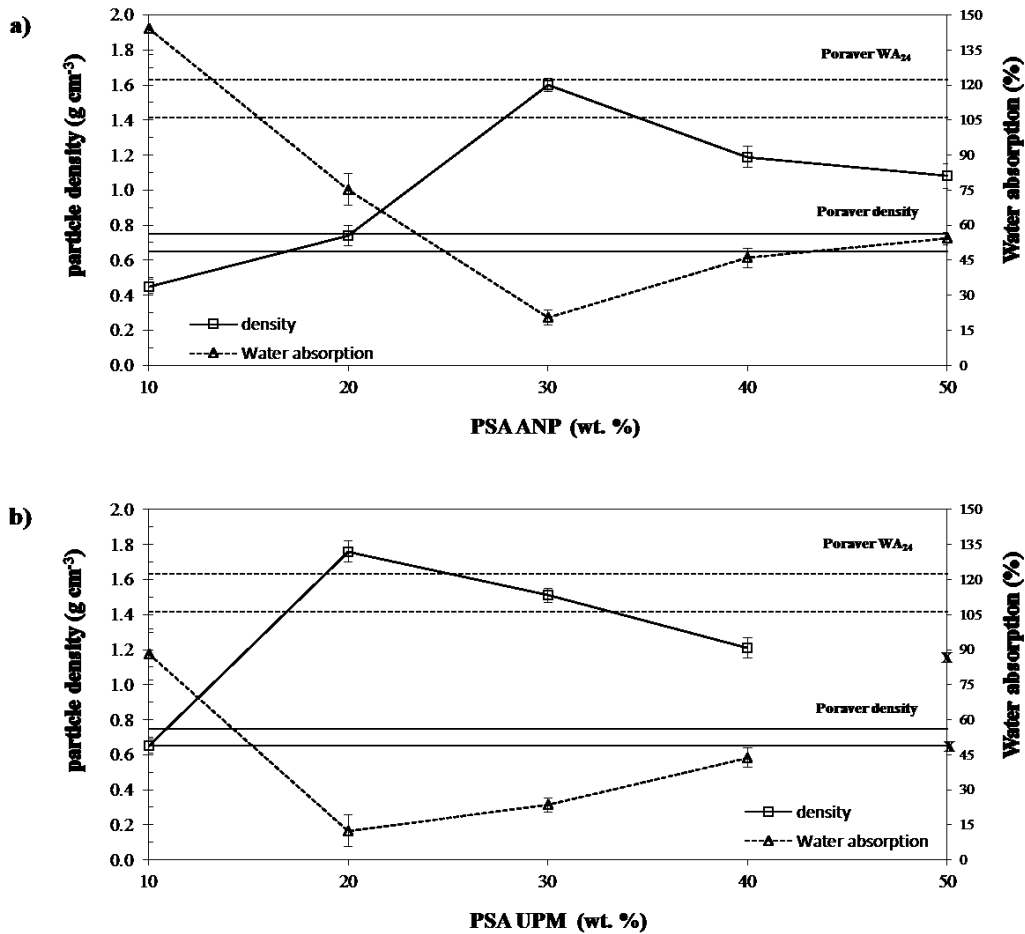


**Figure 5.8** Effect of PSA addition on the density and water absorption of glass-PSA pellets fired at 800 °C for 20 minutes: a) PSA\_ANP and b) PSA\_UPM. All mixes were wet milled for 1h prior to pelletisation and sintering. The two types of ashes behave differently during sintering, with PSA\_ANP exhibiting better sintering reactivity. The 50 PSA\_UPM – 50 glass mixes failed to provide strong testable sintered products. Lightweight materials, with the maximum possible PSA content, are produced for the 80/20 glass/ PSA\_ANP (in wt. %) mix and the 90/10 glass/PSA\_UPM (in wt. %) mix. (n=10)

## 5.4 Effect of sintering time on properties of end-products

### 5.4.1 Effect of sintering time on the 80/20 glass/PSA\_ANP mix

The effect of sintering time on the 80/20 glass/PSA\_ANP pellets fired at 800 °C is shown in Figure 5.9. Microstructural evolution can be described by four distinct stages: a) heating, b) glass softening/gas evolution, c) stabilisation and d) further densification. Initial densification gave place to growth of porosity as the thermally instable species within the PSA decompose during sintering. Based on this data, the optimum sintering time was 10 minutes with LWFs having a density of  $1 \text{ g}\cdot\text{cm}^{-3}$  and WA of 23.2 wt. %. The limitations on pore size increase can be explained by the disintegration of the rigid cell walls of sintered particles reflected on the rapid increase in water absorption rates when sintering between 15 and 20 minutes. Hence, understanding the kinetics of the sintering process is of primary importance. After sintering for 20 minutes, no significant changes were observed in the LWF properties tested, validating that final microstructure has been attained. Microstructural analysis of the pellets, presented in subsequent section, will illustrate in more detail pore growth phenomena during sintering.

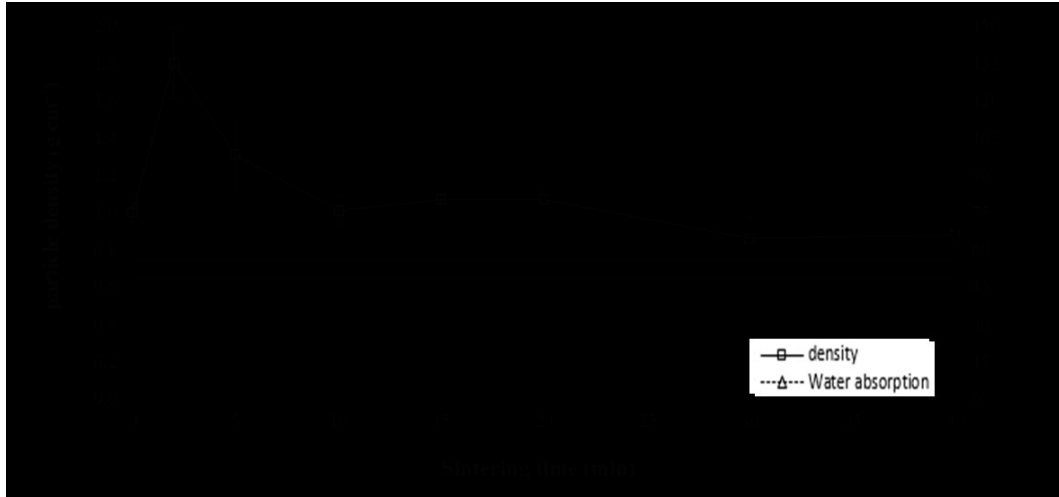


**Figure 5.9** Effect of sintering time on particle density and water absorption of the 20 PSA\_ANP – 80 glass mix when fired at 800 °C. Raw materials were wet milled for 1h prior to pelletising and sintering. Beyond 15 minutes, an abrupt change in permeability of the sintered body was observed indicating piercing of the outer layer of the pellets (n=10).

#### 5.4.2 Effect of sintering time on the 90/10 glass/PSA\_UPM mix

The effect of sintering time on the 90/10 glass/PSA\_UPM pellets fired at 800 °C is shown in Figure 5.10. Similar observations can be made in this case. After sintering for 2 minutes, initial densification of the pellets was recorded. Peak density was as high as  $1.62 \text{ g}\cdot\text{cm}^{-3}$ , similar to peak densities measured for PSA\_ANP-glass mixes as detailed above. A drop in particle density by 60 % occurred with increasing sintering duration. However, water absorption rates were in the region of 80 wt. % for lightweight pellets, which was outside the pre-determined desired water permeability characteristics for LWFs. It is, also, notable that after sintering for more than 30 minutes an increase by 50 % in density was reported compared to density values corresponding to the 5-minute sintering test trials. This was not an expected outcome as it contradicts the concept of '*final density attainment*' based on the principle of equilibrium attainment for the dynamic process of gas evolution and entrapment, after which a pore network is expected to have been developed. It can be, therefore, concluded that continuation of sintering, beyond critical times for each PSA sample, results in complete disintegration of the pore network with further precipitation of solid grains and crystal formations due to smelting. Within the 40-minute time regime investigated in this study, it became obvious that LWFs prepared with PSA\_ANP have more rigid walls surrounding the already formed pores which are not adversely affected by further crystallisation of the matrix as the sintering process is prolonged.

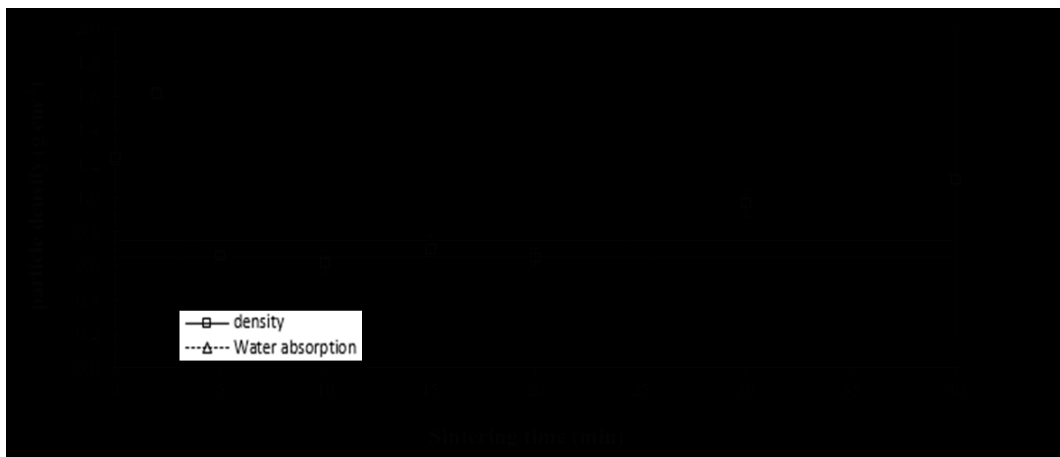


**Figure 5.10** Effect of sintering time on particle density and water absorption of the 90/10 glass/PSA\_UPM mix when fired at 800 °C. Raw materials were wet milled for 1h prior to pelletising and sintering. At 15 minutes, an abrupt change in permeability of the sintered body was observed indicating piercing of the outer layer of the pellets (n=10).

### 5.4.3 Microstructural evolution during sintering

The expansion process of sintered LWFs is a dynamic balance between the evolution of gaseous species from PSA and the inhibiting formation of viscous glass layers able to encapsulate those gases. As demonstrated above, for given glass-PSA composition mixes, controlling sintering time plays a key role in engineering porous structures. This can be demonstrated by the SEM images shown in Figure 5.11. In specific, Figure 5.11a-d illustrates the gradual interconnectivity of pores with increasing sintering dwell times once first pores appear, i.e. beyond the initial heating/densification stage, in the case of wet milled (for 1h) 80/20 glass/PSA\_ANP mixes sintered at 800 °C. In the case of the similarly prepared 90/10 glass/PSA\_UPM mixes, initial densified microstructures give way to porous ones with interconnected pores of up to 200 µm in diameter after 10 minutes of sintering. To allow comparison, micrographs of Poraver and 100 % glass particles are also presented in Figure 5.12.

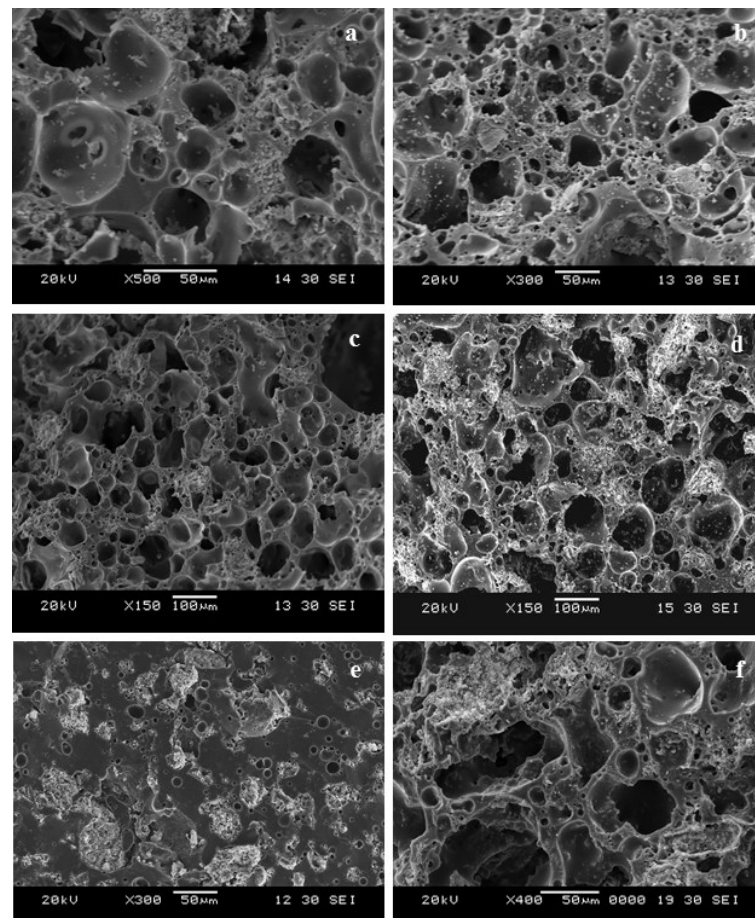


**Figure 5.11** Morphology of LWFs prepared with glass-PSA mixes wet milled for 1h prior to sintering at 800 °C : a-d) Cross-sections of 80/20 glass/PSA\_ANP pellets sintered for 5, 10, 15 and 20 minutes respectively, and e-f) Cross-sections of 90/10 glass/PSA\_UPM pellets sintered for 2 and 10 minutes respectively.

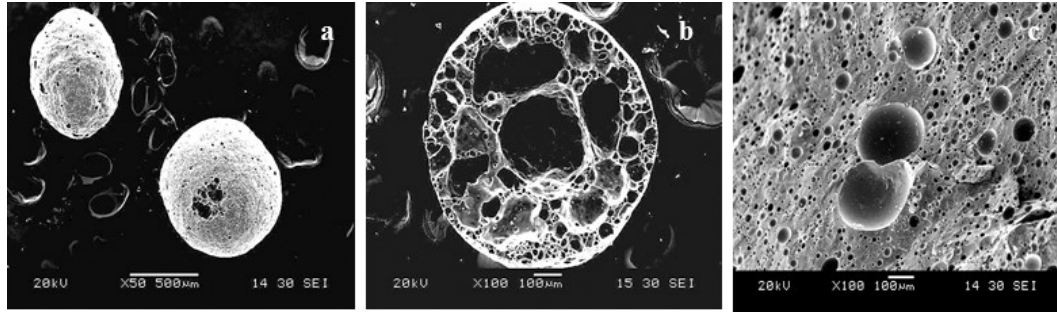


**Figure 5.12** Scanning electron micrographs of: a-b) Commercial LWF Poraver particles of 600-850  $\mu\text{m}$  in diameter and c) 100 % glass pellets sintered at 800  $^{\circ}\text{C}$  for 15 minutes having a particle density of 1.12  $\text{g cm}^{-3}$  and water absorption of 3.8 wt. %.

From the above analysis, it is inferred that the effect of sintering time on a given PSA-glass mix is not only important but it is the one that defines the final microstructure of sintered end-products. With this in mind, following series of experiments focused on investigating the joint effect of sintering time and particle size of formulation mixes.

## 5.5 Effect of particle size of raw materials and sintering time on the properties of 80/20 glass/PSA mixes

### 5.5.1 Physical and microstructural properties of sintered products

In section 5.5.1, it was demonstrated that LWF particles can be produced when wet milling 20 wt. % of PSA\_ANP with glass for 1 hour following by pan-pelletising and sintering at 800  $^{\circ}\text{C}$  for 15 minutes. With regard to glass-PSA\_UPM, the optimum identified mix with the potential to produce LWFs was the one containing 10 wt. % as-received PSA\_UPM as shown in Figure 5.8b. Further processing of the 90/10 glass/PSA\_UPM mix via wet milling for 1 hour and sintering at 800  $^{\circ}\text{C}$  for various times resulted in LWFs of low density but also of high water absorption. To address this issue, increasing the PSA\_UPM content in the mix to 20 wt. % while reducing the particle size of powders was investigated as a viable solution.

The experiments to verify whether LWFs from 80/20 glass-PSA\_UPM mixes could be produced involved varying the particle size of glass-PSA\_UPM mixes via increasing the wet milling time. This helped obtain powder mixes of three distinct particle sizes. Identical processing was employed for the PSA\_ANP samples to allow comparisons both within and between the various PSA-containing sintered products. The wet milling conditions are given in section 4.2.1 and corresponding particle size

distributions are given in Figure 5.13. The mean diameter  $d_{50}$  for the various PSA\_UPM powders produced via 1, 2 and 4h of milling was 15, 16 and 12  $\mu\text{m}$  respectively. The mean diameter  $d_{50}$  for the various PSA\_ANP powders produced via 1, 2 and 4h of milling was 18, 21 and 19  $\mu\text{m}$  respectively.

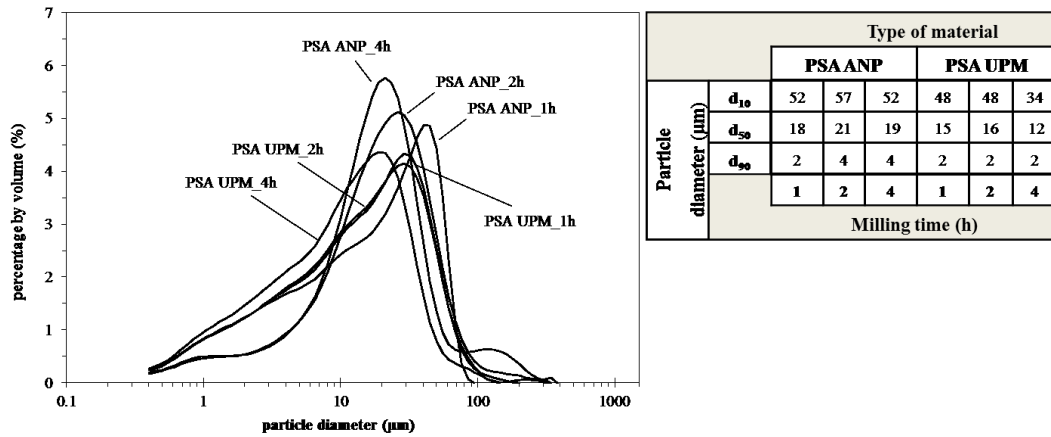


**Figure 5.13** Particle size distributions for the 80/20 glass/PSA mixes achieved after wet milling for 1, 2 and 4 hours. Mixes containing PSA\_UPM showed better size reduction properties compared to the PSA\_ANP ones. At 4 hours of wet milling, PSA\_ANP mixes formed agglomerates. This can be attributed to the reaction of free lime (CaO) present in the PSA\_ANP and water in the mill for the formation of calcium hydroxide according to:  $\text{CaO (s)} + \text{H}_2\text{O (l)} \leftrightarrow \text{Ca(OH)}_2 \text{(aq)}$ .

The effect of wet milling and sintering time on density and water absorption of 80-20 glass-PSA mixes is depicted in Figure 5.14, which also contains data for Poraver. The density of green particles containing PSA\_ANP and PSA\_UPM was  $1.0 \text{ g}\cdot\text{cm}^{-3}$  and  $1.24 \text{ g}\cdot\text{cm}^{-3}$  respectively. In the initial stage of sintering (up to 5 minutes), a densification of the glass-PSA matrix is observed with maximum densities up to  $1.82 \text{ g}\cdot\text{cm}^{-3}$ . As a general observation, the same stages of microstructural evolution, as discussed in section 5.4.3, describe the phenomena of gas evolution and encapsulation within the sintered body wherever a decrease in the density of pellets is measured. It is worth noting that the 80/20 glass-PSA\_ANP mixes wet milled for 2 hours and the 80/20 glass-PSA\_UPM mixes wet milled for 1 hour returned no porous structures when sintered at  $800 \text{ }^\circ\text{C}$  for times varying from 2 to 40 minutes.

As opposed to 80/20 glass/PSA\_ANP mixes, in the case of 80/20 glass/PSA\_UPM mixes wet milled for 1 hour, further sintering did not result in bloating of the particles as confirmed by the minor changes in density and water absorption values. However, the potential for the latter mixes to produce LWF materials increased considerably

when increasing the milling time, i.e. reducing the particle size of the constituents present in the mix. Wet milling such mixes for 2 and 4 hours and sintering at 800 °C for 10 minutes resulted in a density of 1.4 and 0.92 g·cm<sup>-3</sup> reduced by 23 % and 50 % respectively compared to mixes wet milled for only 1 hour. The corresponding water absorption rates were 15 % and 46 %, significantly lower compared to Poraver values.

Increasing milling time had no positive effect on the 80/20 glass/PSA\_ANP mixes, in the sense that the lowest density remained that of 1.0 g·cm<sup>-3</sup> achieved after wet milling such mixes for 1h and sintering for 10 minutes at 800 °C. This had a corresponding water absorption rate of 23 wt. %.

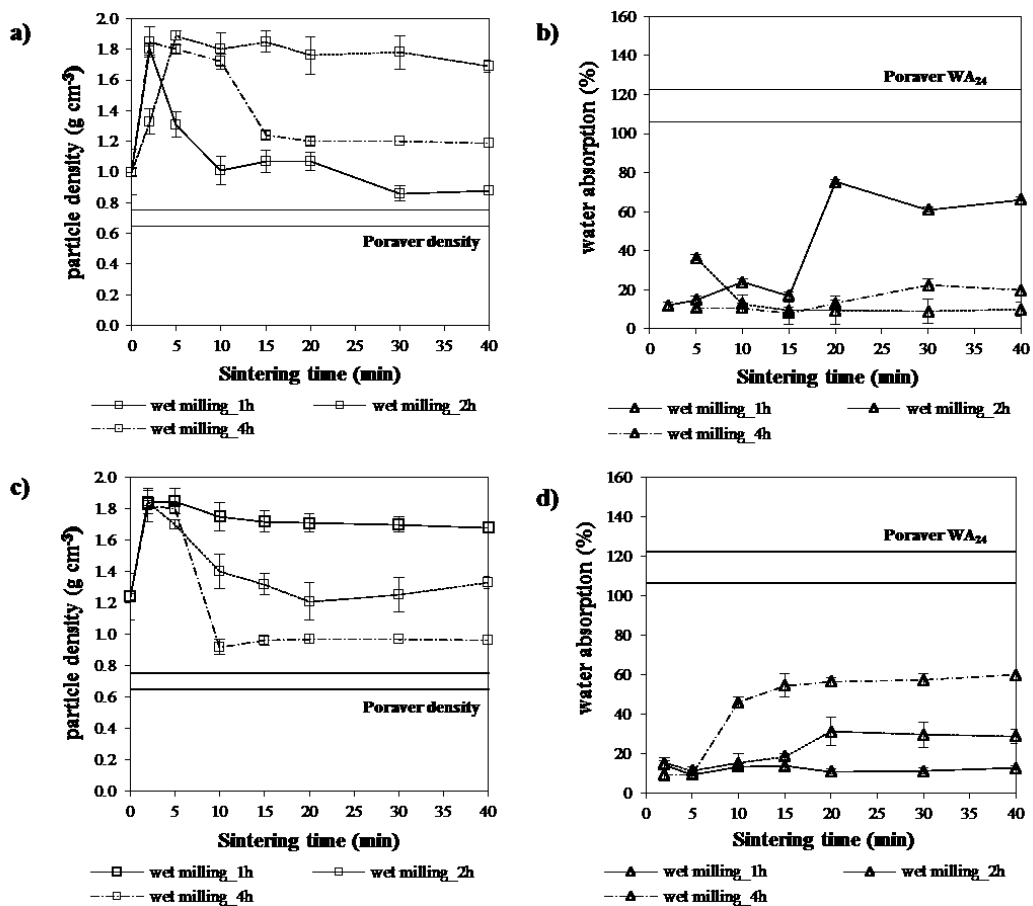


**Figure 5.14** Effect of wet milling and sintering time on (a-b) the particle density and water absorption of 80/20 glass/PSA\_ANP and (c-d) particle density and water absorption of 80/20 glass/PSA\_UPM of sintered pellets at 800 °C (n=10).

The effect of milling time on the 80-20 glass-PSA pellets fired at 800 °C is shown in Figure 5.15. Micrographs of sintered pellets prepared with glass-PSA mixes of different particle size prepared with PSA\_ANP and PSA\_UPM are depicted in Figure

5.15a-c and Figure 5.15d-f respectively. In the case of glass/PSA\_UPM mixes, finer powder mixes resulted in greater porosity during sintering for 20 minutes (final density achieved). This is due to the better homogeneity and fineness of the expanding agent within the glass mix promoting pore formation. Further, increased fineness of glass particles aids the formation of low-viscous vitreous phases at the given temperature of 800 °C. In contrast, increasing wet milling time from 1 hour to 4 hours did not stimulate further pore formation for glass/PSA\_ANP mixes. In fact, wet milling such mixes for 2 hours resulted in no expansion and poor pore formation. This could be attributed to the presence of excessive gas generated early on during heating, i.e. before glass softening took place, due to calcium hydroxide  $\text{Ca}(\text{OH})_2$  species which caused micro-cracks within the body and prevented encapsulation of  $\text{CO}_2$  gas when calcite particles started decomposing. This is to be discussed in detail in Chapter 6.

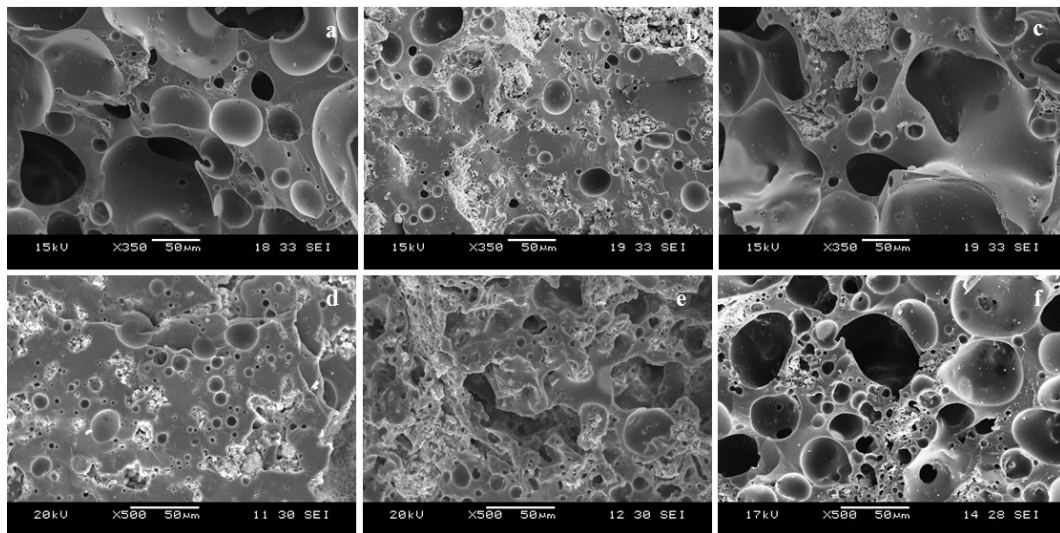


**Figure 5.15** Morphology of 80/20 glass/PSA pellets sintered at 800 °C: Cross-section of 80/20 glass/PSA\_ANP pellets after 20 minutes of sintering for the 1h (a), 2h (b) and 4h (c) wet milling times; Cross-section of 80/20 glass/PSA\_UPM pellets for the 1h (d), 2h (e) and 4h (f) wet milling times.

Based on the above analysis, the optimum LWFs produced were the ones containing 20 wt. % PSA with the remainder being milled glass powder. It was found that the optimum wet milling time for 80/20 glass/PSA\_ANP mixes is 1 hour with optimum properties obtained when sintered at 800 °C for 10 minutes. The effect of sintering time on this type of products has been discussed and illustrated in section 5.5.1 and Figure 5.11.

Hence, here, focus is placed on evaluating the effect of sintering time on the optimum 80-20 glass-PSA\_UPM pellets fired at 800 °C as shown in Figure 5.16. These pellets are produced after wet milling the mix for 4 hours prior to sintering at 800 °C for 10 minutes. As expected, densified structures obtained after 2 minutes of sintering (Figure 5.16a) for all mixes are converted into lightweight porous structures with the increase of sintering duration. However, sintering times higher than 10 minutes led to excessive interconnection of pores and piercing of the vitrified layer formed due to the presence of glass (Figure 5.16c). Optimum sintering time was found to be 10 minutes for this type of mixes (Figure 5.16b). A micrograph of an optimum 80/20 glass/PSA\_UPM spherical LWF capturing a whole approximately spherical sintered particle is shown in Figure 5.17. The pores are evenly distributed within the particle ranging from 25 µm to 50 µm in diameter. This provides LWFs with excellent mechanical properties as it will be discussed below.

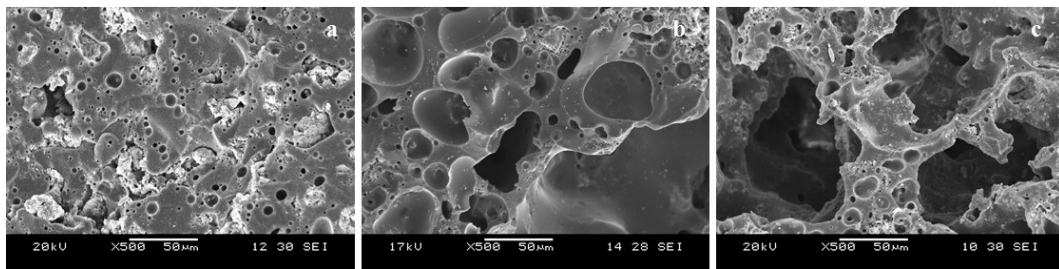


**Figure 5.16** Microstructure of 80/20 glass/PSA\_UPM LWFs sintered at 800 °C: Cross-section of pellets prepared with glass-PSA mixes wet milled for 4h after sintering for 2 minutes (a), 10 minutes (b) and 20 minutes (c).

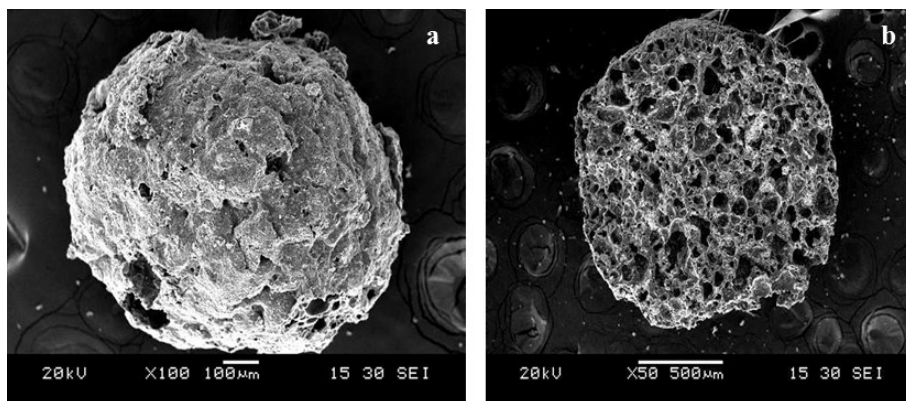


**Figure 5.17** Microstructure of optimum LWFs prepared with glass-PSA\_UPM mixes which were wet milled for 4h prior to being sintered at 800 °C for 10 minutes: a) whole LWF particle and b) cross-section of (a).

Finally, an easy comparison between optimum LWFs prepared with PSA\_ANP and PSA\_UPM can be made by looking at Figure 5.18. It can be seen from the images that optimum glass/PSA\_ANP pellets (Figure 5.18a) are occupied by a network of approximately spherical pores contrast to a more interconnected network of pores found in the optimum glass/PSA\_UPM LWFs. This is also reflected in the lower density and lower water absorption values of the PSA\_ANP pellets.

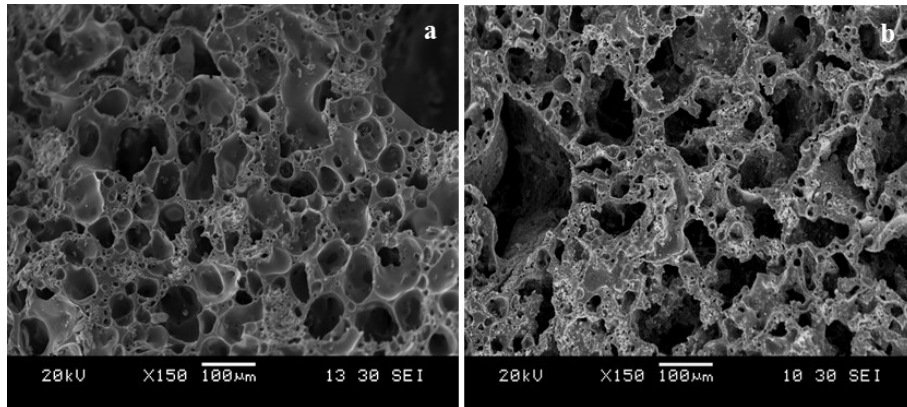


**Figure 5.18** Optimum LWFs produced at 800 °C for 10 minutes with mixes of: a) 80/20 glass/PSA\_ANP wet milled for 1 hour and b) 80/20 glass/PSA\_UPM wet milled for 4 hours.

### 5.5.2 Performance of optimum LWFs of different grain sizes

Commercial LWFs, such as Poraver, can be found in a wide range of particle sizes. Since variations in the properties of each grade have been reported by manufacturers, it was considered essential to assess the physical and mechanical properties of optimum LWFs produced from waste glass and PSA when varying the pellet size from 1 mm to 7 mm. Smaller pellets were obtained using a counter current Eirich mixer operating at an inclination angle of 20° and a pan speed of 85 rpm (clockwise) and rotor speed of 15 m/s (anti-clockwise).

As it can be deduced from Figure 5.19, larger LWF pellets tend to exhibit higher density and lower water absorption rates. The strongest variation in properties was observed in the case of the commercial reference product, where a significant increase in the water absorption rates was measured for the bigger pellets having a diameter between 5 and 7 mm. Optimum LWFs produced with 80/20 glass/PSA mixes have consistent physical properties regardless of the pellet size. This is an additional advantage of optimum LWFs manufactured throughout this study. The benefits of

producing LWFs of various pellet sizes are associated with the versatility of using such materials in a wide range of potential end applications.

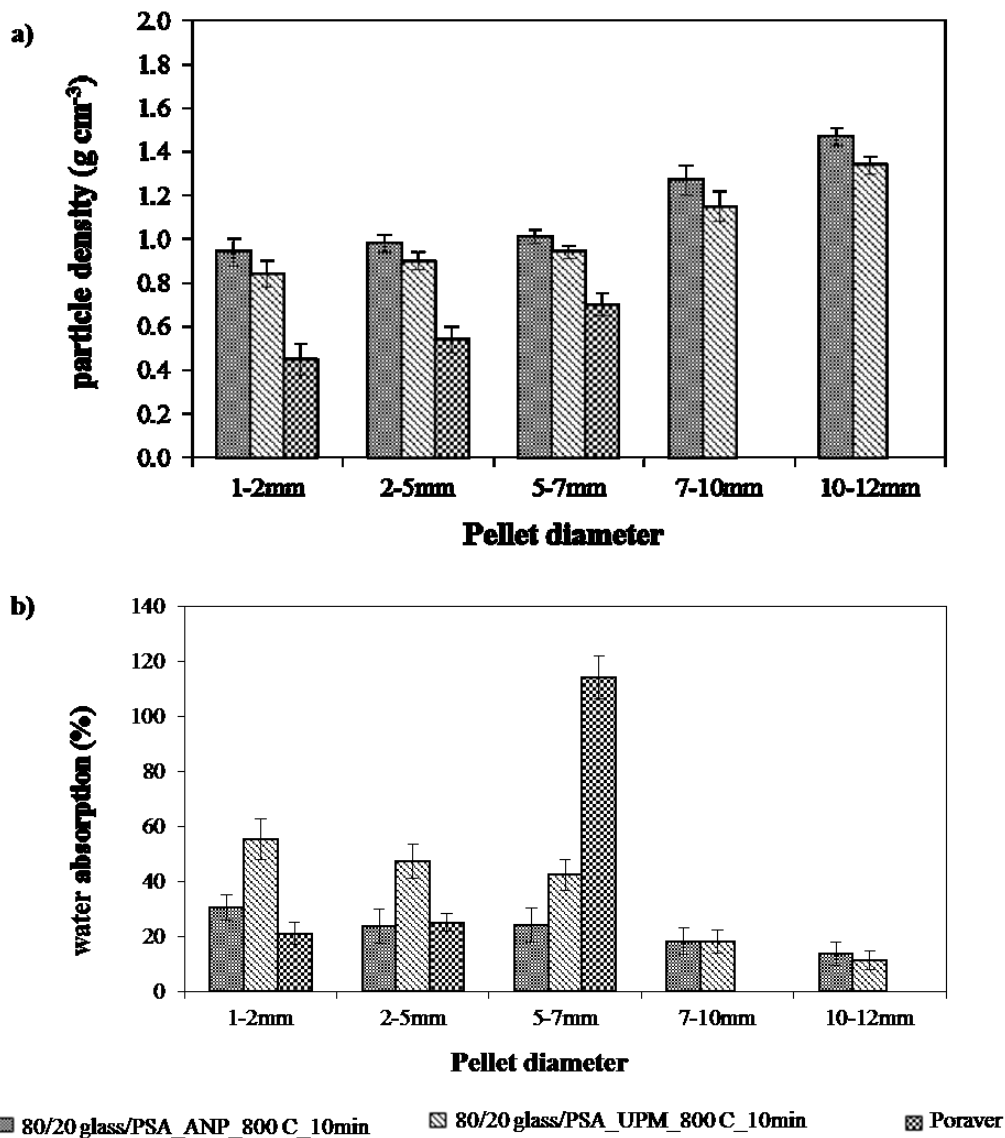


**Figure 5.19** Effect of pellet diameter on particle density (a) and water absorption (b) of optimum 80/20 glass/PSA LWFs and Poraver (n=10).

### 5.5.3 Crushing strength of optimum LWFs

The crushing strength CS(10) of the optimum 80/20 glass/PSA LWFs with pellet sizes ranging from 1-7 mm are compared against Poraver in Table 5.5. Artificial glass-based LWFs with 20 % addition of PSA have consistent mechanical properties regardless of the LWF pellet size. The crushing strength ranges from 2.9-3.1 MPa and this is three times higher than values obtained for the commercially available LWFs, Poraver.

**Table 5.5** Crushing strength of optimum 80/20 glass/PSA LWFs and Poraver LWFs (n=10).

LWF grain size	CS(10) (MPa)		
	PSA_ANP	PSA_UPM	Poraver
1-2 mm	2.9	2.9	1.3
2-5 mm	2.9	3.1	1.1
5-7 mm	3.0	3.1	1.0

High crushing strength values for the 80/20 glass/PSA LWFs are attributed to the rigidity of the microstructure developed after sintering at optimised conditions. These allowed for the establishment of a network of evenly distributed pores within the sintered body, as opposed to large pores found arbitrarily dispersed in the microstructure of Poraver LWFs (see Figure 5.12). Hence, the use of such LWFs in robust structural applications can be recommended.

#### 5.5.4 Mineralogy of optimum 80/20 glass/PSA LWFs

X-ray diffraction data for the optimum 80/20 glass/PSA sintered mixes fired at 800 °C is shown in Figure 5.20. Crystallisation of the original mixes is achieved in both cases resulting in the formation of new crystalline phases.

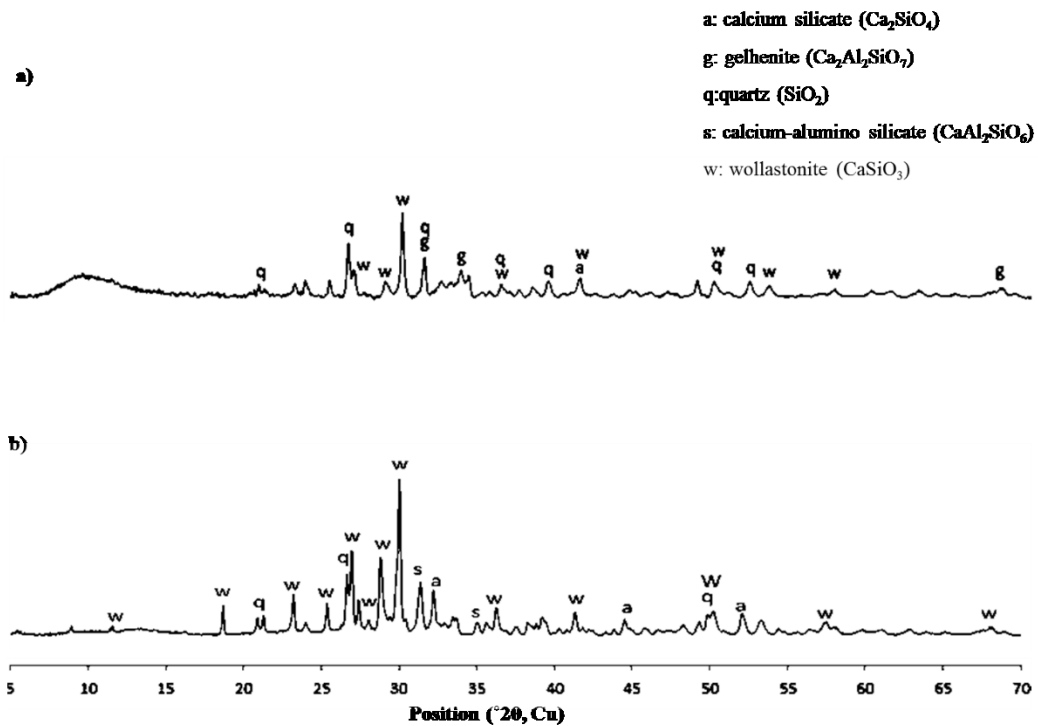


**Figure 5.20** XRD patterns of optimum 80/20 glass/PSA LWFs prepared with 20 wt. % of PSA\_ANP (a) and 20 wt. % of PSA\_UPM (b) sintered at 800 °C for 10 minutes. Representative LWF samples were manually ground to form powders with a mean particle size of 35 μm.

As-received PSA samples demonstrated a rather complex mineralogy with overlapping crystalline phases present, as shown in Figure 5.4. The addition by 80 wt. % of an amorphous waste glass powder to achieve porous sintered structures at a relatively low sintering temperature resulted in extensive crystallisation of the mixes with the formation of new crystalline phases. Calcium silicate ( $\text{Ca}_2\text{SiO}_4$ ), quartz ( $\text{SiO}_2$ ), calcium-alumino silicate ( $\text{CaAl}_2\text{SiO}_6$ ) and wollastonite ( $\text{CaSiO}_3$ ) are the new phases present in the sintered products. These are primarily due to the transformation of gehlenite ( $\text{Ca}_2\text{Al}_2\text{SiO}_7$ ), the major crystalline phase in as-received PSA, in wollastonite as well as the de-vitrification of waste glass powder with high amorphous silica ( $\text{SiO}_2$ ) into quartz crystals. Similar phase transformations have been previously reported by Hernández-Crespo et al. (2011) and Barbieri et al. (2000) when processing hospital waste and municipal incinerator bottom ash into glass-ceramics.

It is to be highlighted that the sintering process employed for the production of LWFs is a single-stage method that involves rapid heat treatment of glass/PSA mixes at the final sintering temperature. Hence, the process of crystallisation and densification of PSA and glass constituents in the powder mix took place simultaneously. This could have adverse effects on the crystallisation of the glass matrix as it has been suggested by Boccaccini et al. (1996). Given that densified structures are obtained early on during sintering, as discussed above, the onset of crystallisation is expected to be delayed. Hence, there were still traces of calcium silicate ( $\text{Ca}_2\text{SiO}_4$ ) and calcium-alumino silicate ( $\text{CaAl}_2\text{SiO}_6$ ) in the sintered products. However, it is appreciated that these peaks on the XRD spectra may also correspond to gehlenite or quartz phases that were difficult to be isolated in the analysis due to the mineralogical complexity of the material and general overlapping of peaks.

## 5.6 Leachability of as-received PSA and optimum 80/20 glass/PSA LWFs

The major leaching controlling factors and mechanisms of release of elements contained in a porous monolithic solid are illustrated schematically in Figure B.1 (Appendix B). Given the inhomogeneity of waste and waste-based materials, the environmental impact that these could potentially have under different conditions needs to be assessed. In this study, pH was considered to be a highly influential chemical factor governing the mechanisms of release of hazardous substances into the environment from as-received PSA samples and sintered glass/PSA LWFs. It is also

a factor with major practical significance considering that potential applications for LWFs include use as building materials in concrete mixes with alkaline properties.

The leaching behaviour of both types of as-received PSA and optimum 80/20 glass/PSA mixes sintered at 800 °C for 10 minutes were assessed applying the pH dependence leaching test using a liquid to solid (L/S) ratio of 10 according to BS-EN 12457-2:2002. This allowed characterisation of leachability characteristics under different pH conditions covering the range from alkaline to acidic. It is a reference test for all extended material evaluation studies, which ensures that leaching of hazardous elements is within acceptable ranges, as set up by the Council Decision 2003/33/EC (see Table B.1 in Appendix B).

### 5.6.1 Acid Neutralisation Capacity (ANC)

The ANC refers to the buffering capacity of the material to maintain the pH levels constant resisting to external chemical attacks caused by the addition of acid/base. The acid neutralisation capacity (ANC) of as-received PSA samples and processed 80/20 glass/PSA LWFs, expressed as the final eluate pH as a function of acid addition in mequivalents of acid per g of solid is shown in Figure 5.21. As described in section 6.3.7, a solution of 4 M of HNO<sub>3</sub> solution was used to induce pH changes. The acid addition is reported in equivalents calculated by:  $\text{Equivalent (m}_{\text{eq}}/\text{ml}) = V * N$ , where  $V$  is the volume of acid (in ml) and  $N$  is the normality of the HNO<sub>3</sub> solution used, which is 4 N in this case.

The as-received PSA samples exhibited a relatively constant rate of pH decrease with acid addition. ANC for as received PSA samples was high compared to that of other waste materials, such as APC residues from municipal solid waste incineration (Quina et al., 2009), incinerator bottom ash (Van der Sloot et al., 2001; Bethanis et al., 2004) and coal fly ash (Georgakopoulos et al., 2010). This can be attributed to the carbonation during aging of the PSA powders, leading to the formation of CaCO<sub>3</sub>, which provided significant buffering capacity particularly at high pH values (Guimaraes et al., 2006; Wahlström et al., 2009).

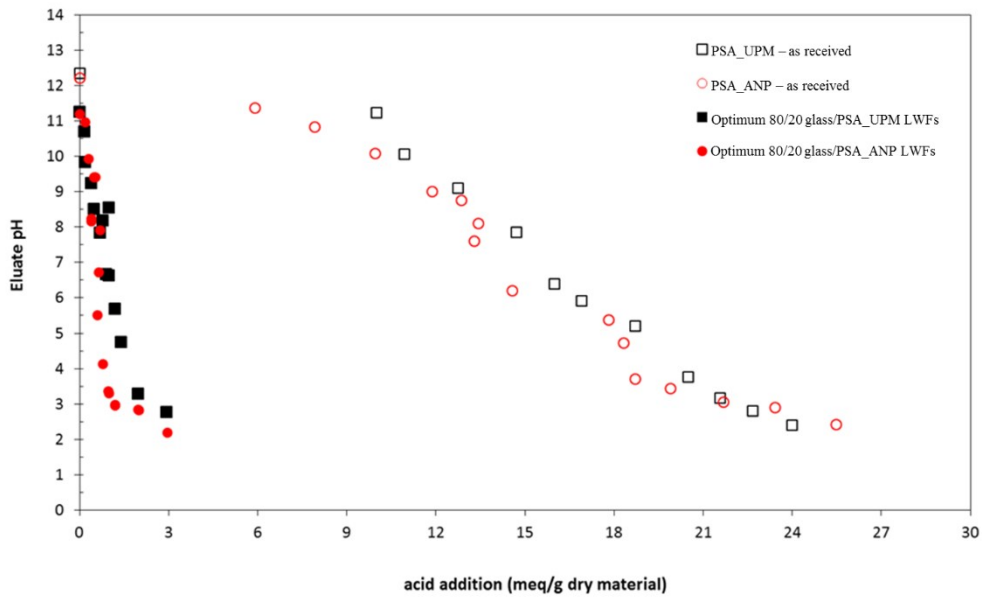
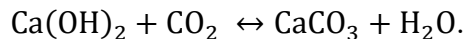


**Figure 5.21** Acid Neutralisation Capacity of the as-received PSA\_ANP and PSA\_UPM samples; 80/20 glass/PSA LWFs sintered at 800 °C for 10 minutes. Sintered LWFs exhibited decreased ANC (n=15).

Calcium carbonate can be formed according to the following reaction:



This reaction may have taken place in the open-air storage areas where PSA was kept before being packed in a sealed bag for transfer to the lab. Also, some gas release was observed when acid solution was added to the solid PSA samples in the test tube. This may correspond to  $\text{CO}_2$  generation from the dissolution of calcite and  $\text{H}_2$  from the reaction with metals, mainly Al which is present in bulk in PSA. The possible routes for the aforementioned gas releases can be described by:

- $\text{CaCO}_3(\text{aq}) + 2 \text{HNO}_3(\text{aq}) \rightarrow \text{Ca(NO}_3)_2(\text{aq}) + \text{CO}_2(\text{g}) + \text{H}_2\text{O}(\text{l})$  and
- $2\text{Al}^0(\text{s}) + 6\text{H}_2\text{O}(\text{l}) \rightarrow 2\text{Al(OH)}_3(\text{s}) + 3\text{H}_2(\text{g})$ .

Regarding sintered products, the solubilisation and removal of alkali metal and alkali metal earth elements during sintering, as well as the dilution of PSA by glass in the optimum mixes, were responsible for the reduction of ANC of optimum sintered LWFs. The addition of glass and crystallisation of glass/PSA mixes during sintering resulted in new phases which advocate the reduction of ANC in the final product. Also, sintering decomposed  $\text{CaCO}_3$  to  $\text{CaO}$  and  $\text{CO}_2$  gas. Lime then formed new amorphous and crystalline phases in the vitrified glass-PSA sintered particles, which had lower reactivity. Wahlström et al. (2009) have reported that the neutralisation potential of

wollastonite and silicate minerals is 40 – 60 % lower than that of carbonate minerals. Finally, depending on the considered element, high ANC of PSA samples may have a positive or a negative effect on the leachability of trace metals (Van der Sloot & Kosson, 2012).

### 5.6.2 Leachate analysis

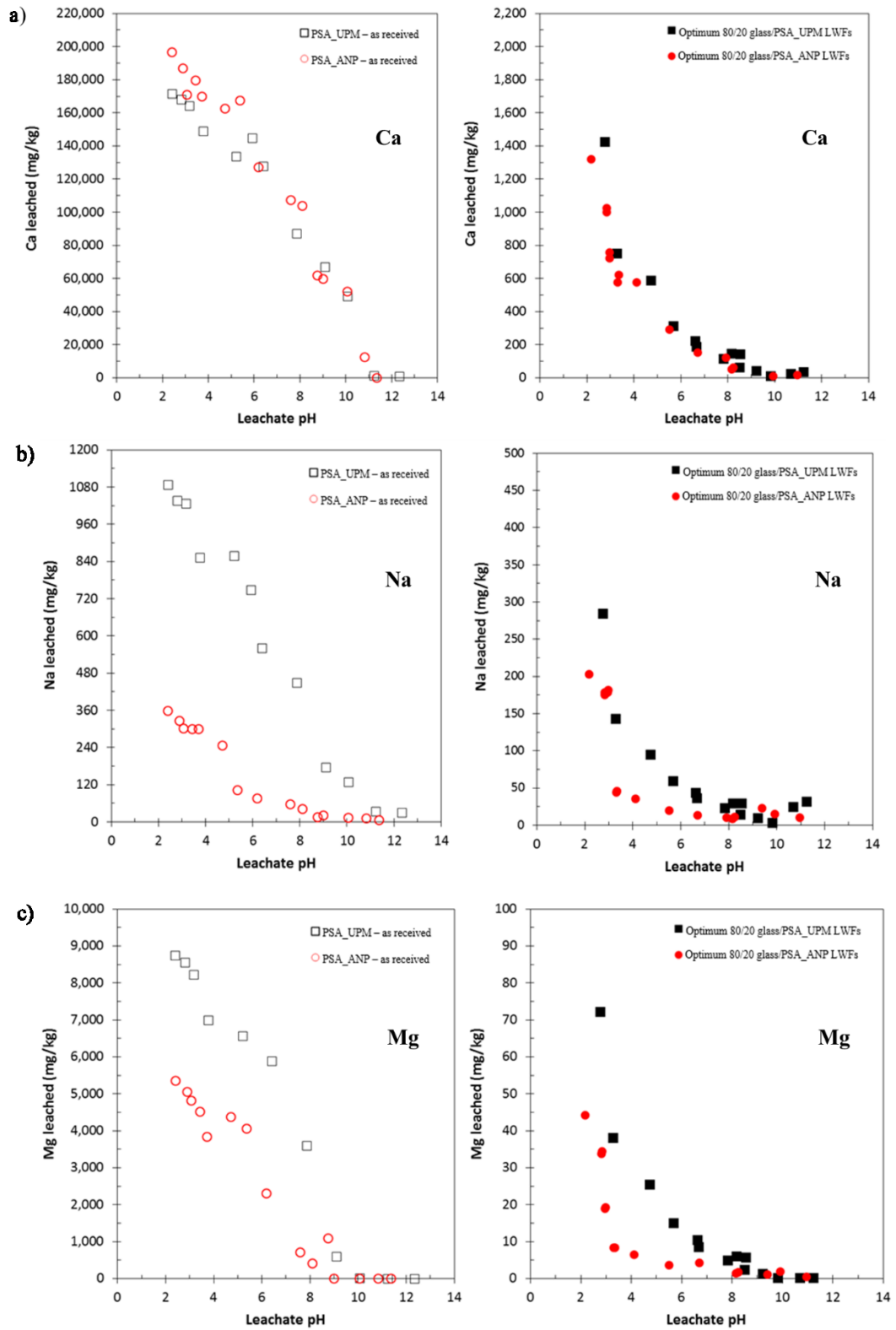
The concentrations of selected alkali and alkali earth metals and heavy metals leached from the as-received PSA powder and optimum 80/20 glass/PSA optimum LWFs produced with both types of PSA and sintered at 800 °C have been plotted as a function of leachate pH and presented in Figures 5.22 to 5.25. Sintering of optimum glass/PSA mixes significantly minimised leachability of all elements contained in the as-received PSA.

#### a) Leaching of alkali metals and alkaline earth metals: Na, K, Ca, Mg

Leaching data for Ca, Mg, Na and K in mg/kg are presented in Figure 5.22. Acidic conditions promoted the dissolution of mineral phases, such as  $\text{CaCO}_3$ ,  $\text{Ca}_2\text{SiO}_4$ ,  $\text{CaO}$ , gehlenite and other Ca-silicates present in the as-received PSA samples. A number of studies have verified similar changes in solubility of such minerals found in different waste residues (Halla et al., 2014; Jones et al., 2015). These changes are of primary importance in deciding on sustainable disposal options.

Below pH 9 solubility of  $\text{Ca}^{+2}$ ,  $\text{Na}^+$ ,  $\text{Mg}^{+2}$  and  $\text{K}^+$  increased drastically in both types of as received PSA.  $\text{Ca}^{+2}$  leaching of as-received PSA increased with acid addition from 1,000 mg/kg at pH 12.5 to about 115,000 mg/kg at pH 5.5 and reached the peak value of 220,000 mg/kg at pH 3. Similar comments can be made for  $\text{Na}^+$ ,  $\text{Mg}^{+2}$  and  $\text{K}^+$  with all reaching maximum leaching concentrations when extreme acidic conditions were imposed. It is notable, though, that in the case of  $\text{Na}^+$ ,  $\text{Mg}^{+2}$  and  $\text{K}^+$ , there was a difference in the amount leached between the two types of ashes. It was found that PSA\_UPM had higher leaching potential with lowering pH, which was up to approximately three times higher for  $\text{Na}^+$  and  $\text{K}^+$  and two times higher for  $\text{Mg}^{+2}$  when compared to corresponding leaching results for PSA\_ANP samples. This suggests the presence of soluble phases containing increased Na, K, Mg-salts found in

PSA\_UPM. It should be noted, however, that extreme acidic conditions are not common in the environment.



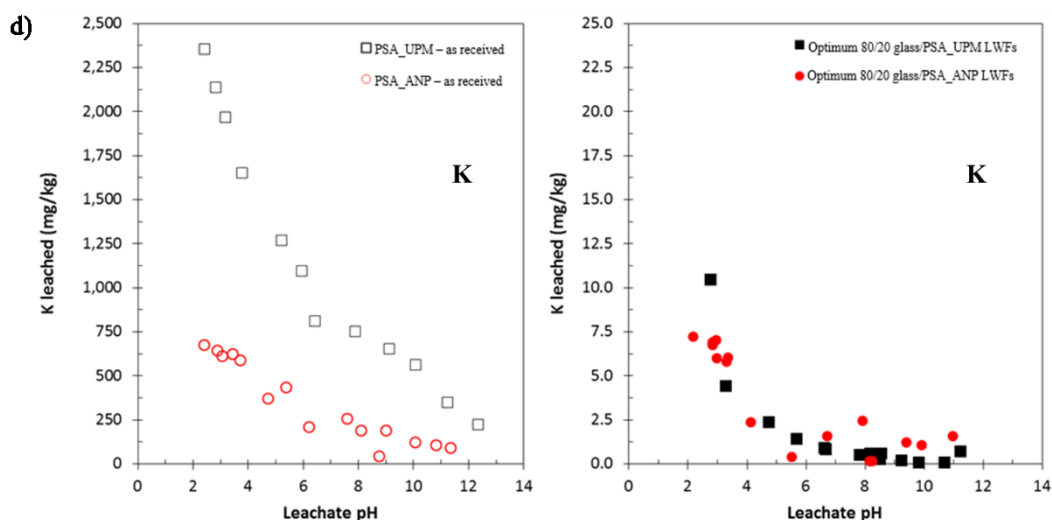


**Figure 5.22** Leaching data for (a) Ca, (b) Na, (c) Mg and (d) K as a function of leachate pH for the as received PSA\_ANP and PSA\_UPM samples (left column) as well as optimum LWFs produced after sintering optimised 80/20 glass/PSA mixes (right column) (n=15).

Leaching of  $\text{Ca}^{+2}$ ,  $\text{Mg}^{+2}$  and  $\text{K}^{+}$  was significantly reduced by two orders of magnitude for LWFs produced with a 20 wt. % addition in milled glass and sintered at 800 °C for 10 minutes when compared to as-received PSA samples. This reduction was still significantly higher than simply accounting for the expected dilution of PSA by glass, which took place to a moderate weight ratio of PSA:glass equal to 1:4. Sintering of optimised 80/20 glass/PSA mixes had a positive effect on leaching of  $\text{Na}^{+}$  minimising the leachability by three times in the case of 80/20 glass/PSA\_UPM LWFs and approximately two times for 80/20 glass/PSA\_ANP LWFs. Sintering significantly reduced  $\text{Ca}^{+2}$  leaching due to the formation of low solubility calcium-silicate minerals, such as wollastonite, and potentially due to incorporation into the glass matrix.

#### **b) Leaching of metals of environmental concern: Al, Fe, Zn, Mn and As**

Leaching data for  $\text{Al}^{+3}$  are presented in Figure 5.23. Given higher  $\text{Al}^{+3}$  concentrations in the as received PSA\_ANP samples, it is expected that leaching of  $\text{Al}^{+3}$  will be prevalent for this type of ash. Hence, leaching of  $\text{Al}^{+3}$  was two times higher for PSA\_ANP as opposed to PSA\_UPM. In both ashes, leaching of Al was recorded at pH regions below 4. Also,  $\text{Al}^{+3}$  became available and was leached from both types of PSA, after initial leaching of alkali and alkaline earth metals at higher pH was initiated. This suggests that  $\text{Al}^{+3}$  was present in less soluble amorphous aluminosilicates phases. Sintering reduces  $\text{Al}^{+3}$  leached concentration by two orders of magnitude in both types

of optimum LWFs. Hence, it can be inferred that much of the  $Al^{+3}$  was encapsulated in more stable crystalline phases.

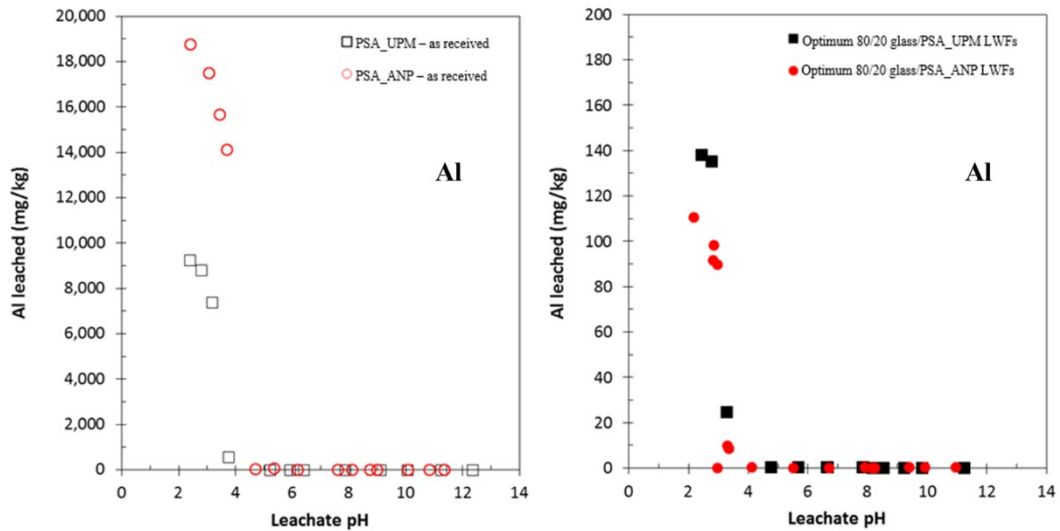


**Figure 5.23** Leaching data for Al as a function of leachate pH for the as received PSA\_ANP and PSA\_UPM samples (left) as well as optimum LWFs produced after sintering optimised 80/20 glass/PSA mixes (right) (n=15).

Leaching data for Fe and Zn are presented in Figure 5.24. Leaching of both Fe and Zn was more prominent for PSA\_UPM samples at low pH conditions. This could be attributed to differences in the feedstock material being incinerated in each mill. Sintered LWF particles exhibited no measurable leaching of Fe or Zn within pH regimes investigated. Hence, the elements were immobilised in the new crystalline phases formed during sintering.

Leaching data for Mn and As are presented in Figure 5.25. Leaching of Mn was again more prominent for as received PSA\_UPM samples at  $pH < 6$ . Maximum Mn release was 170 mg/kg at pH 2.5, which is not of concern given that natural soils have total Mn contents between 450 – 4,000 mg/kg soil (Adriano, 2001). Leaching of As, on the other hand, is of major environmental concern. As leaching was recorded to be in the range of 30 mg/kg for both as received PSA samples, being the maximum allowed level for soils by the UK Environment Agency (2009). Sintered LWFs, though, exhibit no As leachability, which either became inert in the ceramic matrix or decomposed during sintering given volatility of As-containing compounds at temperatures below 800 °C.

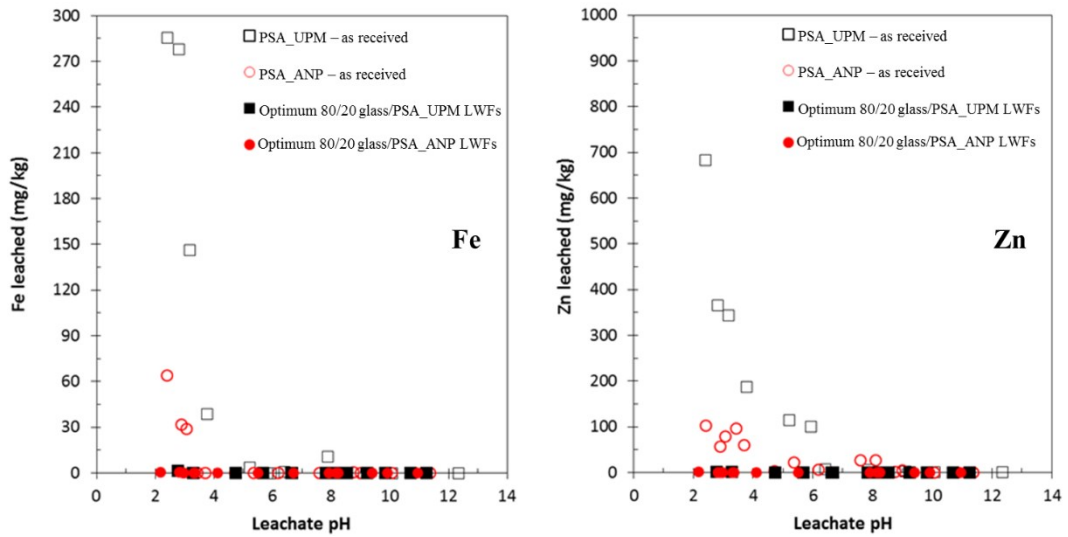


**Figure 5.24** Leaching data for Fe (left) and Zn (right) as a function of leachate pH for the as received PSA\_ANP and PSA\_UPM samples as well as optimum LWFs produced after sintering optimised 80/20 glass/PSA mixes (n=15).

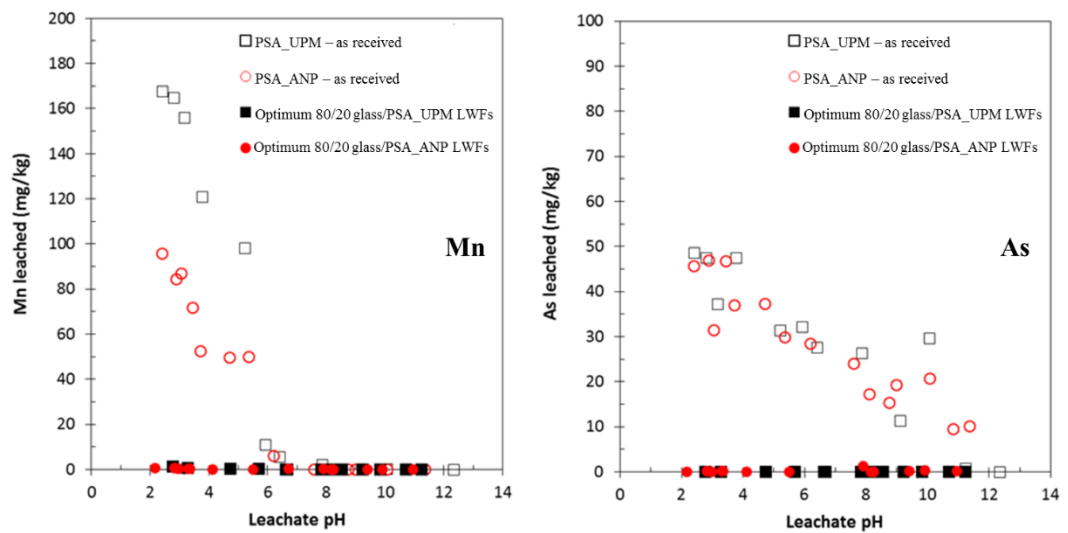


**Figure 5.25** Leaching data for Mn (left) and As (right) as a function of leachate pH for the as received PSA\_ANP and PSA\_UPM samples as well as optimum LWFs produced after sintering optimised 80/20 glass/PSA mixes (n=15).

### 5.6.3 Inclusive leaching behaviour

The metal composition determined by ICP-AES (as described in 4.3.7) of acid digested as-received PSA\_ANP and PSA\_UPM samples is given in Table 5.6. It can be seen that both types of PSA consist primarily of Ca, Al, Mg, K and Na. Trace metals, such as Zn, Mn, Fe, Cu, As and Pb are also present in both ashes. Maximum leaching concentrations of all elements were reported in low pH conditions. Optimum sintered LWFs prepared from 80/20 glass/PSA mixes, as detailed in section 5.6,

immobilised metals of environmental concern which were effectively encapsulated in the vitrified structure of end-products. This makes LWF production from post-consumer mixed colour glass and PSA a promising valorisation option for these materials.

**Table 5.6** Composition of metals on acid digested as-received PSA samples and corresponding maximum leaching concentrations of optimum 80/20 glass/PSA LWFs. Analysis was performed by ICP-AES (n=15).

Determinant	PSA – as-received (mg/kg)		Maximum amount leached from 80/20 glass/PSA LWFs (mg/kg)		
	ANP	UPM	ANP	UPM	at pH
Aluminium (Al)	19,300	10,450	115	139	2.9
Arsenic (As)	51	52	< 0.05	< 0.05	-
Barium (Ba)	56	41	0.6	0.9	2.9
Calcium (Ca)	201,300	223,120	1,380	1,460	2.9
Chlorine (Cl) <sup>1</sup>	334 ppm	0.27 ppm	195 ppm	< 0.1ppm	-
Chromium (Cr)	4.3	4.2	< 0.05	< 0.05	-
Copper (Cu)	87	12	< 0.05	1.0	2.9
Iron (Fe)	78	187	< 0.05	< 0.05	-
Lead (Pb)	89.3	89.2	< 0.05	< 0.05	-
Magnesium (Mg)	5,830	9,320	45	74	2.9
Manganese (Mn)	77	310	< 0.05	1.1	2.9
Nickel (Ni)	14	20	< 0.05	0.2	2.9
Potassium (K)	835	2,670	7.4	10.7	2.9
Sodium (Na)	430	1130	210	385	2.9
Sulphur (S) <sup>1</sup>	< 0.1	0.45	< 0.1	< 0.1	-
Titanium (Ti)	0.1	0.9	< 0.05	0.1	2.9
Vanadium (V)	5	32	< 0.05	< 0.05	-
Zinc (Zn)	115	720	< 0.05	2.0	2.9
Organic C (%) <sup>1</sup>	2.08	1.42	0.78	0.42	-

<sup>1</sup> The chlorides, sulphates and total organic content analysis was carried out at MEDAC Ltd, Surrey, UK. BaCl<sub>2</sub> and AgNO<sub>3</sub> were used as precipitating agents.

## 5.7 Concluding remarks

This chapter discussed the feasibility of producing LWF pellets via rapid sintering from waste mixed colour glass, simply called ‘*glass*’, and paper sludge ash (PSA) supplied by two major paper mills in the UK, Aylesford Newsprint and UPM-Shotton, denoted as ‘PSA\_ANP’ and ‘PSA\_UPM’ respectively. Simple processing technology involving wet milling, pelletising and low temperature sintering, following the paradigm of well-established commercial LWF manufacturers, such as Poraver<sup>®</sup>, was employed.

Full characterisation of the physical and chemical properties of glass and PSA samples was conducted in order to investigate suitability of the materials to form porous microstructures of low density and water absorption. Based on the results, PSA was found to be a refractory material at temperatures below 1180 °C as opposed to glass which started softening at 594 °C. Hence, glass addition was essential to promote sintering reactivity of ‘green’ pellets. Initial screening experiments revealed that only up to 50 wt. % of PSA combined with glass could result in strong sintered pellets, with lightweight structures obtained from low-PSA content mixes (up to 20 wt. % PSA). The two types of ashes exhibited different behavior during sintering, despite similar chemical compositions. This was attributed to the decomposition characteristics of each ash, as illustrated in the TGA analysis. PSA\_ANP presented greater weight loss compared to PSA\_UPM in the temperature range from 600 to 800 °C. This makes PSA\_ANP a stronger candidate as expanding agent for the development of foamed glass microstructures.

In order to address the aforementioned issues, holistic optimisation of all aspects of the process, including powder engineering, formation of ‘green’ pellets and control of sintering temperature and time, was performed. It was found that for the optimum temperature of 800 °C, determined from combining conclusions derived from preliminary experimental and TGA results, particle size of raw materials and sintering time were key parameters affecting the final microstructure. Hence, the joint effect of wet milling and sintering time on properties of 80/20 glass/PSA mixes treated at 800 °C was investigated. These mixes showed great potential to develop LWF materials. A summary of the optimum LWF properties obtained and the optimised conditions under which these were achieved is shown in Table 5.7. Optimum LWFs are compared against Poraver<sup>®</sup>, being the leading LWF product imported in the UK. Results demonstrate that the suggested process is less energy demanding compared to the Poraver LWF production, where the sintering temperature is 900 °C. At the same time, properties of recycled glass/PSA LWFs are comparable or improved to the Poraver ones. The strength-to-density ratios are up to two times higher compared to Poraver LWFs.

Leaching behaviour of selected constituents of environmental concern was also assessed to evaluate environmental impact from both as-received PSA samples and

optimum 80/20 glass/PSA LWFs. High levels of Ca, Na, K, Mg and Al were leached from both types of as-received PSA samples under acidic conditions (pH ~ 3). Results suggest that sintering helped remove, by means of volatilisation, or encapsulate these elements and other hazardous trace metals in new more stable crystalline phases present in the vitrified matrices formed. Hence, despite the fact that sintered LWFs have a low buffering capacity, their use in a wide range of applications can be recommended.

**Table 5.7** Key process parameters to obtain optimum LWF properties

Parameter/property	PSA ANP <sup>1</sup>	PSA UPM <sup>1</sup>	Poraver <sup>1</sup>
Composition (wt. %)	80/20 glass/PSA	80/20 glass/PSA	100 glass
Wet milling time (h)	1	4	na
Sintering temperature (°C)	800	800	900
Sintering time (min)	10	10	-
Pellet size (mm)	0.5 - 7.0	0.5 - 7.0	0.1 - 8.0
Particle density (g cm <sup>-3</sup> )	1.0 ±0.05	0.92 ±0.05	0.75 ±0.05
Loose bulk density (g cm <sup>-3</sup> )	0.60 ±0.05 <sup>2</sup>	0.46 ±0.05 <sup>2</sup>	0.26 ±0.05 <sup>2</sup>
Water absorption (wt. %)	23 ±2	46 ±5	113 ±10
Crushing strength(10) (MPa)	2.9 - 3.0	2.9 - 3.1	1.0 - 1.3
Strength-to-density ratio <sup>3</sup>	3.0	3.4	1.7

<sup>1</sup> All properties assessed relate to LWF particles of 5-7 mm in diameter.

<sup>2</sup> Loose bulk density was measured on LWF particles of 1-2 mm in diameter.

<sup>3</sup> Strength-to-density ratio was obtained by dividing maximum CS(10) by particle density.

The findings indicate significant potential for the manufacture of high-performance LWFs from PSA and recycled glass. In the next chapter, focus is, hence, placed on understanding the mechanisms controlling microstructural evolution during sintering for the glass/PSA binary system.

## CHAPTER 6 Microstructural evolution during sintering

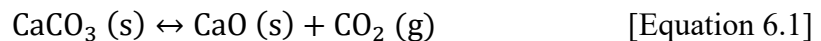
### 6.1 Introduction

A viable lab-scale process for producing lightweight filler materials from waste glass and paper sludge ash (PSA) was established and optimised, as described in Chapter 7. Wet milled glass/PSA mixtures of various particles sizes were processed into fillers through pan-pelletising followed by rapid sintering. The aim of this chapter is to underpin the mechanisms governing the process. Focus was placed on the thermodynamic aspects of the process with a view to enhance product quality and understand the effect of feedstock characteristics and process parameters on final properties.

Expansion of glass/PSA pellets during sintering was attributed to the presence of calcium hydroxide ( $\text{Ca(OH)}_2$ ) and calcium carbonates ( $\text{CaCO}_3$ ). The equilibrium partial pressures for decomposition of these components were calculated to determine the temperatures at which bloating was thermodynamically possible. A simple geometrical argument that explains the limitations of pore growth induced by gas evolution during sintering, accounting for the piercing of the grain molten shell, is also included.

### 6.2 Thermodynamic aspects of calcium hydroxide and calcite decomposition

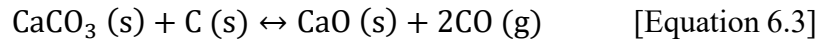
Expansion of a glass bubble by viscous flow is only possible if the pressure in the internal pores of the bubble exceeds the surrounding pressure. Since decomposition of calcite releases carbon dioxide gas ( $\text{CO}_2$ ) further decomposition will halt once the partial pressure of  $\text{CO}_2$  exceeds a critical value, which is a function of the sintering temperature. This can be easily demonstrated by considering the reaction:



The equilibrium constant of the above reaction is equal to the equilibrium partial pressure of  $\text{CO}_2$  according to:  $K = p_{\text{CO}_2}$  [Equation 6.2]

Equilibrium partial pressure of  $\text{CO}_2$  as a function of temperature is shown in Figure 6.1. This data was derived by using free energy data for calcite decomposition in the

SGPS-SGTE database supplied with Fact Sage (Bale et al., 2009), This suggests that the reaction can occur in pure CO<sub>2</sub> at 1 atm once the temperature reaches 1160 K (887 °C). Below this temperature, an embedded calcite particle cannot act as expanding agent given that decomposition will cease before the pressure in the bubble is equal to the surrounding pressure, i.e. the atmospheric. This is not in good agreement with the experimental observations suggesting that bloating of particles can take place at 800 °C. This was attributed to full decomposition of calcite in PSA taking place below that temperature based on TGA analysis of PSA samples. However, PSA also contains residual carbon (Table 5.6). In the presence of free carbon, calcite can decompose according to:



The equilibrium constant of Eq. 8.3 is given by:  $K = p_{\text{CO}}^2$  [Equation 6.4]

As shown in Figure 6.1, decomposition of calcite in the presence of free carbon inducing a pressure on the bubble-shell interface greater than 1 atm continues to take place between ~760 °C and 800 °C. This estimate justifies limited glass/PSA grain bloating during sintering below 800 °C. Hence, residual carbon potentially plays an enabling role in the expansion phenomena.

XRD patterns of PSA samples also indicate that the ash contains free lime, CaO, and/or Portlandite, Ca(OH)<sub>2</sub>. Since the wet milling and pan-pelletising process stages bring PSA particles in contact with water, it is conceivable that free lime is hydrated to Portlandite as well. The decomposition of Ca(OH)<sub>2</sub> is described by:



At high temperatures, the equilibrium constant for this reaction can be written as:

$$K = p_{\text{H}_2\text{O}} \quad [\text{Equation 6.6}]$$

It is clear from Figure 6.1 that this reaction will occur with partial pressures in excess of 1 atm from ~793 K (520 °C) onwards and can therefore, undoubtedly contribute to the expansion of the lightweight fillers.

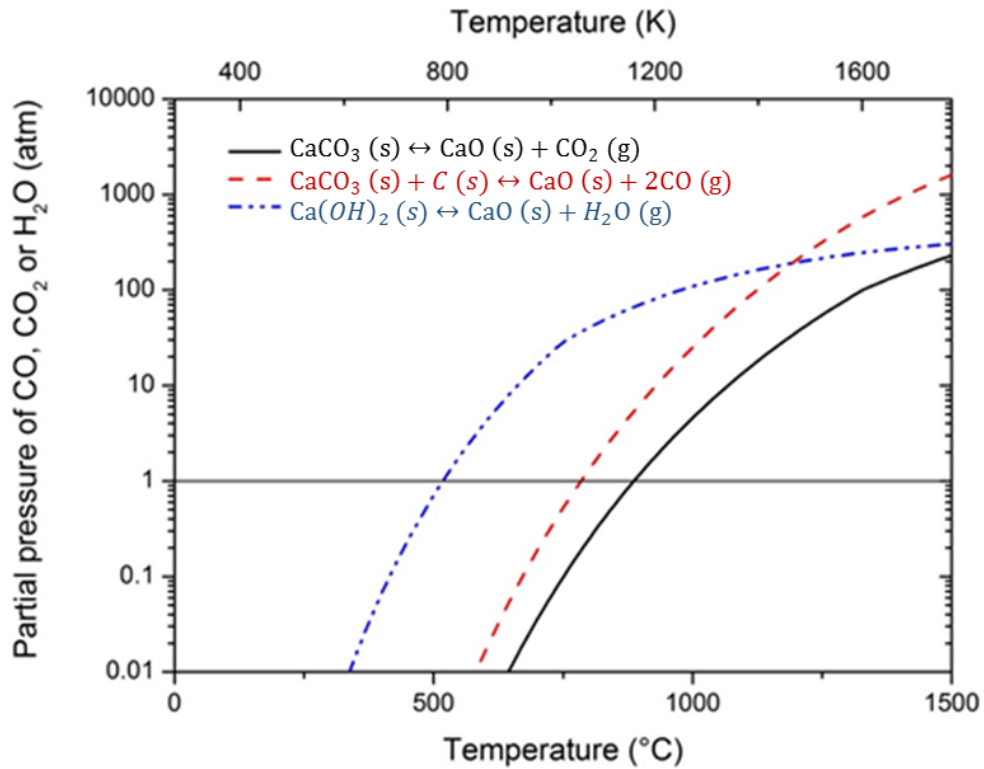


**Figure 6.1** Equilibrium partial pressure of CO, CO<sub>2</sub> or H<sub>2</sub>O as a function of temperature for the decomposition reactions of CaCO<sub>3</sub> (in the absence or presence of free carbon) and Ca(OH)<sub>2</sub>, which could contribute to bloating during rapid sintering provided the sum of the equilibrium partial pressures exceeds 1 atm.

Decomposition of Portlandite and subsequent evolution of water vapour at lower temperatures is also likely to affect glass viscosity. In a study by Matamoros-Veloza et al. (2008), it was highlighted that bound water affected the pore formation during sintering of CRT TV glass, with controlled increasing water content resulting in density decrease. Steam diffused into the glass structural network leads to steady decrease in the glass viscosity and transition temperature  $T_g$  during sintering (Sigoli et al., 2003; Giordano et al., 2008). This effect has been extensively exploited for the expansion of silicate volcanic rocks at high temperatures (700-1300 °C) to produce porous media (Angelopoulos et al., 2013; Klipfel, 1998). In addition to effective bound water content able to give rise to pores during heat treatment of glass/PSA mixes, the molecular concentration of network modifiers such as Na<sub>2</sub>O, K<sub>2</sub>O, MgO, and CaO enable glass melting at lower temperatures (Avramov et al., 2005).

### 6.3 Viscous growth of pores during sintering

The lightweight microstructure is the result of pore formation due to gas evolution and entrapment during sintering. In Chapter 5, when mixing waste glass powder with PSA\_ANP and PSA\_UPM at a weight ratio of glass:PSA = 4:1 followed by rapid sintering, it was assumed that it was predominantly due to the decomposition of calcite content in PSA and the encapsulation of CO<sub>2</sub> gas that highly porous structures were obtained under optimised process conditions. However, maximum porosity is either limited by the amount of calcite present, and hence also by the amount of gas that can be evolved, or when excess gas is present by the piercing of the external walls of the particles. In the case of mechanical deformation of the molten matrix, when high pressures are exerted on the bubble-shell interface, further gas evolved simply escapes from the particle through channel cracks formed.

In principle, if the geometry is that of a spherical pore in a spherical body, the increase in volume could reach its maximum provided the outer walls of the particle resist the pressure developed from gaseous species. However, when many gas particles are growing simultaneously in cells, the cells form a tetrahedron-like stacking (Timoshenko & Goodier, 1984). For such an arrangement, the outer shell of the structure does not necessarily grow at the same rate as the internal pores. This implies that wall piercing will occur.

#### 6.3.1 Volumetric expansion of glass/PSA mixes: Geometrical aspects

It is assumed that each calcite/Portlandite particle in the glass/PSA mixture will give rise to a single pore, which will grow as long as gas evolves from it. By calculating the volume of gas evolved from decomposition of calcium carbonate – even if the molar volume of an ideal gas (22.4 L) at 25 °C and 1 atm pressure is used – it can be shown that the size of the gas bubble upon complete decomposition will be about 8.5 times the size of the particle from which it originated. The size ratio increases to 13.4 when the volume is corrected to a furnace temperature of 800 °C. Therefore, a 5 µm calcite particle can make a pore of about 67 µm, and a 50 µm calcite particle can make a pore of about 668 µm. Given that the mean particle size of the both PSA samples is ~150 µm – although it must be highlighted that these are agglomerated particles – large pores are expected to grow from a single particle.

In the first instance, it will be assumed that there is excess gas. Predicting the structure then, starting from a dense body, becomes a matter of trying to capture at which points the different pores will be interconnected. Since glass and PSA are thoroughly mixed, it is assumed that the calcite particles are homogeneously distributed in the mixtures. Density of pellets at the first sintering stage of ‘heating’, when solely viscous phases are formed with no gas evolution and encapsulation taking place, is assumed to be high. This was verified by initial increase in particle density of sintered particles for sintering times below 5 minutes for both glass/PSA\_ANP and glass/PSA\_UPM mixes.

The microstructure can be projected by considering the volumetric increase of a simple cube before growth of a single pore in its centre pierces the outer walls of the cube. Starting from a cube of edge length  $a_0$ , its original volume, at initial solid densification stage of sintering, is given by:

$$V_{s(t=0)} = a_0^3 \quad \text{[Equation 6.7]}$$

The original pore size,  $D_0$ , is zero. As the pore size increases, the pore volume,  $V_p$ , is given by:

$$V_p = \frac{\pi}{6} D^3 \quad \text{[Equation 6.8]}$$

As long as the pressure in the gas bubble is higher than the pressure surrounding the particle, there will be a driving force for volumetric expansion. The particle will grow until the total volume of the particle is equal to the sum of the volume of the gas at 1 atm and the volume of solid matrix:

$$V_{tot} = \frac{\pi}{6} D^3 + a_0^3 \quad \text{[Equation 6.9]}$$

It is also assumed that the cube retains its shape during expansion. The edge length of the expanded cube,  $a$ , is given by:

$$a = (V_{tot})^{1/3} = \left(\frac{\pi}{6} D^3 + a_0^3\right)^{1/3} \quad \text{[Equation 6.10]}$$

Both the cube and the pore diameter increase with increasing gas release during sintering. The maximum size of the cube,  $a_{max}$ , is expected when wall piercing occurs preventing further gas entrapment and pore growth. The condition for this is that pore diameter,  $D$ , equals  $a_{max}$ , as follows:

$$a_{max} = \left(\frac{\pi}{6} a_{max}^3 + a_0^3\right)^{1/3} \quad \text{[Equation 6.11]}$$

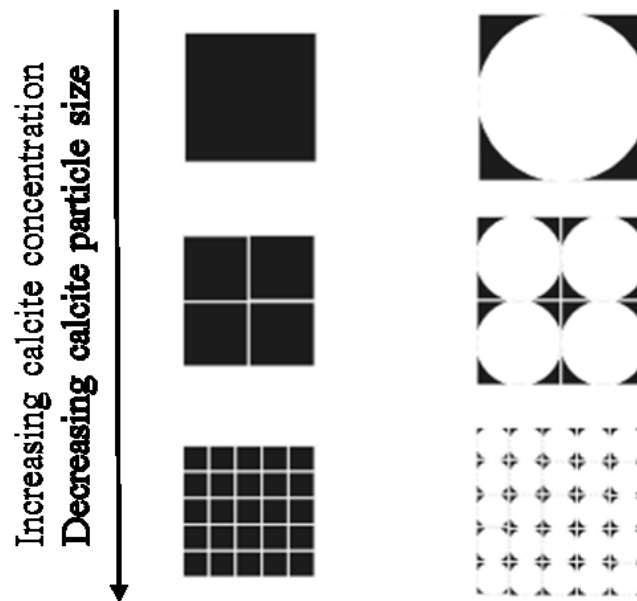
Solving equations 6.10 and 6.11 for the volume ratio yields:

$$\frac{V_{max}}{V_{s(t=0)}} = \frac{a_{max}^3}{a_0^3} = \frac{6}{6-\pi} = 2.10 \quad [\text{Equation 6.12}]$$

The maximum volume attained for a cube cell owing to the growth of a single spherical pore can be approximately twice the size of the initial volume, when gas becomes trapped in the sintered body. This corresponds to an increase in size of:

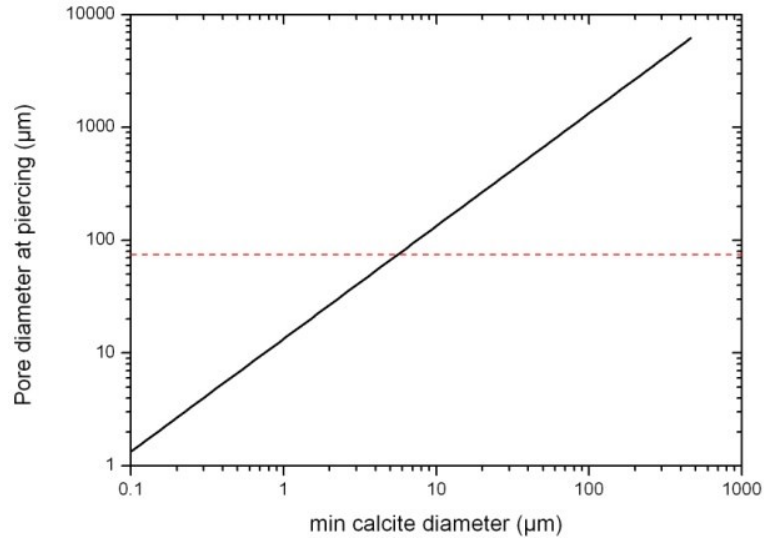
$$\frac{a_{max}}{a_0} = \left(\frac{6}{6-\pi}\right)^{1/3} = 1.28 \quad [\text{Equation 6.13}]$$

Figure 6.2 illustrates schematically that these relations scale with the original size of the cube surrounding a single calcite particle. Hence, the final pore size will depend on the distribution of PSA, i.e. the expanding agent in the mix. The relationship between calcite particle diameter and final pore size can be quantified by assuming calcite particles are evenly distributed in the ‘green’ pellet and that external shell piercing coincides with the largest size a pore can reach.



**Figure 6.2** Schematic of single pores growth into a grid of regular cubes. Single-bubble hollow spherical will give rise to the same scaling during growth and hence the pore size depends on the distribution of the pore former.

As shown in Figure 6.3, the pore sizes at piercing suggest the calcite particles are at least 5  $\mu\text{m}$  in size, which seems reasonable given the particle size distribution of PSA samples. The volume fraction calcite needed to obtain such a porous structure is only about 0.05 % v/v, which confirms that in the 80/20 glass/PSA mixes there will be excess gas.



**Figure 6.3** Predicting final pore size: Maximum pore diameter at piercing as a function of the calcite diameter (black line). The dashed red line indicates a typical pore size at piercing for samples with 20 wt. % ANP ash suggesting the calcite particles are at least 5  $\mu\text{m}$  in size.

Simple geometrical considerations suggest that gas evolution from PSA will be capable of doubling the volume of the particles after sealing before piercing of the outer shell occurs. This is in alignment with the experimental data for optimum 80/20 glass/PSA mixes shown in Figure 5.14a, c: peak densities reached during sintering of 80/20 glass/PSA\_ANP (1h wet milling) and 80/20 glass/PSA\_UPM pellets (4hs wet milling) at 800 °C were 1.85  $\text{g}\cdot\text{cm}^{-3}$  and 1.82  $\text{g}\cdot\text{cm}^{-3}$  with corresponding optimum final densities of  $1.00\pm 0.05$  and  $0.92\pm 0.05$   $\text{g}\cdot\text{cm}^{-3}$  respectively. Hence ignoring any mass loss, the volume ratios are:

$$\text{For glass/PSA\_ANP sintered pellets: } \frac{V_f}{V_0} = \frac{1.85}{1.00} = 1.85 \quad [\text{Equation 6.14}]$$

$$\text{For glass/PSA\_UPM sintered pellets: } \frac{V_f}{V_0} = \frac{1.82}{0.92} = 1.98 \quad [\text{Equation 6.15}]$$

The above ratios fall within the predicted ratio of 2.10 (equation 6.12), allowing for a  $\sim 10\%$  difference between experimental and calculated density values. Hence the geometrical calculation, although highly idealized, describes adequately the limitations on volumetric expansion of lightweight materials during sintering. The size of pores will depend on the calcite particle size and concentration as well as the distribution of PSA in the mix which defines the uniformity of pore formation during sintering. During sintering, the dynamic balance between decreasing viscosity of the siliceous components of the mix and gas evolution from the thermally instable species

in PSA needs to be achieved, by means of controlling the sintering time, before relative sample expansion ratios exceed the values calculated from Equations 6.14 and 6.15.

#### **6.4 Concluding remarks**

Thermodynamic calculations of the equilibrium partial pressure of the decomposition of calcite shows that the partial pressure of CO<sub>2</sub> only reaches 1 atm at 885 °C. This reaction standalone can therefore not be responsible for the expansion of sintered 80/20 glass/PSA particles at 800 °C. However, the calcite decomposition can a pressure of 1 atm at 800 °C if the decomposition of Portlandite and/or burning of residual organic carbon in the ash contribute to the gas formation.

A simple geometric argument was developed to obtain the boundaries for density decrease attained when air-filled bubbles are growing from evenly distributed expanding agents particles. In the highly idealised scenario of a spherical pore growing in a cubic solid volume, the volume can increase by a factor 2.10 before piercing of the cell walls occurs. Despite the simplistic calculation, this prediction does capture the changes in volume observed during lab-scale experiments. Although, in theory, the blowing of a single spherical bubble inside a spherical body could lead to greater volumetric expansion, and hence lower density, the instable viscous growth means that the volume will realistically not increase more than by a factor of 3.33 for this geometry too.

## **CHAPTER 7 Cement mortars: A viable application for glass/PSA LWFs**

### **7.1 Introduction**

This chapter, being the final part of the study on glass/PSA LWF manufacture and end-uses, aims to set a tangible example of upcycling waste streams by innovative product design and development. The prospect to produce lightweight cement mortars with improved thermal-insulation characteristics by incorporating optimum glass/PSA LWF particles, as these were developed from the optimisation study detailed in Chapter 7, was examined. In addition to thermal-insulation and lightweight-associated benefits, recycled glass/PSA LWFs, owing to improved mechanical performance, are considered suitable for use in concrete-based structural components. On the contrary, it needs to be stressed that commercially available LWFs Poraver<sup>®</sup> are primarily used as insulating fill material.

The following series of experiments aimed to substantiate the potential of optimum glass/PSA LWFs in applications where thermal insulation is required. Hence, focus was placed on assessing the heat insulating properties of the lightweight cement mortars produced. Physico-mechanical characteristics were also tested to ensure product alignment with existing standards for masonry mortars.

### **7.2 Materials and preparation of mortars**

All mortar samples were prepared as described in section 4.2.2. The materials used in the preparation of different mixes were given in section 1.1.1. The specific gravity of sand and CEM II used were  $2.6 \text{ g cm}^{-3}$  and  $3.2 \text{ g cm}^{-3}$  respectively. No additives were used to improve the integrity of the mortars given that standard mixes of cement, sand and water gave promising results. Further optimisation of the formulations was out of scope in this study.

Sand substitution with glass/PSA\_ANP, glass/PSA\_UPM and Poraver<sup>®</sup> LWF particles of 1-2 mm in diameter was done on a by weight percentage basis (% w/w). The properties of optimum glass/PSA and Poraver LWFs are given in Table 5.7. The mix designs are shown in Table 7.1. Control samples contained no LWFs, with LWFs systematically replacing sand up to 40 % by mass. A 60 % w/w replacement of sand

by LWFs was also attempted but resulted in non-workable mortar samples. The quantity of water in the mix was kept fixed at a water: cement ratio equal to 0.5. This resulted in flow table slump of approximately 130 mm, which is classified as 'stiff' mortar according to BS EN 1015-6 (British Standards, 1999). Samples were tested in triplicates and the average value of these measurements is reported herein.

**Table 7.1** Composition of mortars containing optimum glass/PSA and Poraver LWFs. Water was added at a fixed water: cement ratio of 0.5. No additives were used.

	Sample ID	Cement (w/w %)	Sand (w/w %)	LWFs (w/w %)
Control mortar	CM	25	75	0
Poraver	10P	25	67.5	7.5
Poraver	20P	25	60	15
Poraver	40P	25	45	30
UPM	10UPM	25	67.5	7.5
UPM	20UPM	25	60	15
UPM	40UPM	25	60	40
ANP	10ANP	25	67.5	7.5
ANP	20ANP	25	60	15
ANP	40ANP	25	45	30

## 7.3 Results and discussion

### 7.3.1 Workability and water absorption

Workability tests were used to determine whether mortar samples with a fixed water/cement ratio of 0.5 could be developed when sand grains are partially substituted by LWFs to produce lightweight cement mortars. Dry, approximately spherical LWF particles of 1-2 mm in size were used. These had an open porosity, calculated according to Equation 6.8, of 23 %, 42 % and 19 % corresponding to glass/PSA\_ANP, glass/PSA\_UPM and Poraver LWFs. Given the presence of porous materials in the mix, water uptake by the pores of the permeable fillers followed by a decrease in the workability of the paste was expected. However, as it can be deduced from workability results shown in Figure 7.1, partial replacement of sand grains by LWFs did not have a significant effect on the workability of the mortars. Within experimental error, mortars containing LWFs up to 40 % w/w have similar workability properties with control mortars samples, with workability values ranging between 120 and 130 mm.

It was only the mortars prepared with glass/PSA\_ANP fillers at 40 % w/w sand substitution that exhibited a low workability of 110 mm. This can be attributed to greater external volume and pore size of such fillers meaning that pores found on the external surface are being saturated with water at an extremely rapid rate when in contact with the available water in the cement paste. Lydon (1972) appreciated that up to 80 % of final water absorption (attained after 24 hours) of a lightweight materials is reached within the first 30 minutes of samples immersed in water. This was confirmed by Valum (1995) when measured the water absorption of different types of expanded clays and shales after 1 hour and 24 hours of submersion in water. Although glass/PSA\_UPM and Poraver LWFs had slower water absorption rates, besides greater or similar with glass/PSA\_ANP open porosity values, further sand replacement by LWFs produced non-workable mortar mixes at the given water/cement ratio condition. Pre-saturation of LWFs used in the mix and/or addition of superplastizicer or water retaining additives could be considered to alleviate such problems (Ferrandiz-Mas et al., 2014).

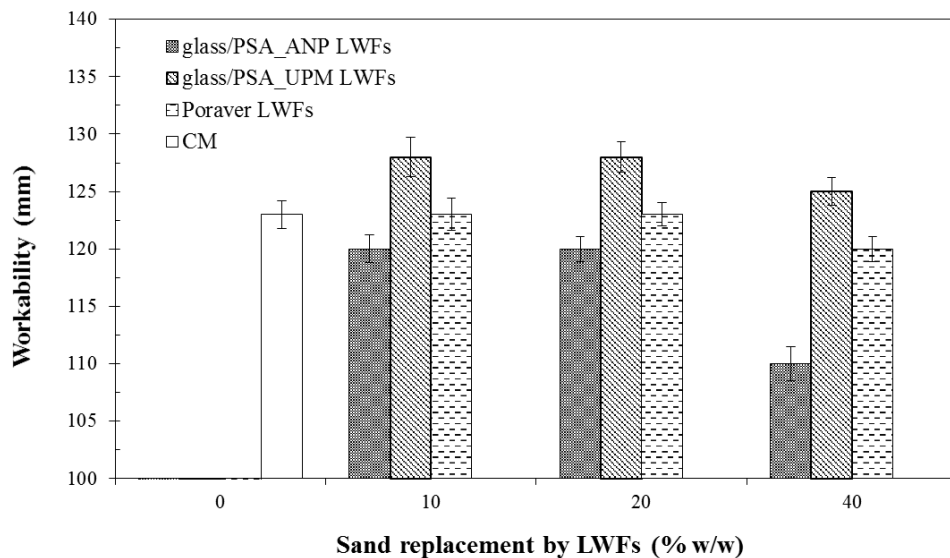


**Figure 7.1** Effect of sand replacement by optimum glass/PSA and Poraver LWFs on workability of cement mortars. CM is the control mortar prepared with a cement:sand:water = 1:3:0.5. The w/c ratio was kept fixed for all samples (n=5).

Many researchers have reported that pre-saturation of lightweight materials used in cement pastes can effectively reduce the amount of mixing water, hence, minimising the risk of early-age cracking during hydration and improving durability of end-products (Zhutovsky et al., 2004; Radlinska et al., 2008; Shen et al., 2015; Henkensiefken et al., 2009). In this study, LWF pre-saturation was not considered

given that water absorption of cement mortars did not alter significantly with the incorporation of LWFs, as shown in Table 7.2. In fact, LWF incorporation led to a decrease in water absorption of mortars up to 25 %, in the case of the 40 % w/w sand replacement by optimum glass/PSA\_ANP filler particles. This corroborates Clarke's (1993) findings on the positive effects high-quality, consistent cement matrix can have on water absorption reduction in lightweight aggregate concrete mixes. It also suggests that, despite initial uptake of water into the pores of fillers, due to the closed cell structure of LWFs used, that water is released back to the cement matrix and becomes available for the hydration reaction. This helps reduce the cracking potential that cement systems with low w/c typically have (Maruyama et al., 2009; De la Varga et al., 2012). Early self-desiccation, i.e. internal drying, was observed when attempted to prepare samples with 60 % w/w sand replacement by LWFs.

**Table 7.2** Water absorption (wt. %) of cement mortars prepared with optimum glass/PSA and Poraver LWFs (n=5).

Sample ID	Water absorption (wt. %)
CM	6.3
10P	6.8
20P	6.2
40P	5.1
10UPM	6.1
20UPM	6.0
40UPM	5.2
10ANP	5.1
20ANP	5.0
40ANP	4.7

### 7.3.2 Dry bulk density and thermal conductivity

The effect of sand replacement by optimum glass/PSA and Poraver LWFs on dry apparent density of cement mortars is shown in Figure 7.2. The predicted density values of mortar samples were calculated according to:

$$\text{Dry apparent density of mortar sample (g} \cdot \text{cm}^{-3}\text{)} = \left( \sum_i \frac{m_i}{\rho_{s,i}} \right)^{-1},$$

where  $m_i$  is the mass fraction of each of the participating constituents of the mix (i.e. sand, cement, LWFs, water) and  $\rho_{s,i}$  is the corresponding apparent density of that

constituent. The calculated density values for the various groups of design mixes are represented by the lines in Figure 7.2.

As expected the density of mortar samples decreased when high density sand particles are replaced by porous and hence lower density LWFs. Control mortar (*CM*) samples had a density of  $2.27 \text{ g}\cdot\text{cm}^{-3}$ , which was similar to the calculated value of  $2.29 \text{ g}\cdot\text{cm}^{-3}$ . Significant decrease in mortar density was achieved when sand was substituted with all types of LWFs by 40 % w/w, with mortar samples containing Poraver, glass/PSA\_ANP and glass/PSA\_UPM particles having a density of 1.50, 1.73 and  $1.62 \text{ g}\cdot\text{cm}^{-3}$  respectively. Overall, the fact that calculated and experimental density values are similar implied that total porosity of mortar samples is low, with no significant air entrapment during the mixing and internal curing of samples. Hence, any effect on the thermal properties will be due to the incorporation of LWFs and not due to changes in air entrapment between the different mixes.

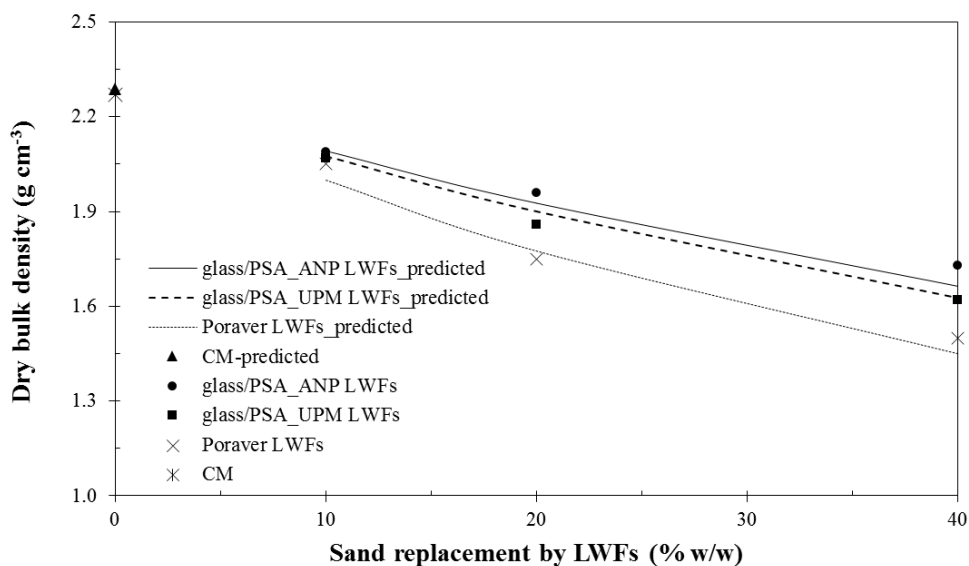


**Figure 7.2** Effect of sand replacement by LWFs (% w/w) on density ( $n=5$ ). *CM* is the control mortar prepared with a cement:sand:water = 1:3:0.5. Lines represent predicted density values based on the mass fraction and skeletal density of each of the mix components.

Figure 7.3 depicts the effect of sand replacement by LWFs on thermal conductivity of dry samples cured for 28 days. Thermal conductivity measurements were conducted as described in 4.3.10. Each point represents the average of thermal conductivity values obtained after testing five faces of two mortar samples. A 40 % w/w sand replacement by LWFs decreased thermal conductivity of mortar samples by 28 % on

average. This is attributed to the air voids due to the porous particles in the mortar matrix. It is also indicative of the expected increase in volume of the mortar by two times on average for any specific sand fraction substituted on a per weight basis, owing to the high inherent skeletal density of sand ( $3.60 \text{ g}\cdot\text{cm}^{-3}$ , measured by He pycnometry) compared to LWFs (skeletal densities were:  $1.52 \text{ g}\cdot\text{cm}^{-3}$  for glass/PSA\_UPM,  $1.77 \text{ g}\cdot\text{cm}^{-3}$  for glass/PSA\_ANP and  $1.83 \text{ g}\cdot\text{cm}^{-3}$  for Poraver LWFs).

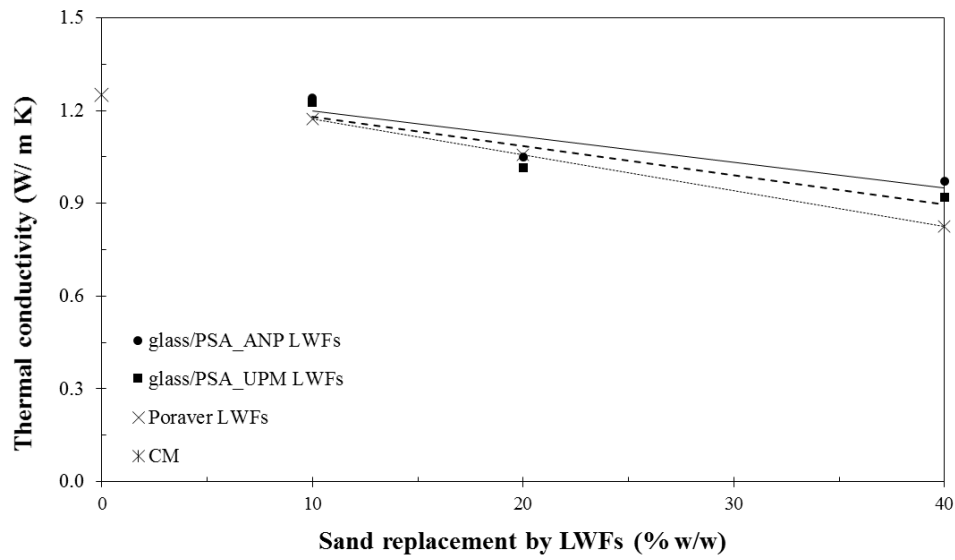


**Figure 7.3** Effect of sand replacement by LWFs (% w/w) on thermal conductivity of mortar samples ( $n=5$ ). Dry samples were used to assess the thermal conductivity using a TT-TC probe. Five faces of samples were tested and average values are reported.

Given that air has low thermal conductivity ( $0.026 \text{ W/m}\cdot\text{K}$ ), it acts as an effective thermal insulator (Wang et al., 2005). Hence, Poraver LWFs, having the highest total porosity of 66 %, when replacing sand into mortars at 40 % w/w, resulted in a decrease in thermal conductivity by 34 % compared to control mortar samples. LWFs from glass/PSA\_ANP and glass/PSA\_UPM in samples with 40 % w/w sand replacement decreased thermal conductivity of mortars by 22 % and 26 % respectively. The effect of total porosity of LWFs on thermal conductivity of mortars becomes more important as the sand replacement by LWFs increases. This data agrees with previously published results (Khedari et al., 2001; Kralj, 2009).

### 7.3.3 Compressive strength and microstructure

Compressive strength data for mortar samples after 28 days curing are shown in Figure 7.4. The compressive strength of control mortar was 46.3 MPa. While there is a

tendency for the compressive strength to decrease with increasing amount of sand replacement with LWFs, replacement levels of 10 and 20 % w/w gave compressive strength values very similar, and in fact slightly higher, than the reference control mortar. This is consistent with higher bulk density values observed for these specimens as shown in Figure 7.5, which correlates density to compressive strength. Of the three replacements, the lowest compressive strength values were recorded for samples prepared with the more porous Poraver LWFs. Apart from the higher porosity contributing to lower strength, the lower crushing strength values for Poraver LWFs might also contribute.

The effect of sand replacement by LWFs on compressive strength of mortars became stronger in the 40 % w/w sand replacement case. This could be explained by either the lower crushing strength of LWFs compared to sand grains or by less effective particle packing of LWFs given the narrow grain size distribution (ranging from 1 to 2 mm) used to replace sand in mortars. Yu et al. (2013) suggested a methodology to design mixes addressing the latter issue that could help improve mechanical properties of cement-based lightweight materials.

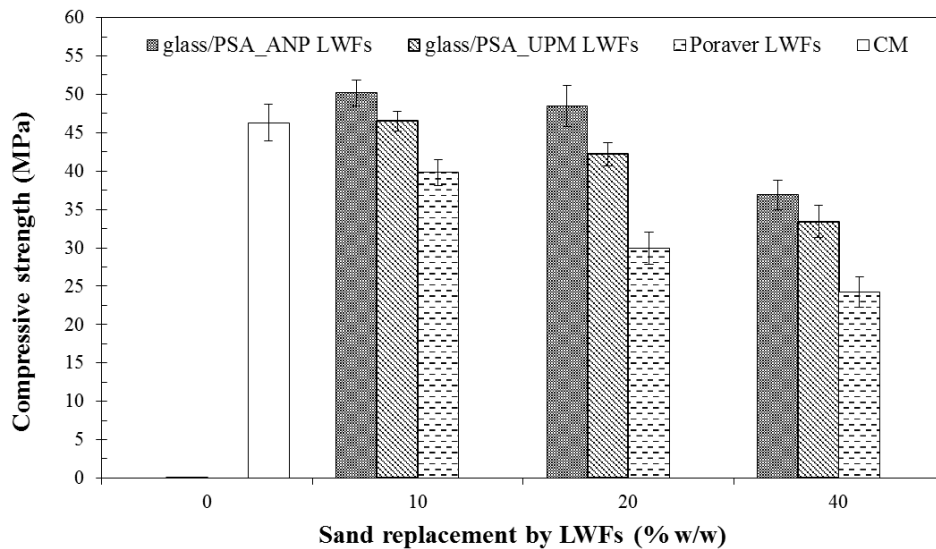


**Figure 7.4** Effect of sand replacement by LWFs (% w/w) on the 28-day compressive strength of saturated mortar samples (n=5).

The increase of lightweight materials in the cement-sand matrix did not cause any disintegration problems in contrast to the report by de Gennaro et al. (2009). All samples produced had high compressive strength which makes them suitable for use in construction applications. For comparison, according to standards BS EN 998-1, 2

(British Standards Institution, 2001; 2003), mortars for masonry and plastering should have compressive strength between 04. – 2.5 MPa. Given high compressive strength for all mortars produced throughout this study, their use in load-bearing elements could also be proposed.

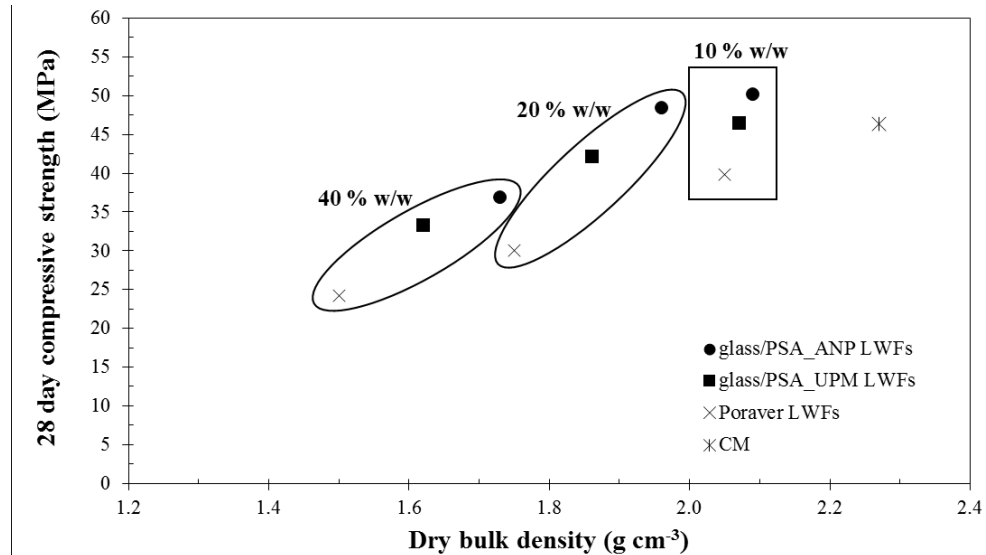


**Figure 7.5** Correlation between dry bulk density of mortars and 28-day compressive strength. Within each subgroup of samples prepared with different % w/w of LWFs, a decrease in strength was observed with decreasing density.

The good performance of the mortars in this work is attributed to the fact that lightweight fillers were evenly distributed across the volume of mortar samples during moulding as well as during curing. Figure 7.6a shows a cross-section of mortar specimen containing 40 % w/w of glass/PSA\_UPM fillers. The filler particles were present in the cement matrix in a uniform manner, alike sand grain distribution in the control mortar samples (Figure 7.6b). Figure 9.6c confirms that no porosity was found in the filler-cement paste interfacial transition zone. The cement matrix adhered well to the LWF particles without phenomena of local densification or clustering observed at the boundary. Moreover, the LWFs on the whole are more rounded and contain less sharp corners, which aids in avoiding stress concentrations. This explains the decent mechanical properties of mortar samples even at the highest LWF addition rate tested (40 % w/w sand). Controlled water absorption by porous particles could also mean that water is not accumulated in the vicinity of the LWFs leading to a narrow interfacial zone with low porosity. This has been reported to act in favour of higher compressive strength (Ducman & Mirtiç, 2014; Lo et al., 2008).

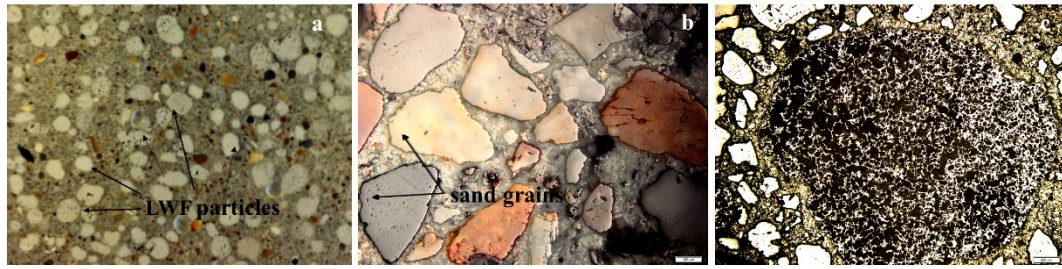


**Figure 7.6** Morphology of lightweight cement mortars: a) Image of cross-section of mortar samples containing 40 % w/w of glass/PSA\_UPM LWFs, b) Optical microscopy micrograph of control mortar showing the distribution of sand grains in the cement matrix and c) LWF particle bonded with the cement paste in mortar sample shown in (a). No pores were developed in the interfacial transition zone of the filler-cement matrix.

#### 7.4 Concluding remarks

This chapter explored the potential of using the optimum LWF materials manufactured from waste glass and paper sludge ash (PSA) in cement mortars. A standard mix of cement (CEM II), normal sand and water at a weight ratio of cement:sand:water equal to 1:3:0.5 was used. Partial substitution of sand by LWFs was possible up to 40 % w/w of sand had no negative effect on the workability of mortars. The workability values achieved, using the flow table method, were below 140 mm, meaning that all mortar samples are characterised as ‘stiff’. Further increase of LWFs in the mortar mix resulted in detrimental decrease in the workability. Adjusting the water content and/or addition of superplasticisers could potentially improve the rheology of the mixes but was not investigated.

Bulk density of mortars reduced with increasing LWF content at a rate approximately following the sand replacement rate. This was expected given the lower particle density of LWFs compared to the sand grains they replaced. Control mortar samples had a bulk density of  $2.29 \text{ g cm}^{-3}$  and that decreased by 35 % on average for samples containing 40 % w/w of LWFs. Lowest bulk density values of  $1.5 \text{ g cm}^{-3}$  were achieved when Poraver particles were used in such mixes. Mortars prepared with optimum glass/PSA\_ANP and glass/PSA\_UPM LWFs had similar densities for any given LWF percentage addition, with glass/PSA\_UPM LWFs resulting in marginally lower mortar densities owing to the lower inherent particle density of these fillers. Low mortar densities were solely attributed to the low density of LWFs and are not

associated with increase in total porosity of samples verified by no significant variations in water absorption of mortars.

Despite low density values, the compressive strength of saturated mortar samples after 28 days of curing were above 25 MPa. Control mortar samples had a compressive strength of 46 MPa. Mortars prepared with Poraver LWFs had the lowest strength values. Compressive strength and bulk density are inversely related. Hence, mortars prepared with glass/PSA\_ANP have improved mechanical properties compared to those containing glass/PSA\_UPM. Sand replacement by glass/PSA\_ANP LWFs up to 20 % w/w resulted in compressive strength increasing by 15 % on average. This can be attributed to optimised bonding between LWF particles and the surrounding cement paste. In general, enhanced mechanical properties of mortar samples containing optimum glass/PSA LWFs compared to those containing Poraver can be justified by higher crushing strength values for this type of materials.

Thermal conductivity of control mortar samples, measured by the TT-TC method, was 1.25 W/ m·K. This decreased by up to 34 % and 22 % in the case of sand replacement by Poraver and glass/PSA LWFs respectively. Decrease in thermal conductivity is associated with total porosity of LWFs. Air-filled voids present in LWFs act as thermal insulators.

Mortars prepared with optimum glass/PSA LWFs have similar or improved properties, in terms of mechanical and thermal insulation performance, compared to the commercial Poraver LWFs. Hence, lightweight cement mortars are a potential viable end-application for glass/PSA LWFs produced in this work.

## CHAPTER 8 PSA-based hydrophobic materials

### 8.1 Introduction

As detailed in previous chapters, grinding was a key step of the production process of LWFs from waste glass and PSA. For that process, initial experiments involved dry milling of high-PSA content mixes in a ball mill. The particles showed high agglomeration during dry milling and hence, stearic acid ( $C_{18}H_{36}O_2$ ) was used as a dispersive medium. Stearic acid, amid other surfactants, has been widely used for the treatment of ceramic powders, such as zirconia (Trunec et al., 2000; Liu et al., 2011) and alumina (Tseng, 2000; Chan & Lin, 2005), to improve their rheological properties prior to injection molding and sintering. In all such cases, adhesion of the surfactant to oxide surface through the functional group carboxyl [-COOH] and orientation of the alkali chain towards the binder mix served to promote wettability of the ceramic powders and lower viscosity of the mixture. In contrast, dry milling PSA with stearic acid resulted in hydrophobisation of the mineral material, which could not be subsequently mixed with water and pelletised to form ‘green’ filler particles. Although dry milling was discarded for grinding PSA and glass/PSA mixes as part of the production process of LWFs, production of hydrophobic PSA was investigated. The production of a hydrophobic powder from PSA was an exciting development in this research project because it represents a high-value use with numerous applications.

Engineering applications where hydrophobic coatings bring tangible benefits include self-cleaning building facades with greater resistance to bio-deterioration, algal growth and general soiling (Spaeth et al., 2006). Other important uses for hydrophobic coatings include bio-fouling-resistant ship hulls and marine infrastructure, anti-icing surfaces and corrosion-resistance applications (Chambers et al., 2006). Finally, the use of hydrophobic agents or additives in concrete mixes is of particular importance for the construction industry. Such additions protect concrete from water ingress and damp, which is associated with deterioration of reinforced concrete assets (Concrete Society, 2013).

Waterproof materials have been inspired by natural systems exhibiting excellent water-repellent and self-cleaning properties, with the most well-known being that of the lotus leaf, described as the ‘*lotus effect*’ (Barthlott & Neinhuis, 1997). This effect

has also been observed in different plants and insects such as rose petals (Feng et al., 2008), cabbage and garden peas (Shirtcliffe et al., 2010), butterfly wings (Fang et al., 2008) and insect wings (Ko et al., 2009). Micro- and nanoscale structures on the surface of these surfaces are responsible for their superhydrophobic properties. In the direction of mimicking naturally-occurring superhydrophobic structures, scientists have focused their research on engineering surfaces with high surface roughness and appropriate chemistry to achieve similar results. Some of the techniques used to induce texture to a surface (i.e. increase the surface area) involve templating, plasma treatment, layer-by-layer deposition and lithography (Yan et al, 2011).

In the present study, focus was placed on investigating hydrophobicity of PSA powders by means of chemical modification of the particle surface, in combination with texturing, given that PSA particles undergo fracturing during dry milling. Hydrophobicity was assessed by measuring the water contact angle (WCA), as described in section 4.3.12. Optimisation of the hydrophobic effect and comparison of hydrophobicity performance between PSA and other inorganic substrate materials was explored. The interaction between PSA and stearic acid was analysed using FTIR to investigate the mechanism responsible for hydrophobicity.

### **8.1.1 Surface functionalization of waste materials**

A typical method of surface chemical modification involves rough particulates on which monolayers of smaller organic molecules with hydrophobic properties are formed. Self-assembling monolayers (SAMs) are physically and/or chemically adsorbed to the surface of the substrate and form layers with a thickness of one molecule. Multiple layers can also be formed in excess of the organic surfactant. The whole procedure is called '*surface functionalization*', as detailed in section 3.5.4, and enables engineering of hydrophobic and superhydrophobic surfaces (Schreiber, 2000).

The use of waste materials and/or industry by-products in the formulation of hydrophobic powders/surfaces is limited to research level. Sakthivel et al. (2013) as well as Yao et al. (2013) chemically modified the surface of coal fly ash (CFA) particles to produce hydrophobic materials. In the former case, one of the methods developed by researchers involved transforming CFA into zeolitic fly ash (ZFA) via conventional refluxing method and functionalising the surface of ZFA via curing in a

stearic acid/NaOH solution at 95 °C until cooling to room temperature. The end-product had a contact angle of 147°. Similarly, Yao et al. (2013) modified the surface of CFA by chemically and thermally treating it with a solution of hot stearic acid and ethanol at 60 °C to achieve hydrophobicity of 148°.

In the literature, the surface functionalization most frequently reported are those related to the modification of calcium carbonate fillers with stearic acid. Calcite is the cheapest commercially available filler material and has been widely used in plastic, rubber, paper and ink industries among others (Price et al., 2004; Shen et al., 2010). Surface modification of calcite particles can be classified into three categories: a) chemical, b) physical and c) mechano-chemical. In the surface modification process of calcite, some modifying reagents such as silane, titanate, phosphate or stearic acid have been used to induce hydrophobic properties. Surface modification of calcite particles with stearic acid is particularly relevant to the present suggested formulations of PSA-based hydrophobic materials, as discussed in the following sections.

## 8.2 Experimental methodology

The materials and preparation methods used to produce hydrophobic particles using PSA and other inorganic substrates were described in sections 4.1.3 and 4.2.3 respectively. Initial observations showed that stearic acid is a promising candidate surfactant for surface functionalization of PSA particles. Dry milling of PSA, of the same origin as those used in the LWF production process, for various times and using different stearic additions was investigated. Optimum processing conditions were determined by assessing the degree of hydrophobicity based on water contact angle measurements of pressed powder samples (see section 4.3.12). These conditions were subsequently applied to other inorganic substrates, which were selected based on their affiliation to the chemical composition of PSA samples. Further optimisation involved applying these conditions to process the optimum substrate identified with various surface functionalising agents (SFAs). In this work capric acid ( $\text{CH}_2(\text{CH}_2)_8\text{COOH}$ ), myristic acid ( $\text{CH}_3(\text{CH}_2)_{12}\text{COOH}$ ), stearic acid ( $\text{CH}_3(\text{CH}_2)_{18}\text{COOH}$ ) and behenic acid ( $\text{CH}_3(\text{CH}_2)_{20}\text{COOH}$ ) have been used to investigate potential correlation between induced hydrophobicity and alkali chain length of fatty acids.

The effect of humidity over time on hydrophobicity was investigated by placing hydrophobic pressed samples in a humidity chamber having a relative humidity of >95 % at  $23 \pm 2$  °C. Samples were also tested for their resistance to heat shocks by measuring the water contact angle of samples after exposure at different temperatures for one 1 hour in a conventional *Lenton* laboratory furnace. Finally, Fourier Transform Infrared Spectroscopy (FTIR) was used to investigate the interaction between optimum hydrophobic particles and acid surface functionalising agents (see section 4.3.6).

### 8.3 Results and discussion

#### 8.3.1 Effect of dry milling time and stearic acid addition on PSA hydrophobicity

The effect of dry milling time on degree of hydrophobicity of PSA\_UPM and PSA\_ANP samples is shown in Figure 8.1a. All samples were prepared with 1 wt. % addition of stearic acid in the PSA mix and the milling duration varied from 1 to 16 hours. As-received PSA samples were hydrophilic, resulting in flat spreading of water droplets on the surface of pressed samples. Water contact angle data indicated that hydrophobicity increased with increasing dry milling time. This suggested that grinding, with simultaneous induced fracturing of solid particles, created new surfaces that were in-situ modified by the surfactant molecules. This surface modification continued until generation of new particle planes ceased due to limitations of the ball mill operational and material-specific conditions. This effect had been also observed in the study of Devarajan et al. (2007) when investigating the synthesis of nanoparticles of  $\text{CaCO}_3$  via ball milling. Hence, in this study, the effect of milling time on hydrophobicity is strong for PSA mixes milled for up to 8 hours. There was no significant change in hydrophobicity after maximum breakage of coarse particles was achieved. This becomes clear when analysing particle size distribution data shown in Figure 8.2. This data correspond to PSA\_ANP samples dry milled in a ball mill for up to 16 hours. Dry ball milling for 16 hours resulted in agglomeration of fine particles rather than further particle size reduction. Dry milled PSA consisted of particles with a  $d_{50}$  between 2-5  $\mu\text{m}$ .

Optimum degree of hydrophobicity was achieved for PSA\_UPM and PSA\_ANP samples after 4 and 8 hours of dry milling with 1 wt. % stearic respectively. Contact angle was measured to be 139.8° for PSA\_UPM and 144.8° for PSA\_ANP samples.

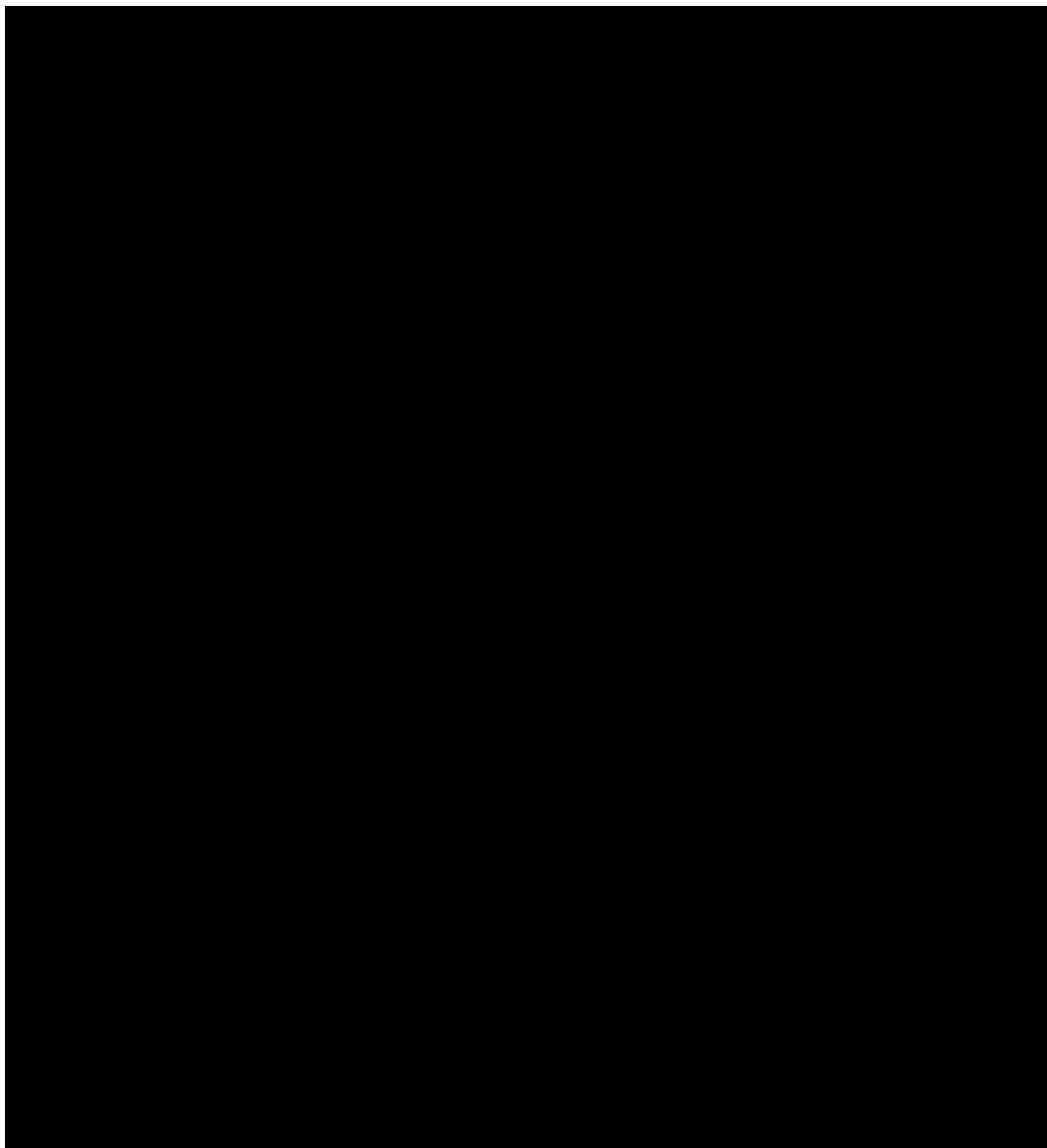


**Figure 8.1** Effect of dry milling time (a) and stearic acid addition (b) on WCA of PSA\_UPM and ANP samples treated with 1 wt. % stearic acid in (a) and dry milled for 4 and 8 hours respectively in (b) (n=10).

Having determined the optimum milling time conditions for each PSA sample, the effect of stearic acid content on hydrophobicity was also investigated. Figure 8.1b depicts a moderate increase in hydrophobicity with increasing stearic acid addition up to 4 wt. %. Further stearic acid increase had no change in hydrophobicity of PSA\_ANP samples and caused marginal hydrophobicity drop for PSA\_UPM samples. The latter effect could be considered negligible accounting for experimental error. For

both PSA samples, highest water contact angles were measured when 4 wt. % stearic acid was used. Based on the above, it is postulated that surface coating of fractured PSA particles via formation of SAMs between PSA and stearic acid components was not only mechanically but also chemically induced. Optimum PSA\_ANP and PSA\_UPM samples, as identified in the above analysis, exhibited a WCA of  $153^\circ$  and  $148^\circ$  respectively. No apparent changes in surface roughness were observed for the pressed samples prepared with as-received PSA ( $1.81\ \mu\text{m}$ ) and PSA milled for 2 h ( $1.79\ \mu\text{m}$ ), 4 h ( $1.77\ \mu\text{m}$ ), 8 h ( $1.78\ \mu\text{m}$ ) and 16 h ( $1.79\ \mu\text{m}$ ) and therefore the variation in hydrophobicity observed is not caused by changes in surface roughness.

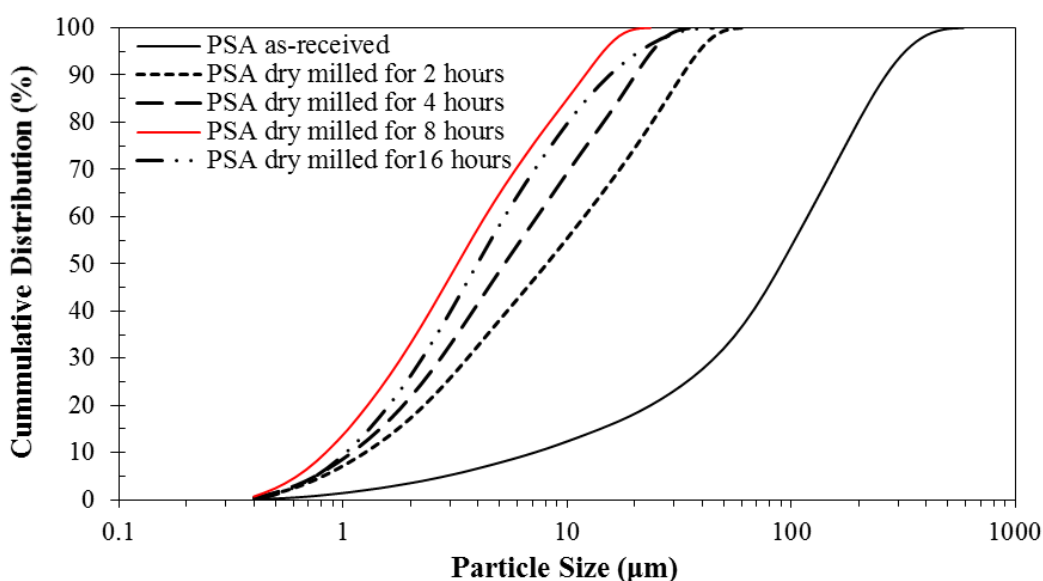


**Figure 8.2** Effect of dry milling time on the PSA\_ANP particle size distribution. Grinding of PSA for 16 hours resulted in agglomeration of particles ( $n=3$ ).

Typical sessile drop images formed on the surfaces of disc samples made from different hydrophobic powders are shown in Figure 8.3. These images are for samples prepared using 1 wt. % stearic acid addition and milled for different times.

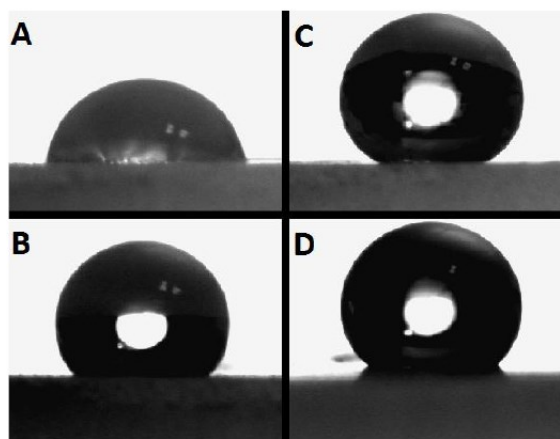


**Figure 8.3** Images of water droplets on hydrophobic surfaces used to determine the water contact angle ( $\theta_c$ ) by the sessile drop method. The droplets shown are for PSA\_ANP dry milled for different times with 1 wt.% addition of stearic acid (A, 2 hours; B, 4 hours; C, 8 hours and D, 16 hours).

### 8.3.2 Effect of SFAs on PSA hydrophobicity under optimum conditions

In order to investigate the effect of various fatty acids on WCA of PSA, optimum milling time for each type of PSA and acid addition of 4 wt. % were kept fixed. The carboxylic acids used were appropriately selected to allow evaluation of potential correlations between hydrophobicity and alkali chain length of surface functionalization agents (SFAs).

Figure 8.4 shows that hydrophobicity is influenced by the SFA used. Increasing the aliphatic chain length resulted in increased hydrophobicity by up to ~26 % when comparing samples treated with capric acid and those treated with stearic acid. This was a statistically significant difference as shown in Appendix C. PSA samples treated with capric acid (10 C-atom chain) had a WCA in the range of ~120°. Stearic acid, with 18 carbon atoms, gives the highest WCA compared to all other saturated fatty acid molecules used. This is in accordance with the findings of Wang et al. (2005) who observed maximum hydrophobicity when stearic acid was used to modify copper surfaces. Similar conclusions were derived from the work of Gomari et al. (2006) when investigated the effect of various C-18 saturated and unsaturated organic acids. In their study, stearic acid provided optimum surface modification of calcite particles through the formation of physi- and chemisorbed SAMs on the mineral surface. Zullig et al. (1988) also established that short chain fatty acids (up to C-12) did not absorb on carbonate surfaces tested. In the present study, stearic acid was, therefore, considered a strong SFA candidate to consistently induce hydrophobicity to PSA.

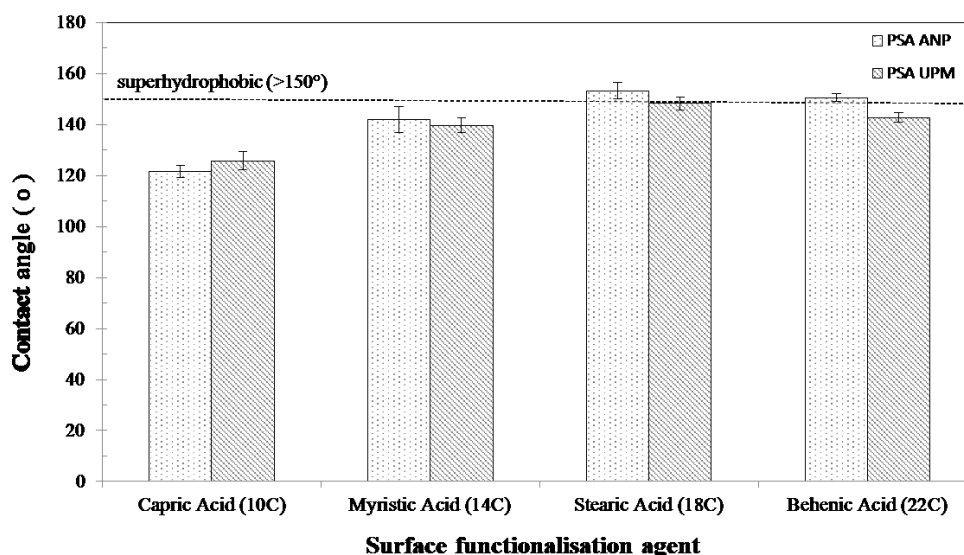


**Figure 8.4** The effect of different surface functionalization agents on the WCA of PSA samples ( $n=10$ ). SFAs used are saturated fatty acids with different carbon chain lengths.

### 8.3.3 Hydrophobicity of different inorganic substrates

In order to understand the specific chemical features of PSA that render it a promising substrate for engineering superhydrophobic particles, alternative inorganic substrates were also treated with stearic acid. Dry milling of mixes was kept fixed at 8 hours as no change in hydrophobicity was observed beyond this time for any of the PSA samples analysed above. Calcium carbonate, lime and silica fume were selected due to association with major elements and mineral phases present in PSA. Other more complex minerals also identified in PSA, such as gehlenite and mayenite, were not possible to find or synthesize within the time frame of the present research project.

The degree of hydrophobicity expressed as WCA for calcium carbonate, lime and silica fume dry milled for 8 hours with 4 wt. % of stearic is depicted in Figure 8.5. Silica fume was hydrophilic and this is in agreement with results previously published by Gomari et al. (2006). Lime is marginally hydrophobic and calcium carbonate is strongly hydrophobic with a WCA of  $140^\circ$ . Surface modification of micro- and nanocalcite particles is attributed to the formation of chemisorbed self-assembled monolayer of calcium stearate on its surface (Jeong et al., 2009; Hait et al., 2013; Mihajlovic et al., 2009).

The studies mentioned above focused on wet grinding of calcite particles with solutions of stearic acid in distilled water or non-polar dispersants such as hexane and

decane. Such methods promoted the dissolution of calcite during milling expressed by:



Simultaneous dissociation of organic acids according to:  $\text{RCOOH} \leftrightarrow \text{RCOO}^- + \text{H}^+$ , also created a tendency of the anionic groups  $[\text{RCOO}^-]$  to reach the calcium cations and form calcium organic salts on the surface of particles via a chemisorption reaction (Hansen et al., 2000).

In the case of the calcium carbonate/stearic acid system, one stearic acid molecule is attached to each  $\text{Ca}^{+2}$  ion to favour the formation of calcium stearate according to:



In the complete monolayer formation, the stearate ions are vertically aligned to the  $\text{Ca}^{+2}$  surface. In excess of surfactant, multilayer physical adsorption due to tail-to-tail arrangement of polar groups occurs. This is typically accompanied by decrease in hydrophobicity given horizontal arrangement of alkyl chains of adsorbed stearic acid to the surface of calcite. Hence, the concentration of surfactant is the key parameter controlling the efficacy of the surface modification (Fekete et al., 1990).

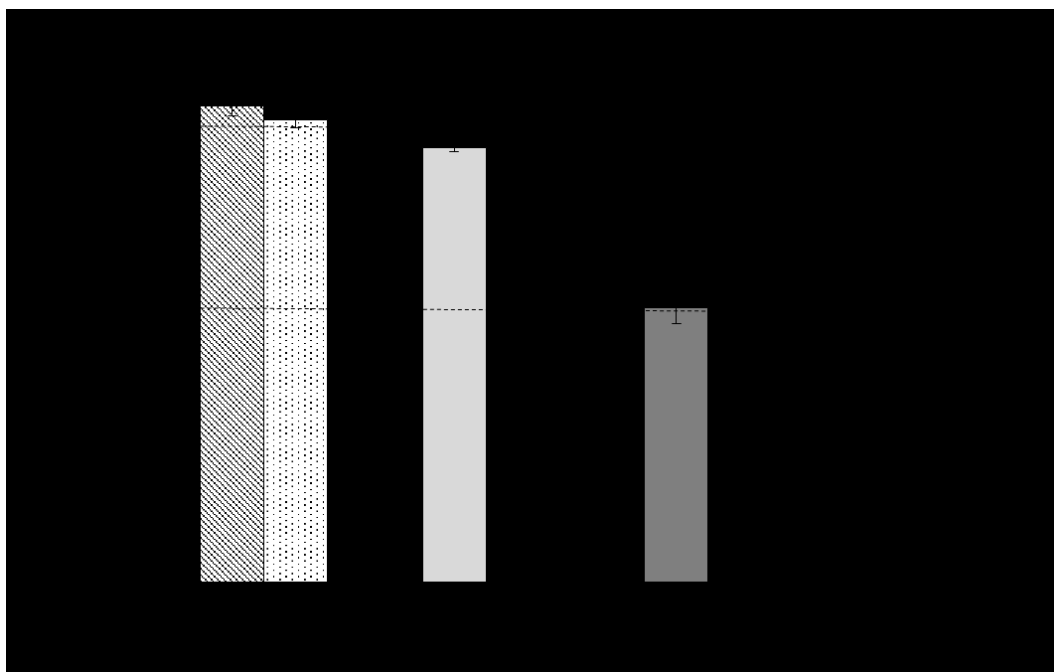


**Figure 8.5** WCA of various inorganic substrates dry milled for 8 hours with 4 wt. % addition of stearic acid (n=10).

In order to better understand the surface modification mechanisms, the effect of stearic acid addition on hydrophobicity of calcium carbonate and lime was investigated and the results are shown in Figure 8.6. Under the 8-hour dry milling conditions applied, it was observed that increasing stearic acid from 2 wt. % to 8 wt. % improved hydrophobicity of calcium carbonate samples expressed by a 4.6 % increase of WCA. The corresponding change in hydrophobicity for lime samples was negligible. This suggested that complete surface modification of calcium carbonate particles could be achieved with an 8 wt. % stearic acid addition giving a WCA of  $\sim 144^\circ$ . In contrast, the lime/stearic acid system did not exhibit strong hydrophobic properties under given processing conditions. There is, therefore, a clear affiliation of stearic acid to calcium carbonate that promotes the formation of calcium stearate hydrophobic monolayers as explained above. It has to be noted that this effect is not associated with particle size effects given that calcium carbonate and lime powders had a  $d_{50}$  of  $8.42 \mu\text{m}$  and  $8.54 \mu\text{m}$  reduced by 85 % and 81 % respectively compared to starting particle size. The equivalent particle size reduction was  $\sim 97$  % for both types of PSA.

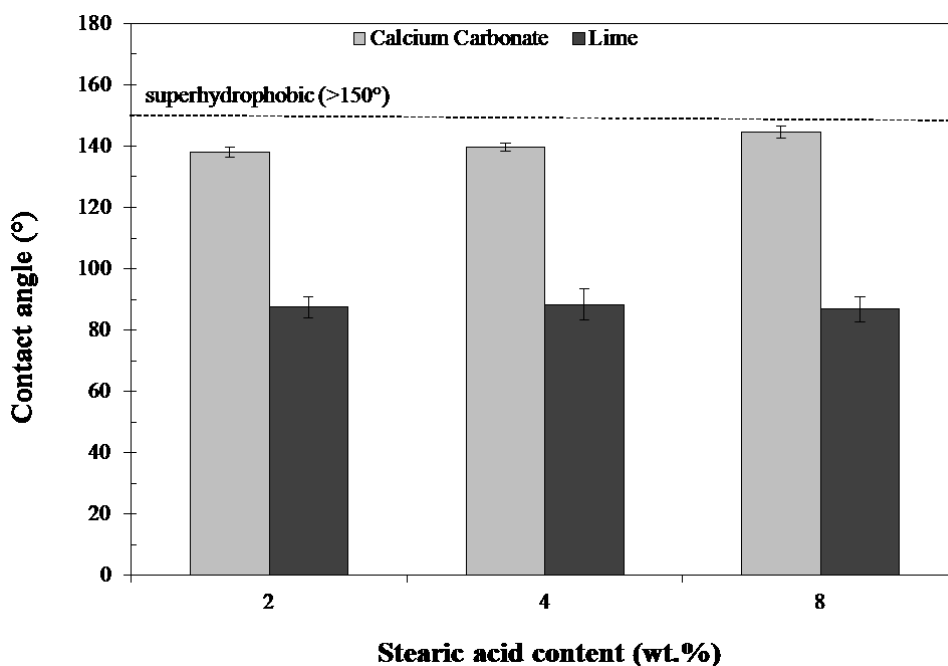


**Figure 8.6** The effect of stearic acid addition (by weight) on calcium carbonate and lime samples dry milled for 8 hours (n=10).

Surface roughness phenomena were also investigated. Dry milled powders were pressed into disc pellets under different pressing pressures prior to measuring WCAs. As depicted in Figure 8.7, calcium carbonate and lime surfaces (dry milled for 8 hours

with 8 wt. % stearic acid addition) had a roughness of  $1.77\ \mu\text{m}$  and  $1.42\ \mu\text{m}$  respectively when applied a force of 25 N (Figure 8.7a). The corresponding values for an applied force of 100 N were  $1.74\ \mu\text{m}$  and  $1.09\ \mu\text{m}$  (Figure 8.7b). It, therefore, seems that lime particles are more susceptible to plastic deformation during pressing. Calcium carbonate samples exhibited heterogeneous roughness profiles with localised asperities along the surface (scattered areas of green and blue colour on surface profiles). This minor, yet present, heterogeneity aids interfacial air entrapment between the water droplet and the hydrophobic substrate favouring a Cassie-Baxter wetting state (see section 4.2.3). These identified differences in surface roughness, however, do not justify the considerable difference in hydrophobicity between calcium carbonate and lime given that corresponding loose powders also had different hydrophobic behavior.

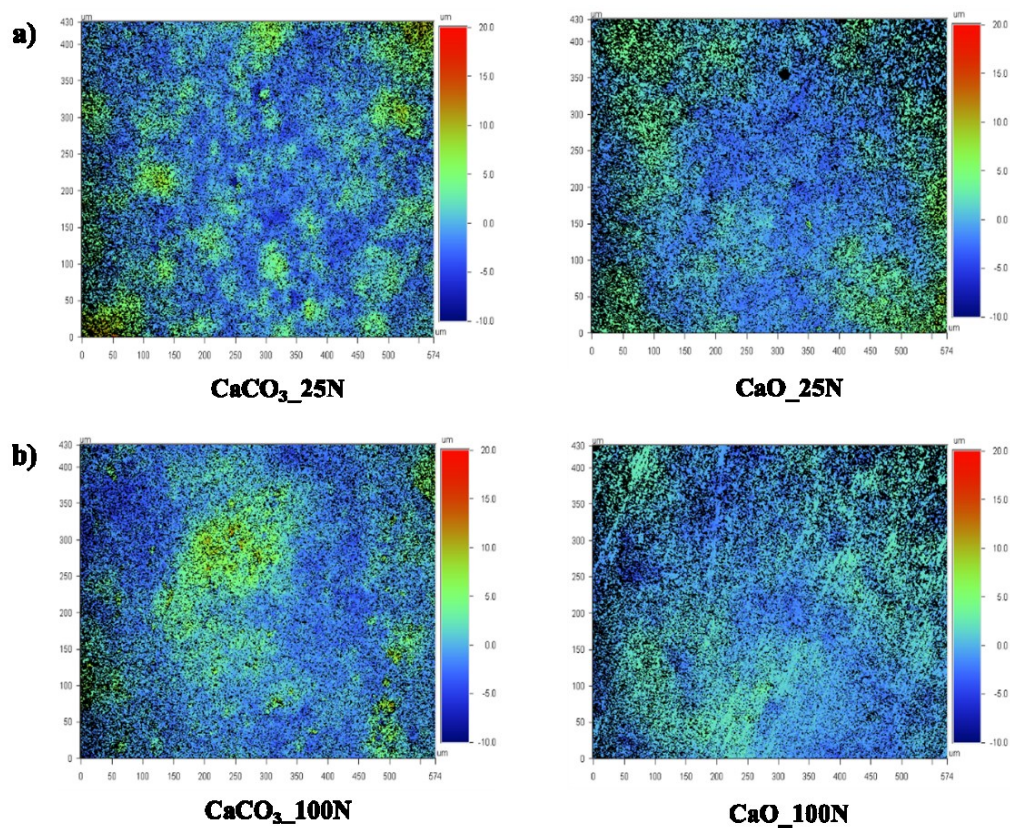


**Figure 8.7** Surface roughness profiles of calcium carbonate and lime powders dry milled for 8 hours with 8 wt. % of stearic acid after pressing them into pellets with an applied force of a 25 N (a) and 100 N (b).

Based on the above analysis, it can be postulated that the resultant hydrophobicity is primarily associated with differences in the chemistry of the materials rather than mechanical deformation and roughness effects. A correlation could, therefore, be

made between PSA and calcium carbonate given similarities in hydrophobicity induced by dry milling and stearic acid surface functionalization.

### 8.3.4 PSA: Formation of a hydrophobic monolayer

FTIR spectra for PSA\_ANP samples prepared with different additions of stearic acid including as-received PSA\_ANP are presented in Figure 8.8. Spectrum A shows the standard absorption pattern for as-received PSA. The presence of absorption bands between 2960 and 2850  $\text{cm}^{-1}$  is ascribed to symmetric and anti-symmetric C-H stretching vibrations of the hydrocarbon moiety and indicated the presence of residual un-burnt hydrocarbons. The intensity of these absorption bands increased significantly with increasing additions of stearic acid. This suggests a solid-like packing of the aliphatic chains similar to that of stearic acid.

The fingerprint region of the FTIR spectra (below 1500  $\text{cm}^{-1}$ ) does not change significantly between the samples and is indicative of PSA chemistry. The most important peaks, which are only present in some of these spectra, are at 1707  $\text{cm}^{-1}$  and 1588  $\text{cm}^{-1}$ . Spectra C and D contain the absorption band at 1588  $\text{cm}^{-1}$ . This is indicative of anti-symmetrical carboxylate ion ( $-\text{COO}^-$ ) stretching and is particularly distinctive of calcium carboxylic (Chen et al., 2010). This implies binding of stearic acid molecules to the substrate surface through reaction with calcium ions to form calcium stearate. The absorption band at 1707  $\text{cm}^{-1}$  in spectra D indicates the presence of free saturated carboxylic acids (1725-1700  $\text{cm}^{-1}$ ) and it can be concluded that for the 8 wt. % addition of stearic acid, surface calcium ions have become the limiting agent for full reaction to calcium stearate monolayers.

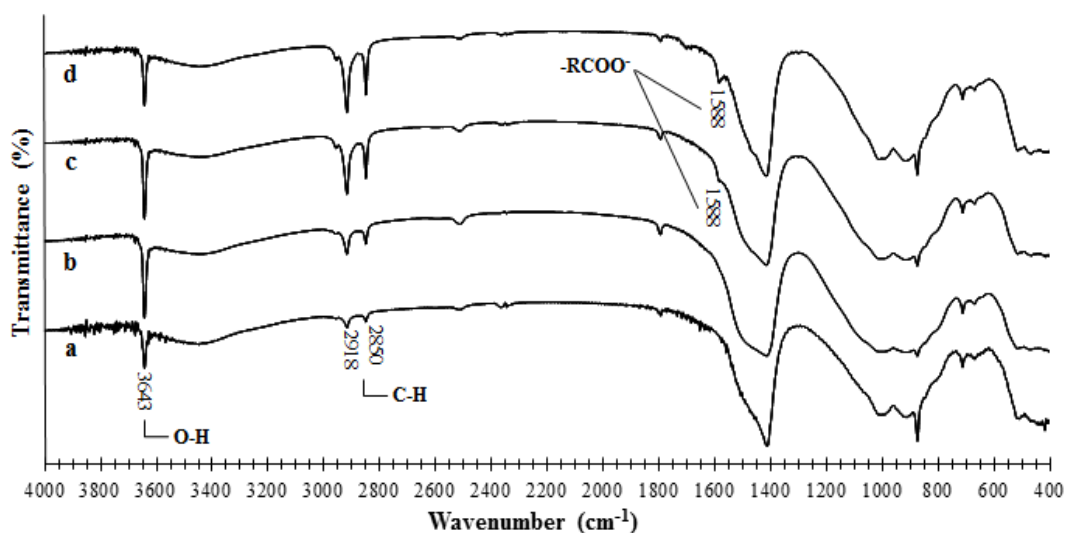


**Figure 8.8** FTIR spectra of PSA powders treated with different stearic acid additions and milled for 8 hours: a) PSA as received; b) 1 wt. % addition; c) 4 wt. % addition and d) 8 wt. % addition. The adsorption band at  $1588\text{ cm}^{-1}$  indicates binding of stearic acid to the substrate surface through the formation of calcium stearate ( $n=3$ ).

### 8.3.5 Heat and humidity resistance

Thermal stability of PSA-based and calcium carbonate hydrophobic powders was evaluated after exposing loose powders at various pre-set temperatures for 1 hour prior to measuring the WCA on pressed disc pellets. As seen in Figure 8.9a, both PSA-based and calcium carbonate hydrophobic samples lost their hydrophobicity when exposed to temperatures higher than  $200\text{ }^{\circ}\text{C}$ . This coincides with the complete decomposition of stearic acid starting at  $200\text{ }^{\circ}\text{C}$  (Figure 8.9b). It is, therefore, attributed to complete desorption of organic molecules bound on the surface of PSA and calcium carbonate particles during the surface modification process. The main exothermal peak and weight loss above  $300\text{ }^{\circ}\text{C}$  on DSC curves of PSA\_ANP (Figure 8.9c) are due to the oxidation of chemically adsorbed stearate ion,  $\text{CH}_3(\text{CH}_2)_{16}\text{COO}^-$ , to the positive surface ions of PSA particles. Although strong interaction has been widely reported between  $\text{Ca}^{+2}$  and stearic acid, as detailed above, other positively charged ions in PSA could have also reacted with stearic acid via a solid-phase reaction during dry grinding, hence contributing to hydrophobisation. Since the chemical adsorption provides the strongest bond between the adsorbates and adsorbents, this exothermic maximum at the highest temperature is ascribed to the oxidation of the chemically adsorbed organic component. The DSC peaks in Figure 8.9c at lower temperatures ( $200\text{--}300\text{ }^{\circ}\text{C}$ ) are attributed to physically adsorbed stearic acid molecules.

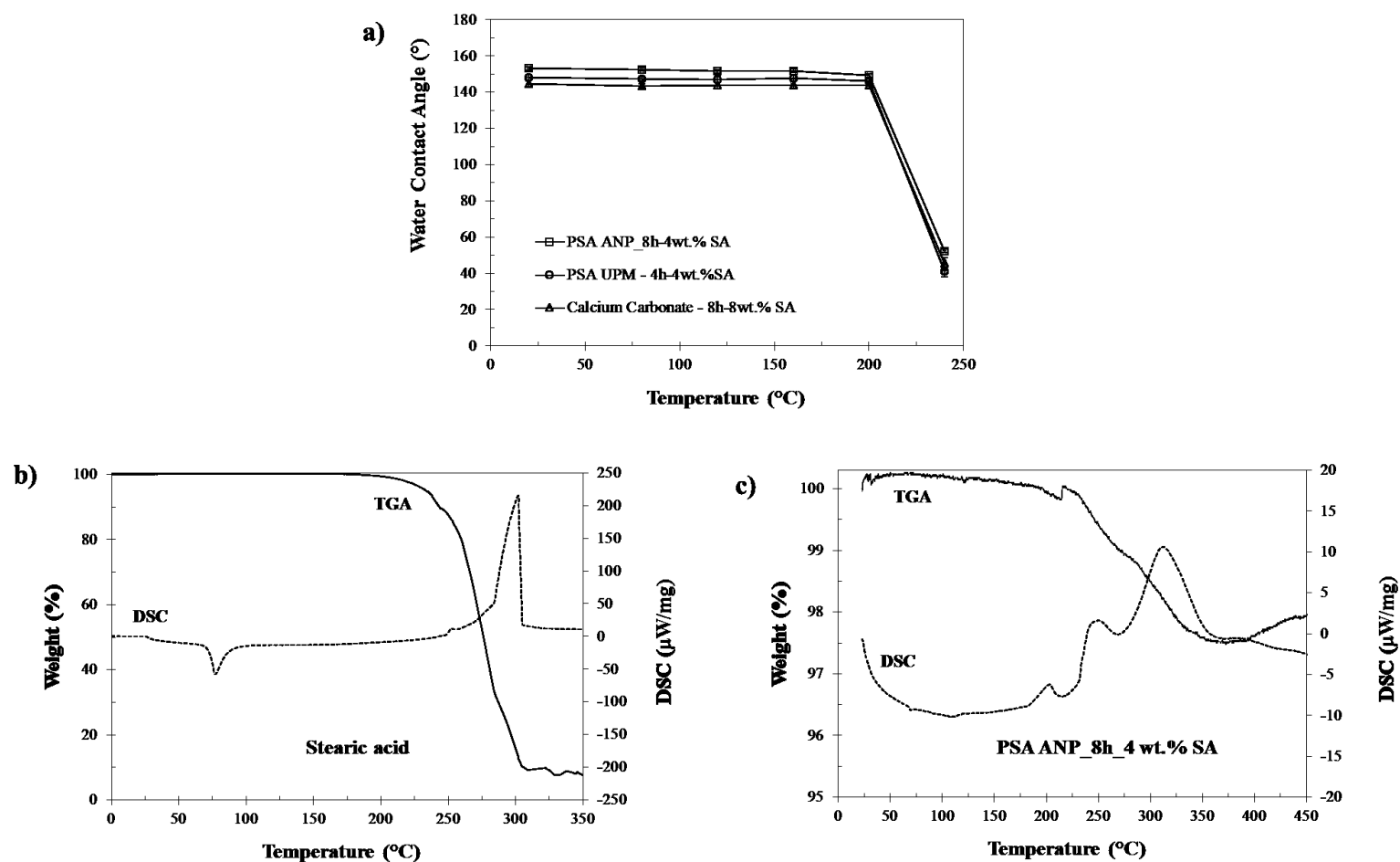


**Figure 8.9** Thermal stability of PSA-based and calcium carbonate hydrophobic powders: a) effect of temperature on WCA of functionalised substrates (n=10), b) TGA/DSC analysis of stearic acid (n=3) and c) TGA/DSC analysis of PSA\_ANP dry milled for 8 hours with 4 wt. % stearic acid (n=3).

The humidity resistance of optimum PSA-based hydrophobic samples was also assessed by exposing pressed hydrophobic disc pellets to high relative humidity (RH) conditions. Samples were placed in a humidity room WCA measurements were taken at distinct times over a period of three months. The RH was kept constant at levels higher than 95 % at  $23\pm 2$  °C. Both types of PSA-based hydrophobic powders showed an initial abrupt decrease in hydrophobicity within the first 24 hours of exposure to humid environment. As depicted in Figure 8.10, hydrophobic PSA\_ANP samples showed a moderate initial decrease of 6 % followed by a more steady decrease in hydrophobicity reaching a final WCA of  $\sim 130^\circ$  at the end of the testing period. In contrast, PSA\_UPM hydrophobic samples showed a more abrupt initial hydrophobicity decrease of 11 % (< 7 days of exposure) followed by a steady state with almost no further deterioration in hydrophobic performance. The overall long-term resistance to humidity for PSA\_ANP and PSA\_UPM was described by a hydrophobicity loss of 16 % and 12 %, respectively. The fundamental difference between the two types of PSA-based hydrophobic powders lies in the initial resistance to a humidity ‘shock’. Finally, it was also macroscopically observed that PSA-based hydrophobic pellets developed high strength over the ‘curing’ period in the humidity chamber. This implies that water molecules were sandwiched between hydrophobic and hydrophilic areas present in the sample creating a water film.

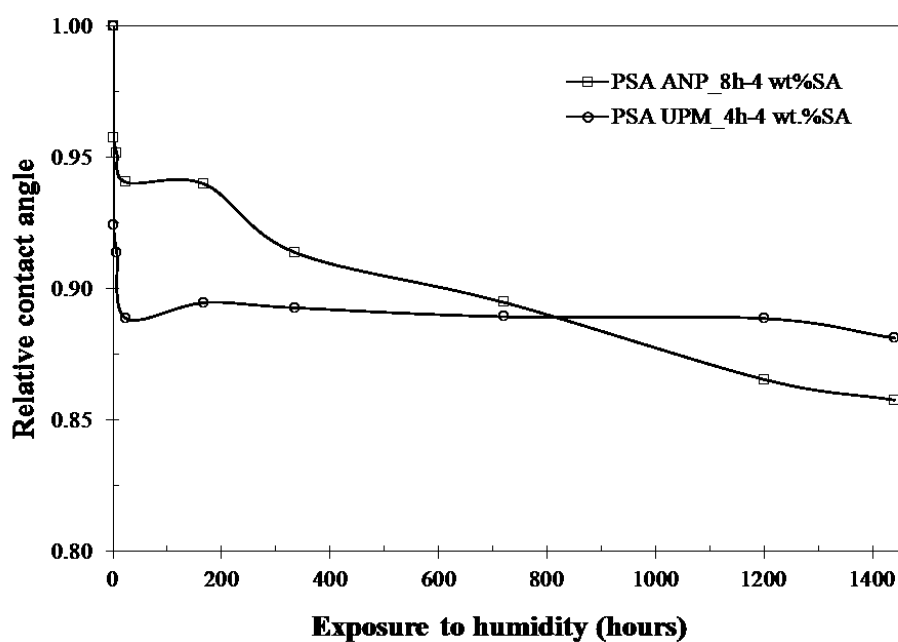


**Figure 8.10** Effect of humidity on hydrophobicity of PSA-based hydrophobic samples (n=3). The relative humidity was kept constant at 95 % at  $23\pm 2$  °C.

## 8.4 Concluding remarks

Paper sludge ash can be modified to form hydrophobic powders via a simple dry milling process in the presence of stearic acid, which acted as the surface functionalization agent. PSA\_ANP formed a super-hydrophobic powder (WCA  $> 150^\circ$ ) when dry milled for 8 hours with a 4 wt. % addition of stearic acid. The optimum processing conditions for inducing hydrophobicity (WCA  $\sim 148^\circ$ ) to PSA\_UPM samples were 4 hours of dry milling with a 4 wt. % addition of stearic acid. Alternative fatty acids were investigated but stearic acid produced the highest WCA. The hydrophobisation mechanism is described by a combination of mechanical (micro-particulate texture induced by dry grinding) and chemical (stearate anions adsorbed on the mineral surface) phenomena. Hence, the suggested mechanism involves physical and chemical adsorption of  $\text{CH}_3(\text{CH}_2)_{16}\text{COO}^-$  on  $\text{Ca}^{+2}$  on the surface of PSA. PSA particles became mechanically activated after prolonged dry milling.

The above was verified by the strong hydrophobic properties of the calcium carbonate/stearic acid binary powder system when processed under identical conditions. Calcium carbonate particles dry milled for 8 hours with 8 wt. % of stearic acid had a WCA of  $144^\circ$ . TGA/DSC analysis of optimum PSA-based hydrophobic powders also confirmed the development of both physically and chemically bonded calcium stearate self-assembling monolayers on the PSA surface. Humidity resistance was marginally higher for optimum PSA\_UPM hydrophobic samples compared to PSA\_ANP samples.

Low-cost PSA-derived super-hydrophobic powders have potential for use in applications where water repellence is beneficial and this includes the development of super-hydrophobic civil engineering infrastructure. Hence, the work presented in this chapter attracted a great amount of attention from other research groups at Imperial College London and construction industry experts. Ongoing research involves investigating the '*hydrophobicity potential*' of alternative carbonates as well as developing liquid hydrophobic formulations with a view to expand the potential applications of solid hydrophobic particles.

## CHAPTER 9 Discussion

The aim of this research project was to develop viable beneficial reuse applications for paper sludge ash (PSA). Initially, lightweight fillers were selected as a promising high-end application for PSA. At a later stage, the opportunity to form hydrophobic PSA-based particles emerged and was also investigated. In the broader context of circular economy, this project achieved to demonstrate that utilisation of resources is possible when innovative technologies are employed and conventional materials-based practices are challenged. What is more stimulating, though, is the use of such resources in novel applications which drives industrial ecology at the micro-level, where resources are locally available, processed and distributed. This has associated environmental and economic benefits.

### 9.1 Production of lightweight fillers from waste glass and paper sludge ash

Artificial lightweight materials are an excellent alternative to quarried aggregates, being light, robust and consistent. The combination of sustainability and high-performance renders waste-based lightweight materials particularly attractive in a variety of construction applications. When added to concrete, insulating properties, frost and fire resistance are enhanced. Light-weight aggregate concrete (LWAC) increases versatility in architectural designs that would, otherwise, not be feasible with normal-weight concrete (Nesbit, 1993). In addition to concrete-bound formulations, porous, heat-insulating materials are used as loose bulk fill, hence reducing the thickness and mass of walls and other structural components. Sealed porous grains are also used as fillers in plastics and paints. The present study focused on producing such lightweight fillers (LWFs) from paper sludge ash (PSA) via a viable rapid sintering manufacturing route.

Previous studies have outlined the utilisation of a variety of wastes for the production of lightweight materials as outlined in section 3.4. The processing of waste materials into lightweight products has also been commercially exploited and a number of production processes have been successfully employed as shown in Table 3.10. They all involve rapid sintering at high temperatures ( $> 900$  °C) in order to achieve porosity. In order to attain desired levels of pore formation, two conditions have to be met during sintering:

- evolution of gases from thermally unstable constituents and
- presence of a viscous liquid phase to entrap the gases.

Drawing upon this fundamental principle and knowledge of past and current industrial practices, processing of waste glass, already widely used for the production of foamed products, and PSA, not previously reported to have been used in a similar process, involved rapid sintering of glass/PSA mixes. Formation of ‘green’ particles meant that waste glass cullet was ground to a fine glass powder which was used throughout the research. Preliminary experiments evaluated the feasibility of sintering pan-pelletised pellets made out of milled glass and as-received PSA mixtures. Particular focus was placed on high-PSA content mixes. However, poor sintering reactivity of PSA particles, as confirmed by dilatometry analysis, diverted, since early stages of this project, the attention to the high-glass/low-PSA content mixes for the production of LWFs. Addition of glass promoted liquid phase sintering due to the formation of a low-viscosity melt that is able to encapsulate any evolving gases. In the glass/PSA system, gas evolution came, primarily, from the decomposition of calcium carbonate in PSA. Hence, PSA acted as an expanding agent in the finely ground glass mixes to produce expanded glass particles.

The two different types of PSA used had similar mineralogical characteristics with major mineral phases being gehlenite ( $\text{Ca}_2\text{Al}_2\text{SiO}_7$ ), calcite ( $\text{CaCO}_3$ ), calcium silicate ( $\text{a}^{\prime}\text{-Ca}_2\text{SiO}_4$ ), lime ( $\text{CaO}$ ) and quartz ( $\text{SiO}_2$ ). Based on TGA/DSC analysis of PSA samples, PSA\_ANP exhibited a weight loss of 8.5 wt. % whereas PSA\_UPM a loss of 6.7 wt. % between 600 °C and 780 °C. This is attributed to the calcium carbonate decomposition ( $\text{CaCO}_3$ ) to calcium oxide ( $\text{CaO}$ ) and calcium dioxide ( $\text{CO}_2$ ). It is the  $\text{CO}_2$  evolving gaseous species that render PSA a suitable candidate as a pore former during sintering of glass/PSA mixes at temperatures above 600 °C. However, in order to achieve adequate softening of the vitreous phases formed during sintering, optimum sintering temperature for glass/PSA pellets was determined to be 800 °C, which corresponds to a glass viscosity value in the range of  $10^{6.6}$  Pa·s. This is in agreement with the upper boundary for glass viscosity in order to achieve foaming of siliceous matrices as determined by Kingery et al. (1976).

Addition of PSA to fine glass powder mixes up to 20 % by weight, followed by rapid sintering for 20 minutes, resulted in lightweight materials (particle density  $<1 \text{ g}\cdot\text{cm}^{-3}$ )

in the case of PSA\_ANP. On the contrary, the corresponding samples prepared with PSA\_UPM exhibited low densities for an addition of up to only 10 % by weight in the glass mix. However, the 80/20 glass/PSA\_UPM also produced lightweight materials when wet milling was applied for 4 hours prior to rapid sintering. This suggests that particle size of the components is of major importance. Also, the reaction of free lime, present in PSA, with water led to the formation of  $\text{Ca(OH)}_2$ . As discussed in section 6.2, the decomposition of  $\text{Ca(OH)}_2$  occurs with partial pressures in excess of 1 atm from  $\sim 793$  K ( $520$  °C) onwards and can therefore, undoubtedly contribute to the expansion of the lightweight fillers.

As shown in Figure 9.1, the viscosity of both 80/20 glass/PSA mixes at  $800$  °C is comparable. In the case of the 80/20 glass/PSA\_ANP system the condition of a  $10^{6.6}$  Pa·s viscosity value is attained at  $804$  °C. The corresponding temperature for the 80/20 glass/PSA\_UPM system is  $798$  °C. Viscosity-temperature data was calculated based on the widely accepted Vogel-Fulcher-Tammann (VFT) equation (Vogel, 1921; Fulcher, 1925):

$$\log(\eta) \text{ (Pa} \cdot \text{s)} = \frac{A+B}{T-T_0} \quad \text{(Equation 9.1).}$$

The  $A$ ,  $B$ ,  $T_0$  parameters are related to chemical composition interactions between components in the silicate melts as modelled by Fluegel (2007) and  $T$  is the temperature in (K). The marginal difference in viscosity at  $800$  °C between the two 80/20 glass/PSA samples is attributed to the higher  $\text{Na}_2\text{O}$  and  $\text{K}_2\text{O}$  content in PSA\_UPM, which favours modification of the glass network by formation of non-bridging oxygen sites, and hence, decreases the glass viscosity. It is to be highlighted that alkali and alkaline earth oxides decrease the glass viscosity in the order  $\text{MgO} < \text{CaO} < \text{SrO} < \text{BaO} < \text{K}_2\text{O} < \text{Na}_2\text{O}$  (strongest effect) (Fluegel, 2007). However, the viscosity difference standalone does not justify the difference in the sintering behavior between the 80/20 glass/PSA mixes prepared with the two types of PSA.

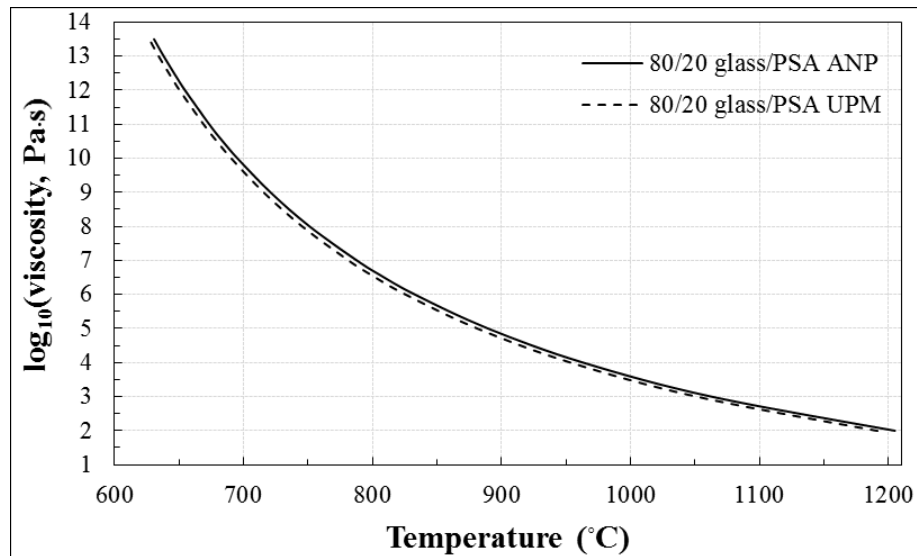


**Figure 9.1** Melt viscosity variations as a function of temperature for the 80/20 glass/PSA mixes prepared with two different types of PSA (PSA\_ANP and PSA\_UPM). Data was calculated according to a literature model (Fluegel, 2007).

It was identified that the particle size of powders to be sintered was a more influential parameter given that finer particles, hence higher particle surface area, increased the contact area between particles and promoted sintering reactivity. This is due to minimization of the distance of the diffusion path (He and Ma, 2005). Wet grinding of raw materials favored the formation of adequate low-viscosity vitreous phases during sintering able to entrap the evolving gases from PSA particles and led to increased porosity. Also, the enabling role of  $\text{Ca}(\text{OH})_2$  phases formed during wet milling, decomposing to produce steam at elevated temperatures, and the fact that grinding of carbonates has been reported to lower their decomposition temperature (Lin and Somasundaran, 1972), contributed to faster growth of bubbles from an early stage during heating of the sintered body. Wet milling of the 80/20 glass/PSA\_ANP samples for more than 1 hour, however, resulted in excessive densification of the structure. This is attributed to the presence of excessive gas being evolved. Based on TGA analysis of both types of as-received PSA samples, it was expected that PSA\_ANP would release a greater amount of gas during sintering. Hence, further wet milling of such samples caused excessive gas liberation that disrupted the integrity of the pore network formed.

In the glass/PSA system, however, it is the joint effect of viscosity levels and gas evolution that defines the final microstructure. Preliminary experiments demonstrated that increase of the foaming agent content (PSA) beyond 20 wt. % in glass mixes was

not followed by decrease in density. This implies that there is a ‘threshold’ value of coarsening of the cellular structure. Smaller pores were likely to be dissolved in larger ones causing increase in the thickness of the cell walls with subsequent density increase. Both viscosity effects, influenced by the particle size distribution and chemical composition of mixes, and gas evolution effects, influenced by the PSA content in the mix, defined the optimum powder characteristics and sintering conditions for each type of glass/PSA formulation.

The effect of sintering time on optimum 80/20 glass/PSA mixes of given particle size characteristics sintered at 800 °C was also investigated. Experimental data revealed that the microstructural evolution during sintering can be described by four distinct stages: a) heating, b) glass softening/gas evolution, c) stabilisation and d) further densification. It is during the glass softening/gas evolution stage that porous materials were formed. Expansion mechanism of sintered pellets is a dynamic balance of the gas liberated and the inhibiting effect of liquid viscosity of the semi-molten matrix. The microstructural evolution of glass/PSA mixes during the LWF production process is schematically shown in Figure 9.2. Raw glass/PSA powder mixes of appropriate particle size were formed into approximately spherical ‘green’ pellets followed by rapid sintering to achieve closed-cell grain particles of various sizes.

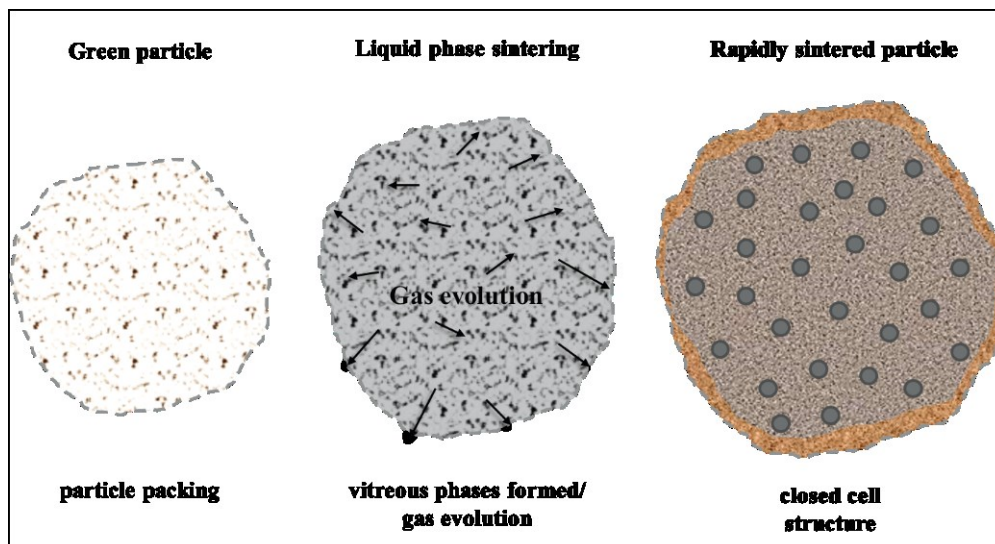


**Figure 9.2** The microstructural evolution of LWF particles from waste glass and paper sludge ash (PSA) is described by the following steps: a) particle packing of initial raw materials, b) bloating of particles during sintering due to gas evolved from PSA constituents being entrapped in the vitrified body and c) final closed-cell porous structures achieved after optimisation of key process parameters.

The final microstructure defined the water absorption and crushing strength properties of sintered products. As expected, density and water absorption were inversely related. For glass/PSA mixes of given composition fired at 800 °C, water absorption variations as a function of sintering time indicated that water absorption is time sensitive. Hence, once maximum bloating was achieved, further sintering led to abrupt increase in water absorption associated with the collapse of the closed-cell pore network and interconnectivity of the pores, as shown in Figure 9.3. The microstructure also determined the crushing strength of LWFs. Glass/PSA samples, having a network of evenly distributed approximately spherical pores, exhibited higher crushing strength-to-density values when compared to commercially available LWF Poraver.

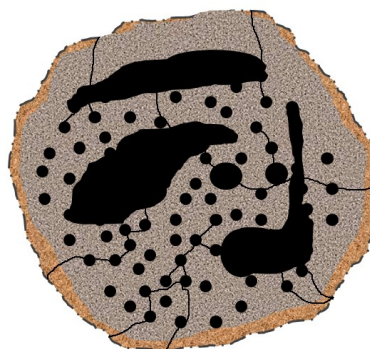


**Figure 9.3** Schematic of porous structures of highly water-absorbent LWF glass/PSA pellets. Sintering of pellets beyond the critical sintering time, as identified for each mix design, resulted in interconnectivity of pores and high water absorption values.

Mineralogical analysis of as-received and optimum 80/20 glass/PSA samples indicated that sintering is responsible for the formation of new crystalline phases. Calcium silicate ( $\text{Ca}_2\text{SiO}_4$ ), quartz ( $\text{SiO}_2$ ), calcium-alumino silicate ( $\text{CaAl}_2\text{SiO}_6$ ) and wollastonite ( $\text{CaSiO}_3$ ) are the new phases present in the sintered products. These are primarily formed due to the transformation of gelhenite ( $\text{Ca}_2\text{Al}_2\text{SiO}_7$ ), the major crystalline phase in as-received PSA, in wollastonite as well as the vitrification of waste glass powder with high amorphous silica ( $\text{SiO}_2$ ) into quartz crystals. Formation of wollastonite is favoured in the excess of calcium oxide. However, given the relatively low sintering temperature, calcium silicate ( $\text{Ca}_2\text{SiO}_4$ ), which is referred to as ‘pseudowollastonite’, was also formed. The higher intensity of the peaks on the optimum 80/20 glass/PSA\_UPM XRD pattern also suggests higher degree of crystallinity favoured by increased sintering reactivity.

Crystallisation of the glass/PSA matrix during sintering at 800 °C is responsible for minimising the leachability of elements of environmental concern under all pH conditions examined. As-received PSA samples had a strong acid neutralisation capacity (ANC). This can be attributed to the carbonation during aging of the PSA powders, leading to the formation of CaCO<sub>3</sub>, which provided significant buffering capacity particularly at high pH values (Guimaraes et al., 2006; Wahlström et al., 2009). The similarity in the leaching curves of Ca, Mg, Na and K of as-received PSA powders supports the possible role of calcite in controlling leaching of alkali metals and alkaline earth metals. Further, heavy metals were immobilised in the new crystalline phases formed or removed by means of volatilisation during sintering. Hence, despite low ANC of sintered glass/PSA LWFs, leaching of hazardous elements is of no concern.

Preparing lightweight cement mortars with glass/PSA LWFs was also investigated. In addition to achieving reduction of density by up to ~28 % when sand was replaced by glass/PSA LWFs, thermal insulation was also improved. This is attributed to the open porosity of the LWFs present in the mortars. Total LWF porosity is inversely related to thermal conductivity. This was expected as air-filled voids within LWFs inhibit heat transfer along the volume of the sample.

## 9.2 PSA-based hydrophobic powders

Surface functionalization phenomena in the PSA/stearic acid system, taking place at room temperature, were investigated in this study. This has not been previously studied. Inducing hydrophobicity on PSA particles via a dry milling method with the use of stearic acid as the surface functionalization agent (SFA) was possible at lab-scale. Exploitation of this feature in construction-related applications include using PSA-based hydrophobic powders as a waterproof concrete additive and/or as coating.

Dry milling of as-received PSA powders with addition of 1 wt. % stearic acid resulted in surface functionalization of PSA particles with hydrophobic characteristics. Increasing the stearic acid content up to 8 wt. % as well as increasing the milling time favoured further hydrophobisation of PSA surfaces. This suggests that surface modification of PSA particles via dry grinding is a cooperative effect of mechanical and chemical modification phenomena.

Dry milling caused the fracture of PSA particles due to high stress developed inside the particles and impact between the grinding media. Dry milling PSA for 16 hours resulted in agglomerated particles due to smaller interparticle distances promoting particle collision. This suggests that deformation of PSA particles ceased once maximum particle size reduction was achieved, which was associated with equipment- and materials-specific limitations. Given that grinding was carried out at room temperature, the modification of PSA particles via stearic acid adsorption was expected to be physical rather than chemical. However, TGA/DSC analysis of optimum hydrophobic particles confirmed that stearate ions were also chemically bonded to polar cationic sites of the inorganic substrate. The mechanical treatment of solids not only multiplied the number of contacts between PSA and stearic acid but also increased the pressure and temperature at the site of contact. This favoured interactions between PSA and stearic acid at the molecular level and led to the formation of stearate salts.

In particular, hydrophobicity of PSA is attributed to the formation of a calcium stearate monolayer on the surface of PSA particles. One stearic acid molecule is attached to one  $\text{Ca}^{+2}$  ion to favour the formation of calcium stearate according to:



The above mechanism is suggested based on experimental data from investigating the effect of dry milling of calcium carbonate, lime and silica fume in the presence of stearic acid. Unlike the rest of the inorganic substrates, dry milling of pure calcium carbonate, under optimum grinding conditions, led to strong hydrophobisation effects similar to the ones observed for as-received PSA samples. Based on previous research findings with regard to surface modification mechanisms of calcium carbonate with stearic acid, inducing hydrophobicity on calcium carbonate particles has been proved possible via steric stabilisation on the surface of calcium carbonate particles (Jeong et al., 2009; Hait et al., 2013; Mihajlovic et al., 2009; Chen et al., 2010).

Surface modification processes, developed in the aforementioned studies, involved either wet milling of nano-sized calcium carbonate particles with stearic acid solvents or dry milling at high temperatures ( $\sim 100^\circ\text{C}$ ). The only less energy-intensive modification process was suggested by Mihajlović et al. (2013) and it involved dry milling calcium carbonate particles with stearic acid for 7 minutes at  $70^\circ\text{C}$ . This

produced chemically and physically bonded monolayers of calcium stearate on calcium carbonate particles with hydrophobic properties when 4 wt. % of stearic acid was added to the mill.

In this study, however, prolonged dry milling times are likely to have increased the temperature at the grain-boundary region that could promote solid-state reactions between exposed  $\text{Ca}^{+2}$  and stearic acid. Based on the above analysis, hydrophobisation of PSA particles is attributed primarily to the surface modification of calcite particles present in PSA by stearic acid, as schematically shown in Figure 9.4.

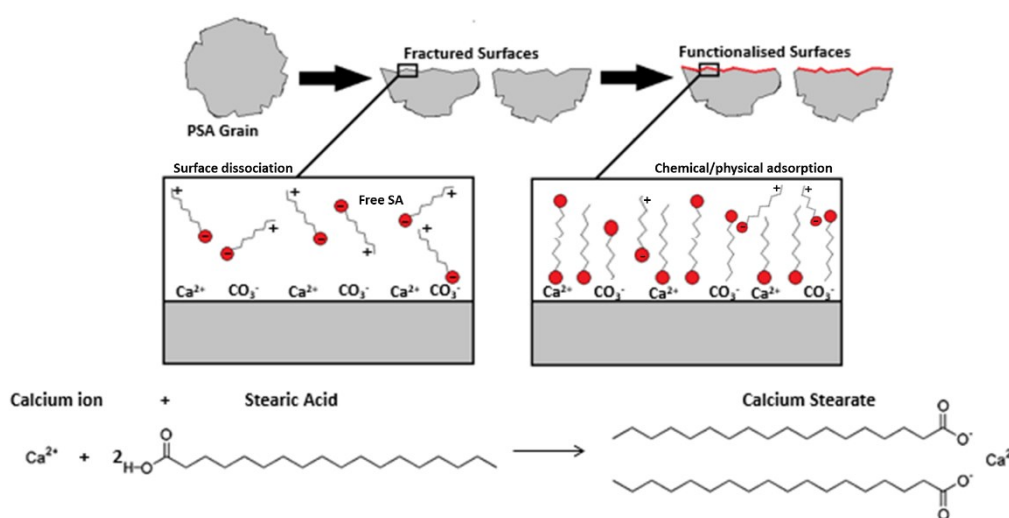


**Figure 9.4** Schematic diagram of the surface functionalization of PSA particles by stearic acid molecules via prolonged dry milling. The possible structure of organic layers formed on fractured surfaces of PSA involves formation of bonds between stearate ions and  $\text{Ca}^{+2}$  from calcite particles present in PSA. Chemisorption reactions led to the formation of a monolayer with the hydrocarbon tails perpendicular to the  $\text{Ca}^{+2}$  surface. Physisorption is also identified due to the local bilayers formed by the tail-to-tail arrangement of hydrocarbon chains. Free stearic acid molecules can also be found.

Higher levels of calcite in the PSA\_ANP samples explain greater hydrophobicity ( $\text{WCA} > 150^\circ$ ) compared to PSA\_UPM samples. It is to be noted, however, that other calcium-containing crystalline phases in PSA could have acted as a source of  $\text{Ca}^{+2}$  ions after breaking of chemical bonds in crystalline phases due to aggressive grinding. TGA was used to differentiate between chemisorbed, intercalated (multilayers) and free stearic acid molecules, which may be found on the surface of PSA particles. TGA data showed that all three forms of stearic acid were present. This caused

inhomogeneous calcium coating and formation of surface bicarbonates explaining scattered hydrophilicity trends when dispersing hydrophobic powders in water.

Recent research at Imperial College London explored the potential to develop liquid superhydrophobic coating formulations using superhydrophobic PSA\_ANP particles. This involved mixing hydrophobic particles with polystyrene (organic adhesive) dissolved in hexane solutions to produce hydrophobic, paint-type solvents. Coatings applied on glass surfaces exhibited hydrophobic properties but resistance against abrasion was low. Also, rigorous agitation-induced shear stresses on hydrophobic particles dispersed in water led to loss of superhydrophobicity (WCA~100°) (Tzouganatos, 2015). Hence, further optimisation of the modification mechanism is required, as proposed in the next chapter.

## CHAPTER 10 Conclusions and Recommendations

The feasibility of producing lightweight filler materials from paper sludge ash and waste glass was investigated. Given collaboration with the UK paper industry, initial focus was placed on maximising PSA content in glass/PSA mix designs. Dry grinding of PSA samples was employed in an attempt to enhance the identified poor sintering reactivity of as-received PSA. Although, this was not achieved, the addition of stearic acid during the dry grinding process resulted in the unexpected effect of inducing hydrophobicity to PSA particles. This outcome gave a new perspective to the research project which also explored the surface functionalization of PSA particles with the aid of appropriate organic surface modifiers.

The findings indicate significant potential for the manufacture of high-performance LWFs containing PSA that is currently disposed of to landfill or used in low-value applications. PSA-based hydrophobic powders consist a novel application with great commercial potential.

### 10.1 Thesis conclusions

Key conclusions derived from the present PhD thesis are:

1. As-received PSA, supplied by the UK paper mills Aylesford Newsprint Ltd. and UPM-Shotton Ltd., had low sintering reactivity. Addition of waste glass promoted sintering. Hence, at the temperature of 800 °C, glass/PSA mixes, with up to a glass:PSA ratio of 4:1, produced foamed glass particles suitable for use as lightweight fillers. This sintering temperature is considerably lower compared to a sintering temperature of 900 °C employed for the production of Poraver<sup>®</sup>, a leading commercially available LWF.
2. The mechanisms controlling microstructural evolution during sintering of the 80/20 glass/PSA (% w/w) feedstocks are:
  - evolution of gases from the thermally unstable constituents present in PSA and
  - presence of the viscous glassy phase able to entrap the gases evolved.

Addition of fine waste glass powder, with a softening point determined at 594 °C, provided adequate low-viscosity vitreous phases during sintering able to lead to rigid glass/PSA structures. In the glass/PSA system, PSA addition acts as the

expanding agent owing to decomposition of, primarily, calcite species, formed by carbonation of PSA during aging. PSA\_ANP had higher calcite content compared to PSA\_UPM.

3. Wet milling 80/20 glass/PSA mixes favours the formation of calcium hydroxide ( $\text{Ca(OH)}_2$ ) through reaction between free lime ( $\text{CaO}$ ) present in PSA and water. Optimum wet milling times for the 80/20 glass/PSA\_ANP and PSA\_UPM mixes were 1 hour and 4 hours, respectively. Decomposition of  $\text{Ca(OH)}_2$  at high temperatures played an enabling role in pore growth.
4. Sintering time was critical in attaining expansion and sealing of the vitrified layer formed during sintering of the 80/20 glass/PSA mixes. Early-stage densification was followed by interconnectivity of pores after sintering for 10 minutes, manifested by abrupt changes in water absorption rates.
5. Optimum spherical pellets of glass/PSA had twice the strength-to-density ratios of Poraver<sup>®</sup> LWFs and exhibited up to 88 % lower water absorption.
6. Incorporation of the optimum 80/20 glass/PSA LWFs in cement mortars by means of partial substitution of sand grains by 40 % w/w, reduced thermal conductivity by 22 %, compared to control mortar samples.
7. Dry grinding PSA with stearic acid resulted in superhydrophobic powders due to the physi- and chemisorption of stearate ions on  $\text{Ca}^{+2}$  fracture PSA surfaces.
8. PSA exhibited the highest hydrophobicity among calcium carbonate, lime and silica fume substrates treated under the same milling conditions. Stearic acid provided optimum surface modification of PSA particles in contrast to capric, myristic and behenic acid.
9. Both plastic deformation of PSA particles, induced via grinding, and concentration of stearic acid determined the nature and extent of adsorption of stearic acid molecules on PSA particles. Superhydrophobic PSA-based powders were produced with 4 wt. % addition of stearic acid when dry milled for 8 hours.

## 10.2 Recommendations for further work

Based on research completed to date, it was shown that the production of LWFs from a glass/PSA system is feasible when rapid sintering takes place. A separate dry grinding method showed potential for converting PSA particles into hydrophobic powders. Further optimisation of these processes is recommended in order to address

key issues, as raised below, in order to make more informed decisions on the potential of PSA as an alternative raw material for the production of LWF and hydrophobic additives.

- In the present study, two types of PSA were used establishing that optimum sintering conditions examined were material-specific. It is, therefore, proposed that the variation in the composition of PSA and/or glass over time, geographical location and source of supply is further investigated.
- Sintering of the optimum the 80/20 glass/PSA mixes was found to be considerably time-sensitive, with sintering time greatly influencing the final microstructure of end-fillers. Hence, it is recommended that a kinetic model is developed allowing for predictions of final properties in a more quantitative way. This could serve as a tool for making informed decisions in potential optimisation studies of scaling up the proposed technology. An inclusive model accounting for viscous and gas evolution flows, would also have associated economic benefits, given that time-dependent experiments are costly and time-consuming.
- The underlying driver for the manufacturing of waste-derived LWFs and hydrophobic powders is the valorisation of PSA in added-value applications. Hence, the total CO<sub>2</sub> emissions embodied throughout the life cycle of the products need to be considered. A cradle-to-cradle approach is required in order to evaluate the sustainability credentials of end-products and environmental impact. In parallel with technical feasibility, economic viability of the suggested processes needs to be appraised through detailed cost-benefit analysis.
- Dry grinding PSA with stearic acid resulted in hydrophobicity. Recent research at Imperial College showed that optimum superhydrophobic particles did not retain their strong hydrophobic properties when rigorously agitated in water. An alternative processing method based on typical surface modification methods applied to calcite particles should be investigated.
- If PSA-based hydrophobic materials are to be used in concrete, an effective way of in-situ hydrophobisation of PSA particles in a cement/PSA system should be investigated. Alternative processing methods need to be explored for the development of spray- or membrane-type hydrophobic coatings.
- Incorporation of glass/PSA LWFs and PSA-based hydrophobic powders in polymer and paint formulations should also be investigated.

## REFERENCES

- Adriano, D.C. (2001) Trace elements in terrestrial environments. Biogeochemistry, bioavailability and risks of metals. Springer-Verlag, New York.
- Anagnostopoulos, I.M. & Stivanakis, V.E. (2009) Utilization of lignite power generation residues for the production of lightweight aggregates. *Journal of Hazardous Materials*, 163, pp. 329–336.
- Angelopoulos, P.M., Gerogiorgis, D.I. & Paspaliaris, I. (2013) Model-Based Sensitivity Analysis and Experimental Investigation of Perlite Grain Expansion in a Vertical Electrical Furnace. *Industrial & Engineering Chemistry Research*, 52(50), pp. 17953-17975.
- ASTM C-1113-99 (Reapproved 2004) Standard Test Method for thermal conductivity of refractories by hot wire (Platinum Resistance thermometer technique).
- Avramov, I., Vassilev, T.S. & Penkov, I. (2005) The glass transition temperature of silicate and borate glasses. *Journal of Non-Crystalline Solids*, 351, pp. 472-476.
- Babu, D.S., Babu, K.G. & Tiong-Huan, W. (2006) Effect of polystyrene aggregate size on strength and moisture migration characteristics of lightweight concrete. *Cement and Concrete Composites*, 28(6), pp. 520-527.
- Bai, J., Chaipanicha, A., Kinuthia, J.M., O'Farrella, M., Sabira, B.B., Wilda, S., Lewis, M.H. (2003) Compressive strength and hydration of wastepaper sludge ash-ground granulated blastfurnace slag blended pastes. *Cement and Concrete Research*, 33, pp. 1189–1202.
- Bale, C.W., Bélisle, E., Chartrand, P., Deckerov, S.A., Eriksson, G., Hack, K., Jung, I.-H., Kang, Y.-B., Melançon, J., Pelton, A.D., Robelin, C. & Petersen, S. (2009) FactSage thermochemical software and databases — recent developments. *Calphad*, 33(2), pp. 295-311.
- Barbieri, L., Corradi, A. & Lancellotti, I. (2000) Bulk and sintered glass-ceramics by recycling municipal incinerator bottom ash. *Journal of the European Ceramic Society*, 20 (10), pp. 1637-1643.
- Barriga, Méndez, S.A., Camara, J., Guerrero, F. & Gasco, G. (2010) Agricultural valorisation of de-inking paper sludge as organic amendment in different soils. *Thermal Analysis and Calorimetry*, 99, pp. 981–986.
- Barthlott, W. & Neinhuis, C. (1997) Purity of the sacred lotus, or escape from contamination in biological surfaces. *Planta*, 202 (1997), pp. 1–8.

- Beauchamp, C.J, Boulanger, R., Matte, R. & Saint-Laurent, G. (2002) Examination of the contaminants and performance of animals fed and bedded using de-inking paper sludge. *Archives of Environmental Contamination and Toxicology*, 42, pp. 523–528.
- Bernardo, E., Castellan, R. & Hreglich, S. (2007) Sintered glass-ceramics from mixtures of wastes. *Ceramics International*, 33 (1), pp. 27–33.
- Bethanis, S., Cheeseman, C.R. & Sollars C.J. (2004). Effect of sintering temperature on the properties and leaching of incinerator IBA. *Waste Management Resources*, 22 (4), pp. 225-264.
- Bijen, J.M.J.M. (1986) Manufacturing Processes of Artificial Lightweight Aggregates From Fly Ash. *The International Journal of Cement and Lightweight Concrete*, 8(3), pp. 191-199.
- Blengini, G.A., Bustoa, M., Fantoni, M. & Fino, D. (2012) Eco-efficient waste glass recycling: Integrated waste management and green product development through LCA. *Waste Management*, 32, pp. 1000-1008.
- Boccaccini, A.R., Stumpfe, W. Taplin, D.M.R. & Ponton, C.B. (1996) Densification and crystallization of glass powder compacts during constant heating rate sintering. *Materials Science and Engineering*, A219, pp. 26-31.
- British Glass Manufacturers' Confederation. (2009) UK Glass Manufacture 2008: A mass balance. London, British Glass Manufacturer's Confederation.
- British Standards Institution (2001) EN 998-2:2001 Specification for mortar for masonry. Part 2: Masonry mortar. London, British Standards Institution.
- British Standards Institution (2003) BS EN 998-1:2003 Specification for mortar for masonry. Part 1: Rendering and plastering mortar. London, British Standards Institution.
- British Standards Institution. (1997) BS EN 10545-3:1997. Ceramic tiles. Part 3: Determination of water absorption, apparent porosity, apparent relative density and bulk density. London, British Standards Institution.
- British Standards Institution. (1997) BS EN 12457-2:2002. Compliance test for leaching of granular waste materials and sludges. One stage batch test at a liquid to solid ratio of 10 l/kg for materials with particle size below 4 mm (without or with size reduction). London, British Standards Institution.

- British Standards Institution. (1999) BS EN 1015-3:1999. Methods of test for mortar for masonry. Determination of consistence of fresh mortar (by flow table). London, British Standards Institution.
- British Standards Institution. (1999) BS EN 1015-6:1999. Methods of tests for mortar for masonry: Determination of bulk density of fresh mortar. London, London, British Standards Institution.
- British Standards Institution. (2002) BS 13055-1:2002. Lightweight aggregates. Part 1: Lightweight aggregates for concrete, mortar and grout. London, British Standards Institution.
- British Standards Institution. (2002) BS EN 13657:2002. Characterization of waste — Digestion for subsequent determination of aqua regia soluble portion of elements. London, British Standards Institution.
- British Standards Institution. (2005) BS EN 196-1:2005. Methods of testing cement- Part 1: Determination of strength. London, British Standards Institution.
- British Standards Institution. (2013) BS EN1097-11:2013. Tests for mechanical and physical properties of aggregates. London, British Standards Institution.
- Callies, M. & Quéré, D. (2005) On water repellency. *Soft Matter*, 1, pp. 5-61.
- Cassie, A.B.D. & Baxter, S. (1944) Wettability of porous surfaces. *Transactions of the Faraday Society*, 40, pp. 546–551.
- Chambers, L.D., Stokes, K.R., Walsh, F.C. & Wood, R.J.K. (2006) Modern approaches to marine antifouling coatings. *Surface & Coatings Technology*, 201, pp. 3642–3652.
- Chan, T-Y. & Lin, S-T. (2005) Effects of stearic acid on the injection molding of alumina. *Journal of the American Ceramic Society*, 78(10), pp. 2746-2752.
- Chandra, S. & Berntsson, L. (2003) *Lightweight Aggregate Concrete*. New York, USA. William Andrew Publishing.
- Cheeseman, C.R, Makinde, A. & Bethanis, S. (2004) Properties of lightweight aggregate produced by rapid sintering of incinerator bottom ash. *Resources, Conservation and Recycling*, 43, pp. 147–162.
- Cheeseman, C.R. & Viridi, G.S. (2005) Properties and microstructure of lightweight aggregate produced from sintered sewage sludge ash. *Resources, Conservation and Recycling*, 54(1), pp. 18-30.

- Chen, Y, Ji, X., Zhao, G., Wang, X. (2010) Facile preparation of cubic calcium carbonate nanoparticles with hydrophobic properties via a carbonation route. *Powder Technology*, 200, pp. 144–148.
- Chindaprasirt, P., Jaturapitakkul, C. & Rattanasak, U. (2009) Influence of fineness of rice husk ash and additives on the properties of lightweight aggregate. *Fuel*, 88, pp. 158–162.
- Cioffi, R., Colangelo, F., Montagnaro, F. & Santoro, L. (2011) Manufacture of artificial aggregate using MSWI bottom ash. *Waste Management*, 31(2), pp. 281-288.
- Clarke, J.L. (1993) *Structural Lightweight Aggregate Concrete (First Edition)*. Glasgow, Blackie Academic & Professional, an imprint of Chapman & Hall, Wester Cleddens Road, Bishop Briggs.
- Concrete Society (2013) The influence of integral water-resisting admixtures on the durability of concrete. CS, 174 (Camberley).
- Confederation of European Paper Industries (CEPI) (2010) About Paper: Papermaking History. [Online]. Available from: <http://www.cepi.org/aboutPaper> [Accessed 3rd November 2014].
- Confederation of European Paper Industries (CEPI) (2011) Maximum value from paper for recycling –Towards a multi-product paper mill. CEPI.
- Confederation of European Paper Industries (CEPI) (2013) Sustainability Report 2013. CEPI.
- Confederation of Paper Industries (CPI) (2014) Code of good practice for landspreading paper Mill sludges. CPI.
- Constructing Excellence (2008) ‘Construction and Sustainable Development’, Plain English. [Online] Available from: <http://www.constructingexcellence.org.uk> [Accessed 20th January 2015].
- Cusido, J.A. & Soriano, C. (2011) Valorization of pellets from municipal WWTP sludge in lightweight clay ceramics. *Waste Management*, 31, pp. 1372-1380.
- De Gennes, P.G. (1985) Wetting – statics and dynamics. *Reviews of Modern Physics*, 57(3), pp. 827–863.
- De la Varga, I., Castro, J., Bentz, D.P. & Weiss, W.J. (2012) Application of internal curing for mixtures containing high volumes of fly ash. *Cement and Construction Composites*, 34(9), pp. 1001–1008.

- de' Gennaro, R., Graziano, S.F., Cappelletti, P., Colella, A., Dondi, M., Langella, A. & de' Gennaro, M. (2009) Structural concretes with waste-based lightweight aggregates: from landfill to engineered materials. *Environmental Science Technology*, 43, pp. 7123-7129.
- DEFRA (2009) Codes of Good Agricultural Practice. Defra, UK.
- Demeyer, A & Verloo, M (1999) Evaluation of paper sludge as organic fertiliser for growth of ryegrass on a Belgian clay soil. *Agrochimica*, 43, pp. 243-250.
- Demharte, A. (1998) Polyurethane rigid foam, a proven thermal insulating material for applications between +130 °C and -196 °C. *Cryogenics*, 38, pp. 113–117.
- Department for Business Innovation & Skills (BIS) (2010) Estimating the amount of CO<sub>2</sub> emissions that the construction industry can influence. BIS
- Devarajan, A., Khadar, M.A. & Chattopadhyay, K. (2007) Effect of ball milling on chemically synthesized nanoparticles of CaCO<sub>3</sub>. *Materials Science and Engineering A*, 452-453, pp. 395-400.
- Doel, A. (2007) Lightweight aggregates for use in concrete. *Concrete*, 41, pp. 36-37.
- Ducman, V. & Mirtiç, B. (2014) Water vapour permeability of lightweight concrete prepared with different types of lightweight aggregates. *Construction and Building Materials*, 68, pp. 314-319.
- Ducman, V., Mladenovic, A. & Suput, J.S. (2002), Lightweight aggregate based on waste glass and its alkali-silica reactivity. *Cement and Concrete Research*, 32, pp. 223–226.
- Dunster, A.M. (2007) Case study: Paper sludge and paper sludge ash in Portland cement manufacture. Characterisation of Mineral Wastes, Resources and Processing technologies – Integrated waste management for the production of construction material, University of Leeds, UK.
- Engel, P. & Moore, B. (1998) Recycled mills seek options to turn deinking residuals into resources. *Pulp & Paper*, 72(4), pp. 83–88.
- Environment Agency (2007) Environmental Permitting (England and Wales) Regulations. SI 2007 No. 3538. [Online]. Available from: [http://www.opsi.gov.uk/si/si2007/uksi\\_20073538\\_en\\_1](http://www.opsi.gov.uk/si/si2007/uksi_20073538_en_1) [Accessed 7 November 2012].
- Environment Agency (2009) Science Report SC050021/ arsenic SGV: Soil Guideline Values for inorganic arsenic in soil. Environment Agency, Bristol.

- ESCSI (2004) Structural Lightweights' Holistic Contribution to Sustainable Development. [Online] Available from: [http://www.escsi.org/uploadedFiles/Technical\\_Docs/General\\_Information/7700.0%20SLWA%20Holistic%20Contribution%20to%20Sustainable%20Development.pdf](http://www.escsi.org/uploadedFiles/Technical_Docs/General_Information/7700.0%20SLWA%20Holistic%20Contribution%20to%20Sustainable%20Development.pdf) [Accessed: February 1st 2013].
- European Commission (1999) Directive 99/31/EC: The landfill of waste, European Commission.
- European Commission (2000) Directive 2000/76/EC: Incineration of waste. European Commission.
- European Commission (2003) Council Decision 2003/33/EC: Establishing criteria and procedures for the acceptance of waste at landfills pursuant to Article 16 of and Annex II to Directive 1999/31/EC, European Commission.
- European Commission (2004) Directive 2004/62/EC: Packaging and Packaging Waste. European Commission.
- European Commission (2011) Roadmap to a Resource Efficient Europe. European Commission. [Online] Available from: [http://ec.europa.eu/environment/resource\\_efficiency/about/roadmap/index\\_en.htm](http://ec.europa.eu/environment/resource_efficiency/about/roadmap/index_en.htm) [Accessed 10th December 2015].
- European Commission (2014) Best Available Techniques (BAT) Reference Document for the Production of Pulp, Paper and Board. European Commission.
- Fang, Y., Sun, G., Cong, Q., Chen, G.H. & Ren, L.Q. (2008) Effects of methanol on wettability of the non-smooth surface on butterfly wing. *Journal of Bionic Engineering*, 5, pp. 127-133.
- Fava, G., Ruello, M.L. & Corinaldesi, V. (2011) Paper mill sludge ash as supplementary cementitious material. *Journal of Materials in Civil Engineering*, 23, pp. 772-776.
- Fekete, E. & Pukanszky, B., Toth, A. & Bertoti, I. (1990) Surface Modification and Characterization of Particulate Mineral Fillers. *Journal of Colloid and Interface Science*, 135(1), pp. 200-208.
- Feng, L., Zhang, Y.A., Xi, J.M., Zhu, Y., Wang, N., Xia, F. & Jiang, L. (2008) Petal effect: a superhydrophobic state with high adhesive force. *Langmuir*, 24, pp. 4114–4119.

- Fenter, P., Eisenberger, P. & Liang, K.S. (1993) Chain-length dependence of the structures and phases of  $\text{CH}_3(\text{CH}_2)_{n-1}\text{SH}$  self-assembled on Au(111). *Physical Review Letters*, 70(16), pp. 2447–2450.
- Ferrandiz-Mas, V., Bond, T., Garcia-Alcocel, E. & Cheeseman, C.R. (2014) Lightweight mortars containing expanded polystyrene and paper sludge ash. *Construction and Building Materials*, 61, pp. 285-292.
- Fluegel, A. (2007) Glass viscosity calculation based on a global statistical modelling approach. *Glass Technology: European Journal of Glass Science and Technology Part A*, 48(1), pp. 13-30.
- Fox, H.W & Zisman, W.A (1950) The spreading of liquids on low energy surfaces. I. polytetrafluoroethylene. *Journal of Colloid Science*, 5(6), pp. 514-531.
- Frías, M. García, R., Vigil, R. & Ferreiro, S. (2008) Calcination of art paper sludge waste for the use as a supplementary cementing material. *Applied Clay Science*, 42, pp. 189-193.
- Fulcher, G. S. (1925) Analysis of recent measurements of the viscosity of glasses. *Journal of the American Ceramics Society*, 8, pp. 339–355.
- Furlani, E., Tonello, G., Maschio, S., Aneggi, E., Minichelli, D., Bruckner, S. & Lucchini, E. (2011) Sintering and characterisation of ceramics containing paper sludge, glass cullet and different types of clayey materials. *Ceramics International*, 37, pp. 1293–1299.
- Georgakopoulos, A., Filippidis, A., Kassoli-Fournaraki, A., Fernandez-Turiel, J-L., Lorens, J-F. & Mousty, F. (2010) Leachability of major and trace elements of fly ash from Ptolemais power station, Northern Greece. *Energy sources*, 24, pp. 103-113.
- German, R.M., Suri, P. & Park, S.J. (2009) Review: Liquid phase sintering. *Journal of Materials Science*, 44, pp. 1-39.
- Giordano, D., Russell, J. K. & Dingwell, D.B. (2008) Viscosity of magmatic liquids: A model. *Earth and Planetary Sciences Letters*, 271, pp. 123–134.
- Gomari, K.A.R., Denoyel, R. & Hamouda, A.A. (2006) Wettability of calcite and mica modified by different long-chain fatty acids (C18 acids) *Journal of Colloid and Interface Science*, 297, pp. 470–479.
- Guimaraes, A.L., Okuda, T., Nishijima, W. & Okada, M. (2006) Organic carbon leaching behaviour from incinerator bottom ash. *Journal of Hazardous Materials*, 137(2), pp. 1096-1101.

- Hait, S.K.D., Christopher, J., Chen, Y., Hodgson, P. & Tuli, D.K. (2013) Preparation and evaluation of hydrophobically modified core shell calcium carbonate structure by different capping agents. *Powder Technology*, 235, pp. 581-589.
- Halla, C., Large, D.J., Adderley, B. & West, H.M. (2014) Calcium leaching from waste steelmaking slag: Significance of leachate chemistry and effects on slag grain mineralogy. *Minerals Engineering*, 65, pp. 156-162.
- Hansen, G., Hamouda, A.A. & Denoyel, R. (2000) The effect of pressure on contact angles and wettability in the mica/water/n-decane system and the calcite+stearic acid/water/n-decane system. *Colloids and Surfaces A: Physicochemical and Engineering Aspects*, 172(1-3), pp. 7-16.
- He, Z. & Ma, J. (2005) Constitutive modelling of alumina sintering: grain-size effect on dominant densification mechanism. *Computational Materials Science*, 32, pp. 196-202.
- Henkensiefken, R., Bentz, D.P., Nantung, T. & Weiss, W.J. (2009) Volume change and cracking in internally cured mixtures made with saturated lightweight aggregate under sealed and unsealed conditions, *Cement and Concrete Composites*, 31(7), pp. 427–437.
- Hernández-Crespo, M.S., Romero, M. & Rincón, J.Ma. (2006) Nucleation and crystal growth of glasses produced by a ceramic plasma arc-process. *Journal of the European Ceramic Society*, 26, pp. 1679–1685
- Huanga, S.-C., Changb, F.-C., Lob, S.-L., Lee, M.Y., Wang, C.-F. & Lin, J.-D. (2007) Production of lightweight aggregates from mining residues, heavy metal sludge, and incinerator fly ash. *Journal of Hazardous Materials*, 144, pp. 52–58.
- Integrated Pollution Prevention and Control (IPPC) (2013). Reference Document on Best Available Techniques in the Pulp and Paper Industry. European Commission, European Commission.
- Jenkins, R. (1999) X-Ray Fluorescence Spectrometry. 2nd edition, John Wiley & Sons, Inc., New York, USA.
- Jeong, S.-B., Yang, Y.-C., Chae, Y.-B. & Kim, B.G. (2009) Characteristics of the Treated Ground Calcium Carbonate Powder with Stearic Acid Using the Dry Process Coating System. *Materials Transactions*, 50(2), pp. 409-414.
- Jones, B.E.H., Haynes, R.J. & Phillips, I.R. (2015) Influence of amendments on acidification and leaching of Na from bauxite processing sand. *Ecological Engineering*, 84, pp. 435-442.

- Karamanov, A., Dzhantov, B., Paganelli, M. & Sighinolfi, D. (2013) Glass transition temperature and activation energy of sintering by optical dilatometry. *Thermochimica Acta*, 553, pp. 1-7.
- Karamberi, A. & Moutsatsou, A. (2005) Participation of coloured glass cullet in cementitious materials. *Cement and Concrete Composites*, 27, pp. 19–27.
- Kazmiruk, V. (2012) Scanning Electron Microscopy. [Online] InTech Publishing. Available from: <http://www.intechopen.com/books/scanning-electron-microscopy> [Accessed 5th June 2015].
- Khedari, J., Suttisonk, B., Pratinthong, N. & Hirunlabh, J. (2001) New lightweight composite construction materials with low thermal conductivity. *Cement and Concrete Composites*, 23(1), pp. 65–70.
- Kim, H., Biswas, J. & Choe, S. (2006) Effects of stearic acid coating on zeolite in LDPE, LLDPE, and HDPE composites. *Polymer*, 47, pp. 3981–3992.
- Kingery, W.D., Bowen, H.C. & Uhlmann, D.R. (1976) Introduction to Ceramics, 2nd Edition, John Wiley and Sons, New York.
- Klipfel, A., Founti, M., Zähringer, K., Martin, J. P. & Petit, J. P. (1998) Numerical simulation and experimental validation of the turbulent combustion and perlite expansion process in an industrial perlite expansion furnace. *Flow Turbulence and Combustion*, 60, pp.283–300.
- Ko, H., Lee, Y.J., Park, H.C., Byun, B.-K. & Lukes, J.R. (2009) Wetting Characteristics of Insect Wing Surfaces. *Journal of Bionic Engineering*, 6, pp. 63-70.
- Kourti, I. & Cheeseman, C. R. (2010) Properties and microstructure of lightweight aggregate produced from lignite coal fly ash and recycled glass. *Resources, Conservation and Recycling*, 54, pp.769-775.
- Kralj, D. (2009) Experimental study of recycling lightweight concrete with aggregates containing expanded glass. *Process Safety and Environmental Protection*, 97, pp. 267-273.
- Kudra, T., Gawrzynski, Z., Glaser, R., Stanislawski, J. & Poirier, M. (2002) Drying of pulp and paper sludge in a pulsed fluid bed dryer. *Drying Technology*, 20 (4-5), pp. 917-933.
- Lin, I.J. & Somasundaran, P. (1972) Alteration in properties of samples during their preparation by grinding. *Powder Technology*, 30, pp. 171-179.

- Lin, Y., Chen, H., Chan, C.-M. & Wu, J. (2011) Effects of coating amount and particle concentration on the impact toughness of polypropylene/CaCO<sub>3</sub> nanocomposites. *European Polymer Journal*, 47, pp. 294–304.
- Liu, W., Xie, Z., Yang, X., Wu, Y., Jia, C., Bo, T. & Wang, L. (2011) Surface modification mechanism of stearic acid to zirconia powders induced by ball milling for water-based injection molding. *Journal of the American Ceramic Society*, 94(5), pp. 1327-1330.
- Lo, Y.T., Cui, H.Z., Tang, W.C. & Leung, W.M (2008) The effect of aggregate absorption on pore area at interfacial zone of lightweight concrete. *Construction and Building Materials*, 22(4), pp. 623-628.
- Lydon, F.D. (1972) Concrete Mix Design. London, Applied Science Publishers, pp. 148.
- Mahmood, T. & Elliott, A. (2006) A review of secondary sludge reduction technologies for the pulp and paper industry. *Water Research*, 40, pp. 2003-2122.
- Mäkinen, L., Ämmälä, A., Körkkö, M. & Niinimäki, J. (2013) The effects of recovering fibre and fine materials on sludge dewatering properties at a deinked pulp mill. *Resources, Conservation & Recycling*, 73(1), pp. 11–16.
- Maldonado-Bandala, E.E., Nieves-Mendozal, D., Romero-López, R., Tobias-Jaramillo, R. Almeraya-Calderón, F., Barrios-Durstewitz, C.P., Núñez Jaquez, R.E. (2015) Electrochemical and Mechanical Properties of Lightweight Concrete Blocks with Expanded Polystyrene Foam. *International Journal of Electrochemical Science*, 10, pp. 472-485.
- Manakasettharn, S., Taylor, J.A. & Krupenkin, T. (2011) Superhydrophobicity at Micron and Submicron Scale. *Comprehensive Nanoscience and Technology*, 4, pp. 383-411.
- Manikandan, R. & Ramamurthy, K. (2007) Influence of fineness of fly ash on the aggregate pelletization process. *Cement & Concrete Composites*, 29, pp. 456–464.
- Marinoni, N., D’Alessio, D., Diella, V., Pavese, A. & Francescon, F. (2013) Effects of soda-lime-silica waste glass on mullite formation kinetics and micro-structures development in vitreous ceramics. *Journal of Environmental Management*, 124, pp. 100-107.
- Maruyama, I., Kanematsu, M., Noguchi, T., Iikura, H., Teramoto, A. & Hayano, H. (2009) Evaluation of water transfer from saturated lightweight aggregate to

- cement paste matrix by neutron radiography, *Nuclear Instruments and Methods in Physics Research*, 605 (1–2), pp. 159–162.
- Matamoros-Veloza, Z., Rendón-Angeles, J.C., Yanagisawa, K., Cisneros-Guerrero, M.A., Cisneros-Guerrero, M.M. & Aguirre, L. (2008) Preparation of foamed glasses from CRT TV glass by means of hydrothermal hot-pressing technique. *Journal of the European Ceramic Society*, 28(4), pp. 739-745.
- Matteucci, F., Dondi, M. and Guarini, G. (2002) Effect of soda-lime glass on sintering and technological properties of porcelain stoneware tiles. *Ceramics International*, 28, pp. 873–880.
- Mihajlović, S.R., Sekulic, Ž., Dakovic, A., Vučinić, D., Jovanovic, V. & Stojanovic, J. (2009) Surface properties of natural calcite filler treated with stearic acid. *Ceramics – Silikáty*, 53 (4), pp. 68-275.
- Mihajlović, S.R., Vučinić, D.R., Sekulić, Z.T., Milićević, S.Z. & Kolonja, B.M. (2013) Mechanism of stearic acid adsorption to calcite. *Powder Technology*, 245, pp. 208-216.
- Modolo, R., Ferreira, V.M, Machado, L.M., Rodrigues, M. & Coelho, I. (2011) Construction materials as a waste management solution for cellulose sludge. *Waste Management*, 31, pp. 370–377.
- Monte, M.C., Fuente, E., Blanco, A. & Negro, C. (2009) Waste management from pulp and paper production in the European Union. *Waste Management*, 29, pp. 293-308.
- Moo-Young, H.K. & Zimmie, T.F. (1996) Geotechnical properties of paper mill sludge for use in landfill covers. *Journal of Geotechnical Engineering*, pp. 768-775.
- Mozaffari, E., Farrell, M.O., Kinuthia, J.M. & Wild, S. (2006) Improving strength development of wastepaper sludge ash by wet-milling. *Cement & Concrete Composites*, 28, pp. 144–152.
- Mozaffari, E., Kinuthia, J.M., Bai, J. & Wild, S. (2009) An investigation into the strength development of Wastepaper Sludge Ash blended with Ground Granulated Blastfurnace Slag. *Cement and Concrete Research*, 39, pp. 942–949.
- Mueller, A., Sokolova S.N. & Vereshagin, V.A (2008) Characteristics of lightweight aggregates from primary and recycled raw materials. *Construction and Building Materials*, 22, pp. 703-712.

- Occhionero, M.A. & Halloran, J.W. (1984) The influence of Green Density upon sintering. In: Kuczynski, G.C., Miller, A.E. & Sargent, G.A. (eds.) *Materials Science Research*, pp. 89-102.
- Ochoa de Alda, J.A.G. (2008) Feasibility of recycling pulp and paper mill sludge in the paper and board industries. *Resources, Conservation and Recycling*, 52, pp. 965–972.
- Olmeda, J., Sanchez de Rojas, M.I., Frias, M., Donatello, S. & Cheeseman, C.R. (2013) Effect of petroleum (pet) coke addition on the density and thermal conductivity of cement pastes and mortars. *Fuel*, 107, pp. 138–146.
- Owens, P. L. (1993) Lightweight aggregates for structural concrete. In: Clarke, J. L. (ed.) *Structural lightweight aggregate concrete*. UK, Chapman & Hall, pp. 1-17.
- Patankar, N.A (2003) On the modeling of hydrophobic contact angles on rough surfaces. *Langmuir*, 18(15), pp. 1249-1253.
- Phillips, V. R., Kirkpatrick, N., Scotford, I.M., White, R.P. & Burton, R.G.O. (1997) The use of paper sludge ashes on agricultural land. *Bioresource Technology*, 60, pp. 73-80.
- Pontikes, Y., Christogerou, A., Angelopoulos, G. N., Rambaldi, E., Esposito, L. & Tucci, A. (2005) Use of scrap soda–lime–silica glass in traditional ceramics. *Glass technology*, 46 (2), pp. 200-206.
- Price, G.J. & Ansari, D.M.A. (2004) Surface modification of calcium carbonates studied by inverse gas chromatography and the effect on mechanical properties of filled polypropylene. *Polymer International*, 53, pp. 430–438.
- PwC and CPA Report. (2012) Material Gains in Sustainability. Available from: <http://pwc.blogs.com/files/pwc-cpa-material-gains.pdf> [Accessed 23rd January 2016].
- Quina, M.J., Bordado, J.C.M. & Quinta-Ferreira, R.M. (2009) The influence of pH on the leaching behaviour of inorganic components from municipal solid waste APC residues. *Waste Management*, 29, pp. 2483–2493.
- Radlinska, A., Raja bi pour, F., Bucher, B., Henkensiefken, R., Sant, G. & Weiss, J. (2008) Shrinkage mitigation strategies in cementitious systems: A closer look at sealed and unsealed material behavior. *Journal of the Transportation Research Board*, 2070, pp. 59–67.
- Ramamurthy, K. & Harikrishnan, K.I. (2006) Influence of binders on properties of sintered fly ash aggregate. *Cement & Concrete Composites*, 28, pp. 33–38.

- Resource Association (2014) ReQIP – Recycling Quality Information Point. [Online] Available from: <http://www.resourceassociation.com/recycling-quality-specifications> [Accessed 6th February 2015].
- Ribeiro, P., Albuquerque, A., Quinta-Nova, L. & Cavaleiro, V. (2010) Recycling pulp mill sludge to improve soil fertility using GIS tools. *Resources, Conservation and Recycling*, 54, pp. 1303-1311.
- Roulia, M., Chassapis, K., Kapoutsis, J. A., Kamitsos, E. I. & Savvidis, T. (2006) Influence of thermal treatment on the water release and the glassy structure of perlite. *Journal of Material Science*, 41, pp. 5870–5881.
- Rungruanga, P., Grady, B.P. & Supaphola, P. (2006) Surface-modified calcium carbonate particles by admicellar polymerization to be used as filler for isotactic polypropylene. *Colloids and Surfaces A: Physicochemical and Engineering Aspects*, 275 (1-3), pp. 114-125.
- Sakthivel, T., Reid L., D., Goldstein, I., Hench, L. & Seal, S. (2013) Hydrophobic high surface area zeolites derived from fly ash for oil spill remediation. *Environmental Science & Technology*, 47 (11), 5843-5850.
- Schmidt, K., Qiu, X., Mathis, N. & Chaplin, G. (2006) Evaluation of thermal interface materials using the modified hot wire technique. In: Dinwiddie RB, White MA, McElroy DL, editors. Proceedings of the 16th international thermal expansion symposium.
- Schreiber, F. (2000) Structure and growth of self-assembling monolayers. *Progress in Surface Science*. 65 (5–8), pp. 151-257.
- Segui, P., Aubert J.E., Husson, B. & Measson, M. (2012) Characterization of wastepaper sludge ash for its valorization as a component of hydraulic binders. *Applied Clay Science*, 57, pp. 79-85.
- Shen, D., Jiang, J. Shen, J., Yao, P. & Jiang, G. (2015) Influence of prewetted lightweight aggregates on the behavior and cracking potential of internally cured concrete at an early age. *Construction and Building Materials*, 99, pp. 260–271.
- Shen, J., Song, Z., Qian, X. & Yang, F. (2010) Carboxymethyl cellulose/alum modified precipitated calcium carbonate fillers: Preparation and their use in papermaking. *Carbohydrate Polymers*, 81(3), pp. 545-553.
- Shirtcliffe, N. J., McHale, G., Atherton, S. & Newton, M. I. (2010) An introduction to superhydrophobicity. *Advances in Colloid and Interface Science*, 161 (1–2), pp. 124-138.

- Sigoli, F.A., Feliciano, S., Giotto, M.V., Davolos, M.R. & Jafelicci, M. (2003) Porous silica matrix obtained from Pyrex glass by hydrothermal treatment — characterization and nature of the porosity. *Journal of the American Ceramic Society*, 86, pp. 1196-1201.
- Sivakumar, S., Pradip, P.C. Kapur, P.C. & Malghan, S.G. (1998) A size interval-by-size interval marching algorithm for modelling grain growth in the intermediate stage of sintering. *Physicochemical and Engineering Aspects*, 133, pp. 173-182.
- Smith, R. & Tanford, C. (1973) Hydrophobicity of long chain n-alkyl carboxylic acids, as measured by their distribution between heptane and aqueous solutions. *Proceedings of the National Academy of Sciences USA*, 70(2), pp. 289–293.
- Spaeth, M., Solga, A., Barthlott, W. & Cerman, Z. (2006) Funktionale bautenoberflächen: wie testet man mikrobiellen bewuchs? *Altbauinstandsetzung*, 11, pp. 203–14.
- Spathi, C. (2011) Influence of raw material particle aggregate properties size on artificial lightweight. MSc thesis. Imperial College London.
- Steiger, R.W & Hurd, M.K. (1978) Lightweight insulating concrete for floors and roof decks. *Concrete Construction*, 23 (7), pp. 411–422.
- Sweeney, S.M. & Mayo, M.J. (2002) Green density-based sintering predictions.
- Timoshenko, S.P. & Goodier, J.N. (1984) Theory of Elasticity. *Engineering Societies Monographs*, New York: McGraw-Hill.
- Trunec, M., Dobšák P. & Cihlár, J. (2000) Effect of powder treatment on injection moulded zirconia ceramics. *Journal of the European Ceramic Society*, 20, pp. 859-866.
- Trutschler, J.D. (1999) Fibre recovery—reducing operating costs and sludge. *Paper Technology*, 40 (7), pp. 97–100.
- Tseng, W.-J. (2000) Influence of surfactant on rheological behaviors of injection–molded alumina suspensions. *Materials Science and Engineering A*, 289(1-2), PP. 116-122.
- Tzouganatos, I. (2015) Hydrophobic coatings from paper sludge ash. MSc Thesis, Imperial College London.
- Valum, R. S. (1995) Production, Construction and Quality Control of High Performance LWA Concrete for Marine and Other Severe Exposure Environments Structural Lightweight Aggregate (LWA) Concrete Summit, May 25-26, 1995. North Carolina.

- Van der Sloot, H.A., & Kosson, D.S. (2012) Use of characterisation leaching tests and associated modelling tools in assessing the hazardous nature of wastes. *Journal of Hazardous Materials*, 207-208, pp. 6-43.
- Van der Sloot, H.A., Kosson, D.S. & Hjelm, O. (2001) Characteristics, treatment and utilisation of residues from municipal waste incineration, *Waste Management*, 21, pp. 753-765.
- Vogel, D. H. (1921) Temperaturabhängigkeitsgesetz der viskosität von flüssigkeiten. *Zeitschrift für Physikalische Chemie*, 22, pp. 645–646.
- Vozár, L. (1996) A Computer-Controlled Apparatus for Thermal Conductivity Measurement by the Transient Hot Wire Method, *Journal of Thermal Analysis*, 46, pp. 495-505.
- Vrana, T. & Bjork, F. (2009) Frost formation and condensation in stone-wool insulations. *Construction Building Materials*, 23(5), pp. 1775–1187.
- Wahlström, M. Laine-Ylijoki, J., Kaartinen, T. & Hjelm, O. (2009) Acid neutralization capacity of waste - specification of requirement stated in landfill regulations. Copenhagen, Nordic Council of Ministers.
- Wang, K-S., Tsen, C-J., Chiou, I-J. & Shih M-H. (2005) The thermal conductivity mechanism of sewage sludge ash lightweight materials. *Cement and Concrete Research*, 35, pp. 803–809.
- Wang, S., Feng, L., Liu, H., Sun, T., Zhang, X. & Jiang L. (2005) Manipulation of surface wettability between superhydrophobicity and superhydrophilicity on copper films. *ChemPhysChem*, 6, pp. 1475– 1478.
- Waseda, Y., Matsubara, E. & Shinoda, K. (2011) X-Ray Diffraction Crystallography. Springer Berlin Heidelberg, Germany.
- Wei, Y-L., Lin, C-Y., Ko, K-W. & Wang, H.P. (2011) Preparation of low water-sorption lightweight aggregates from harbour sediment added with waste glass. *Marine Pollution Bulletin*, 63(5-12), pp.135-140.
- Wenzel, R.N. (1936) Resistance of solid surfaces to wetting by water. *Industrial and Engineering Chemistry*, 28(8), pp. 988-994.
- WRAP (2004) Research into using recycled waste paper residues in construction products. WRAP Project code: PAP009-011. WRAP, UK.
- WRAP (2007) Paper Sludge Ash: A technical report on the production and use of paper sludge ash. WRAP, UK.

- WRAP (2013) Glass Flow 2012. [Online] Available from: <http://www.wrap.org.uk/sites/files/wrap/GlassFlow%20Final%20Report.pdf> [Accessed: December 3rd 2014].
- Yan, S., Sagoe-Crentsila, K. & Shapiro, G. (2011) Reuse of de-inking sludge from wastepaper recycling in cement mortar products. *Journal of Environmental Management*, 92 (8), pp. 2085-2090.
- Yan, Y.Y., Gao, N. & Barthlott, W. (2011) Mimicking natural superhydrophobic surfaces and grasping the wetting process: A review on recent progress in preparing superhydrophobic surfaces. *Advances in Colloid and Interface Science*, 169(2), pp. 80-105.
- Yao, N., Zhang, P., Song, L., Kang, M., Lu, Z. & Zheng, R. (2013) Stearic acid coating on circulating fluidized bed combustion fly ashes and its effect on the mechanical performance of polymer composites. *Applied Surface Science*, 279, pp. 109-115.
- Young, T. (1805) An essay on the cohesion of fluids. *Philosophical Transactions*, pp. 65-87.
- Yu, Q.L, Spiesz, P. & Brouwer, H.J.H. (2013) Development of cement-based lightweight composites – Part 1: Mix design methodology and hardened properties. *Cement and Concrete Composites*, 44, pp. 17-29.
- Zhou, X., Zheng, F., Li, H., Lu, C. (2010) An environment-friendly thermal insulation material from cotton stalk fibers. *Energy and Buildings*, 42(7), pp. 1070–1074.
- Zhutovsky, S., Kovler, K. & Bentur, A. (2004) Assessment of Water Migration Distance in Internal Curing of High Strength Concrete, in ACI SP-220 Autogenous Deformation of Concrete, American Concrete Institute (O. M. Jensen, D. P. Bentz and P. Lura, Eds). Farmington Hills, MI, pp. 181–200.
- Zullig, J.J. & Morse, J.W. (1988) Interaction of organic acids with carbonate mineral surfaces in seawater and related solutions: I. Fatty acid adsorption. *Geochimica et Cosmochimica Acta*, 52, pp. 1667-1678.

## APPENDIX A

Table A.1 summarizes the properties rendering waste materials hazardous, as described in Annex III of the Waste Framework EU Directive 2008/98/EC on waste.

**Table A.1** Properties of wastes which render them hazardous

<b>H1</b>	'Explosive': substances and preparations which may explode under the effect of flame or which are more sensitive to shocks or friction than dinitrobenzene.
<b>H2</b>	'Oxidizing': substances and preparations which exhibit highly exothermic reactions when in contact with other substances, particularly flammable substances.
<b>H3-A</b>	'Highly flammable': — liquid substances and preparations having a flash point: below 21 °C (including extremely flammable liquids), or — substances and preparations which may become hot and finally catch fire in contact with air at ambient temperature without any application of energy, or — solid substances and preparations which may readily catch fire after brief contact with a source of ignition and which continue to burn or to be consumed after removal of the source of ignition, or — gaseous substances and preparations which are flammable in air at normal pressure, or — substances and preparations which, in contact with water or damp air, evolve highly flammable gases in dangerous quantities.
<b>H3-B</b>	'Flammable': liquid substances and preparations having a flash point equal to or greater than 21 °C and less than or equal to 55 °C.
<b>H4</b>	'Irritant': non-corrosive substances and preparations which, through immediate, prolonged or repeated contact with the skin or mucous membrane, can cause inflammation.
<b>H5</b>	'Harmful': substances and preparations which, if they are inhaled or ingested or if they penetrate the skin, may involve limited health risks.
<b>H6</b>	'Toxic': substances and preparations (including very toxic substances and preparations) which, if they are inhaled or ingested or if they penetrate the skin, may involve serious, acute or chronic health risks and even death.
<b>H7</b>	'Carcinogenic': substances and preparations which, if they are inhaled or ingested or if they penetrate the skin, may induce cancer or increase its incidence.
<b>H8</b>	'Corrosive': substances and preparations which may destroy living tissue on contacts.
<b>H9</b>	'Infectious': substances containing viable micro-organisms or their toxins which are known or reliably believed to cause disease in man or other living organisms.
<b>H10</b>	'Teratogenic': substances and preparations which, if they are inhaled or ingested or if they penetrate the skin, may induce non-hereditary congenital malformations or increase their incidence.

- 
- H11** 'Mutagenic': substances and preparations which, if they are inhaled or ingested or if they penetrate the skin, may induce hereditary genetic defects or increase their incidence.
- H12** Substances and preparations which release toxic or very toxic gases in contact with water, air or an acid.
- H13** Substances and preparations capable by any means, after disposal, of yielding another substance, e.g. a leachate, which possesses any of the characteristics listed above.
- H14** 'Ecotoxic': substances and preparations which present or may present immediate or delayed risks for one or more sectors of the environment.
-

## APPENDIX B

The major leaching controlling factors and mechanisms of release of elements contained in a porous monolithic solid are illustrated schematically in Figure B.1. Valorisation, reuse and ultimate disposal of waste materials will depend on the potential interactions with water. This interaction, called ‘leaching’, is a complex reactional process of transfer of pollutants to the environment which relates to toxicity and eco-toxicity. This research project focused on the effect of pH variations on leachability of bulk and trace elements present in PSA and optimum 80/20 glass/PSA LWFs.

The pH-dependence test conducted is a compliance test used to determine if the waste complies with specific reference leaching limits (**Table B.1**). The same test was performed to assess the leachable potential of constituents present in sintered LWFs. However, it should be noted that aggregates should comply with appropriate standards relevant to the end-use they are destined for.

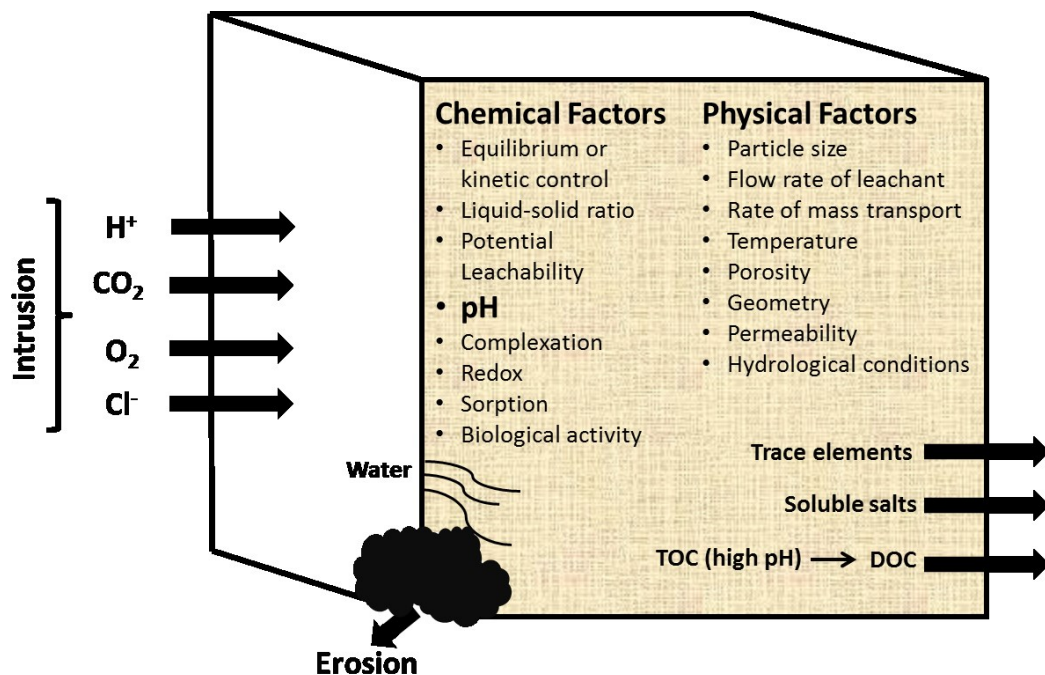


**Figure B.1** Leaching controlling factors and mechanisms of release of elements into the environment when a porous solid material comes in contact with a liquid, called the ‘leachant’. In this study, pH was selected as an important factor to investigate.

**Table B.1** Leaching limit values for inert, non-hazardous and hazardous granular wastes calculated at L/S=10 l/kg for total release (Adapted from Council Decision 2003/33/EC).

Element or substance	Inert Wastes	Non-hazardous wastes	Hazardous waste acceptable at non-hazardous waste landfills	Hazardous waste acceptable at hazardous waste landfills
<b>As</b>	0.5	2	2	25
<b>Ba</b>	20	100	100	300
<b>Cd</b>	0.04	1	1	5
<b>Cr (total)</b>	-	10	10	70
<b>Cu</b>	2	50	50	100
<b>Hg</b>	0.01	0.2	0.2	2
<b>Mo</b>	0.5	10	10	30
<b>Ni</b>	0.4	10	10	40
<b>Pb</b>	0.5	10	10	50
<b>Sb</b>	0.06	0.7	0.7	5
<b>Se</b>	0.1	0.5	0.5	7
<b>Zn</b>	4	50	50	200
<b>Cl</b>	880	15000	15000	25000
<b>F</b>	10	150	150	500
<b>SO<sub>4</sub></b>	1000	20000	10000	25000

## APPENDIX C

The statistical significance of the difference in mean WCA values of hydrophobic PSA samples prepared with capric and stearic acid, as presented in Figure 8.4, was assessed using the t-test method (see section 4.4.1). Hence, the hypothesis  $H_0$  was that the mean WCA values of both types of hydrophobic PSA are equal versus  $H_1$  that assumes they are different.

In the case of PSA ANP, the mean WCA values for capric acid- and stearic acid-modified PSA samples were  $121.6^\circ$  and  $153.2^\circ$  respectively. The corresponding variances were 5.3 and 6.2. The sample size equals 10 in both cases. Using the '*ttest*' function in Excel (calculation based on Equation 4.18) and for a two-tailed test at a prescribed confidence level of 5 % ( $\alpha=0.05$ ), the returned p-value was  $7.52 \cdot 10^{-7}$  ( $=2 \times 3.76 \cdot 10^{-7}$ , for a two-tailed test), which is a lot lower than the  $\alpha$ -value of 0.05. Hence, the null hypothesis was rejected, meaning that the means are significantly different.

Similarly, in the case of PSA UPM, the mean WCA values for capric- and stearic-modified PSA samples were  $125.7^\circ$  and  $148.3^\circ$  respectively. The corresponding variances were 5.3 and 6.2. The sample size equals 10 in both cases. The p-value was  $18.1 \cdot 10^{-6}$  ( $=2 \times 9.05 \cdot 10^{-6}$ ). Hence, the difference in hydrophobicity between capric and stearic acid-treated PSA samples is statistically significant in this case as well.